SIMULATED SPACE RADIATION:

EFFECTS ON MURINE BEHAVIOR AND NEUROGENESIS

APPROVED BY SUPERVISORY COMMITTEE

Amelia J. Eisch, Ph.D.

_____

Ann M. Stowe, **Ph.D.**

_____

Dwight C. German, Ph.D.

_____

Jerry W. Shay, Ph.D.

_____

Sandeep Burma, Ph.D.

_____

DEDICATION

I am extremely fortunate enough to be blessed with two amazing mentors. First, I would like to thank Dr. Amelia Eisch for accepting me initially in her lab, and then her willingness to keep me on as a graduate student through the move to UPENN. I know this took a tremendous amount of effort and patience to coordinate our almost daily chat sessions, but you made it feel as if you had never left UTSW. I would also like to tremendously thank Dr. Ann Stowe for graciously taking me into her lab as her own. You had the ability to make me feel welcomed from the moment I transitioned into your lab and your accommodation has allowed me to remain on a project I am truly passionate about. I would also like to thank my wife, Lauren, for trusting in me enough to move to Texas, supporting, and encouraging me through the entire graduate school process. Also gratitude goes out to our dog Henry, for providing a constant source of laughter during this intense dissertation process. Finally I would like to thank my family for urging me to continue my education to this level. All of these people have provided tremendous support in my career and I certainly would not be where I am without you.

SIMULATED SPACE RADIATION:

EFFECTS ON MURINE BEHAVIOR AND NEUROGENESIS

by

Cody William Whoolery

DISSERTATION

Presented to the faculty of the Graduate School of Biomedical Sciences

The University of Texas Southwestern Medical Center

In Partial Fulfillment of the Requirements

For the Degree of

DOCTOR OF PHILOSOPHY

The University of Texas Southwestern Medical Center

Dallas, Texas

May, 2018

SIMULATED SPACE RADIATION:

EFFECTS ON MURINE BEHAVIOR AND NEUROGENESIS

Publication No. _____

Cody Whoolery, BS

The University of Texas Southwestern Medical Center, 2017

Supervising Professors: Amelia Eisch, Ph.D. & Ann M. Stowe, Ph.D.

Abstract

An unavoidable consequence of deep space exploration is exposure to high-atomic number, high-energy (HZE) particles, such as ^{28}Si or ^{56}Fe, that comprise galactic cosmic radiation (GCR). It is widely believed that GCR is damaging to the brain, as HZE particle exposure decreases rodent hippocampal dentate gyrus neurogenesis as well as function (e.g. learning and memory). While this raises concern that GCR will compromise astronaut health and mission success, most data have been collected

using a specific set of parameters: 2 month old mice or rats (age-equivalent to a teenage human) irradiated with ^{56}Fe. For this dissertation, I have filled three major knowledge gaps with regards to space radiation, brain, and behavior, which are described in the five chapters of my dissertation. In my introductory chapter, **Chapter 1**, I provide the essential background needed to understand the research chapters, including an overview of the hippocampus, the process of neurogenesis and how radiation affects it, and in-depth look at the published literature on how space radiation influences the central nervous system (CNS). In **Chapter 2**, I present my published work (Whoolery et al. 2017) on how dentate gyrus neurogenesis is changed at two timepoints post-^{28}Si irradiation (24 h and 3 months), and explain how ^{28}Si-induced changes in dentate gyrus neurogenesis compares to the effects seen after exposure to other previously-studied ions. In **Chapter 3**, I present my submitted work on how dentate gyrus-dependent behaviors are changed after 6 month old mice are exposed to mission-relevant doses of ^{56}Fe. I test mice on many behavioral paradigms, but the most striking results come from two pattern separation tasks: the aversive Contextual Discrimination Fear Conditioning (CDFC) task and the appetitive Location Discrimination (LD) task which is performed on the Lafayette Bussey touchscreen platform. As I show in **Chapter 3**, mice exposed to ^{56}Fe radiation display surprisingly improved performance on both CDFC and LD, findings which are discussed in relation to mission-critical behaviors and prior results on space radiation-induced changes in behavior. In **Chapter 4,** I expand on the operant touchscreen data provided. Specifically, I investigate whether the ^{56}Fe-induced improvement in pattern separation is transient and if it is sex-specific. In my conclusion chapter, **Chapter 5**, I summarize the

main conclusions of Chapters 2-4, provided future directions for each project, possible mechanisms that may underlie this improvement in pattern separation, and end with my thoughts on remaining challenges in the field and obstacles that need to be overcome.

TABLE OF CONTENTS

PUBLICATIONS

Whoolery CW, Walker AK, Richardson DR, Lucero MJ, Reynolds RP, Beddow DH, Clark KL, Shih H- Y, LeBlanc JA, Cole MG, Amaral WZ, Mukherjee S, Zhang S, Ahn F, Bulin SE, DeCarolis NA, Rivera PD, Chen BPC, Yun S, Eisch AJ. Whole-Body Exposure to ^{28}Si-Radiation Dose-Dependently Disrupts Dentate Gyrus Neurogenesis and Proliferation in the Short Term and New Neuron Survival and Contextual Fear Conditioning in the Long Term. Radiation Research. 2017. 188(5):532-551; PMID: 28945526, NIHMSID: 920999, DOI: 10.1667/RR14797.1

Whoolery CW, Lucero MJ, Reynolds RP, Ito N, Redfield RL, Richardson DR, Shih H, Rivera PD, Chen BPC, Yun S, Birnbaum SG, Stowe AM, Eisch AJ Space radiation unexpectedly enhances pattern separation yet diminishes dentate gyrus neurogenesis in C57BL/6J mice. *In preparation.*

Whoolery CW, Eisch AJ. Space radiation-induced behavioral effects: a comprehensive review of current CNS behavior studies. Invited focused review for The Health Risks for Extraterrestrial Environments (THREE). *In preparation.*

Ortega SB, Latchney SE, Torres V, **Whoolery CW**, Noorbhai IZ, Poinsatte K, Selvaraj UM, Benson MA, Meeuwissen AJM, Plautz EJ, Kong X, Goldberg MP, Monson NL, Eisch AJ, Stowe AM. B Cells directly mediate functional recovery and neuronal viability following stroke. *In preparation.*

LIST OF FIGURES

Figure 3-1. On an aversive contextual discrimination fear conditioning (CDFC) task, mice exposed to whole body ^{56}Fe irradiation (IRR) at 6-month of age discriminate two contexts earlier than mice exposed to Sham IRR.

Figure 3-2. On an appetitive touchscreen task, mice exposed to whole body ^{56}Fe IRR at 6-month of age distinguish two similar visual cues earlier and with greater percent correct than mice exposed to Sham IRR.

Figure 3-3. Stereological quantification reveals fewer immature dentate gyrus neurons (DCX+ cells) 4 months post-whole body ^{56}Fe particle radiation.

Supplemental Figure 3-1. Contextual Discrimination Fear Conditioning (CDFC) paradigm.

Supplemental Figure 3-2. Contextual fear conditioning (CFC) paradigm.

Supplemental Figure 3-3. CFC and anxiety are unaffected in mice exposed to whole body Fractionated (Frac) or Non-Fractionated (Non-Frac) ^{56}Fe radiation.

Supplemental Figure 3-4. Locomotion and pain threshold are generally unaffected in mice exposed to whole body Frac or Non-Frac ^{56}Fe radiation in maturity.

Supplemental Figure 3-5. On an aversive fear conditioning task, mice exposed to ^{28}Si irradiation (IRR) at 7-month of age discriminate two contexts faster and more consistently than mice exposed to Sham IRR.

Supplemental Figure 3-6. On an appetitive touchscreen task, mice exposed to ^{56}Fe IRR at 6-month of age show no changes in rule based learning.

Figure 4-1. Analysis of Location Discrimination performance 6 months post-IRR reveal no differences in training or pattern separation performance in male mice.

Figure 4-2. On an appetitive touch screen task, female mice exposed to ^{56}Fe IRR at 6-

Figure 5-9. Long-term CDDO delivery decreases the innate lymphoid cells in Sed mice.

LIST OF TABLES

LIST OF ABBREVIATIONS

2-cyano-3,12-dioxooleana-1,9 (11)-dien-28-oic acid, CDDO; 3'-Diaminobenzidine, DAB; Bromodeoxyuridine, BrdU; Brookhaven National Laboratory, BNL; Central Nervous System, CNS; Context Discrimination Fear Conditioning, CDFC; Contextual Fear Conditioning, CFC; Cornu Ammonis 1, CA1; Cornu Ammonis 3, CA3; Dentate Gyrus, DG; Doublecortin, DCX; Double Stranded Break, DSB; Entorhinal Cortex, Ent; Fractionation, Frac; Galactic Cosmic Radiation, GCR; Granule cell, GC; Granule Cell Layer, GCL; (Centi) Gray, (c)Gy; Green fluorescent protein, GFP; High Atomic Number and High Energy, HZE; Hours, h,hrs; International Space Station, ISS; Irradiation, IRR; Linear Energy Transfer, LET; Location Discrimination, LD; Minute, min; Month, mo; Mossy Fiber, mf; NASA Space Radiation Laboratory, NSRL; National Institute of Health, NIH; Neuronal Stem Cell, NSC; Open Field, OF; Paired Associates Learning, PAL; Pairwise Discrimination, PD; Phosphate Buffered Saline, PBS; Radial Glia-like Stem Cells, RGL; Reversal Learning, Rev; Schaffer Collateral, sc; seconds, sec; Subiculum, Sub; Subgranular Zone, SGZ; University of Texas Southwestern Medical Center, UTSW; Visiomotor Conditional Learning, VMCL

QUESTIONS ASKED IN THIS THESIS

Chapter 2

1. Does ^{28}Si radiation exposure affect proliferation and neurogenesis in the young adult mouse hippocampus 24 hours post-irradiation?
2. Does ^{28}Si radiation exposure affect proliferation, neurogenesis, and survival in the young adult mouse hippocampus 3 months post-irradiation?

Chapter 3

3. Do mature male mice exposed to whole body ^{56}Fe radiation have altered pattern separation ability when tested on an aversive platform?
4. Do mature male mice exposed to whole body ^{56}Fe radiation have altered pattern separation ability when tested on an appetitive platform?

Chapter 4

5. Do mature female mice exposed to whole body ^{56}Fe radiation have altered pattern separation ability when tested on an appetitive platform?
6. Are ^{56}Fe radiation-induced improvements in pattern separation (using appetitive touchscreen platform) long-lasting?

CHAPTER 1: INTRODUCTION

Hippocampus and the hippocampal dentate gyrus

History

The earliest mentions of the hippocampus date back to 1587, where Arantius first compared the floor of temporal horn of the lateral ventricle to a seahorse, the latin term being hippocampus (Duvernoy 2005). As time went on, this brain region garnered additional names that referred to a “silkworm” or a “rams horn”, cornu ammonis, after ammon, the egyptian god Ammun Kneph). Eventually, the field adapted the terminology to refer to the entire ventricular perfusion solely as the hippocampus. This region is then further broken down into two cortical laminae rolled up inside each other, one is the cornu ammonis (or CA region) and the other is the fascia dentata, now referred to as the dentate gyrus (DG; **Fig. 1-1**) (Duvernoy 2005).

However, it wasn’t until 1957 when the famous “Patient H.M”, later revealed to be Henry Molaison, brought the spotlight to hippocampus for its function. Specifically, Henry Molaison suffered considerably from extreme seizures (Scoville & Milner 1957). This condition left him totally incapacitated to the point that it was recommended that he undergo a medial temporal-lobe resection which extended into the hippocampus. To a normal individual, this patient displayed ordinary reasoning and understanding during conversations. However patient H.M had a significant loss to his short-term memory. For example, the report highlights that the patient would forget that he had eaten lunch a mere half-hour earlier, or reread the same magazines over and over without finding their contents familiar (Scoville & Milner 1957). Since this insightful study occurred, a

vast amount of literature has focused on the hippocampus to parse out the exact role it plays in cognition in a wide variety of animal models and humans. For purposes of this work, many of the studies that will be discussed throughout will be specific for a rodent model, as all of the work presented in later chapters is specific to mice.

Hippocampal Development and Structure

In early development, the CA and DG regions are continuous and linear (Duvernoy 2005). As development progresses, the DG starts to become concave and the CA region starts to bulge into the ventricular space, allowing the DG to form two interlocking U-shaped laminae by slipping beneath the medial end of the CA (**Fig. 1-1**) (Duvernoy 2005). While this is occuring, the hippocampus is migrating in a mammal dependent manner. Specifically in humans, the hippocampus follows the lateral telencephalic vesicle, starting from the interventricular foramen and curving up and back, and then down and under to form the temporal lobe (Duvernoy 2005). However in rodents this migration is incomplete, as the telencephalic vesicle ceases before the formation of a complete temporal lobe (Duvernoy 2005). As a result, it is viewed that the dorsal hippocampus in rodents correlates to the posterior hippocampus in primates, and thus, the ventral hippocampus relates to the anterior hippocampus in primates (Fanselow & Dong 2010). This is important to keep in mind when we discuss the functionality of these regions in rodents (i.e dorsal performs primarily cognitive function and ventral relates to stress, emotion, and affect), as each cognitive process is shifted across this axis in the primate as well (Fanselow & Dong 2010).

Fortunately, this migration does not affect two aspects of the hippocampus, the DG structure or the signaling circuitry, as both have been shown to be highly conserved across a variety of animals including rodents, cats and primates (Fanselow & Dong 2010; Treves et al. 2008).

For instance, the DG is a trilaminar structure made up of a molecular layer, a granule cell layer, and the hilus (**Fig. 1-1**). The molecular layer, or outer most layer, is relatively cell free and is comprised mostly of either dendrites from the granule shaped neurons in the dentate or axons from the entorhinal cortex (Treves et al. 2008). The granule cell layer (GCL), or middle layer, is primarily composed of densely packed granule shaped neuron cell bodies (~10 μm in diameter). As these neurons mature, though the process of neurogenesis that will be discussed later, they send their dendrites up to the molecular layer and pass their axons through the Hilus. The Hilus, or deepest layer, runs between the suprapyramidal and infrapyramidal blade of the GCL. This layer contains mostly axons from the GCL and mossy cells, though 25-30% less concentrated than the granule cells (Treves et al. 2008).

As briefly mentioned above, this conserved structure allows for similar circuitry to exist across species. For example the granule neurons in the GCL will receive signals (dendritic processes synapsing in the molecular layer) from the entorhinal cortex via the perforant path (**Fig. 1-1**) (Fanselow & Dong 2010). These granule neurons will then send information through the Hilus to the CA3 large pyramidal cells via mossy fibers (**Fig. 1-1**). The CA3 will then either relay back on itself or project signals through the

schaffer collateral to the small pyramidal cells of the CA1, where it will then be sent to the subiculum (**Fig. 1-1**). However, as this thesis project did not directly aim to manipulate the hippocampus in a circuit specific manner, this information is purely a simplified summary for referencing purposes to highlight the basic hippocampal circuitry. There is a large body of literature attempting to map these highly complex processes that have not been discussed and can be reviewed separately (Fanselow & Dong 2010).

Hippocampal Functionality and Mechanism

Although rodents provide easier access for structural brain mapping, one key downside of using animal models to mimic human disease is the rodents inability to verbally interact with us. As a result, we as scientists are challenged to design appropriate behavioral tests that can get at key traits - such as learning, memory, spatial navigation, pattern separation, or defensive fear responses - following a particular manipulation of interest; whether it be a disease model, exposure to radiation, or drug exposure.

Classically, experiments targeting these behavioral traits would use simplistic tests ranging from non-aversive (i.e. no fear) to high aversion (i.e. highly fear-based) behavioral paradigms. For instance a simple non-aversive learning and memory test that experimenters often use is the Novel Object Recognition (NOR) task, which takes advantage of a rodents natural instinct to investigate something new (Antunes & Biala 2012). For this test, the rodent is exposed to two identical items in a novel environment before having one of the items replaced with a new object (Antunes & Biala 2012). A

rodent that does not have any memory impairments will naturally spend more time investigating the novel object compared to the familiar object (Antunes & Biala 2012). The NOR task has been expanded to look at non-aversive spatial memory, called novel spatial location task, by moving one of the two familiar objects in the chamber to a different corner (vs. switching it out for a new object) (Antunes & Biala 2012). Without memory impairment, a rodent will spend more time investigating the item that has been moved compared to the familiar item.

Other simple spatial memory tests include some of the arm maze tasks - e.g. the radial arm maze, T-maze or Y-maze - or the slightly aversive barnes maze. Specifically, the various arm mazes test a rodent's ability to spatially navigate around a chamber to find a food reward (Vorhees & Williams 2014). These tests can vary the number of enclosed arms involved (depending on experimenter preference) but the general principle is to measure the latency of time it takes for a rodent to get the reward or the number of entries into a previously entered arm (Vorhees & Williams 2014). Rodents with better spatial navigation will spend less time and enter empty arms less often than spatially impaired rodents (Vorhees & Williams 2014). Additionally, the Barnes maze takes advantage of a rodents natural aversion to being in brightly lit open spaces. Specifically rodents are placed on a elevated open platform with holes around the perimeter and either bright lights, a tone, or a fan blowing on them to increase their aversion to sitting on the platform (Vorhees & Williams 2014). The objective is to measure the time it takes for a rodent to find the escape box beneath one of the open holes (Vorhees & Williams 2014). Rodents with impaired spatial memory or learning will continue to randomly

search the holes for the escape box, but a unimpaired rodent will eventually learn where the hole is and head directly to it (Vorhees & Williams 2014).

Far more stressful spatial memory tasks are the morris water maze test and Contextual Fear Conditioning. For example, the Morris Water Maze (MWM) is conducted in a circular pool (usually with white opaque water) with either a submerged platform or a platform slightly above the water so that a rodent swimming in the pool can stand on the platform (Vorhees & Williams 2014). The rodent must use cues outside of the circular pool to find the platform located in one of the 4 quadrants of the pool. Rodents with better spatial learning/memory will spend less time searching for the platform as the number of trials increases. The benefit of this type of trial is that it avoids the need to food restrict the rodents (Vorhees & Williams 2014). With the Contextual Fear Conditioning (CFC) test, the stress associated with food restricting (any of the arm mazes) and forcing a rodent to swim (MWM) is replaced with pain fear (Vorhees & Williams 2014). Specifically a rodent is briefly placed into a novel environment and administered a foot shock with a tone. The rodent is then placed back into the environment it received the shock and it's time spent freezing is recorded. Animals with unaffected spatial memory will spend more time freezing in the environment, as they will then associate the environment with a stressful foot shock (Fanselow & Dong 2010).

Many early functional studies tied the hippocampus to learning, memory, spatial navigation, or defensive fear responses by lesioning the hippocampus and testing the ability of a rodent to perform some of the cognitive tasks mentioned above. For

instance, using spatial memory tasks, such as the water maze, radial arm maze, and contextual fear conditioning, it was found that a lesion of the anterior/dorsal hippocampus - but not posterior/ventral - impaired the acquisition of spatial navigation using a water maze and radial arm maze, as well as reduced freezing in fear conditioning (Moser et al. 1995; Kim & Fanselow 1992; Pothuizen et al. 2004; Phillips & LeDoux 1992). For recognition memory, rats with hippocampal lesions spent less time exploring novel objects or previously encountered objects placed in a novel location (Clark et al. 2000; Mumby et al. 2002). Finally, for defensive fear-related responses, rats with hippocampal lesions to the ventral half of the hippocampus, via Ibotenic acid, exhibited little open arm avoidance in elevated plus maze, and decreased neuroendocrine responses to stress during confinement in brightly lit chamber (Kjelstrup et al. 2002). Interestingly, this fear-related experiment was also in agreement with the spatial memory work, as these ventral lesions did not induce any deficits in spatial memory - using contextual fear or water maze - that was found in some of the dorsal lesioning experiments mentioned above (Moser et al. 1995; Kim & Fanselow 1992; Pothuizen et al. 2004; Fanselow & Dong 2010; Kjelstrup et al. 2002).

Although crude, these early lesioning experiments provided some of the first link between the hippocampus and these cognitive processes. However, it also highlighted the need for more region- (or cell-) specific studies to identify possible underlying mechanisms. For example, one explanation for this spatial memory phenomenon is likely driven by the high density of pyramidal “place cells” located in the dorsal hippocampus (O’Keefe & Dostrovsky 1971; Jung et al. 1994). Specifically, these place

cells fire as an animal enters a specific location in an environment (Bird & Burgess 2008). The firing pattern they then produce will create a stable representation of the animals location memory (independent of orientation) that will last for several weeks (Bird & Burgess 2008). These place cells are then supported by “head direction” cells in the subiculum (for coding head position in space) and grid cells in the entorhinal cortex (for path integration) (Fanselow & Dong 2010; Bird & Burgess 2008). In fact, as place cells are thought to be important for pattern separation (differentiating between two similar contexts) and pattern completion (ability to retrieve additional surrounding features bound to a specific place representation), the presentation of a partial cue can stimulate the retrieval of a full environment where the observer had been (Bird & Burgess 2008).

With the development of key technologies, such as optogenetics, recent work has been able to take this connection a step further. Specifically, using channelrhodopsin, it was shown that reactivation of the hippocampal neurons, which were activated during fear conditioning, was sufficient to induce freezing behavior when placed in a separate context and had no effect on rodents who were not exposed to an aversive environment (Liu et al. 2012). Taken together, these studies highlight the impactful role cell specific hippocampal manipulations can play on cognition and thus support investigations targeting the highly unique process of neurogenesis in the dentate gyrus of the hippocampus.

Dentate Gyrus Neurogenesis

Overview

Neurogenesis, the term used to describe the process of making new neurons, was originally believed to occur only during embryonic development (Altman & Das 1965). However, by using radiolabeled thymidine, Altman and Das were able to disprove this theory over 50 years ago and provide some of the first evidence that neurogenesis occurs in the granule cell layer of the DG (Altman & Das 1965). Since this discovery, much work has been done to tie the cell specific process of neurogenesis to many of the hippocampal dependent behaviors mentioned above - spatial navigation, learning and memory, fear response - as well as multiple disease states not mentioned - such as schizophrenia, major depression, addiction, and anxiety (Gonçalves et al. 2016). In this section, I will provide an overview of neurogenesis and explain how it relates to the radiation-induced cognitive changes that this thesis aims to address. However, as the ever expanding breadth of neurogenic markers could be discussed in detail for a review in itself (von Bohlen Und Halbach 2007), this section will primarily focus on the markers used in this thesis to define the various stages of neurogenesis (**Fig. 1-2**).

Stages of Neurogenesis

Radial Glia-like Stem Cells

The DG is unique in that it contains a region, called the subgranular zone (SGZ), that is one of two major neurogenic niches in the mammalian brain necessary (Bond et al. 2015). Specifically, neural stem cells (NSC) in the SGZ must pass through a variety of stages to reach maturity over a 6 week timeframe (**Fig. 1-2**) (Gonçalves et al. 2016).

Initially, these NSC's, also called radial glia-like NSC (RGL or Type-1 cells), have radial projections that extend into the DG (**Fig. 1-2**) (Bonaguidi et al. 2012). However, much is still unknown about this cell population beyond their ability to either self-renewal, give rise to astrocytes or neuronal precursor cells (Type-2 cells), and their relatively quiescent state that allows them to withstand cell stressors (such as radiation exposure) to maintain genomic integrity over the animals lifetime (Bond et al. 2015; Rivera et al. 2013; Bonaguidi et al. 2012). Some contrasting studies have attempted to determine the maintenance of this quiescence and suggest they replicate a few rounds before re-entering quiescence, while other studies demonstrate these cells die off after replication or become astrocytes (Bond et al. 2015). In addition, two separate transgenic mouse lines specifically designed to label NSC's in the SGZ (Nestin-CreER^{T2} and GLAST::CreER^{T2}), found that NSC's do not contribute to neurogenesis equally, as only Glutamate Aspartate Transporter (GLAST) derived cells contribute to neurogenesis following either ablation or stimulation (DeCarolis et al. 2013). In addition, they found the stem cell pool of these radial glial like (RGL) NSC are heterogeneous, as some GLAST immunopositive (+) cell populations were nestin+ and nestin immunonegative (-) (DeCarolis et al. 2013).

Interestingly, these GLAST+ and Nestin+ cells only make up two markers for this stage, as additional markers can range from structural proteins to transcription factors and even include DNA altering factors including epigenetic regulatory elements and nucleotide analogs (Gonçalves et al. 2016). Taken together, this highlights the careful consideration that must be taken when selecting a specific cell marker for these types of

studies. For instance, GLAST+ and Nestin+ cells only overlap in the RGL cell stage, with nestin is expressed in the neural progenitor cells (NPC or Type-2 cells) that RGL cells give rise (DeCarolis et al. 2013).

Nonradial Neural Progenitor Cells

Like RGL NSC's, neural progenitor cells (NPC) have the ability to either self renew or give rise to neuronal progeny, called neuroblasts (or Type-3 cells) (Gonçalves et al. 2016; Suzuki et al. 2010; Bonaguidi et al. 2012). These NPCs lack the radial projections into the DG but can still contain parallel processes along the granule cell layer (**Fig. 1-2**) (Bonaguidi et al. 2012). Additionally, they are more mitotic than RGL cells, relatively speaking, as most are still not in the cell cycle (Bonaguidi et al. 2012) - allowing for endogenous and exogenous labeling of the proliferating cells (Bonaguidi et al. 2012). For instance, Ki67 is an endogenous protein expressed during mitosis and the G1, S, and G2 phases of the cell cycle and is expressed throughout the body in actively dividing cells, including progenitor cells in the DG (Scholzen & Gerdes 2000). Whereas bromodeoxyuridine (BrdU) is an exogenously introduced thymidine analog that incorporates itself into the DNA of actively dividing cells during the S phase of the cell cycle (Mandyam et al. 2007). Once incorporated, BrdU can then be permanently detected in the cell (or its progeny) for the rest of the cells life, allowing researchers the ability follow the cells maturity over time (Mandyam et al. 2007). In fact, researchers have also been able to colocalize BrdU and Ki67 to determine the length of the cell cycle (14 hrs total) and time for BrdU to be taken up (15 minutes) to help explain precursor proliferation kinetics and cell fate (Mandyam et al. 2007). However, because

of its endogenous expression, Ki67 is often prefered over BrdU for studies where BrdU injections are either infeasible due to the toxicity and mutagenesis, or for cells that divide rapidly, as BrdU is halved every time the cell divides and thus can lead to underestimations of cell division (Kim et al. 2009; Curtis et al. 2011).

Neuroblasts and Immature Neurons

As mentioned above, NPC's in the SGZ will give rise to newborn neuroblasts, which in turn can either self-renew or differentiate into immature neurons before becoming mature neurons (**Fig. 1-2**) (Ming & Song 2011; Lee et al. 2006). Once derived, neuroblasts will slowly migrate into the inner granule cell layer where they can develop into immature neurons by extend dendritic processes into the molecular layer and axons into the hilus (Ming & Song 2011). During this period, the endogenous microtubule protein doublecortin (DCX) is constitutively expressed and can be used for cell labeling (Brown et al. 2003). Specifically, DCX was first discovered in patients with mutated DCX alleles due to its developmental role in cell migration in the brain, leading to Double Cortex Syndrome (des Portes et al. 1998; Gleeson et al. 1998). However, since its discovery, DCX is a widely-used marker for inter-neurogenesis stages, as it is up-regulated during the final stages of proliferation and is down-regulated around the time mature neuronal markers start to be expressed (i.e. NeuN) (Brown et al. 2003). However, only a small subset of neuroblast cells will end up integrating into the hippocampal circuitry as mature neurons, and in fact, as many as 81% of cells entering neurogenesis will be depleted within the first 8 days (Sierra et al. 2010).

The underlying mechanism for this phenomenon is only partially understood, as a vast amount of literature has tied many intracellular (cell cycle regulators, transcription factors and epigenetic regulators) and extracellular (growth factors, neurotrophins, cytokines and hormones) regulators of neurogenesis (Ming & Song 2011). However, the integration of neuroblasts and immature neurons into the neuronal circuitry follows a conserved sequence (Ge et al. 2008). Initially, newborn granule cells express the Cl^- importer $GABA_AR$, NKCC1, a receptor for γ-aminobutyric acid (GABA) (Ge et al. 2008). This receptor imports chloride into a cell and consequently depolarizes the cell early on by tonic GABA (GABA which diffused out of synaptic cleft)(Ge et al. 2008). As the cell develops into an immature neuron, NKCC1 expression levels decreases while the $GABA_AR$ KCC2 (chloride exporter) is upregulated. This receptor shift gradually convert the cell to be hyperpolarized by GABA over a period of 2-3 weeks until it is indistinguishable from a mature neuron (Ge et al. 2008; Ming & Song 2011).

Interestingly, this transition from excitatory to inhibitory GABA signaling overlaps with the glutamate-dependent critical survival period of newborn neurons (Ge et al. 2008). Specifically, it was shown by electrophysiological analysis that glutamate receptors are present in immature neurons and NR1 deletion does not reduce progeny survival until 2-3 weeks after being born (Ge et al. 2008). It is believed that this integration stage is a critical period for survival, as these immature neurons experience enhanced plasticity which may provide an advantage over mature neurons for selective formation and stabilization of synaptic connections (Ming & Song 2011).

Function of Postnatal Neurogenesis

Given that neurogenesis only occurs in two primary locations in the adult mammalian brain, it should be of no surprise that researchers have been interested in uncovering related diseases. For instance, neurogenic regulators in the SGZ play a role in Alzheimer's disease, double cortex syndrome, fragile X syndrome, Rett syndrome, schizophrenia, as well as many other additional mental disorders (Ming & Song 2011). As a result, rodent data showing stress, radiation exposure, and aging decrease neurogenesis yet exercise, learning in an enriched environment, and antidepressants all increased neurogenesis drove excitement for the clinical benefit neurogenesis may provide for many CNS diseases (Scharfman & Hen 2007). However, this excitement was tempered after neurogenesis was also shown to be pathologically upregulated after stroke or prolonged seizures, which can lead to inappropriate migration, differentiation, and integration of many of these new neurons (Scharfman & Hen 2007). Additionally, increased neurogenesis can also have beneficial effects on some behavior tests, such as CFC, yet ablation of neurogenesis can lead to improvements in certain working memory paradigms (Scharfman & Hen 2007).

Although these correlative studies provide valuable insight into the functionality of neurogenesis, highly causative studies are necessary to determine the true role neurogenesis plays on various cognitive processes. For instance, neurogenesis has been causatively linked to contextual pattern separation, a high-resolution and translationally-relevant hippocampal-dependent learning ability required to distinguish two similar contexts (Clelland et al. 2009; A. Sahay et al. 2011). In order to do this,

researchers have used a variety of techniques - including radiation exposure and transgenic mouse lines - to manipulate neurogenesis prior to rodent performance (Clelland et al. 2009; A. Sahay et al. 2011). Specifically, pattern separation has been assessed via Context Discrimination Fear Conditioning (CDFC) in an aversive shock-based paradigm or by Location Discrimination (LD) in an appetitive touchscreen-based paradigm (Sahay et al. 2011; T. J. McHugh et al. 2007; McTighe et al. 2009). For example, correlative studies exposed 2 month C57Bl/6J female mice to hippocampal-directed X-ray radiation (5 Gy fractionated dose of 3 times a day, every 4 days, for 3 days total) 2 months prior to appetitive-based pattern separation testing (Clelland et al. 2009). They found that the irradiated cohort required additional trials to reach criterion when shown the easy separation display. This tie of decreased DCX+ granule cells to the decrease in pattern separation was then causative established using transgenic mice. For instance, Nakashiba et al. exposed Tg1xTg3-TeTX transgenic mice to 15 Gy (300 kV) of hippocampal-directed X-Ray radiation at 3-4 months of age. This radiation exposure decreased performance in the CDFC paradigm, i.e. freezing similar amounts in the shock and non-shock contexts for a longer duration than the non-irradiated control mice. They showed inhibition of mature neuron signaling did not change pattern separation ability until signaling from younger mature neurons (NeuN+) was blocked (Nakashiba et al. 2012). In addition, other transgenic mouse lines have been used to either induce survival or death of adult-generated neurons prior to pattern separation testing. Specifically, prevention of cell death at 4 months of age improved pattern separation (using the CDFC paradigm, mice discriminated earlier)(Sahay et al. 2011). Furthermore, by inducing cell death at 2 months of age, pattern separation (using the

CDFC paradigm) could be impaired (i.e mice discriminate between the similar contexts later than control mice) (Tronel et al. 2012).

In the following chapters of this thesis, I will present data that build on what is known about hippocampal-directed radiation exposure to both neurogenesis and cognitive function by exposing rodents to simulated whole-body space radiation. As this radiation source is not readily available here on Earth, a broad overview of the radiation features will be discussed in the next section prior to an in-depth overview of where the space radiation field is today.

Space Radiation Effects On Brain Structure And Function

Space Radiation Overview

Physical and Molecular Properties

Humans are increasingly being exposed to various forms of ionizing radiation, such as X-ray exposure for doctor visits, nuclear accidents, solar and environmental radionuclide exposure, etc. (Hladik & Tapio 2016). This is of particular concern as ionizing radiation can directly interact with DNA, causing single base mutations, single-stranded breaks, or double-stranded breaks, or indirectly by ionizing water in the body to create hydroxyl radicals that can attack DNA (Mahaney et al. 2009). Due to these biological processes, strong evidence suggests an increasing number of deleterious effects on the brain, including disrupted neurogenesis and impaired cognition (Hladik & Tapio 2016). Thus, as the variety of ionizing radiation sources rise, more work will be needed to ensure human safety (Hladik & Tapio 2016).

In this thesis, all data are centered around ionizing high(H)-atomic number (Z), high-energy (E) particles (HZE). HZE particles are fundamentally different from other common forms of ionizing radiation (such as X-ray or γ-rays) due to their deposition of energy along a linear track (**Fig. 1-3**) (Nelson 2003a; Cucinotta et al. 2014). For instance, as electromagnetic radiation (photons) interacts with tissue, a photon beam dislodges electrons and becomes scattered from its original direction, diffusely spreading the beam into an even radiation exposure (Nelson 2003a). As a result, these photons exponentially deposit their energy as a function of depth, with the highest deposit of energy near the surface of tissue (Nelson 2003a). However, HZE particles have a high charge on the nucleus of the particle. This allows for Coulomb's law to dominate the interaction, and thus deposits its energy along the track in a Z^2/V^2 (where Z is atomic number and V is velocity) relationship (Nelson 2003a). As a result, much of the energy is released around the stopping point of the particle within the tissue, referred to as the “Bragg Peak”. However, in addition to the ionization along the track, HZE particles also eject secondary electrons, called delta rays, during their molecular interactions. These delta rays can then be absorbed by surrounding tissue as secondary ionizing particles, creating a “bottle brush” pattern when viewed on photographic emulsions (Nelson 2003a). Lastly, HZE particle damage can be further extended by nuclear interactions. Specifically, HZE particles can produce secondary particles by fragmenting when they come in contact with other nuclei (Nelson 2003a; Cucinotta et al. 2013). This fragmentation can then produce smaller ions (e.g. protons,

neutrons, helium, etc.) that create their own ionizing tracks (Nelson 2003a; Cucinotta et al. 2013).

The ionization damage HZE particles produce is also unique. For example, the majority of cell damage arising from radiation types, such as X-ray, is primarily in the form of single-stranded breaks (Ward 1988). For HZE particles, a cluster of simultaneously damaged DNA sites can occur if they lie along the particle track, with concentrated doses near the ion stopping point (Nelson 2003a). As a result, a 0.1 Gy dose could equate to around 80,000 Gy to the nucleosome alone (Cucinotta et al. 2000). This interaction leads to a larger proportion of double-stranded breaks to single-stranded breaks (Nelson 2003a).

Global Relevance

Fortunately, the damaging effects of HZE particles are not readily felt here on Earth or in the International Space Station, as the Earth's magnetosphere repels high charge nuclei with energies below about 1000 Mev/μ (Cucinotta et al. 2014). However, with an increasing interest in deep space exploration, (i.e long-term lunar or missions to Mars), the relevance of HZE particle damage begins to become a concern (Cucinotta et al. 2013). With most GCR in space ranges in the 100's of cm, shielding will not be a viable countermeasure (Cucinotta et al. 2014). Thus particle accelerators - similar to the one at Brookhaven National Laboratories (BNL) - have been used to simulate various components of GCR in an attempt to mimic the whole body radiation exposure that

astronauts are bound to receive (Cucinotta et al. 2014; Jandial et al. 2018).

In addition, traditional cancer radiotherapy for using photons that make up a large portion of GCR, has led to some success treating patients with a variety of malignancies (Schlaff et al. 2014). Unfortunately this approach has drawbacks, including increasing radioresistance and a lack of local directed radiation control that can increase toxicity and damage to healthy tissues/structures (Schlaff et al. 2014). As a result, heavy particle radiation centers (mostly heavy carbon) have been built throughout the world (Schlaff et al. 2014). With these centers, researchers show favorable results in malignancies that are traditionally radioresistant or constrained anatomically by the body - such as glioblastoma multiforme (intracranial), lung (thoracic), and rectal carcinoma - due to their ability to spare the healthy surrounding tissue while delivering a higher biological dosage (via controlment of the Bragg peak) to the tumor (Schlaff et al. 2014).

Simulation of Space Radiation On Earth

In order to test HZE particles here on Earth, ground-based accelerators, such as the one at NASA's Space Radiation Laboratory [NSRL, Brookhaven National Laboratory (BNL); Upton, NY], are needed to mimic space radiation. With these accelerators, scientists have attained essential knowledge necessary for creating our basic understanding of HZE particles and their effects on the CNS (Jandial et al. 2018). For instance, based on the 80 papers listed in **Table 1-1**, it is generally believed that HZE radiation is detrimental to the CNS. Specifically, 12.5% of this work has looked at

neurogenesis (all showing radiation-induced decrease in neurogenesis) and ~96% of these 80 papers have shown some form of deficit in cognitive testing (specific behavior tests included in **Table 1-1**). However, there are still key questions unanswered. How does radiation affect females or older rodents, of “astronaut-age”? How do lower doses of radiation affect brain and behavior? What kind of brain and behavior influence does exposure to mixed beams have? Are there even more relevant cognitive behaviors we can probe for radiation sensitivity?

The necessity of these questions emerges after closer examination of the published literature. For example, only 15% (12/80) of studies include female rodents and only 29% (23/80) use rodents >6 months of age, which would be the age equivalence of the average 34 year old astronaut (Jackson Laboratory 2018; NASA no date). Surprisingly, 81% (65/80) of these studies exposed lab rodents to well over the the predicted dose astronauts will receive on the way to Mars. Lastly, technology has been limited in its ability to provide mixed beam radiation (Gifford & Magazine 2014; Cucinotta & Durante 2006; Kim et al. 2015). However, recent technological advancement allows scientists the ability to better simulate the GCR spectrum experience in deep space missions by irradiating with a mixed radiation beam (Kim et al. 2015). As the field currently stands though, only one study has been able to provide data on mixed beam effects to the CNS (Kiffer et al. 2018).

As you will see, in this thesis I tackle many of the unanswered questions. In **Chapter 2** and **Chapter 4,** I provide insight into how ground-based space radiation influences

neurogenesis and performance on the operant touchscreen platform of female rodents, respectively. In **Chapter 3** and **Chapter 4,** I examine how ground-based space radiation at 6 months of age influences rodent behavior. Also in **Chapter 3**, I examine how ground-based space radiation influences the ability of rodent's to pattern separate - discriminate two similar visual contexts - under both aversive and appetitive testing conditions. In **Chapter 5** I provide an overview of the main findings of each chapter, describe plans to investigate mixed beam radiation in order to better understand GCR effects on the CNS, and discuss the translational relevance this approach has over traditional techniques. While more work is certainly needed to expand on this dissertation, the data provided here lay the groundwork for these questions, highlighting the role age, sex, and ion play on HZE related cognitive effects.

‘

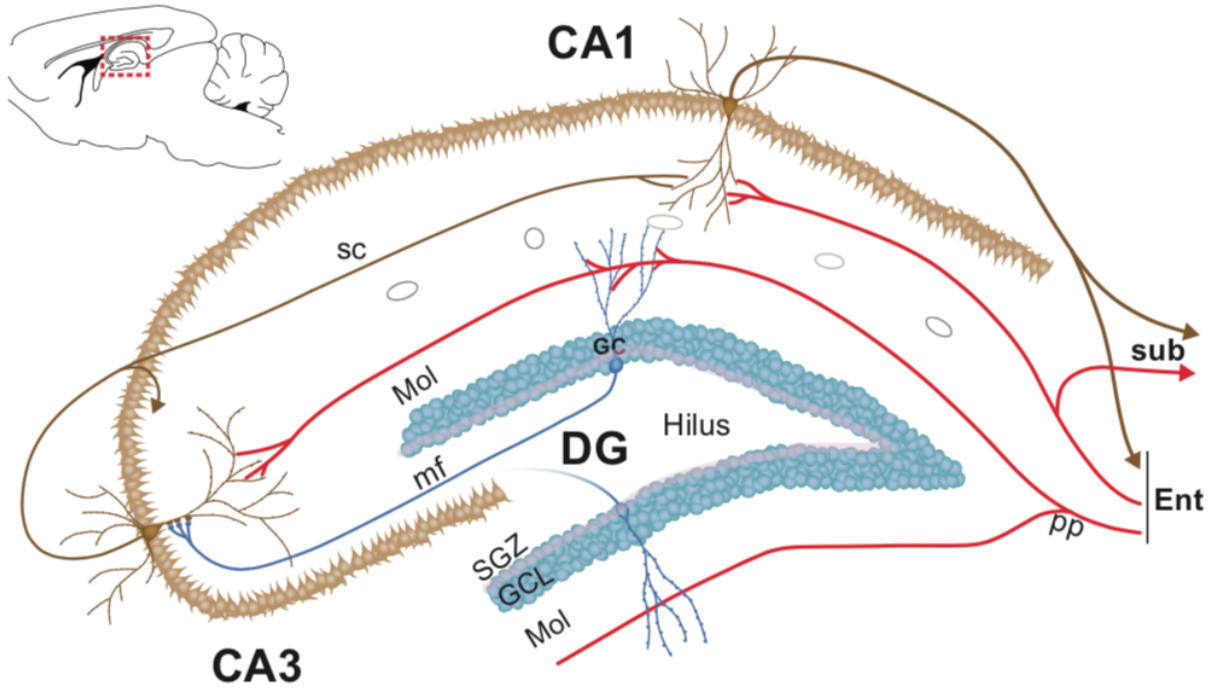

Figure 1-1. Schematic of basic hippocampal circuitry. Various regions of the entorhinal cortex (Ent) will send signals to the hippocampus along the perforant path (pp). Granule shaped neurons in the subgranular zone (SGZ) or granule cell layer (GCL) will extend their dendritic processes into the molecular layer (Mol) to synapse onto the perforant path. From here, these granule neurons will extend their axons through the Hilus to the large pyramidal cells in the CA3 via mossy fibers (mf). The CA3 cells will then either relay back onto itself or extend axons through the Schaffer collateral (sc) to the small pyramidal cells in the CA1. Finally, the CA1 cells will extend processes either to the subiculum (sub) or back to the entorhinal cortex. The Entorhinal cortex will also synapse in the CA region, for instance, so that grid cells in the entorhinal

cortex can support place cells during spatial navigation/memory. (Figure provided by Ryan P. Reynolds and modified with permission.)

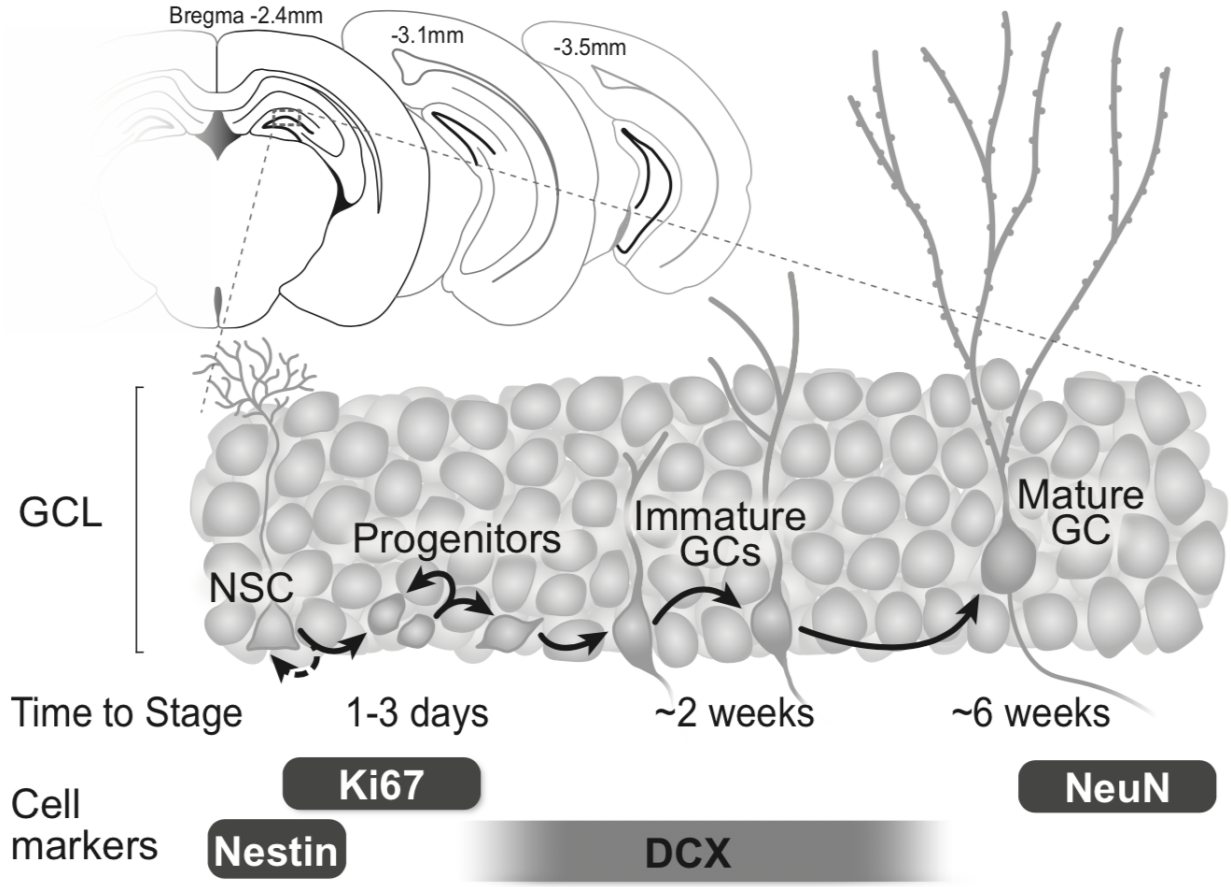

Figure 1-2. Neurogenesis overview from neuronal stem cells to mature granule cells. For a neuronal stem cell to become a mature granule cell, it must slowly advance through a variety of cell stages. During this time (about 6 weeks in rodents or >6 month in monkeys; (Kohler et al. 2011), scientists can use unique cell markers to track cell progress. Initially, the first two types of cells in the process, Neuronal Stem Cells (NSC) and progenitors, possess the ability for either self renewal or differentiation into later neurogenesis stages. During this time, a select population of NSC will express Nestin, as well as very early progenitor cells. When both of these cells leave quiescence and begin to proliferate, they will express the short lived cell cycle marker, Ki67. The cells will slowly differentiate from progenitors to immature neurons, increasing the expression

of the microtubule protein doublecortin (DCX). As the cell continues to mature, it will decrease DCX expression and slowly express the fully mature neuronal marker, NeuN. Importantly, the thymidine analog BrdU will be used in the second chapter as a marker for proliferation and survival. This specific marker is incorporated into the DNA during S phase of the cell cycle, but omitted from the figure above because it is dependent on the time of injection. However, its specific role in this process can be seen in **Fig. 2-1**. In addition, the markers shown in this figure are important markers for this thesis only. For a more extensive list of current neurogenesis markers please see (Gonçalves et al. 2016; von Bohlen Und Halbach 2007). (Modified and reprinted with permission from Whoolery et al., 2017)

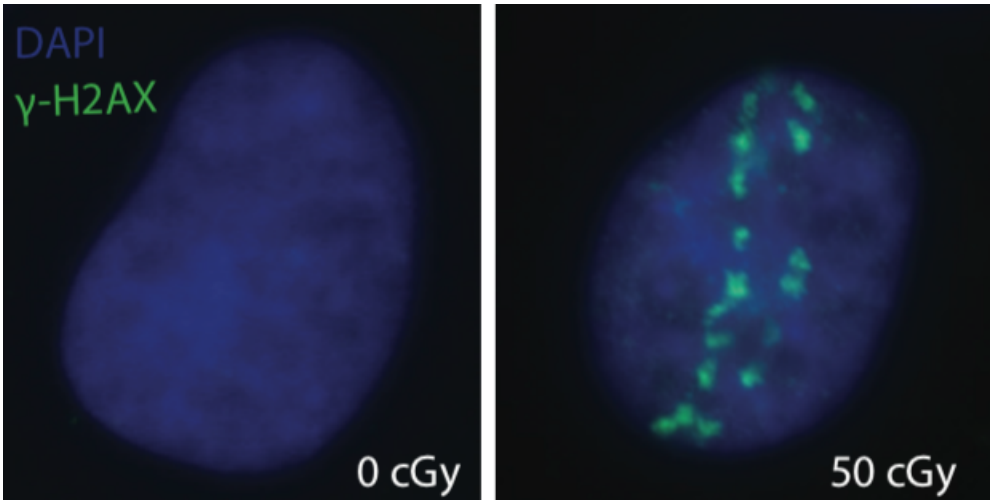

Figure 1-3. Linear HZE tracks can be seen using the DNA damage marker γ-H2aX. These images are courtesy of Angela Kim, Brookhaven National Laboratory, NY and were created at Nasa Space Radiation Laboratories during the Nasa Space Radiation Summer School in Brookhaven, NY on June, 2015. Briefly, NT2 cells were irradiated with either 0 or 50 cGy of 600 MeV ^{56}Fe at NSRL in June, 2015. One hour after radiation exposure, cells were fixed with 4% PFA and fluorescently immunostained the following day with the DNA double stranded break marker, anti-phosphorylated histone γ-H2aX (Green, 1:750 dilution). Cells were counterstained with the nuclear, DNA binding, DAPI stain (blue). Cells irradiated with 50 cGy (right image) show a defined DSB track structure compared to sham NT2 cells (left image).

Table 1-1. Cited literature involving HZE radiation exposure in rodent CNS studies.

Space irradiation effects on brain and behavior table | Rodents>6 months | Neurogenesis study | Doses<0.3 Gy | Rodents>6 months & Doses <0.3

PROTONS (H)

TITLE	First author	Year	Last author	Animal used	Sex	Age at IRR	HZE Particle	Dose (Gy)	Dose Rate (Gy/min)	LET (MeV/n)	Age at Testing	Behavior test	Brain Region
Late effects of 1H irradiation on hippocampal physiology	Kiffer	2018	Allen	C57BL/6 mice	M	6 mo	H	0.5 and 1	0.35-0.55	150	9 mo post-irr	Y-maze	Hippocampus
Effects of 1H + 16O Charged Particle Irradiation on Short-Term Memory and Hippocampal Physiology in a Murine Model	Kiffer	2018	Allen	C57BL/6 mice	M	6 mo	H and O	0.5 H and 1 hr later 0.1 O	0.18–0.19 (H) and 0.18–0.33 (O)	150 MeV/n (H) and 600 MeV/n (O)	9 mo	Y-maze	Hippocampus
Bi-directional and shared epigenomic signatures following proton and 56Fe irradiation	Impey	2017	Raber	Mouse: C57Bl/6J	M	6 mo	H and Fe (Fe data is from prior study)	0, 1 H, compared to 0.1 and 0.2 Gy Fe	Not given	150	6 mo or 11 mo	NOR, Water maze, Environment test	Hippocampus
Long-Term Deficits in Behavior Performances Caused by Low- and High-Linear Energy Transfer Radiation	Patel	2017	Welford	Mouse: C57Bl/6J	M	3 mo	H, Si, Fe, gamma	0, 0.1, 1, 2.5	0.05-0.5	1000, 300, 600	8-12 mo	OF, rotarod, NO, T maze	Hippocampus (DG)
Proton irradiation induces persistent and tissue-specific DNA methylation changes in the left ventricle and hippocampus	Impey	2016	Raber	Mouse: C57Bl/6J	M	6 mo	H	1	Not provided	1000	22 weeks post-IRR	No behavior	Hippocampus, left ventricle
Effects of Proton and Combined Proton and 56Fe Radiation on the Hippocampus	Raber	2016	Nelson	Mouse: C57Bl/6J	M	2 mo	H and Fe	0, 0.1, 0.5 H, or 0, 0.1 H then 0.5 Fe 1d later, or 0, 0.5 Fe	Not provided	150, 600	3 mo or 5 mo	CFC, NOR	Hippocampus
A Single Low Dose of Proton Radiation Induces Long-Term Behavioral and Electrophysiological Changes in Mice	Bellone	2015	Vlkolinsky	Mouse: B6D2F1/J	M	3 mo	1H	0, 0.5	1.5-2.5	150	2.75 mo, retested at 6-9 mo. Ephys at 11 mo	MWM (Cued, spatial test, probe test), Barnes maze,	Hippocampus
Targeted Overexpression of Mitochondrial Catalase Prevents Radiation-Induced Cognitive Dysfunction	Parihar	2015	Limoli	Mouse: MCAT (Tg)	M	2 mo	H	0, 0.5, 2	0.5	150	3 mo	NOR, OiP, morphology	Hippocampus (CA1)
28Silicon Irradiation Impairs Contextual Fear Memory in B6D2F1 Mice	Raber	2015	Turker	Mouse: B6D2F1	M, F	6-7 mo	H, Si, Ti	0.5	?	1000	9-10 mo	CFC, cued fear	Hippocampus, Amygdala
Lack of reliability in the disruption of cognitive performance following exposure to protons	Rabin	2015	Baxter	Rat: Sprague-Dawley	M	200-225g	H	0, 35, 50,80, 100, 150, 200; 0, 25, 50, 100, 125; 0, 25, 50, 100. Some head only, some whole body.	Not provided	150 or 1000	1-2 mo post-IRR (NOR). 2-3 mo post-IRR (operant respondi ng)	NOr, operant responding	NA
Radiation-Induced Alterations in Synaptic Neurotransmission of Dentate Granule Cells Depend on the Dose and Species of Charged Particles	Marty	2014	Spigelman	Mouse: C57Bl/6J	M	2.5 mo	H	0, 0.1, 0.5, 1	?	600.5	Sac'd at ~5.5 mo	Ephys	Hippocampus (DG)
Effects of Age on the Disruption of Cognitive Performance by Exposure to Space Radiation	Rabin	2014	Carrihill-Knoll	Rat: Sprague-Dawley	M	~2 mo (200 - 225g)	H, O, Si, Ti, Fe	0.001-2 (dose varied by animal and group)	.05-1 Gy given within 3-4min (dose rate varied by group)	380-1100 (LET varied by group)	3-19 mo (age varied by group)	NOR	Hippocampus
Central nervous system effects of whole-body proton irradiation.	Sweet	2014	O'Banion	Mouse: C57Bl/6J	M,F	10-12 w	H	0, 0.1, 0.5, 1, 2 or 0, 0.1, 1	0.044-0.21 or 0.7-0.162	1000	48 hrs or 1, 3, 6, 12 months	CFC and cued	Hippocampus, Amygdala
Effects of Exposure to 56Fe Particles or Protons on Fixed-ratio Operant Responding in Rats	Rabin	2002	Jenkins	Rat: Sprague Dawley	M	250-275 g	Fe, H	H: 4 Fe: 1, 2	Not Given	250 or 1000	Not Given	AFR	Striatum

Helium (He)

TITLE	First author	Year	Last author	Animal used	Sex	Age at IRR	HZE Particle	Dose (Gy)	Dose Rate (Gy/min)	LET (MeV/n)	Age at Testing	Behavior test	Brain Region
Persistent nature of alterations in cognition and neuronal circuit excitability after exposure to simulated cosmic radiation in mice	Parihar	2018	Limoli	C57BL/6J	M	6 mo	He	0, 0.05, 0.3	0.05	400	6, 15, 52 weeks post-IRR	OF, Temporal Order, Object in Place, EPM, Forced Swim, MWM, and Fear Conditioning/Extinction.	Hippocampus and Cortex
Age as a factor in the responsiveness of the organism to the disruption of cognitive performance by exposure to HZE particles differing in linear energy transfer	Rabin	2018	Shukitt-Hale	Rats: Fischer 344	Does not indicate	7 week, 2, 11, and 15 mo	He, O, Ti	0.01, 0.05, or 0.1 cGy He; 0.1 or 0.5 cGy O; 1 or 10 cGy Ti	Does not say. IRR does not exceed 3-4 min	1000 (He and O); 500 (Ti)	2-3 mo post-IRR and 7-8 mo post-IRR (tested twice)	Plus maze and Ascending FR operant	Amygdala and striatum

Comparison of the Effectiveness of Exposure to Low-LET Helium Particles (4He) and Gamma Rays (137Cs) on the Disruption of Cognitive Performance	Rabin	2015	Shukitt-Hale	Rat: Sprague-Dawley	M	IRR @ 225-250 grams	γ-ray; 4He	0, 0.5, 1, 2, 4; 0, 0.001, 0.005, 0.01, 0.05, 0.1	0.5-5	1000	1-5 mo	EPM, NOR, FRR, NSL	Hippocampus, amygdala, striatum, perirhinal ctx

CARBON (12C)													
TITLE	**First author**	**Year**	**Last author**	**Animal used**	**Sex**	**Age at IRR**	**HZE Particle**	**Dose (Gy)**	**Dose Rate (Gy/min)**	**LET (MeV/n)**	**Age at Testing**	**Behavior test**	**Brain Region**
Effects of Age on the Disruption of Cognitive Performance by Exposure to Space Radiation	Rabin	2014	Carrihill-Knoll	Rat: Sprague-Dawley	M	~2 mo (200 - 225g)	H, O, Si, Ti, Fe	0.001-2 (dose varied by animal and group)	.05-1 Gy given within 3-4min (dose rate varied by group)	380-1100 (LET varied by group)	3-19 mo (age varied by group)	NOR	Hippocampus
Operant responding following exposure to HZE particles and its relationship to particle energy and linear energy transfer	Rabin	2011	Shukitt-Hale	Rats: Sprague-Dawley	M	4 mo	C,O,Si,Ti	0.001-0.15	0.05-0.1	290,380, 500, 600, 1000, 1100	6-8 wks	FRR	Striatum
High-LET Radiation Induces Inflammation and Persistent Changes in Markers of Hippocampal Neurogenesis	Rola	2005	Fike	Mice: C57BL/6J	M	2.5 mo	C and Fe	0, 1, 2, 3	0.87 Fe & 1.23 C	1000 Fe & 290 C	9 mo post-IRR	no behavior examined	

OXYGEN (16O)													
TITLE	**First author**	**Year**	**Last author**	**Animal used**	**Sex**	**Age at IRR**	**HZE Particle**	**Dose (Gy)**	**Dose Rate (Gy/min)**	**LET (MeV/n)**	**Age at Testing**	**Behavior test**	**Brain Region**
Early effects of 16O radiation on Neuronal Morphology and Cognition in a Murine Model	Carr	2018	Allen	C57BL/6 mice	M	6 mo	O	0, 0.1, 0.25, 1 Gy	0.21-0.26	600	2 weeks post-IRR	Y-maze	Hippocampus
Effects of 1H + 16O Charged Particle Irradiation on Short-Term Memory and Hippocampal Physiology in a Murine Model	Kiffer	2018	Allen	C57BL/6 mice	M	6 mo	H and O	0.5 H and 1 hr later 0.1 O	0.18–0.19 (H) and 0.18–0.33 (O)	150 (H) and 600 (O)	9 mo	Y-maze	Hippocampus
Whole-Body Oxygen (16O) Ion-Exposure-Induced Impairments in Social Odor Recognition Memory in Rats are Dose and Time Dependent	Mange	2018	Davis	Long-Evans rats	M	6 mo	O	0.05, 0.25	0.05-0.25	1000	7 mo and 12 mo	Social order recognition	Hippocampus and SVZ
Age as a factor in the responsiveness of the organism to the disruption of cognitive performance by exposure to HZE particles differing in linear energy transfer	Rabin	2018	Shukitt-Hale	Rats: Fischer 344	Does not indicate	7 week, 2, 11, and 15 mo	He, O, Ti	0.01, 0.05, or 0.1 cGy He; 0.1 or 0.5 cGy O; 1 or 10 cGy Ti	Does not say. IRR does not exceed 3-4 min	1000 (He and O); 500 (Ti)	2-3 mo post-IRR and 7-8 mo post-IRR (tested twice)	Plus maze and Ascending FR operant	Amygdala and striatum
Cosmic radiation exposure and persistent cognitive dysfunction	Parihar	2016	Limoli	Mouse: (Thy1-EGFP)MJrsJ (Tg) Rat:Wistar	M	Mice 6 month Rat 7-9 month	O, Ti	0, 0.05, 0.3	0.05-0.25	600	3-6 mo post IRR	NOR, OiP, Temporal order (TO), attention set shifting, CFC, EPM	multiple
What happens to your brain on the way to Mars?	Parihar	2015	Limoli	Mouse: (Thy1-EGFP)MJrsJ (Tg)	M	6 mo	O, Ti	0, 0.5, 0.3	0.5-1	600	7.5 mo	NOR, OiP	mPFC
16Oxygen irradiation enhances cued fear memory in B6D2F1 mice	Raber	2015	Turker	Mouse: B6D2F1	M, F	6 mo	O	0, 0.4, 0.8, 1.6	Not given, but check Kronenberg 2009	250	7 mo	CFC, CuF	Hippocampus, amygdala
Acute Effects of Exposure to 56Fe and 16O Particles on Learning and Memory	Rabin	2015	Shukitt-Hale	Rat: Sprague-Dawley	M	~2 mo	HEAD ONLY O, Fe	0, 0.05 or 0, 0.25	0.05	600	7-8 wks	NOR	Multiple
Comparison of the Effects of Partial- or Whole-Body Exposures to 16O Particles on Cognitive Performance in Rats	Rabin	2014	Gomes	Rat: Sprague-Dawley	M	~2 mo	O	0, 0.01, 0.05, 0.1, 0.25	0.01-0.1	1000	~2.25 mo, 2.75 mo, 4 mo, 7 mo	EPM, NOR, FRR, NSL	Hippocampus
Effects of Age on the Disruption of Cognitive Performance by Exposure to Space Radiation	Rabin	2014	Carrihill-Knoll	Rat: Sprague-Dawley	M	~2 mo (200 - 225g)	H, O, Si, Ti, Fe	0.001-2 (dose varied by animal and group)	.05-1 Gy given within 3-4min (dose rate varied by group)	380-1100 (LET varied by group)	3-19 mo (age varied by group)	NOR	Hippocampus
Exposure to 16O-Particle Radiation Causes Aging-Like Decrements in Rats through Increased Oxidative Stress, Inflammation and Loss of Autophagy	Poulouse	2011	Rabin and Shukitt-Hale	Rat: Sprague-Dawley	M	~2 mo	O	.05, .5, 1	.25-.5	1000	1 day and 2.5 mo	No behavior	Hippocampus
Operant responding following exposure to HZE particles and its relationship to particle energy and linear energy transfer	Rabin	2011	Shukitt-Hale	Rats: Sprague-Dawley	M	4 mo	C,O,Si,Ti	0.001-0.15	0.05-0.1	290,380, 500, 600, 1000, 1100	6-8 wks	FRR	Striatum

SILICON (28Si)													
TITLE	First author	Year	Last author	Animal used	Sex	Age at IRR	HZE Particle	Dose (Gy)	Dose Rate (Gy/min)	LET (MeV/n)	Age at Testing	Behavior test	Brain Region
Impaired Attentional Set-Shifting Performance after Exposure to 5 cGy of 600 MeV/n 28Si Particles	Britten	2018	Tessa	Rat: Sprague-Dawley	M	old? retired breeder	Si, and previous work with Fe, Ti	0, 0.05, 0.15, 0.20. And 1 Gy for Fe and Ti	0.2	600	3 mo post-irradiation	ATSET (attentional set shifting) assay - simple discrimination (SD)	PFC
Epigenetic determinants of space radiation-induced cognitive dysfunction	Acharya	2017	Baulch	Mouse: C57Bl/6J	M	6 mo	Si	0, 0.2	0.2	600	7 mo	OF, NOR, OiP, Temporal Order (TO)	hippocampus, medial prefrontal cortex (mPFC) and perirhinal cortex
Long-Term Deficits in Behavior Performances Caused by Low- and High-Linear Energy Transfer Radiation	Patel	2017	Welford	Mouse: C57Bl/6J	M	3 mo	H, Si, Fe, gamma	0, 0.1, 1, 2.5	0.05-0.5	1000, 300, 600	8-12 mo	OF, rotarod, NO, T maze	Hippocampus (DG)
Whole-body exposure to 28Si-radiation dose-dependently disrupts dentate gyrus neurogenesis and proliferation in the short term and new neuron survival and contextual fear conditioning in the long term	Whoolery	2017	Eisch	Mouse: Nestin-GFP and C57Bl/6J	M, F	~2.5 mo	Si	0, 0.2, 1	1	300	~6 mo	CFC	Hippocampus
28Silicon Irradiation Impairs Contextual Fear Memory in B6D2F1 Mice	Raber	2015	Turker	Mouse: B6D2F1	M, F	6-7 mo	Si, Ti, H	0, 0.4, 0.8, 1.6	Not given	263	9-10 mo	CFC, cued fear	Hippocampus, Amygdala
Radiation-Induced Alterations in Synaptic Neurotransmission of Dentate Granule Cells Depend on the Dose and Species of Charged Particles	Marty	2014	Spigelman	Mouse: C57Bl/6J	M	2.5 mo	Si	0, 0.25, 1	Not given	600.5	Sac'd at ~5.5 mo	Ephys	Hippocampus (DG)
28Silicon Radiation-Induced Enhancement of Synaptic Plasticity in the Hippocampus of Naïve and Cognitively Tested Mice	Raber	2014	Vlkolinsky	Mouse: C57Bl/6J	M	~2 mo	Si	0.25, 1	Not given	600	~5 mo	CFC, Ephys	Hippocampus
Effects of Age on the Disruption of Cognitive Performance by Exposure to Space Radiation	Rabin	2014	Carrihill-Knoll	Rat: Sprague-Dawley	M	~2 mo (200 - 225g)	H, O, Si, Ti, Fe	0.001-2 (dose varied by animal and group)	.05-1 Gy given within 3-4min (dose rate varied by group)	380-1100 (LET varied by group)	3-19 mo (age varied by group)	NOR	Hippocampus
28Silicon Radiation Impairs Neuronal Output in CA1 Neurons of Mouse Ventral Hippocampus without Altering Dendritic Excitability[]/	Rudobeck	2014	Vlkolinsky	Mouse: C57Bl/6	M	~2.5 mo	Si	0, 0.25, 1	0.2-0.6	600	~5.5 mo	Ephys	Hippocampus (CA1)
Operant responding following exposure to HZE particles and its relationship to particle energy and linear energy transfer	Rabin	2011	Shukitt-Hale	Rats: Sprague-Dawley	M	4 mo	C,O,Si,Ti	0.001-0.15	0.05-0.1	290,380, 500, 600, 1000, 1100	6-8 wks	FRR	Striatum

Calcium (40Ca)													
TITLE	First author	Year	Last author	Animal used	Sex	Age at IRR	HZE Particle	Dose (Gy)	Dose Rate (Gy/min)	LET (MeV/n)	Age at Testing	Behavior test	Brain Region
Sex- and dose-dependent effects of calcium ion irradiation on behavioral performance of B6D2F1 mice during contextual fear conditioning training	Raber	2016	Turker	Mouse: B6D2	M, F	6 mo	Ca	0, 0.165, 0.33, 1.32	?	942	9 mo	CFC, extinction	Hippocampus

Titanium (48Ti)													
TITLE	First author	Year	Last author	Animal used	Sex	Age at IRR	HZE Particle	Dose (Gy)	Dose Rate (Gy/min)	LET (MeV/n)	Age at Testing	Behavior test	Brain Region
Age as a factor in the responsiveness of the organism to the disruption of cognitive performance by exposure to HZE particles differing in linear energy transfer	Rabin	2018	Shukitt-Hale	Rats: Fischer 344	Does not indicate	7 week, 2, 11, and 15 mo	He, O, Ti	0.01, 0.05, or 0.1 cGy He; 0.1 or 0.5 cGy O; 1 or 10 cGy Ti	Does not say. IRR does not exceed 3-4 min	1000 (He and O); 500 (Ti)	2-3 mo post-IRR and 7-8 mo post-IRR (tested twice)	Plus maze and Ascending FR operant	Amygdala and striatum
Exposure to Mission-Relevant Doses of 1 GeV/n 48Ti Particles Impairs Attentional Set-Shifting Performance in Retired Breeder Rats	Hadley	2016	Britten	Rat: Wistar (retired breeders)	M	6-11 mo (Avg 7 mo)	Ti	0, 0.1, 0.15, 0.2	0.2	1000	3 mo post-IRR	AtSet (CDR and CD)	Executive Function

Cosmic radiation exposure and persistent cognitive dysfunction	Parihar	2016	Limoli	Mouse: (Thy1-EGFP)MJrsJ (Tg) Rat:Wistar	M	Mice 6 month Rat 7-9 month	O, Ti	0, 0.05, 0.3	0.05-0.25	600	3-6 mo post IRR	NOR, OiP, Temporal order (TO), attention set shifting, CFC, EPM	multiple
What happens to your brain on the way to Mars?	Parihar	2015	Limoli	Mouse: (Thy1-EGFP)MJrsJ (Tg)	M	6 mo	Ti , O	0, 0.5, 0.3	0.5-1	600	7.5 mo	NOR, OiP	mPFC
28Silicon Irradiation Impairs Contextual Fear Memory in B6D2F1 Mice	Raber	2015	Turker	Mouse: B6D2F1	M, F	6-7 mo	Ti, Si, H	0, 0.2, 1.4	Not given	1000	9-10 mo	CFC, cued fear	Hippocampus, Amygdala
Effects of Age on the Disruption of Cognitive Performance by Exposure to Space Radiation	Rabin	2014	Carrihill-Knoll	Rat: Sprague-Dawley	M	~2 mo (200 - 225g)	H, O, Si, Ti, Fe	0.001-2 (dose varied by animal and group)	.05-1 Gy given within 3-4min (dose rate varied by group)	380-1100 (LET varied by group)	3-19 mo (age varied by group)	NOR	Hippocampus
Operant responding following exposure to HZE particles and its relationship to particle energy and linear energy transfer	Rabin	2011	Shukitt-Hale	Rats: Sprague-Dawley	M	4 mo	C,O,Si,Ti	0.001-0.15	0.05-0.1	290,380, 500, 600, 1000, 1100	6-8 wks	FRR	Striatum

Iron (56Fe)													
TITLE	First author	Year	Last Author	Animal used	Sex	Age at IRR	HZE Particle	Dose (Gy)	Dose Rate (Gy/min)	LET (MeV/n)	Age at Testing	Behavior test	Brain Region
Changes in the Hippocampal Proteome Associated with Spatial Memory Impairment after Exposure to Low (20 cGy) Doses of 1 GeV/n 56Fe Radiation	Britten	2017	Dutta	Rat: Wistar	M	130 g	Fe	0, 0.2	Not given	1000	3 mo post-IRR	Barnes Maze	Hippocampus
Bi-directional and shared epigenomic signatures following proton and 56Fe irradiation	Impey	2017	Raber	Mouse: C57Bl/6J	M	6 mo	H and Fe (Fe data is from prior study)	0, 1 H, compared to 0.1 and 0.2 Gy Fe	Not given	150	6 mo or 11 mo	NOR, Water maze, Environment test	Hippocampus
Long-Term Deficits in Behavior Performances Caused by Low- and High-Linear Energy Transfer Radiation	Patel	2017	Welford	Mouse: C57Bl/6J	M	3 mo	H, Si, Fe, gamma	0, 0.1, 1, 2.5	0.05-0.5	1000, 300, 600	8-12 mo	OF, rotarod, NO, T maze	Hippocampus (DG)
Performance in hippocampus- and PFC-dependent cognitive domains are not concomitantly impaired in rats exposed to 20 cGy of 1 GeV/n 56Fe particles	Britten	2016	Macadat	Rat: Wistar	M	612 g	Fe	0, 0.2	0.2	1000	14-16 weeks old	AtSet, Barnes Maze	Hippocampus and PFC, basal forebrain, ant & post cingulate orbitofrontal ctx
Impaired Spatial Memory Performance in Adult Wistar Rats Exposed to Low (5-20 cGy) Doses of 1 GeV/n (56)Fe Particles	Britten	2016	Wyrobek	Rat: Wistar	M	6-11 mo	Fe	0.05, 0.1, 0.15, 0.2	0.2	1000	3 mo post-IRR	Barnes Maze	Hippocampus
Short- and long-term effects of 56Fe irradiation on cognition and hippocampal DNA methylation and gene expression	Impey	2016	Raber	Mouse: C57Bl/6J	M	6 Mo	Fe	0, 0.1, 0.2, or 0.4	Not clear	600	2 or 20 weeks post-IRR	NOR, Water maze, Environment test	Hippocampus
Effects of Proton and Combined Proton and 56Fe Radiation on the Hippocampus	Raber	2016	Nelson	Mouse: C57Bl/6J	M	2 mo	H and Fe	0, 0.1, 0.5 H, or 0, 0.1 H then 0.5 Fe 1d later, or 0, 0.5 Fe	Not provided	150, 600	3 mo or 5 mo	CFC, NOR	Hippocampus
Effect of behavioral testing on spine density of basal dendrites in the CA1 region of the hippocampus modulated by 56Fe irradiation	Raber	2016	Fike	Mouse: C57Bl/6J	M	2 mo	Fe	0, 0.5	Not given	600	5 mo	Exploratory behavior, habituation	Hippocampus (CA1, CA3, DG)
Neurogenic Effects of Low-Dose Whole-Body HZE (Fe) Ion and Gamma Irradiation	Sweet	2016	O'Banion	Mouse: C57Bl/6J	M	8-10 weeks	Fe	0, 0.01, 0.03, 0.1, 0.3, 1	1	1000	2 days or 1 mo post-IRR	no behavior examined	Hippocampus
Individual Variations in Dose Response for Spatial Memory Learning Among Outbred Wistar Rats Exposed From 5 to 20 cGy of 56Fe Particles	Wyrobek	2016	Britten	Rat: Wistar	M	6-11 mo	Fe	0, 0.05, 0.1, 0.15, 0.2	Not given	1000	3 mo post-IRR	Barnes Maze	Hippocampus
56Fe irradiation-induced cognitive deficits through oxidative stress in mice	Yan	2016	Zhang	SPF-class Kunming	M	6-8 weeks	Fe	0.5, 1, 2	1	600	1 mo post-IRR	MWM	Hippocampus
56Fe Irradiation Alters Spine Density and Dendritic Complexity in the Mouse Hippocampus	Allen	2015	Fike	Mouse: C57Bl/6J	M	2 mo	Fe	0, 0.5	Not given	600	5 mo	Locomotion and habituation	Hippocampus
Acute Effects of Exposure to 56Fe and 16O Particles on Learning and Memory	Rabin	2015	Shukitt-Hale	Rat: Sprague-Dawley	M	~2 mo	Fe, O	0, 0.25 or 0, 0.05	0.25	600	7-8 wks post-IRR	NOR	Multiple
Exposure to mission relevant doses of 1 GeV/Nucleon (56)Fe particles leads to impairment of attentional set-shifting performance in socially mature rats	Britten	2014	Lonart	Rat: Wistar	M	~1.5 mo, 6-11 mo	Fe	0, 0.1, 0.15, 0.2	0.5	1000	~4.5 mo, 9-14 mo	AtSet	PFC, basal forebrain, ant & post cingulate, orbitofrontal ctx
(56)Fe Particle Exposure Results in a Long-Lasting Increase in a Cellular Index of Genomic Instability and Transiently Suppresses Adult Hippocampal Neurogenesis in Vivo	Decarolis	2014	Eisch	Mouse: Nestin-GFP, Nestin-CreER(T2)/R26R:YFP	M, F	1.5-2 mo	Fe	0, 1	1	300 or 1000	Sac'd at: 1, 7, 90 d post-IRR	None	Hippocampus (DG)

Radiation-Induced Alterations in Synaptic Neurotransmission of Dentate Granule Cells Depend on the Dose and Species of Charged Particles	Marty	2014	Spigelman	Mouse: C57Bl/6J	M	2.5 mo	Fe	0, 0.25, 1	Not given	594.7	Sac'd at ~5.5 mo	Ephys	Hippocampus (DG)
Effects of Age on the Disruption of Cognitive Performance by Exposure to Space Radiation	Rabin	2014	Carrihill-Knoll	Rat: Sprague-Dawley	M	~2 mo (200-225g)	H, O, Si, Ti, Fe	0.001-2 (dose varied by animal and group)	.05-1 Gy given within 3-4min (dose rate varied by group)	380-1100 (LET varied by group)	3-19 mo (age varied by group)	NOR	Hippocampus
Early effects of whole-body (56)Fe irradiation on hippocampal function in C57BL/6J mice	Haley	2013	Raber	Mouse: C57Bl/6J	M, F	Not given	Fe	0, 0.1, 0.2, 0.5	Not given	600	2-4 wks after IRR	MWM, NOR, CFC	Hippocampus
Effects of whole body 56Fe radiation on contextual freezing and Arc-positive cells in the dentate gyrus	Raber	2013	Fike	Mouse: C57Bl/6J	M	2 mo	Fe	0, 0.5, 1	Not given	600	5 mo	FCF, CuF	Hippocampus (DG)
Acute and Fractionated Exposure to High-LET 56Fe HZE-Particle Radiation Both Result in Similar Long-Term Deficits in Adult Hippocampal Neurogenesis	Rivera	2013	Eisch	Mouse: Nestin-GFP, Nestin-CreER(T2)/R26R-YFP	M, F	~2.5 mo	Fe	0, 0.2x5, 1	0.2 or 1	300	Sac'd 1d or 3 mo post-IRR	None	Hippocampus (DG)
Changes in Gene Expression in the Rat Hippocampus Following Exposure to 56Fe Particles and Protection by Berry Diets	Shukitt-Hale	2013	Joseph	Rat: Sprague-Dawley	M	2 mon	Fe	1.5, 2.5	1	1000	1 week or 2 mo post-IRR	no behavior examined	Hippocampus
Low (20 cGy) Doses of 1 GeV/u 56Fe-Particle Radiation Lead to a Persistent Reduction in the Spatial Learning Ability of Rats	Britten	2012	Lonart	Rat: Wistar	M	~1.5 mo	Fe	0, 0.2, 0.4, 0.6	0.5	1000	4.5 mo	Barnes Maze	Hippocampus
Galactic Cosmic Radiation Leads to Cognitive Impairment and Increased Aβ Plaque Accumulation in a Mouse Model of Alzheimer's Disease	Cherry	2012	O'Banion	Mouse: APPswe/PSEN1dE9 (APP/PS1)	M, F	3.5 mo	Fe	0, 0.1, 1	0.1-1	1000	M: 9.5 mo F: 7 mo	CFC, NOR, cued tone response	Hippocampus, PFC
Executive function in rats is impaired by low doses (20 cGy) of 1 GeV/u (56)Fe particles	Lonart	2012	Britten	Rat: Wistar	M	130 g	Fe	0, 0.2	0.5	1000	90 d post-IRR	AtSet	PFC, basal forebrain, ant & post cingulate, orbitofrontal ctx
Interaction between age of irradiation and age of testing in the disruption of operant performance using a ground-based model for exposure to cosmic rays	Rabin	2012	Carrihill-Knoll	Rats: Fischer-344	M	2, 7, 12, 16 mo	Fe; Head, neck, shoulder area only	0, 0.25, 0.5, 1.5, 2	0.5-1	1000	4-6, 9-11, 14-16, 18-20 mo post-IRR	FRR	Striatum
LONG-TERM EFFECTS OF 56FE IRRADIATION ON SPATIAL MEMORY OF MICE: ROLE OF SEX AND APOLIPOPROTEIN E ISOFORM	Villasana	2011	Raber	human apoE3- and apoE4-targeted replacement mice on the C57Bl/6J background	M and F	2 mon	Fe, Head only	3	Not given	600	13 mon post-IRR	MWM, CFC, OF, Zero Maze	Hippocampus, Amygdala
Dynamic characteristics of 56Fe-particle radiation-induced alterations in the rat brain: magnetic resonance imaging and histological assessments	Huang	2010	Obenaus	Rat: Sprague-Dawley	M	2	Fe	0,1,2,4	1-3	600	0.25-18 months post-IRR	No behavior examined	Hippocampus, entorhinal cortex, retrosplenial cortex, and thalamus
Low (60 cGy) Doses of 56Fe HZE-Particle Radiation Lead to a Persistent Reduction in the Glutamatergic Readily Releasable Pool in Rat Hippocampal Synaptosomes	Machida	2010	Britten	Rat: Wistar	M	~180g	Fe	0, 0.6	0.5	1000	3 & 6 mo post-IRR	Ephys/LTP	Hippocampus (CA1)
High-LET radiation-induced response of microvessels in the Hippocampus.	Mao	2010	Nelson	Mouse: C57Bl/6J	M	2.5 mo	Fe	0, 0.5, 2, 4	1.5-2.5 avg	600	8.5, 14.5 mo	Hipp volume, microvessel quant.	Hippocampus (CA1, DG)
Effects of heavy particle irradiation and diet on object recognition memory in rats	Rabin	2009	Foster	Rat: Sprague-Dawley	M	200-225g or 250-275g	Fe; Head, neck, shoulder area only	0, 0.5, 0.8, 1, 1.5, 2 or 0, 1.5	1	1000	2-3 mo post-IRR	NO	Hippocampus
Quiescent adult neural stem cells are exceptionally sensitive to cosmic radiation	Encinas	2008	Steindler	nestin-CFPnuc reporter mouse line	Not given	2 mo	Fe	0, 1	Not given	1000	1 day post IRR	None	Hippocampus
Memory impairment, oxidative damage and apoptosis induced by space radiation: ameliorative potential of alpha-lipoic acid. stress in mice: Protective effect of -lipoic acid	Manda	2008	Anzai	Mouse: C57BL	M	2 mo	Fe	0, 1.5	0.88	500	1, 7, 15, and 30 d post-IRR	MWM, SMA	Hippocampus, cerebellum, blood
Space radiation-induced inhibition of neurogenesis in the hippocampal dentate gyrus and memory impairment in mice: ameliorative potential of the melatonin metabolite, AFMK	Manda	2008	Anzai	Mouse: C57BL	M	2 mo	Fe	0, 2	0.88	500	4 mo	MWM, SMA	Hippocampus
Hippocampal Neurogenesis and Neuroinflammation after Cranial Irradiation with 56Fe Particles	Rola	2008	Fike	Mice: C57BL/6J	M	2 mo	Fe	0.5, 1, 2, 4	5	600	2 mo post-IRR	no behavior examined	Hippocampus
Amphetamine-induced taste aversion learning in young and old F-344 rats following exposure to 56Fe particles	Carrihill-Knoll	2007	Carey	Rat: Fischer 344	M	2, 7, 12, 16 Mo	Fe	0.25, 0.5, 1.5, 2	1	1000	3-4 d post-IRR	Conditioned Taste Aversion (CTA)	striatum

HIGH-ENERGY (HZE) RADIATION EXPOSURE CAUSES DELAYED AXONAL DEGENERATION AND ASTROGLIOSIS IN THE CENTRAL NERVOUS SYSTEM OF RATS	Cummings	2007	Mandell	Rat: Sprague-Dawley	Not given	Not given	Fe	0,4	Not Given	600	1, 6, and 12 mo	None	cerebral cortex
Dietary modulation of the effects of exposure to 56Fe particles	Rabin	2007	Carey	Rat: Sprague Dawley	M	175-200g at start of expt. Fed diet 2 mon prior to IRR	Fe; Head, neck, shoulder area only	1.5 Gy	1-1.5	1000	Up to 1 yr	None	None
Elevated plus-maze performance of Fischer-344 rats as a function of age and of exposure to 56Fe particles	Rabin	2007	Foster	Rat: Fischer 344	M	2 (n = 40), 7 (n = 30), 12 (n = 40), and 16 (n = 30) months of age at IRR	Fe; Head, neck, shoulder area only	0.25-2 Gy	Not Given	1000	1 or 4 mo post-IRR	EPM	Hippocampus and Amygdala
Beneficial effects of fruit extracts on neuronal function and behavior in a rodent model of accelerated aging	Shukitt-Hale	2007	Joseph	Rat: Sprague-Dawley	M	4 mon	Fe	1.5	Not given	1000	1 mon post IRR	MWM	Striatum
Interaction between age and exposure to 56Fe particles on behavior and neurochemistry	Shukitt-Hale	2006	Joseph	Rat: Fischer 344	M	7 mo and 16 mo	Fe	0,1,2	1-1.5	1000	6-7 weeks post-IRR	MWM	Hippocampus
Hippocampal neurogenesis and PSA-NCAM expression following exposure to 56Fe particles mimics that seen during aging in rats	Casadesus	2005	Joseph	Rat: Sprague-Dawley	M	2 mo	Fe	0, 2.5	1	1000	28 days post-IRR	no behavior examined, but see Casadesus 2004	Hippocampus
A Longitudinal Study of Operant Responding in Rats Irradiated when 2 Months Old	Rabin	2005	Shukitt-Hale	Rat: Sprague Dawley	M	2 mo 225-250g	Fe	1, 1.5, 2	1-1.5	1000	7, 11, and 15 mo	AFR	Striatum
High-LET Radiation Induces Inflammation and Persistent Changes in Markers of Hippocampal Neurogenesis	Rola	2005	Fike	Mice: C57BL/6J	M	2.5 mo	C and Fe	0, 1, 2, 3	0.87 Fe & 1.23 C	1000 Fe & 290 C	9 mo post-IRR	no behavior examined	Hippocampus
The effects of heavy particle irradiation on exploration and response to environmental change	Casadesus	2004	Joseph	Rat: Sprague-Dawley	M	3 mo (400-500 g)	Fe	0, 1.5	1	1000	3 mo post-IRR	Open field with NO and NL included in chamber	Hippocampus
The Effects of Low-Dose, High-LET Radiation Exposure on Three Models of Behavior in C57BL/6 Mice	Pecaut	2004	Nelson	Mouse: C57Bl/6	F	~2.25 mo	Fe	0, 0.1, 0.5, 2	0.1-1.3	1000	~2.75, 3.25, then 4.25 mo	OF, rotorod, acoustic startle	Amygdala
Indicators of Hippocampal Neurogenesis are Altered by 56Fe-Particle Irradiation in a Dose-Dependent Manner	Rola	2004	Fike	Mice: C57BL/6J	F	2.5 mo	Fe	0,1,2,3	0.16-0.44 & 0.67-0.87	1000	2 mo post-IRR	no behavior examined	Hippocampus
COGNITIVE DEFICITS INDUCED BY 56FeRADIATION EXPOSURE	Shukitt-Hale	2003	Joseph	Rat: Sprague-Dawley	M	3 mo	Fe	0, 1	1	1000	9 mo post-IRR	RAM	Hippocampus
Brain Signaling and Behavioral Responses Induced by Exposure to 56Fe-Particle Radiation	Denisova	2002	Joseph	Rat: Sprague-Dawley (Taconic)	M	2 mo	Fe	0, 1.5	1	1000	5-7 weeks post-IRR, testing took 2 weeks	Radial Arm Maze	Hippocampus
Effects of heavy particle irradiation and diet on amphetamine- and lithium chloride-induced taste avoidance learning in rats	Rabin	2002	Joseph	Rat: Sprague-Dawley	M	175-200g	Fe	1.5	1-1.5	1000	2-3 days post-IRR	CTA	Dopaminergic system
Effects of Exposure to 56Fe Particles or Protons on Fixed-ratio Operant Responding in Rats	Rabin	2002	Jenkins	Rat: Sprague Dawley	M	250-275 g	Fe, H	H: 4 Fe: 1, 2	Not Given	250 or 1000	Not Given	AFR	Striatum
Spatial Learning and Memory Deficits Induced by Exposure to Iron-56-Particle Radiation	Shukitt-Hale	2000	Joseph	Rat: Sprague-Dawley	M	3 mo	Fe	0, 1.5	1	1000	1 mo post-IRR	MWM	Hippocampus
Deficits in the Sensitivity of Striatal Muscarinic Receptors Induced by 56Fe Heavy-Particle Irradiation: Further "Age-Radiation" Parallels	Joseph	1993	Harris	Rat: Sprague-Dawley	M	200-300 g	Fe	0, 0.1, or 1	1	600	2-3 days after IRR	None	Striatial
Possible "Accelerated Striatal Aging" Induced by 56Fe Heavy-Particle Irradiation: Implications for Manned Space Flights	Joseph	1992	Dalton	Rat: Sprague-Dawley	M	200-300 g	Fe	0.1, 0.25, 0.5, 1	1	600	3-180 days post IRR	Wire Suspension test	Neostriatum
An Assessment of the Behavioral Toxicity of High-Energy Iron Particles Compared to Other Qualities of Radiation	Rabin	1989	Joseph	Rat: Crl:CD BR VAF/Plus	M	300-400 g	Fe	0, 0.05, 0.1, 0.2, 0.3, 0.4, 0.5, 1.5	0.1	600	Right before IRR	Taste Aversion	Area postrema

Table 1-1. Cited literature involving HZE radiation exposure in rodent CNS studies. This table was cumulatively compiled of all papers published from 1989-2018

over the length of this dissertation (2014-2018) using a variety of strategies with the last date being April,11th that this table was checked. Initially, standard literature searches through pubmed or google scholar were used for key phases such as: GCR, HZE, space radiation, CNS, and cognition to form a foundation. From here, the table was expanded by performing a reverse search on the citation list of the published literature. In addition, as the specific details of each study were added to the table, close attention would be given to the work each individual article would cite. Finally, the listserv for the SPACELINE Current Awareness Lists was closely monitored for any new publications that were posted on the NASA Task Book for work that was derived from NASA support (2014-present). The goal of this table was to compile literature that was strictly centered around two main characteristics relevant to this dissertation: *1) Does the study provide behavioral data from laboratory animals following HZE exposure? 2) Does the study provide neurogenesis data from laboratory animals following HZE exposure?* The resulting table was then color coordinated to visually highlight the studies targeting neurogenesis (orange), rodents at or above 6 months of age at IRR exposure (yellow), doses less than 0.3 Gy (blue), using both low dose and older mice (green), and those testing low doses on neurogenesis (alternating blue and orange cells in a single row). All ion types used were listed in purple and are given in order from smallest (H) to largest (^{56}Fe) ion. Within these subsets, each article is in descending order by year and then alphabetically by first author last name.

CHAPTER 2: WHOLE-BODY EXPOSURE TO ^{28}SI-RADIATION DOSE-DEPENDENTLY DISRUPTS DENTATE GYRUS NEUROGENESIS AND PROLIFERATION IN THE SHORT TERM AND NEW NEURON SURVIVAL AND CONTEXTUAL FEAR CONDITIONING IN THE LONG TERM

Published and reprinted with permission from: **Whoolery CW**, Walker AK, Richardson DR, Lucero MJ, Reynolds RP, Beddow DH, Clark KL, Shih H- Y, LeBlanc JA, Cole MG, Amaral WZ, Mukherjee S, Zhang S, Ahn F, Bulin SE, DeCarolis NA, Rivera PD, Chen BPC, Yun S, Eisch AJ. Whole-Body Exposure to ^{28}Si-Radiation Dose-Dependently Disrupts Dentate Gyrus Neurogenesis and Proliferation in the Short Term and New Neuron Survival and Contextual Fear Conditioning in the Long Term. Radiation Research. 2017. 188(5):532-551; PMID: 28945526, NIHMSID: 920999, DOI: 10.1667/RR14797.1

Abstract

Astronauts traveling to Mars will be exposed to chronic low doses of galactic cosmic space radiation, which contains highly charged, high-energy (HZE) particles. ^{56}Fe-HZE-particle exposure decreases hippocampal dentate gyrus (DG) neurogenesis and disrupts hippocampal function in young adult rodents, raising the possibility of impaired astronaut cognition and risk of mission failure. However, far less is known about how exposure to other HZE particles, such as ^{28}Si, influences hippocampal neurogenesis and function. To compare the influence of ^{28}Si exposure on indices of neurogenesis and hippocampal function with previous studies on ^{56}Fe exposure, 9-week-old C57BL/6J and Nestin-GFP mice (NGFP; made and maintained for 10 or more generations on a

C57BL/6J background) received whole-body ^{28}Si-particle-radiation exposure (0, 0.2 and 1 Gy, 300 MeV/n, LET 67 KeV/μ, dose rate 1 Gy/min). For neurogenesis assessment, the NGFP mice were injected with the mitotic marker BrdU at 22 h post-irradiation and brains were examined for indices of hippocampal proliferation and neurogenesis, including Ki67+, BrdU+, BrdU+NeuN+ and DCX+ cell numbers at short- and long-term time points (24 h and 3 months post-irradiation, respectively). In the short-term group, stereology revealed fewer Ki67+, BrdU+ and DCX+ cells in 1-Gy-irradiated group relative to nonirradiated control mice, fewer Ki67+ and DCX+ cells in 0.2 Gy group relative to control group and fewer BrdU+ and DCX+ cells in 1 Gy group relative to 0.2 Gy group. In contrast to the clearly observed radiation-induced, dose-dependent reductions in the short-term group across all markers, only a few neurogenesis indices were changed in the long-term irradiated groups. Notably, there were fewer surviving BrdU+ cells in the 1 Gy group relative to 0- and 0.2-Gy-irradiated mice in the long- term group. When the short- and long-term groups were analyzed by sex, exposure to radiation had a similar effect on neurogenesis indices in male and female mice, although only male mice showed fewer surviving BrdU+ cells in the long-term group. Fluorescent immunolabeling and confocal phenotypic analysis revealed that most surviving BrdU+ cells in the long-term group expressed the neuronal marker NeuN, definitively confirming that exposure to 1 Gy ^{28}Si radiation decreased the number of surviving adult-generated neurons in male mice relative to both 0- and 0.2-Gy-irradiated mice. For hippocampal function assessment, 9-week-old male C57BL/6J mice received whole-body ^{28}Si-particle exposure and were then assessed long-term for performance on contextual and cued fear conditioning. In the context test the animals that received

0.2 Gy froze less relative to control animals, suggesting decreased hippocampal-dependent function. However, in the cued fear conditioning test, animals that received 1 Gy froze more during the pretone portion of the test, relative to controls and 0.2- Gy-irradiated mice, suggesting enhanced anxiety. Compared to previously reported studies, these data suggest that ^{28}Si radiation exposure damages neurogenesis, but to a lesser extent than ^{56}Fe radiation and that low-dose ^{28}Si exposure induces abnormalities in hippocampal function, disrupting fear memory but also inducing anxiety-like behavior. Furthermore, exposure to ^{28}Si radiation decreased new neuron survival in long-term male groups but not females suggests that sex may be an important factor when performing brain health risk assessment for astronauts traveling in space.

Introduction

As the push for space exploration continues with plans by NASA to send humans to Mars by 2030 (United States. National Aeronautics and Space Administration 2015), understanding how high-linear energy transfer (LET) galactic cosmic radiation (GCR) effects the brain and behavior has become a top priority. Current shielding strategies are ineffective at blocking the high atomic number, high-energy (HZE) particles, including ^{56}Fe and ^{28}Si, which comprise space radiation (Nelson 2003a; Durante 2014; Vuolo et al. 2016; Gemignani et al. 2015; Hagen 1989; Bucker & Facius 1981). Thus, it is crucial to assess how exposure to HZE radiation influences the brain at both a cellular and behavioral level. Ground-based accelerators have been used for many years to mimic space radiation, and recent developments in technology have allowed NASA's Space Radiation Laboratory [NSRL, Brookhaven National Laboratory (BNL); Upton, NY] to provide mixed beam radiation to better simulate the GCR spectrum (Kim et al. 2015).

While these GCR simulation experiments are crucial to understanding the effects of HZE particles on brain and behavior, the effects of individual particles on the central nervous system (CNS) may vary depending on dose and energy (Rabin et al. 2011). In fact, understanding how individual particles alter both brain and behavior will enhance efforts to accurately model and predict how the GCR spectrum encountered during deep space missions alters brain and behavior (Rabin et al. 2007; Norbury et al. 2016), particularly in regards to experiments using mission-relevant doses of 0.25 Gy or less (Cucinotta et al. 2014).

The vast majority of studies that examine the influence of HZE particles on the central nervous system (CNS) involve exposure of laboratory animals to ^{56}Fe. In contrast, there have been few studies examining the influence of smaller charged particles, such as ^{28}Si (Cucinotta et al. 2014), on the CNS, particularly after low-dose exposure. As for CNS cellular analysis, ^{56}Fe exposure was shown to be detrimental to neurogenesis in the postnatal hippocampal dentate gyrus (DG) (Rola, Raber, et al. 2004; Sweet et al. 2016; Rivera et al. 2013; N. A. DeCarolis et al. 2014; Manda et al. 2008), a dynamic process closely linked to learning, memory and mood regulation. For example, 2-month-old mice exposed to 0.3 or 1 Gy ^{56}Fe radiation have fewer proliferating/differentiating DG cells shortly after irradiation (24–48 h). Also, using well-established indices of neurogenesis (Brown et al. 2003; Kee et al. 2002; Eisch et al. 2000; Lagace et al. 2010; Kuhn & Peterson 2008; Taupin 2007), published studies have shown that 2-month-old mice exposed to 1 Gy ^{56}Fe have fewer surviving bromodeoxyuridine-immunoreactive (BrdU+) cells and immature neurons, as labeled with doublecortin (DCX), at longer

times post-irradiation (1-3 months) (Sweet et al. 2016; Rivera et al. 2013). In contrast to work in ^{56}Fe, to our knowledge there have been no published studies examining DG neurogenesis after ^{28}Si irradiation. As for CNS function, there is an ion-specific effect on the hippocampal-based learning task, contextual fear conditioning (CFC), where mice learn that a context is associated with a foot shock (Phillips & LeDoux 1992). For example, it has been reported that 2-month-old C57BL/6J mice exposed to ^{56}Fe (0.1-0.5 Gy) freeze as much as nonirradiated mice in a shock- associated context (Haley et al. 2013; Raber et al. 2016). ^{56}Fe-exposed mice also freeze similarly to nonirradiated mice in a companion test to CFC, cued fear conditioning (FC), which is both hippocampal- and amygdalar-dependent and whose results can reflect anxiety-like behaviors (Haley et al. 2013). In contrast to the absence of ^{56}Fe-radiation effects on CFC and cued FC, ^{28}Si appears to have a dose-dependent effect on CFC. For example, 2- month-old C57BL/6J mice exposed to 1 Gy ^{28}Si learn CFC similar to nonirradiated mice, but mice exposed to 0.25 Gy ^{28}Si freeze more in a shock-associated context relative to control mice (Raber et al. 2014), suggesting improved hippocampal- dependent learning at this lower dose. It is unknown how ^{28}Si influences performance in the companion cued FC test. Thus, more information on how ^{28}Si-particle exposure influences these key indices of brain and behavior, DG neurogenesis, CFC and cued FC, is warranted to allow generalization across HZE particles, particularly in 2- month-old mice for which most data exist.

To fill these knowledge gaps, here we examined how ^{28}Si- particle exposure influences key measures of brain and behavior that have previously been evaluated after ^{56}Fe-

particle exposure in 2-month-old mice. Specifically, we examined DG neurogenesis, including measures of neural progenitors, immature neurons and surviving cells, in male and female mice at short- and long-term time points (24 h and 3 months) after 0, 0.2 and 1 Gy whole-body ^{28}Si- particle exposure. In addition, CFC and cued FC were examined at the long-term time point. We observed that whole-body ^{28}Si radiation dose-dependently disrupts DG neurogenesis and proliferation in the short term and new neuron survival in the long term. In addition, male mice exposed to ^{28}Si radiation performed abnormally in a dose- dependent manner in CFC and cued FC in the long term, suggesting abnormal hippocampal and amygdalar function. These findings expand what is known about the influence of HZE particles on the brain and behavior in young adult mice, particularly in regards to mission-relevant doses, thus enabling better predictions about how single- and multiple- particle events may influence the astronaut brain and behavior during deep space missions.

Methods

Animals

For the neurogenesis studies, Nestin-GFP (NGFP) male (n=39) and female (n=32) mice were used. NGFP mice were developed in C57BL/6 oocytes (Yamaguchi et al. 2000), and maintained on a C57BL/6J background for 10 or more generations at UT Southwestern Medical Center (UTSW) prior to their use in these studies (N. A. DeCarolis et al. 2014; Eisch et al. 2000; Petrik et al. 2012; Lagace et al. 2008). For the behavioral studies, C57BL/6J males (n = 21) were used (Jackson Laboratory, Bar Harbor, ME). All mice were housed 4/cage, kept on a 12:12 h light-dark schedule (lights on 06:00) and given ad libitum access to food and water. At 9 weeks of age, all mice

were shipped to BNL and were allowed to acclimate for five days prior to exposure **(Fig. 2-1A)**. At 22 h post-irradiation, all NGFP mice received a single intraperitoneal (i.p.) injection of the thymidine analog BrdU 150 mg/kg, 10 mg/ml in 0.9% saline and 0.001 M NaOH, consistent with our previously reported studies (N. A. DeCarolis et al. 2014; Rivera et al. 2013; DeCarolis et al. 2013). One-half of the NGFP mice (for neurogenesis studies), identified as the ‘‘short-term’’ group, were sacrificed 2 h after BrdU injection and 24 h post-irradiation **(Fig. 2-1A)** at BNL. The remaining half of the NGFP mice (for neurogenesis studies) and all of the C57BL/6J mice (for behavioral studies) were collectively identified as the ‘‘long-term’’ group, and were shipped back to UTSW for behavioral testing and sacrifice at a later time point (3 months after BrdU and irradiation; **Fig. 2-1A**). Short- and long-term animals were all weighed 24 h prior to exposure. Long-term mice were also weighed at 24 h and 3 months post-irradiation to verify similarity with preirradiation weights and the lack of a long-term effect on bodyweight, respectively (data not shown). Experimental protocols were approved by the Animal Care and Use Committees of UTSW and BNL, and mice were treated in accordance with National Institutes of Health (NIH) guidelines.

Irradiations

Irradiations were performed at BNL, similar to our previously reported work (N. A. DeCarolis et al. 2014; Rivera et al. 2013). ^{28}Si particles were produced at the Alternating Gradient Synchrotron Booster at BNL and transferred to the experimental beam line in the NSRL facility (BNL no date). The delivered beam was 20 x 20 cm with a uniformity of 5%. Mice were placed individually into clean, well-ventilated 50-ml conical tubes, and

tubes were placed perpendicular to the beam such that the beam was centered with the mouse heads. The mice were then whole-body irradiated with 1 Gy (n = 23) or 0.2 Gy (n = 25) ^{28}Si particles (300 MeV/n, LET 67 KeV/μ) at a dose rate of 1.0 Gy/min. Control animals were handled and placed in conical tubes for a similar amount of time as irradiated mice, but were not exposed to the beam. The NGFP mice (for neurogenesis data) were tested in the Fall 2011 NSRL campaign, while the C57B/6J mice (for behavior data) were tested in the Summer 2013 NSRL campaign.

Immunohistochemistry

To quantify cells in the many stages of neurogenesis in the DG granule cell layer (Kempermann et al. 2004), the entire DG (including sections anterior and posterior to the DG) was processed for immunohistochemistry for neurogenesis-relevant markers (**Fig. 2-1B**). We opted not to quantify neural stem cells since they are unchanged after ^{56}Fe exposure (DeCarolis et al. 2014; Rivera et al. 2013). Either 24 h or 3 months post-irradiation **(Fig. 2-1A**), NGFP mice were anesthetized with chloral hydrate (250 mg/kg, i.p.) and underwent intracardial perfusion with ice-cold 0.1 M phosphate- buffered saline (PBS) followed by 4% paraformaldehyde for fixation, as previously described elsewhere (DeCarolis et al. 2014; Rivera et al. 2013). Extracted brains were immersed for 24 h in 4% paraformaldehyde in 0.1 M PBS at 4°C for post-fixation, followed by at least 3 days of immersion in 30% sucrose in 0.1 M PBS with 0.01% sodium azide for cryoprotection. For each animal, the entire brain was sectioned at 30 μm in a 1:9 series (coronal plane) and stored in 1x PBS with 0.01% sodium azide at 4°C until processing for

immunohistochemistry.

Slide-mounted immunohistochemistry for BrdU+, Ki67+, DCX+ and NeuN+ cells in DG was performed as previously described elsewhere (DeCarolis et al. 2014; Rivera et al. 2013; Lagace, Whitman, Noonan, Ables, DeCarolis, Arguello, Donovan, Fischer, Farnbauch, Beech & Others 2007). Briefly, one entire series of the hippocampus (every ninth section) was slide-mounted onto charged slides. Antigen retrieval was performed using 0.01 M citric acid (pH 6.0) at 100°C for 15 min, followed by washing in PBS at room temperature. Next, endogenous peroxidase activity was inhibited by means of incubation with 0.3% hydrogen peroxide (H_2O_2) for 30 min. For BrdU immunohistochemistry, two additional steps were performed to allow the antibody access to DNA inside the cell nucleus: permeabilization and denaturation. Permeabilization was performed using 0.1% Trypsin in 0.1 M Tris and 0.1% CaCl2, and denaturation was performed using 2 N HCl in 1X PBS. Nonspecific binding was blocked with 3% serum (donkey) and 0.3% Triton X in PBS for 1 h.

After blocking and pretreatment steps, sections were incubated with rat-α-BrdU (1:400, Accurate Chemical & Scientific Corp., Westbury, NY), rabbit-α-Ki67 antibody (1:500, Fischer Scientific, Freemont, CA), goat-α-DCX (1:8,000, Santa Cruz Biotechnology, Dallas, TX), or mouse-α-NeuN (1:500, EMD Millipore, Billerica, MA) in 3% serum and 0.3% Tween 20 overnight. For single labeling immunohistochemistry, primary antibody incubation was followed by 1X PBS rinses, incubation with biotinylated secondary antibodies [biotin-donkey-α-rat-IgG, biotin-donkey-α-rabbit-IgG or biotin-don- key-α-

goat-IgG, all 1:200 (Jackson ImmunoResearch Laboratories Inc., West Grove, PA)] for 1 h, 1X PBS rinses, and incubation with an avidin-biotin complex for 90 min (ABC Elite, Vector Laboratories, Burlingame, CA). After another set of rinses in 1X PBS, immunoreactive cells were visualized with incubation with metal-enhanced diaminobenzidine (Fisher Scientific, Pittsburgh, PA) for 5-10 min. Lastly, slides were incubated for ~2 min in the nuclear counterstain, Fast Red (Vector Laboratories), dehydrated through a series of increasing ethanol concentrations and coverslipped using DPX. For NeuN+BrdU+ fluorescent double labeling, after BrdU pretreatment (above), slide-mounted tissue was incubated in BrdU and NeuN antibodies simultaneously overnight at room temperature, and in secondary antibodies [for BrdU, biotinylated donkey-α-rat; for NeuN, DyLight 649 donkey-α-mouse; all 1:200 (Jackson ImmunoResearch)] simultaneously for 1 h. Tissue was then incubated in ABC, and the BrdU signal was amplified with Tyramide-Cy2 (PerkinElmer Inc., Waltham, MA).

Stereological Cell Counts

BrdU+, Ki67+ and DCX+ DAB cells were quantified in line with stereology principles using an Olympus BX-51 microscope at 400X by an observer blind to experimental groups as described previously (Lagace et al. 2010; Walker et al. 2015; S. Yun et al. 2016). Immunopositive cells were quantified in every ninth coronal section in the granule cell layer (GCL) in the DG, spanning the entire anterior-posterior axis of the hippocampus (-0.82 mm to -4.33 mm from bregma). As the entire DG was examined using stereology, the number of sections per animals varied per stereology principles (Mouton 2009; West 2012; Howard & Reed 2004). However, the number of DG

sections/mouse (mean ± SEM) for each group was as follows: for short-term, 11.03 ± 0.18 (0 Gy control: 11.55 ± 0.34; 0.2 Gy: 10.55 ± 0.27; 1 Gy: 11 ± 0.30); for long-term, 11.37 ± 0.13 (0 Gy control: 11.2 ± 0.20; 0.2 Gy: 11.23 ± 0.26; 1 Gy: 11.5 ± 0.19). Stereology was performed under brightfield microscopy, and total cell counts were multiplied by 9 to account for the whole DG. Data are presented as total GCL cell counts in all mice (**Figs. 2-7A**) and broken into group by sex (**Figs. 2-7B**). Data are also presented by sex along the longitudinal axis of the DG (distance from bregma, **Figs. 2-7C, 2-7D**). Photomicrograph images were captured using the Olympus DP Manager Program and were imported into software program Adobe Illustrator for design of manuscript figures.

Confocal Phenotyping

NeuN+BrdU+ co-localization analysis of tissue from mice 3 months post-irradiation (long-term cohort) was performed as previously described elsewhere (Lagace et al. 2010; van Praag et al. 1999). Briefly, tissue was selected from mice whose BrdU+ DAB cell counts were representative of the mean [n = 8 (4 male, 4 female) per controls, 0.2 Gy and 1 Gy groups]. BrdU+ cells in the GCL were first identified under an epifluorescent microscope (Olympus BX51) with 10x and 40x objectives by an observer blind to treatment group. Using a Leica pinhole confocal microscope (TCS SP8, 40x oil objective; Buffalo Grove, IL), previously identified BrdU+ cells spanning the anterior-posterior axis of the DG (distance from bregma range: -1.63 to -3.79 mm) were examined via z-stacks through full-section thickness (20 μm) by an additional observer blind to treatment. Step sizes of 0.5 μm were used, as were wavelengths of 489 and

654 nm laser lines to excite BrdU and NeuN signals with emission wavelengths of 506 and 673 nm, respectively. Scans were analyzed using Leica LAS X software, and BrdU+ cells were determined to be NeuN+ or NeuN- based on fluorescence intensity profiling (and histograph analysis) as well as orthogonal sectioning. Either 50 cells/group were examined, or in the case of 1 Gy dose, all BrdU+ cells were examined. Confocal phenotyping data are presented as percentage of BrdU+ cells that were also NeuN+ [calculated as (BrdU+NeuN+)/(BrdU+) * 100] (**Fig. 2-6F**). To calculate the number of BrdU+ neurons 3 months post-irradiation (one way of assessing ‘‘new neurons’’ or ‘‘surviving neurons’’; **Table 2-2**), the percentage of BrdU+ cells that were also NeuN+ was multiplied by the BrdU+ cell counts collected via stereology. For images, raw confocal scans were exported to Adobe Photoshop, and RGB channel adjustments were made by bringing white marker to the edge of the histogram. Images were then imported into Adobe Illustrator for cropping and placed into the figure. For clarity and presentation purposes, the pseudocolored NeuN channel (Cy5) was shifted to magenta (**Fig. 2-6E**).

Contextual Fear Conditioning and Cued Fear Conditioning

CFC and cued FC were performed as previously described elsewhere (Raber et al. 2015; Drew et al. 2010) with the following modifications, male mice went through three phases of the test: training (day 1), CFC (day 2) and FC (day 2) (**Fig. 2-8A**). Mice were habituated to the behavior room for 1 h each day prior to training and testing. On day 1, mice were trained to associate a novel context (standard FC chamber, grid flooring, no odor, house lights on; Med Associates Inc., St. Albans, VT) with a shock. Specifically, 2

min after placement in the chamber, an auditory cue (80 db white noise, 30 s duration) was played (Med Associates Inc.), which co-terminated with a 0.5 mA shock (2 s duration). This cued-shock pairing was repeated two more times during the 6-min training session on day 1, with 1 min between cued-shock presentations. On day 2, mice were tested for CFC by being placed for 5 min in the same context as used for day 1 training, but no auditory cue or foot shock was presented. Also on day 2, but 2 h after CFC, mice underwent auditory cued FC testing where they were placed for 6 min in a novel context (plastic flooring, triangular roof, vanilla odor, house lights on). After 3 min, the tone from day 1 was presented for 3 min. For training and testing sessions, freezing behavior was assessed using Video Freezet software (Med Associates Inc.), compiled for each phase of each session (e.g., pretone, during tone), and presented as percentage time freezing for each phase.

Statistical Analyses

Data are reported as mean ± SEM. Statistical analyses were performed using Prism software version 7 (GraphPad Software Inc., LaJolla, CA). Statistical significance was defined as $P \leq 0.05$. Statistical outcomes are reported in the Results section, as well as in **Figs. 2-8**, with details of statistical analyses provided in **Table 2-1**: short-term cohort (24 h post-irradiation, **Figs. 2-4**); **Table 2-2:** long- term cohort and cellular phenotyping (3 months post-irradiation, **Figs. 5-7**) and **Table 2-3**: CFC and cued FC data irrespective of gender (males and females combined) and behavioral data, statistical analyses were performed using one-way analysis of variance (ANOVA; variable of treatment: 0, 0.2 and 1 Gy), and Bonferroni multiple comparison post hoc tests were

used (**Figs. 2-7A** and **8B-D**). For total cell counts or phenotypic analysis considering treatment and sex, statistical analyses were performed using two-way ANOVA, and Bonferroni multiple comparison post hoc tests were used on male or female data, per our planned comparisons **(Figs. 2-7B-D)**. BrdU+ cell survival rate was calculated as (1-death%) * 100, where death percentage = [(24 h BrdU+ group cell counts) - (3 month BrdU+ group cell counts)/(24 h BrdU+ cell counts)], similar to prior work (Eisch et al. 2000). For cellular analysis, only animals with a full representative set of hippocampal sections were analyzed, per stereological principles. For the assessment of outliers, the ROUT test was performed with Q = 1%. Three outliers were discovered and removed prior to subsequent analysis (2 animals from Ki67+ and 1 animal from DCX+ stains in the long-term group).

Results

Proliferation and Neurogenesis are Dose-Dependently Reduced at 24 h post-irradiation in ^{28}Si-Irradiated vs. Control Animals

At 24 h post-irradiation the effects of whole-body ^{28}Si exposure **(Figs. 2-4)** on DG proliferation and neurogenesis (**Fig. 2-1B**) were evaluated using stereological assessment of immunoreactive cells. As cells in distinct phases of the cell cycle can be differentially affected in regards to physiological manipulations, two markers were used to measure proliferation: the endogenous cell cycle marker Ki67, which labels the nucleus of cells in all phases of the cell cycle (**Fig. 2-2**) (Mandyam et al. 2007), and the exogenously-administered thymidine analog BrdU, which labels the nucleus of cells in S phase at the time of BrdU injection (**Fig. 2-3**) (Eisch et al. 2000; Eisch 2002). Ki67+ and BrdU+ cell counts in the short-term group reveal levels of DG proliferation at 24 h post-

irradiation. However, we also used a widely-accepted measure of neurogenesis for the 24 h post-irradiation group (Francis et al. 1999; Rao & Shetty 2004; Couillard-Despres & Winner 2005; Brown et al. 2003; Kempermann et al. 2003; Knoth et al. 2010). The number of cells immunoreactive for the neuronal fate commitment marker DCX (**Fig. 2-4**).

As previously shown elsewhere (Mandyam et al. 2007; Lagace et al. 2010), Ki67+ cells in the DG had intensely-stained, irregularly-shaped nuclei (**Fig. 2-2A**). In regards to Ki67+ cell numbers, ^{28}Si radiation had a dose-dependent effect on total Ki67+ cell numbers (**Fig. 2-2A and Table 2-1**). Post hoc analyses revealed that 0.2 and 1 Gy ^{28}Si exposure resulted in fewer Ki67+ cells relative to controls (20 and 61% reduction, respectively) (**Fig. 2-2A and Table 2-1**). Also, there were fewer Ki67+ cells after 1 Gy relative to 0.2 Gy ^{28}Si exposures (51% reduction; **Fig. 2-2A**). Subsequent analyses performed to assess possible differences between male and female mice revealed main effects of both sex and treatment and an interaction of sex and treatment (**Table 2-1**). Specifically, in males there were fewer Ki67+ cells after 0.2 and 1 Gy exposures relative to controls (22 and 64% reduction, respectively) (**Fig. 2-2B and Table 2-1**) and fewer Ki67+ cells after 1 Gy relative to 0.2 Gy exposures (54% reduction) (**Fig. 2-2B and Table 2-1**). In females, there were fewer Ki67+ cells after 1 Gy irradiation relative to controls (49% reduction) (**Fig. 2-2B and Table 2-1**). However, the lack of additional radiation effects on Ki67+ cells in female mice may be influenced by the lower control levels in female vs. male mice (**Fig. 2-2B**), as suggested by the interaction of sex and treatment (**Table 2-1**).

DG function varies with distance from bregma and indices of DG neurogenesis are often correlated with DG function (Scharfman 2011; Jonas & Lisman 2014; Kesner 2007; Amaral et al. 2007; Snyder et al. 2012; Sahay et al. 2007; Jinno 2011). Therefore, in addition to total cell Ki67+ numbers (condensed from quantification throughout the longitudinal axis of the DG), we also analyzed cell counts for male and female mice across their respective distance from bregma to evaluate the sensitivity of proliferation throughout the coronal axis. For males and females, analyses of these data (by two-way ANOVA) revealed main effects of both bregma and radiation as well as an interaction (**Table 2-1**). Specifically, male mice that were exposed to 1 Gy had fewer Ki67+ cells at almost every bregma position relative to controls and animals that were exposed to 0.2 Gy (**Fig. 2-2C**). Male mice that received a 0.2 Gy dose had fewer Ki67+ cells at discrete bregma positions in the middle and posterior DG relative to controls (**Fig. 2-2C**). However, female mice that received a 1 Gy dose had fewer Ki67+ cells at only three bregma positions relative to controls and 0.2 Gy (**Fig. 2-2D**).

As with Ki67+ cells, DG BrdU+ cells examined at 24 h post-irradiation (2 h after BrdU injection) presented intensely stained nuclei (**Fig. 2-3A**) clustered along the subgranular zone (SGZ) (Mandyam et al. 2007). As for BrdU+ cell counts, ^{28}Si exposure had an effect on total BrdU+ cell numbers (**Fig. 2-3A and Table 2-1**). Specifically, post hoc analyses revealed there were fewer BrdU+ cells after 1 Gy ^{28}Si irradiation relative controls (71% reduction) (**Fig. 2-3A and Table 2-1**). Also, there were fewer BrdU+ cells after 1 Gy relative to 0.2 Gy ^{28}Si irradiation (67%) (**Fig. 2-3A**). Subsequent

consideration of treatment and sex (two-way ANOVA) revealed a main effect of treatment only, and not of sex (**Table 2-1**). This was somewhat surprising, as a main effect of sex was observed with the proliferation marker, Ki67 (**Fig. 2-2B and Table 2-1**) but not with this S-phase marker, BrdU (**Fig. 2-3B and Table 2-1**) (Eisch & Mandyam 2007), suggesting cell cycle stage-dependent susceptibility to HZE radiation. For BrdU+ cell numbers in males, there were fewer BrdU+ cells after 1 Gy irradiation relative to controls (74%; **Fig. 2-3B, Table 2-1**) and fewer BrdU+ cells after receiving 1 Gy relative to a 0.2 Gy dose (69%; **Fig. 2-3B and Table 2-1**). In females, there were fewer BrdU+ cells after receiving 1 Gy relative to controls (64%; **Fig. 2-3B and Table 2-1**), and fewer BrdU+ cells after receiving 1 Gy relative to a 0.2 Gy dose (63%; **Fig. 2-3B and Table 2-1)**.

For males, consideration of treatment and bregma (two- way ANOVA) revealed main effects of both variables as well as an interaction effect (**Table 2-1**). Specifically, male mice that were exposed to 1 Gy had fewer BrdU+ cells at many bregma positions relative to 0.2-Gy-exposed animals and controls (**Fig. 2-3C**). Male mice that were exposed to 0.2 Gy had fewer BrdU+ cells at discrete posterior DG bregma positions relative to controls (**Fig. 2-3C**). For females, consideration of treatment and bregma (two-way ANOVA) also revealed main effects of both variables as well as an interaction (**Table 2-1)**. However, female mice that were exposed to 1 Gy had fewer BrdU+ cells at only three bregma positions relative to controls and only five bregma positions relative to 0.2 Gy animals (**Fig. 2-3D**).

We next assessed neurogenesis in the 24 h post-irradiation group using DCX cell counts, a widely-accepted measure of neurogenesis (Francis et al. 1999; Rao & Shetty 2004; Couillard-Despres & Winner 2005; Brown et al. 2003; Kempermann et al. 2003; Knoth et al. 2010). As shown elsewhere (Noonan et al. 2010; Lagace, Whitman, Noonan, Ables, DeCarolis, Arguello, Donovan, Fischer, Farnbauch, Beech & Others 2007), DCX+ cells in the SGZ and granule cell layer (GCL) present a range of cellular morphologies, with approximately one-half presenting the morphology of an immature GCL neuron: an oval- or tear-drop-shaped soma (**Fig. 2-4A**) with a thin apical process, which branches after exiting the GCL and entering the DG molecular layer. As for DCX+ cell counts, ^{28}Si radiation had an effect on total DCX+ cell numbers (**Fig. 2-4A and Table 2-1**). Specifically, post hoc analyses revealed fewer DCX+ cells after 0.2 and 1 Gy ^{28}Si irradiation relative to controls (18% and 50% reduction, respectively; **Fig. 2-4A and Table 2-1**). Also, there were fewer DCX+ cells after 1 Gy ^{28}Si irradiation relative to 0.2 Gy ^{28}Si irradiation (39%; **Fig. 2-4A**). Subsequent consideration of treatment and sex (two- way ANOVA) revealed main effect of treatment only, with no effect of sex (**Table 2- 1**). Specifically, in males there were fewer DCX+ cells after 1 Gy irradiation relative to controls (50%; **Fig. 2-4B and Table 2-1**), and fewer DCX+ cells after 1 Gy irradiation relative to 0.2 Gy irradiation (41%; **Fig. 2-4B and Table 2-1**). In females, there were fewer DCX+ cells after 1 Gy irradiation relative to controls (50%; **Fig. 2-4B and Table 2-1**).

For males, consideration of treatment and bregma (two-way ANOVA) revealed main effects of both variables as well as an interaction effect (**Table 2-1**). Specifically, male

mice exposed to 1 Gy had fewer DCX+ cells at many bregma positions relative to 0.2-Gy-exposed and control groups (**Fig. 2-4C**). Male mice exposed to 0.2 Gy had fewer DCX+ cells at discrete anterior and posterior DG bregma positions relative to controls (**Fig. 2-4C**). For females, consideration of treatment and bregma (two-way ANOVA) also revealed main effects of both variables, as well as an interaction effect (**Table 2-1**). However, female mice exposed to 1 Gy had fewer DCX+ cells at many bregma positions relative to nonirradiated controls, and only two bregma positions relative to 0.2-Gy-irradiated mice (**Fig. 2-4D**). Female mice exposed to 0.2 Gy had fewer DCX+ cells at discrete posterior DG bregma positions relative to controls (**Fig. 2-4D**).

Three Months after ^{28}Si Irradiation, Proliferation and Neurogenesis are Similar among Irradiated and Control Groups, whereas New Neuron Survival is Reduced, Particularly in Irradiated Male Mice

Three months after whole-body ^{28}Si exposure (**Figs. 5–7**), the effects on DG proliferation (Ki67+ cells), neurogenesis (DCX+ cells), surviving neurons (BrdU+, BrdU+NeuN+ cells) and cell survival rate (BrdU+ cells 3 months vs. 24 h) were evaluated in the long-term group using stereological assessment of immunoreactive cells. As for Ki67+ cell numbers between short- and long-term groups in control mice, those at 3 months post-irradiation had approximately one-third of the Ki67+ cell numbers compared to control animals at 24 h post-irradiation, as expected, based on the age-induced decrease in proliferation (Rao et al. 2006; Ben Abdallah et al. 2010). However, in regards to the effect of radiation on Ki67+ cell numbers, at 3 months after ^{28}Si irradiation, a similar total Ki67+ cell numbers was observed in irradiated and control

animals (**Fig. 2-5A and Table 2-2**). Subsequent consideration of treatment and sex (two-way ANOVA) revealed main effects of both variables as well as an interaction of sex and treatment (**Table 2-2**). Specifically, in male mice there were fewer Ki67+ cells at 3 months after 1 Gy relative to 0.2 Gy irradiation (34% reduction; **Fig. 2-5B and Table 2-2**), with no post hoc changes seen in female mice. However, the lack of radiation effects on Ki67+ cells in female mice may be influenced by the lower control levels in female vs. male mice (**Fig. 2-5B**), as suggested by the interaction of sex and treatment (**Table 2-2**). In both males and females, two-way ANOVA revealed main effects of treatment and bregma on Ki67+ cell numbers (**Table 2-2**). Specifically, at 3 months post-irradiation, male mice that received 1 Gy irradiation had fewer Ki67+ cells at three anterior bregma positions relative to controls and 0.2-Gy-irradiated mice (**Fig. 2-5C**). Female mice that were exposed to 1 Gy had fewer Ki67+ cells at only one bregma position relative to controls (**Fig. 2-5D**), and female mice that were exposed to 0.2 Gy had fewer Ki67+ cells at three bregma positions relative to controls, with two of them being posterior (**Fig. 2-5D**).

BrdU is bioavailable in the adult mouse for ~15 min (Mandyam et al. 2007). Thus, a BrdU injection, followed by a period of weeks, can be used to ‘‘birth date’’ cells and follow them into maturity. Therefore, unlike the BrdU+ cells in the short-term group, which represent proliferating cells, BrdU+ cells in the long- term group represent ‘‘surviving’’ cells. Qualitatively, DG BrdU+ cells in the long-term group looked like neurons: solitary, round, intensely stained nuclei, many with a punctate staining pattern, in the SGZ and GCL (**Fig. 2-6A**). In regards to BrdU+ cell counts in the long-term group,

^{28}Si radiation had a dose-dependent effect on total BrdU+ cell numbers at 3 months post-irradiation (**Fig. 2-6A and Table 2-2**). Specifically, post hoc analyses revealed fewer BrdU+ cells at 3 months after exposure to 1 Gy ^{28}Si radiation relative to 0.2 Gy and control groups (57 and 71% reduction, respectively; **Fig. 2-6A and Table 2-2**). Subsequent consideration of treatment and sex (two-way ANOVA) revealed main effects of both variables (**Table 2-2**). In males, post hoc analyses revealed fewer BrdU+ cells at 3 months after exposure to 1 Gy relative to 0.2 Gy and control animals (71% and 64%, respectively; **Fig. 2-6B and Table 2-2**). In contrast, exposure to radiation did not affect BrdU+ cell numbers in this female long-term group. The lack of radiation effects on BrdU+ cell numbers in female mice at 3 months post-irradiation may be due to the low number of BrdU+ cells in control female relative to control male groups (**Fig. 2-6B)**, a difference that was not evident in the short-term control female vs. male groups (**Fig. 2-3B**).

In both males and females, a two-way ANOVA revealed main effects of both radiation and bregma position, with the males also having an interaction (**Table 2-2**). Specifically, male mice exposed to 1 Gy had fewer BrdU+ cells at numerous bregma positions relative to 0.2 Gy and control groups (**Fig. 2-6C**), while male mice exposed to 0.2 Gy had fewer BrdU+ cells at a single anterior bregma location relative to controls at 3 months post-irradiation (**Fig. 2-6C**). Female mice exposed to 1 Gy had fewer BrdU+ cells at only one bregma location relative to 0.2 Gy and control groups (**Fig. 2-6D**).

While most surviving BrdU+ DG cells become neurons (Cameron et al. 1993; Canales 2016; Kempermann et al. 2015; Zhao et al. 2008), manipulations can sometimes change the fate of the cells, for example, driving astrogenesis instead of neurogenesis (Dranovsky et al. 2011). We tested the effect of ^{28}Si radiation on the fate of BrdU+ cells at 3 months post-irradiation (and at 3 months after BrdU administration) by co-labeling with antibodies against BrdU and the neuronal nuclear protein NeuN and performing phenotypic analysis using confocal microscopy (**Fig. 2-6E and F**). As expected, the nuclei of BrdU+ cells in the long-term (3 months) post-irradiation group co-labeled with NeuN (**Fig. 2-6Ei and Eiii**), even throughout the z plane of optical sectioning (**Fig. 2-6Eiv**). The percentage of BrdU+ cells that were also NeuN+ was collected to reflect the proportion of adult-generated cells that were neurons. A two-way ANOVA revealed no main effect of sex or treatment, and no interaction (**Table 2-2**), and the percentage of BrdU+ and NeuN+ co-labeled cells was approximately 100% for all treatment groups (**Fig. 2-6F**). Multiplication of the number of BrdU+ cells (**Fig. 2-6B**) by these percentages (**Fig. 2-6F**; see Methods) resulted in a dose-dependent decrease of surviving adult-generated neurons in exposed animals relative to controls in males but not in females, strikingly similar to the BrdU+ cell numbers (**Fig. 2-6B**).

While these data show that the number of surviving, new neurons is decreased in male mice that were irradiated relative to control male mice, there is an additional consideration: perhaps this decrease is already evident in the ‘‘starting’’ value of BrdU cells in the 24 h group. Therefore, in addition to quantifying BrdU+ cells and neuron numbers at 3 months post-irradiation in exposed vs. control animals, we also calculated

the BrdU+ cell survival rate. The proportion of BrdU+ cells at 3 months post-irradiation was represented as a fraction of the ‘‘starting’’ value of BrdU+ cells at 24 h post-irradiation (see Methods). With this approach, BrdU+ cell survival rate was similar across groups (percentage surviving: controls, 18%; 0.2 Gy, 18%; 1 Gy, 23%). When sex was considered, exposed groups again had similar survival rates compared to their respective control groups (data not shown). Therefore, although the number of surviving BrdU+ cells and neurons is decreased in exposed vs. controls at 3 months post-irradiation (**Fig. 2-6A** and **Table 2-2**, see Results), the survival rate of BrdU+ cells (change in BrdU+ cell numbers in exposed and control groups between the 24 h and 3 month time points) was similar in exposed and control mice.

As for DCX+ cell count between short- and long-term control groups, at 3 months post-irradiation controls, had approximately a quarter of DCX+ cells compared to controls at 24 h post-irradiation, as expected, based on the age- induced decrease in neurogenesis (Rao et al. 2006; Ben Abdallah et al. 2010). For the long- term group, ^{28}Si radiation had an effect on total number of DCX+ cells (**Fig. 2-7A and Table 2-2**). Specifically, post hoc analyses revealed there were fewer DCX+ cells after ^{28}Si exposure to 1 Gy relative to 0.2 Gy (23% reduction; **Fig. 2-7A and Table 2-2**). Neither 0.2 Gy nor 1 Gy exposure was significantly different from controls. Subsequent consideration of treatment and sex (two-way ANOVA) revealed main effects of treatment only (**Table 2-2)**, with post hoc analyses revealing no major changes within each sex (**Fig. 2-7B**).

For males, consideration of treatment and bregma (two- way ANOVA) revealed main effects of both variables (**Table 2-2**). Specifically, male mice exposed to 1 Gy had fewer DCX+ cells at one bregma position relative to controls, and a few bregma positions relative to 0.2 Gy exposure (**Fig. 2-7C**). For females, consideration of treatment and bregma (two-way ANOVA) only revealed main effects across bregma but not treatment (**Table 2-2**).

Three Months after ^{28}Si Irradiation, Male Mice Show a Dose-Dependent Disruption of Contextual Fear Memory and Increased Freezing in a Novel Environment

Since neurogenesis has been linked to disrupted performance on CFC, and since ^{28}Si exposure caused a long-term decrease in surviving BrdU cells and new neurons, we next examined whether ^{28}Si exposure caused a behavioral change. We focused on male mice, because they showed the greatest influence of ^{28}Si radiation on surviving new neurons in the long term. Specifically, 3 months after whole-body ^{28}Si irradiation, the radiation effects on hippocampal- and amygdala-dependent learning were evaluated in long-term mice using CFC and cued FC (**Fig. 2-8A**). While the C57BL/6J mice used for CFC and cued FC were treated the same as the NGFP mice used for the neurogenesis studies, the animals used for behavioral testing were irradiated two years after the NGFP mice and were not given BrdU injection after irradiation. Similar to our previously reported work (DeCarolis et al. 2014), NGFP and C57BL/6J mice had body mass and weight gain throughout the experiment, and radiation exposure had no effect on weight gain in either mouse strain (data not shown).

Regarding CFC, ^{28}Si exposure had an effect on percentage freezing time in the context test (**Fig. 2-8B and Table 2-3**), with post hoc analyses revealing that mice exposed to 0.2 Gy froze less relative to controls (nearly relative to 1 Gy exposure; P = 0.053). Regarding the cued FC, ^{28}Si exposure had an effect on percentage freezing time in the pretone phase of the test (**Fig. 2-8C and Table 2-3**). Specifically, post hoc analyses revealed that mice exposed to 1 Gy spent more time freezing relative to 0.2 Gy and control animals when placed in a novel environment prior to hearing the tone (**Fig. 2-8C and Table 2-3**). In contrast, there was no radiation effect on percentage freezing time during tone (**Fig. 2-8D and Table 2-3**). Taken together, these data suggest a dose-dependent effect of ^{28}Si radiation on CFC and cued FC, where mice exposed to 0.2 Gy had worse hippocampal-dependent memory, but mice exposed to 1 Gy had increased freezing in general, indicating anxiety.

Discussion

An important consideration for future travel into deep space is the potentially damaging effects of heavy particle space radiation to the CNS (Cucinotta et al. 2014). A unique aspect of the current study is the focus on ^{28}Si effects on adult hippocampal DG neurogenesis and hippocampal-dependent behavior. Prior to this work, to our knowledge, nothing was known about how ^{28}Si exposure influenced neurogenesis, and little was known about how ^{28}Si exposure influenced behavior. Here we show that whole-body exposure to ^{28}Si radiation reduces mouse hippocampal DG proliferation and neurogenesis in the short term, and decreases new neuron survival in the long term. We also show that ^{28}Si radiation interferes with performance on the hippocampal-dependent

CFC task and a 1 Gy dose induces anxiety-like behavior. As discussed below, these findings are important additions to the growing body of knowledge on how HZE particles influence the brain and behavior.

While it is important to perform studies in fully mature, astronaut age-equivalent animals (Rabin et al. 2012), we performed the current studies in young adult mice to enable a better comparison with the vast majority of published neurogenesis work, which focused on approximately 2-month-old rodents that are exposed to space radiation (Sweet et al. 2016; DeCarolis et al. 2014; Rivera et al. 2013; Manda et al. 2008; Raber et al. 2004). In our work presented here, ^{28}Si radiation was shown to dose- dependently decrease DG proliferation (Ki67+ cell numbers) and neurogenesis (DCX+ cell numbers) in the short term. Additionally, ^{28}Si radiation decreased the number of surviving new DG neurons in the long term. Specifically, we observed this decrease in surviving new DG neurons only in males, although the lack of decrease in females may be a consequence of a floor effect. These ^{28}Si radiation- induced decreases in DG neurogenesis are similar to, but less robust than, previously reported ^{56}Fe radiation-induced changes in neurogenesis (Sweet et al. 2016; DeCarolis et al. 2014; Rivera et al. 2013; Rola, Otsuka, et al. 2004). For example, for DCX, which is a well-accepted marker of immature neurons and neurogenesis (Couillard-Despres & Winner 2005; Brown et al. 2003), whole-body 1 Gy ^{28}Si exposure (current results) and 1 Gy ^{56}Fe (DeCarolis et al. 2014; Rivera et al. 2013; Rola, Otsuka, et al. 2004) exposure were shown to decrease DCX+ DG cell numbers in the short term. However, our current data show that ^{28}Si-irradiated and control mice have similar DCX+ cell numbers in the long term, with just a

decrease in DCX+ cells in mice exposed to 1 Gy relative to 0.2 Gy. In contrast, it was previously shown that ^{56}Fe-exposed mice still have decreased DCX+ cell numbers, compared to control mice, in the long term (Rivera et al. 2013). Other published data, on 1 Gy ^{56}Fe- radiation exposure, shows a robust decrease in DCX+ cells in the anterior DG at 1 month post-irradiation (Sweet et al. 2016), while our 1 Gy ^{28}Si-radiation exposure data presented in this work shows a modest decrease in DCX+ cells in the anterior DG (bregma, –1.63) at 3 months post-irradiation. In regards to proliferation, ^{28}Si-irradiated and control mice have similar Ki67+ cell numbers in the long term. Thus, our data suggest ^{28}Si radiation has a more transient and less potent long-term influence on the process of DG neurogenesis than ^{56}Fe. The mechanism underlying the differential influence of ^{28}Si compared to ^{56}Fe on DCX+ cell numbers is unknown. However, the larger initial track size and delta-ray damage produced by ^{56}Fe vs. ^{28}Si (Rabin et al. 2011) may explain the greater long- term negative effect of ^{56}Fe on proliferation and this measure of neurogenesis.

In addition to looking at indices of neurogenesis in the overall DG, we also examined it in regards to distance from bregma. This is useful, since the hippocampus varies in function along its longitudinal axis, as in the rodent: the more anterior/dorsal/septal hippocampus is linked to spatial learning and memory, and the more posterior/ventral/ temporal hippocampus is linked to emotion and mood regulation (O'Leary & Cryan 2014; Moser & Moser 1998; Tanti & Belzung 2013; Jarrard et al. 2012; Grivas et al. 2003; Abchiche & Others 2016; Kheirbek & Hen 2011). Because neurogenesis is linked to both spatial memory and mood (Canales 2016; Kheirbek & Hen 2011; Sanghee Yun

et al. 2016), examination along the septotemporal axis allows insight into DG neurogenesis that may be associated with specific changes in function (Lagace et al. 2006; Latchney et al. 2014; Mahar et al. 2016; Wu & Hen 2014). In fact, inducible manipulation of neurogenesis in the anterior compared to posterior DG disrupts spatial versus emotionally-linked hippocampal function, respectively (Wu & Hen 2014). In the current work, surviving BrdU+ cells at 3 months after ^{28}Si irradiation in male mice are dose-dependently decreased in the anterior DG, but decreased irrespective of dose in the posterior DG. This suggests that ^{28}Si radiation may dose-dependently impair spatial learning and memory, but also interfere with mood regulation irrespective of dose. While other work has examined the influence of ^{56}Fe radiation on neurogenesis via stereology of the entire DG (DeCarolis et al. 2014; Rivera et al. 2013), those data have been published as total immunoreactive DG cell numbers and not according to bregma. Consideration of this functional gradient of the hippocampus, and the biochemical, cellular and neuroanatomical gradients that accompany it, may enable more hypothesis-driven experiments for future work into the functional effect of space radiation on hippocampal function.

Indeed, our bregma analysis revealing fewer BrdU+ surviving cells in the anterior DG at 3 months after ^{28}Si irradiation (**Fig. 2-6**) fits with our reported ^{28}Si radiation- induced disruption of spatial learning and memory (CFC) and emotionally-linked memory (cued FC; **Fig. 2-8**). Specifically, in the context test, 0.2-Gy-irradiated mice froze less relative to controls, suggesting decreased hippocampal-dependent function. However, in cued FC, 1-Gy-irradiated mice froze more during the pretone portion of the test relative to 0.2

Gy and controls, suggesting enhanced anxiety (Gresack et al. 2010; Maren et al. 2013; Izquierdo et al. 2016). These data raise several discussion points. First, while these data suggest a ^{28}Si radiation dose-dependent effect on memory and/or anxiety, a HZE-induced effect has also been observed at low doses with titanium-48 [^{48}Ti (0.3 Gy)] but not ^{56}Fe (0.1, 0.5 and 2 Gy) (Parihar et al. 2016; Pecaut et al. 2004). Importantly, these data indicate the utility of employing the cued FC as well as CFC testing, because without the cued FC we might have concluded that 1 Gy irradiated mice had ‘‘normal’’ hippocampal-dependent function, while only the 0.2 Gy irradiated mice had worse hippocampal function. A second point of discussion is that these data are notable in their contrast with prior behavioral testing with ^{28}Si radiation in young adult mice. For example, young adult mice exposed to a similar dose (0.25 Gy) of whole-body ^{28}Si radiation, also tested at 3 months post-irradiation, displayed increased CFC freezing (Raber et al. 2014), in contrast to our decreased CFC freezing shown here. While increased freezing can be an index of anxiety, cued FC was not assessed. It is possible that this difference could be due to the lower energy used in our experiments [300 MeV vs. 600 MeV, as in ref. (Raber et al. 2014)], as lower-energy particles can be more damaging than higher-energy particles (Rabin et al. 2011). Of course, age at time of exposure plays a role in the behavioral effects of ^{28}Si radiation, as has also been shown with other ions (Parihar et al. 2016; Rabin, Shukitt-Hale & Carrihill-Knoll 2014a). For example, mice exposed to ^{28}Si radiation at 6-7 months old were resistant to radiation-induced deficits in CFC at doses <1.6 Gy (Raber et al. 2015a). However, our goal here was to work with young adult mice to enable comparison with prior published studies in

which other ions were examined.

This raises our third discussion point: how does the ^{28}Si radiation-induced disruption of hippocampal function, assessed here using CFC, compare to that induced by other ions? Only a few studies have examined CFC in young adult mice after HZE-particle exposure, and it is challenging to compare these to our work. For example, young adult mice exposed to protons (150 MeV) have shown increased freezing at low dose (0.1 Gy) with no change at higher doses (0.5, 1 Gy) at 1 month post-irradiation, and no change in any group at 3 months post-irradiation (Raber et al. 2016). However, cued FC was not reported as being assessed, so it remains possible that increased freezing at 0.1 Gy proton irradiation was due to anxiety, not improved memory. In another study, mice exposed to ^{56}Fe (0.1-0.5 Gy) were reported to have no deficits in CFC at 2-4 weeks post-irradiation (Haley et al. 2013), although the age at the time of exposure was not provided. Another way to answer this question is to widen the comparison to all studies investigating HZE-induced behavioral changes in young adult mice after exposure to mission-relevant doses (>1 Gy and ideally >0.2 Gy). From this perspective, there is increasing evidence that lower doses of ^{56}Fe (as low as 0.2 Gy), ^{28}Si (0.005 Gy), ^{16}O (0.01 Gy), ^{12}C (0.05 Gy), protons (0.1 Gy) or combined exposure (e.g., protons and ^{56}Fe) impede hippocampal, striatal and executive function in young adult rats and mice (Raber et al. 2016; Rabin et al. 2011; Yan et al. 2016; Bellone et al. 2015; Rabin et al. 2009; Britten et al. 2011; V. K. Parihar et al. 2015; Rabin, Shukitt-Hale, Carrihill-Knoll, et al. 2014; Rabin et al. 2015; Carrihill-Knoll et al. 2007; Rabin et al. 1989; Britten et al. 2014) in an energy- dependent manner. Although there is a relative paucity of

behavioral studies using ^{28}Si radiation, our data show that exposure to 0.2 Gy ^{28}Si radiation induces deficits in hippocampal function even at 3 months post-irradiation.

The neural mechanisms underlying the ^{28}Si-induced behavioral changes we report here are unknown. In other published work with these ^{28}Si doses, no change in key electrophysiological parameters in the mouse DG was reported at 3 months post-irradiation (Marty et al. 2014), although those data were generated with more energetic (and perhaps less damaging) ^{28}Si particles than ours. Might these behavioral changes be due instead to ^{28}Si radiation-induced changes in neurogenesis? Certainly, DG neurogenesis is functionally important in hippocampal-dependent tasks (Ming & Song 2011; Tannenholz et al. 2014; Aimone et al. 2014; Kempermann 2002; Christie & Cameron 2006). Notably, the mice in our current study have fewer surviving adult-generated DG neurons in both the anterior and posterior DG (**Fig. 2-6A, E and F**) as well as disrupted CFC performance at 3 months post-irradiation (**Fig. 2-8**), a task that engages the posterior hippocampus. Since this is a correlation, it is not feasible or appropriate from our data to conclude that the ^{28}Si radiation-induced decrease in neurogenesis causes the disruption in CFC. More association studies may strengthen this correlation, e.g., if exposure to radiation disrupts other behaviors that specifically involve adult-generated neurons (Oomen et al. 2014; Vivar & van Praag 2013; Jonas & Lisman 2014). Of course, only a causative study can truly reveal this relationship. For example, if selective and inducible elevation of the activity of adult-generated neurons rescues ^{28}Si radiation-induced disruption of CFC (Sahay et al. 2011; Hill et al. 2015), then a causative link may be inferred. In fact, one may not even expect a relationship

between the number of new neurons and performance on hippocampal tasks (Leuner et al. 2006), since this disconnect has already been shown after exposure to low-LET proton radiation (Sweet et al. 2014). There are other measures relevant to neurogenesis, beyond new neurons, which are proposed to contribute to DG function (e.g., dendritic complexity), and these merit evaluations in HZE-exposed animals in future studies, along with consideration of the functional heterogeneity that is evident in the rodent hippocampus (O'Leary & Cryan 2014; Kheirbek & Hen 2011).

One caveat of this study is that our neurogenesis findings (that ^{28}Si radiation damages DG newborn neuron survival), and our behavioral findings (that low doses of ^{28}Si induce abnormalities in hippocampal function, disrupting fear memory but also inducing anxiety) are collected from NGFP mice and C57BL/6J mice, respectively. Another caveat is that the mice were exposed to ^{28}Si during different NSRL campaigns. While we cannot say for certain that these differences do not have an effect on our conclusions, i.e., the behavior of NGFP would be different from C57BL/6J mice (or vice versa), several lines of evidence suggest that it is reasonable to generalize our conclusions across these mouse lines. First, the NGFP mouse line was created in C57BL6 oocytes, and was maintained on a C57BL/6J background for 10 or more generations prior to use in this study. Supporting the broad utility of this mouse line for neurogenesis research, the NGFP mouse line is commonly used to explore fundamental and advanced concepts in neurogenesis research, and is often used interchangeably with C57BL/6 mice (Yamaguchi et al. 2000; DeCarolis et al. 2013; Kempermann et al. 2003; Gebara et al. 2015; Sawamoto et al. 2001; Kronenberg et al.

2003; Tozuka et al. 2005; Filippov et al. 2003; Walter et al. 2011; Knobloch et al. 2013; Wang et al. 2005; Plümpe et al. 2006; Steiner et al. 2004; Fukuda et al. 2003), and such findings have informed seminal and widely-accepted models of the DG neurogenesis (Kempermann et al. 2004; Ming & Song 2011). Also supporting the similarity of these mouse lines, NGFP mice are also commonly used in publications where neurogenesis data come from NGFP mice and behavior data come from C57BL/6 mice (Steiner et al. 2004; Wolf et al. 2010; Wolf et al. 2011). There is also published work showing similar effects of HZE-induced changes in neurogenesis in NGFP and other mouse lines (Rivera et al. 2013; DeCarolis et al. 2014). In addition, NGFP mice respond similarly to the contextual and cued fear conditioning paradigm used here (Petrik et al. 2012), and have grossly similar measurements of anxiety, social avoidance and spatial learning as C57BL/6 mice (Klein et al. 2016; Ehninger & Kempermann 2006; Petrik et al. 2012; Lagace et al. 2010). Finally, many conclusions in the field on HZE- induced changes in the brain and behavior have been generalized across mutant mouse strains, rodents, different NSRL campaigns, to humans and even for computer modeling, as supported by the contents of review publications and even the titles of primary research works (Cucinotta et al. 2014; Parihar et al. 2015; Cucinotta et al. 2015; Koike et al. 2005; Rabin & Shukitt-Hale 2014; Nelson et al. 2016; O'Banion n.d.; Boice 2017). It is clearly important to acknowledge the potential differences in these mouse strains, as we do here, and future studies should strive to minimize variables of strain and irradiation date. However, by emphasizing both the differences and similarities in our mouse strains in this work, we feel it is reasonable to conclude that in our mice, whole-body exposure to ^{28}Si radiation dose-dependently disrupts DG neurogenesis and proliferation in the short

term and new neuron survival and CFC in the long term.

In conclusion, this work was specifically done in young adult mice to facilitate comparison with the many prior studies exposing young adult mice to other ions. However, it is important that future work examine whether older mice, which are closer in age to that of astronauts, are similarly influenced by ^{28}Si (Rabin, Shukitt-Hale & Carrihill-Knoll 2014a). Indeed, as mentioned above, previous work with another mouse strain has revealed that these animals, which were 6–7 months old at time of exposure, were unimpaired in CFC at low doses of ^{28}Si and only showed impairment after 1.6 Gy ^{28}Si irradiation (Raber et al. 2015a). Sex will be another important factor to assess as the number of female astronauts rises, since basic research has demonstrated sex-specific responses to space radiation (Rabin et al. 2013; Raber et al. 2016; Rola, Otsuka, et al. 2004). Here, we show robust and similar effects on neurogenesis indices in male and female mice in the short term, with more subtle sex-dependent differences in the long term. Whether these time-dependent effects are truly sex-dependent or merely less robust in females merit a study with larger cohort numbers per sex. In addition to the importance of sex, and the age at irradiation, it will be useful to assess the mechanisms underlying the changes in neurogenesis and hippocampal-dependent function reported here, such as radiation-induced changes in inflammation (Cucinotta et al. 2014).

These findings expand what is known about the influence of HZE particles on the brain and behavior in young adult mice, particularly in regards to mission-relevant doses, thus

enabling better predictions about how single- and multiple- particle events may affect the astronaut brain and behavior during deep space missions.

Chapter 2, Figures

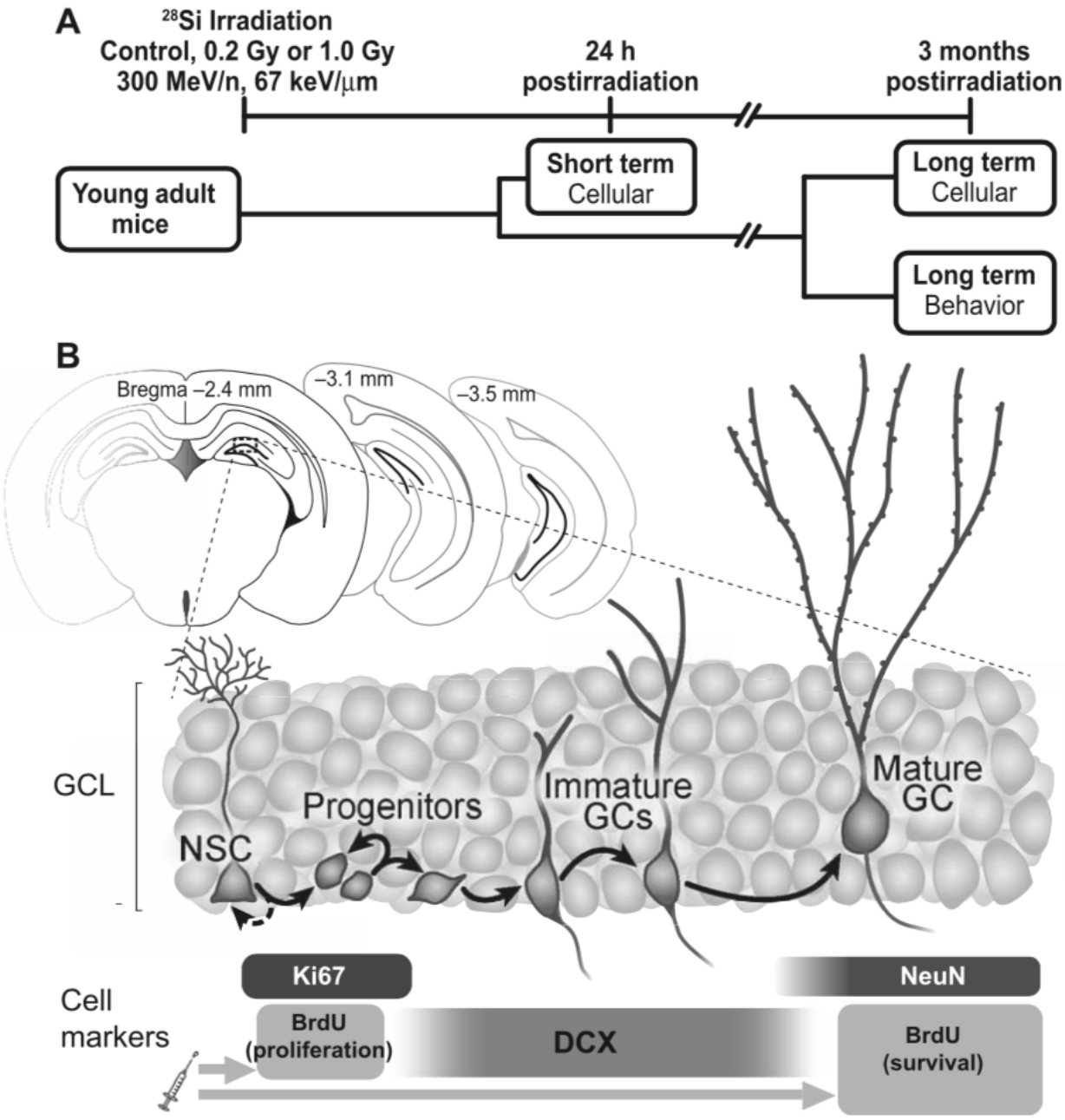

Figure 2-1. Schematic of experimental design and stages of neurogenesis. Panel A: Timeline of experiment to examine short-term (24 h) and long-term (3 months) effects of ^{28}Si radiation on cellular indices of neurogenesis (short- and long-term) and behavior (long-term) in young adult mice (9 weeks old at exposure). **Panel B**: Schematic depicting the stages of neurogenesis in the DG granule cell layer (GCL) to emphasize that neurogenesis is a process, not a time point (34). Cells immunopositive for neurogenesis-relevant markers were quantified in the DG GCL (dotted rectangle) along the entire longitudinal axis of the hippocampus; three sample coronal sections along the bregma axis are shown. The magnified GCL depicts cells in various stages of neurogenesis, from neural stem cell and progenitor, to immature and then mature DG granule cell (GC). Antibodies against the endogenous proteins Ki67, doublecortin (DCX) and NeuN label proliferating progenitors, immature neurons and mature neurons respectively. When injected i.p., the exogenous S-phase marker BrdU incorporates into the DNA of proliferating cells. Antibodies against BrdU label proliferating cells (2 h after BrdU injection) and surviving cells (3 months after BrdU injection).

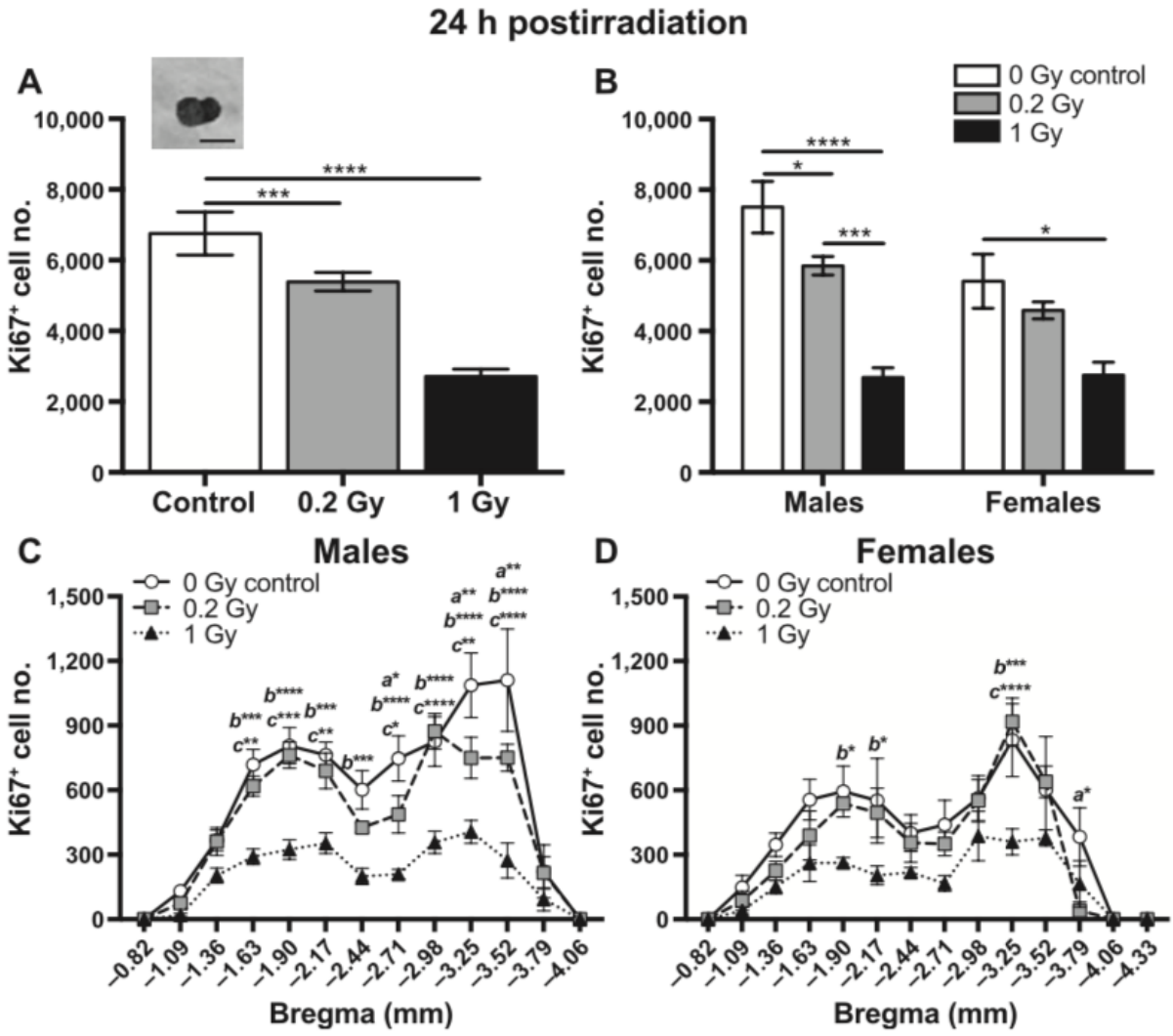

Figure 2-2. Twenty-four h after whole-body ^{28}Si irradiation, DG GCL proliferation was reduced, as measured by stereology of Ki67+ cells. Panel A: Stereological quantification of total GCL Ki67+ cells (inset: representative photomicrograph). Controls, n = 11; 0.2 Gy, n = 11; and 1 Gy, n = 10. **Panel B**: Stereological quantification of total GCL Ki67+cells by sex.For males,n=7 per group (controls,0.2Gy and 1Gy).For females:controls,n= 4;0.2Gy,n=4;and1Gy,n=3.**Panels C and D**: Quantification of GCL Ki67+ cells across the bregma in male and female mice, respectively. *P<0.05,

**P<0.01, ***P<0.001, ****P<0.0001. a Controls vs. 0.2 Gy; b controls vs. 1 Gy; c 0.2 Gy vs. 1 Gy. Scale bar = 10 um.

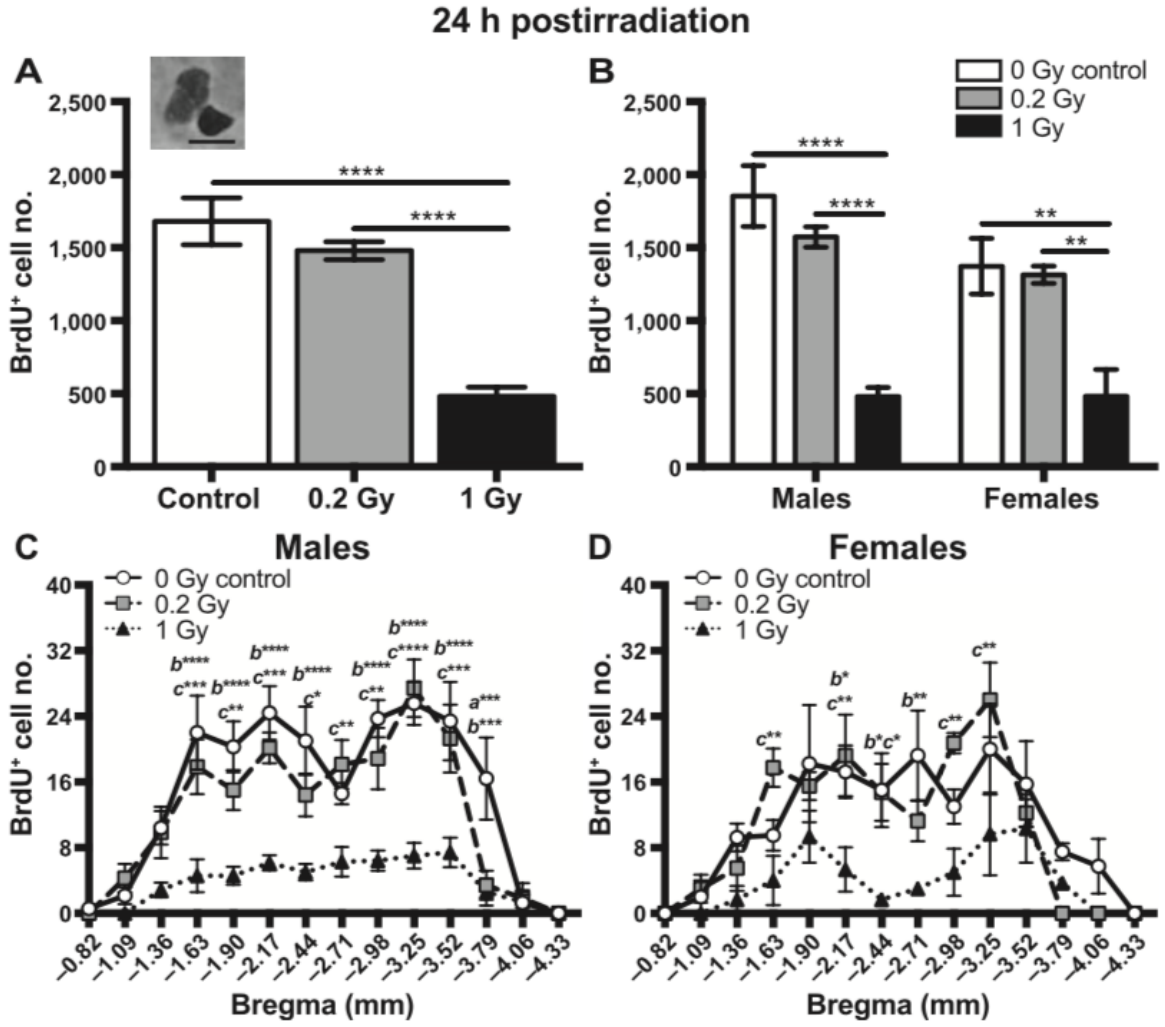

Figure 2-3. Twenty-four h after whole-body ^{28}Si irradiation, DG GCL proliferation was reduced, as measured by stereology of BrdU+ cells. Panel A: Stereological quantification of total GCL BrdU+ cells (inset: representative photomicrograph). Controls, n = 11; 0.2 Gy, n = 11; and 1 Gy, n = 10. **Panel B**: Stereological quantification of total GCL BrdU+ cells by sex. For males: n = 7 per group (controls, 0.2 Gy and 1 Gy). For females: controls, n = 4; 0.2 Gy, n = 4; and 1Gy, n = 3. **Panels C and D**: Quantification of GCL BrdU+ cells across the bregma in male and female mice, respectively. *P<0.05, **P<0.01, ***P<0.001, ****P<0.0001. a Controls vs. 0.2 Gy; b controls vs. 1 Gy; c 0.2 Gy vs. 1 Gy. Scale bar = 10 um.

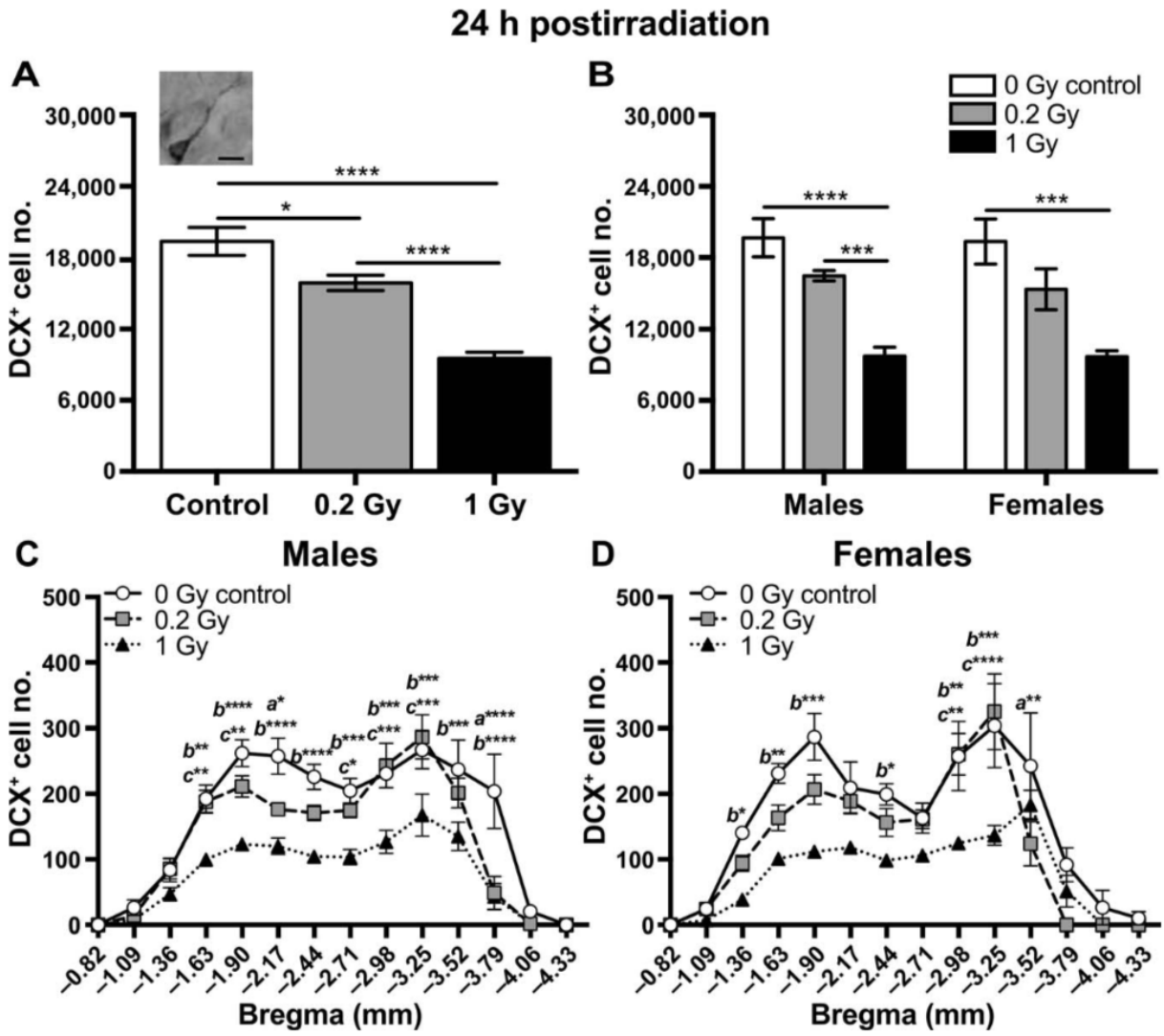

Figure 2-4. Twenty-four h after whole-body ^{28}Si irradiation, DG neurogenesis was reduced, as measured by stereology of DCX+ cells. Panel A: Stereological quantification of total DCX+ cells (inset: representative photomicrograph). For controls, n = 11, 0.2 Gy = 11, 1 Gy = 10. **Panel B**: Stereological quantification of total GCL DCX+ cells by sex. For males: controls, n = 7; 0.2 Gy, n = 7; and 1 Gy, n = 7. For females: controls, n = 4; 0.2 Gy, n = 4; and 1 Gy, n = 3. **Panels C and D**: Quantification of GCL DCX+ cells across the bregma in male and female mice, respectively. *P<0.05,

**P<0.01, ***P<0.001, ****P<0.0001. *a* Controls vs. 0.2 Gy; *b* controls vs. 1 Gy; *c* 0.2 Gy vs. 1 Gy. Scale bar = 10 um.

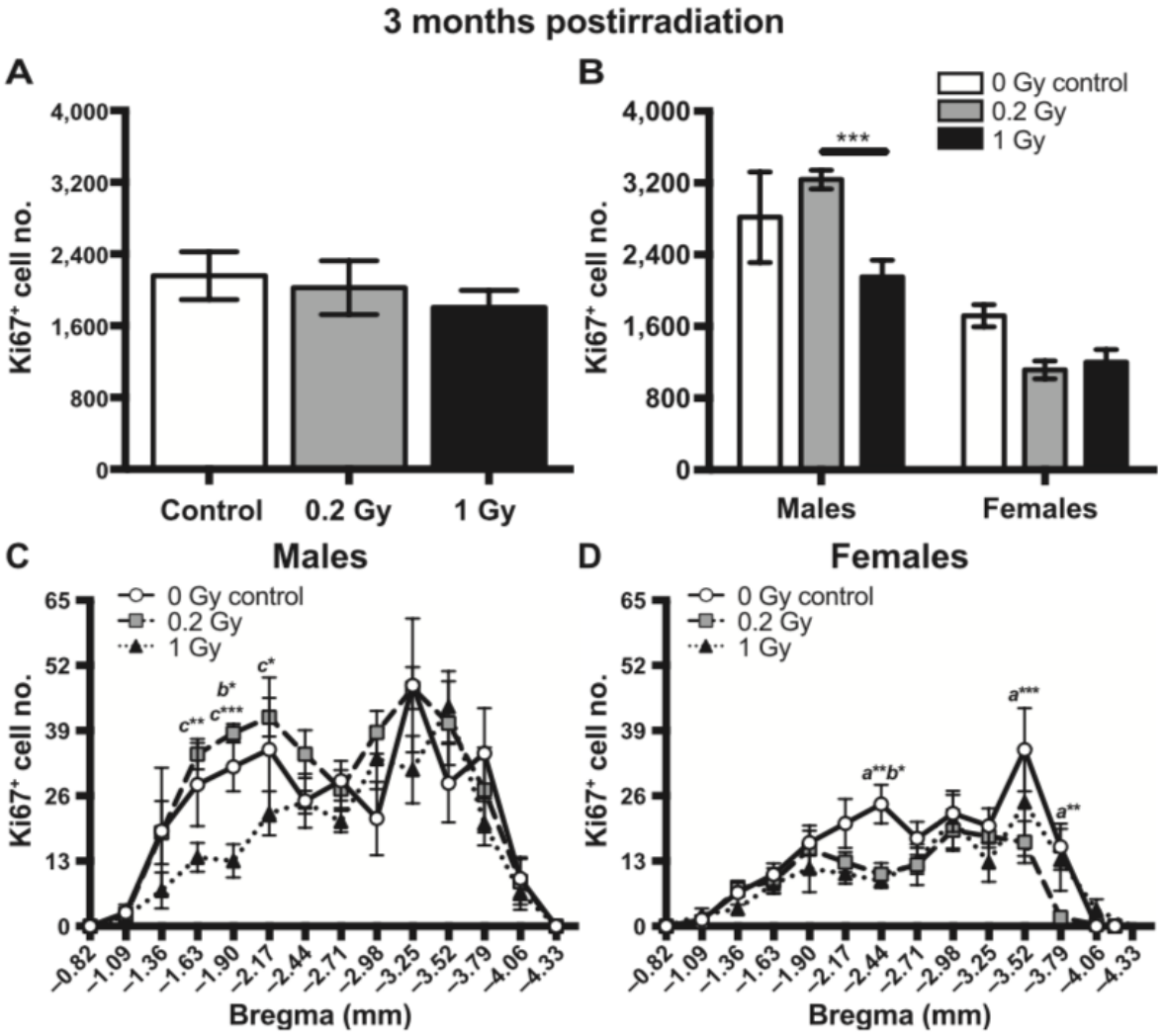

Figure 2-5. At three months post-irradiation, proliferation in irradiated mice recovers compared to controls after whole-body exposure to ^{28}Si, as measured by stereology of Ki67+ cells. Panel A: Stereological quantification of total Ki67+ cells. For controls, n = 10; for 0.2 Gy, n = 14; and for 1 Gy, n = 11. **Panel B**: Stereological quantification of total GCL Ki67+ cells by sex. For males: controls, n = 4; 0.2 Gy, n = 6; and 1 Gy, n = 7. For females: controls, n = 6; 0.2 Gy, n = 8; and 1 Gy, n = 4. **Panels C** and D: Quantification of GCL Ki67+ cells across the bregma in male and female mice,

respectively. *P<0.05, **P<0.01, ***P<0.001. *a* Controls vs. 0.2 Gy; *b* controls vs. 1 Gy; *c* 0.2 Gy vs. 1 Gy.

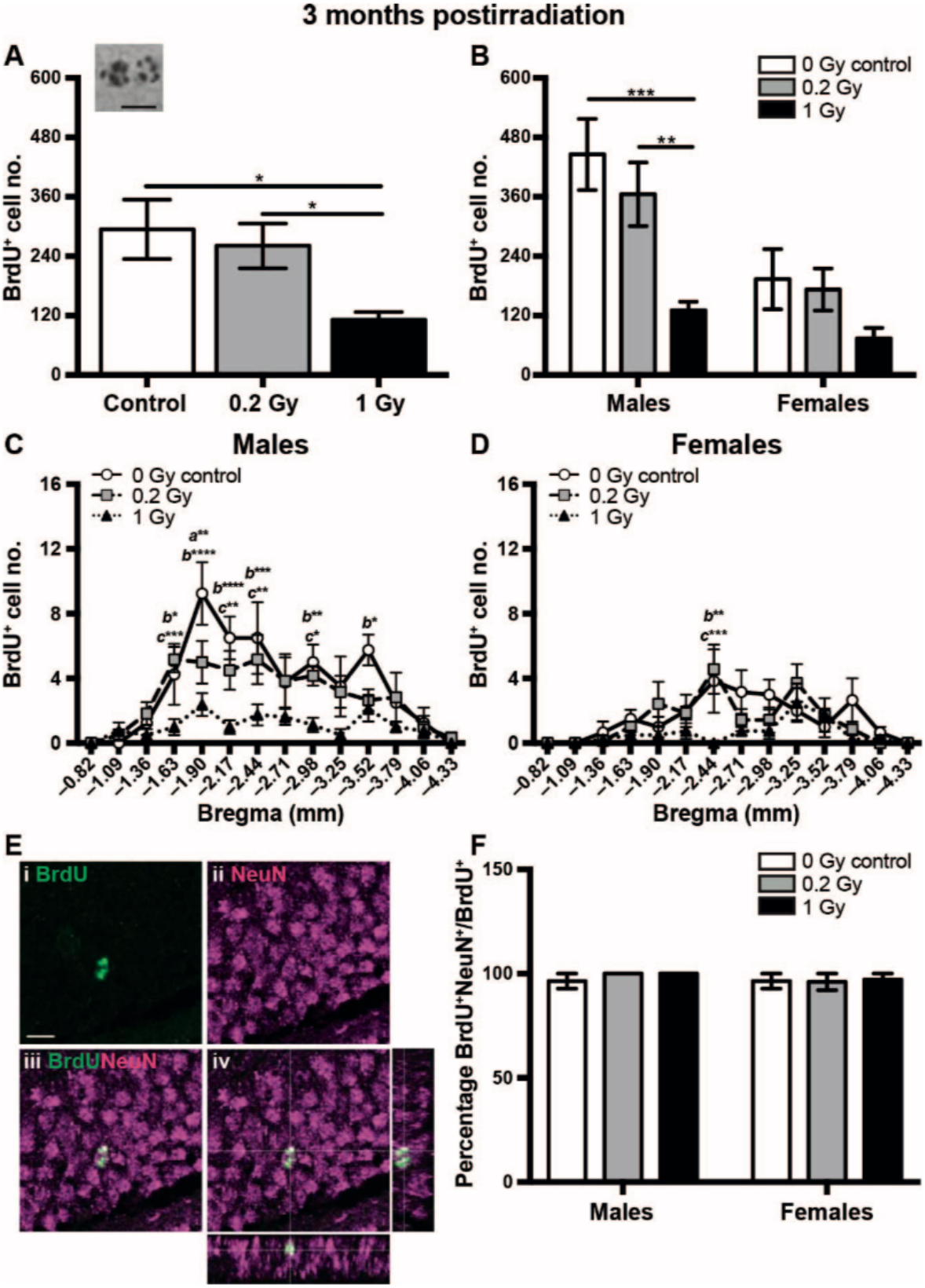
3 months postirradiation
A
BrdU+ cell no.
600
480
360
240
120
0
Control
0.2 Gy
1 Gy
B
0 Gy control
0.2 Gy
1 Gy
Males
Females
C
Males
D
Females
Bregma (mm)
E
i BrdU
ii NeuN
iii BrdUNeuN
iv
F
Percentage BrdU+NeuN+/BrdU+
150
100
50

Figure 2-6. Three months post-irradiation, whole-body exposure to ^{28}Si reduces new neuron cells, as measured by stereology and confocal phenotypic analysis of BrdU+ cells. Panel A: Stereological quantification of total GCL BrdU+ cells (inset: representative photomicrograph). For control, n = 10; for 0.2 Gy, n = 13; and for 1 Gy, n = 12. **Panel B**: Stereological quantification of total GCL BrdU+ cells by sex. For males: controls, n = 4; 0.2 Gy, n = 6; and 1 Gy, n=8. For females: controls, n = 6; 0.2 Gy, n = 7; and 1 Gy, n = 4. **Panels C and D**: Quantification of GCL BrdU+ cells across the bregma in male and female mice, respectively. **Panel Ei–iv**: Representative confocal photomicrographs of BrdU+NeuN+ cells. Single channel photomicrographs are shown of BrdU+ cells (i: green, 489 nm excitation) and NeuN+ cells (ii: magenta, 654 nm excitation), with the merged image (iii). Orthogonal presentation is shown of BrdU+NeuN+ cells, along with xz and yz planes (iv). **Panel F**: Percentage of BrdU+ cells that are NeuN+ in male and female mice (subset of mice in panel A near mean). Males: controls, n = 4; 0.2 Gy, n = 4; 1 Gy, n = 4. Females: controls, n = 4; 0.2 Gy, n = 4; 1 Gy, n = 4. *P<0.05, **P<0.01, ***P<0.001, ****P<0.0001. *a* Controls vs. 0.2 Gy; *b* controls vs. 1 Gy; *c* 0.2 Gy vs. 1 Gy. Scale bar = 10 um.

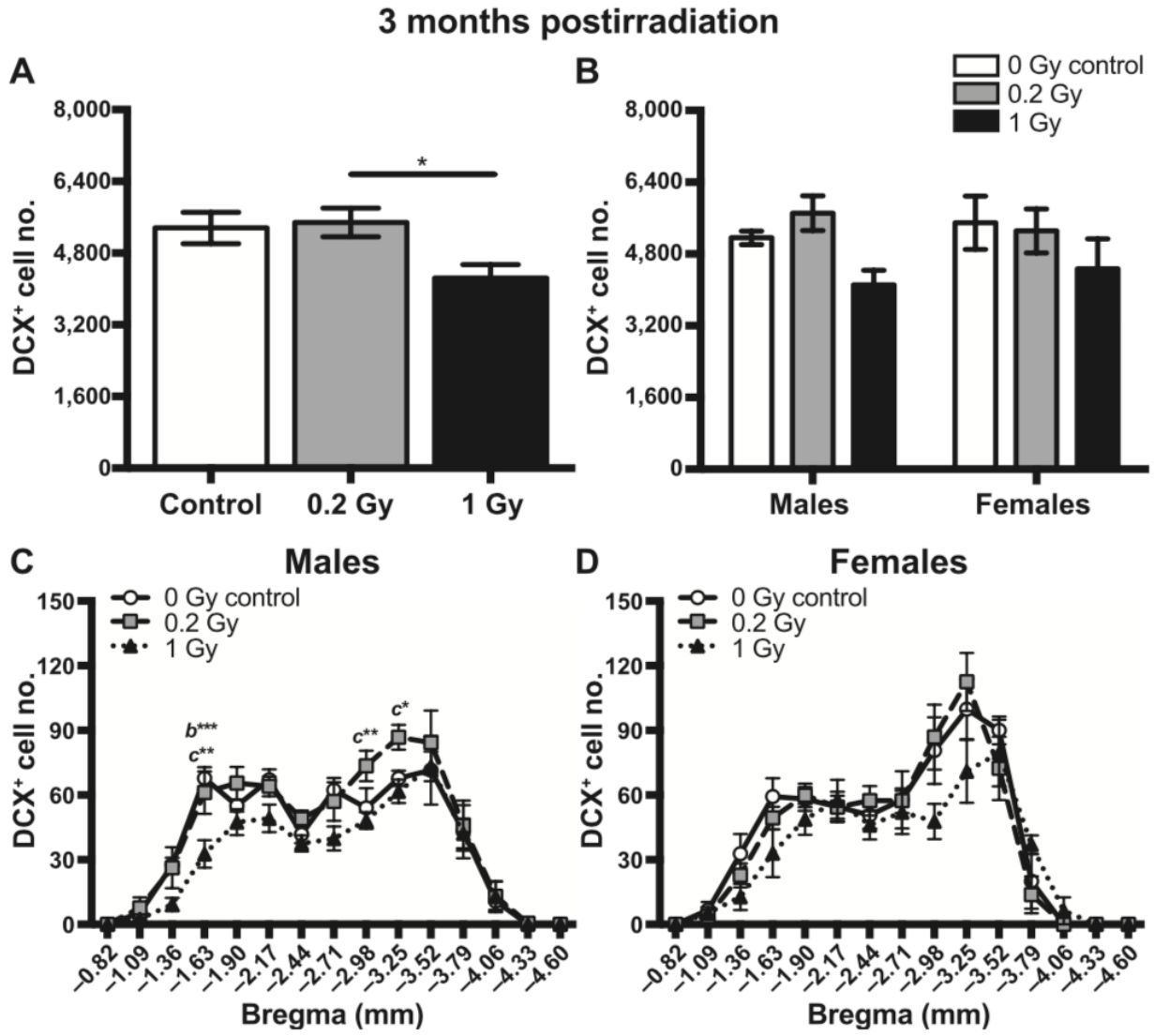

Figure 2-7. Three months post-irradiation, neurogenesis in irradiated mice recovers compared to controls after whole-body exposure to ^{28}Si, as measured by stereology of DCX+ cells. Panel A: Stereological quantification of total DCX+ cells. For controls, n = 10; for 0.2 Gy, n = 14; and for 1 Gy, n = 11. **Panel B**: Stereological quantification of total GCL DCX+ cells by sex.For males: controls, n = 4; 0.2 Gy, n = 6; and 1 Gy, n = 7. For females: controls, n = 6; 0.2 Gy, n = 8; and 1 Gy, n = 4. **Panels C and D**: Quantification of GCL DCX+ cells across the bregma in male and female mice, respectively. *P<0.05, **P<0.01, ***P<0.001. *b* Controls vs. 1 Gy; *c* 0.2 Gy vs. 1 Gy.

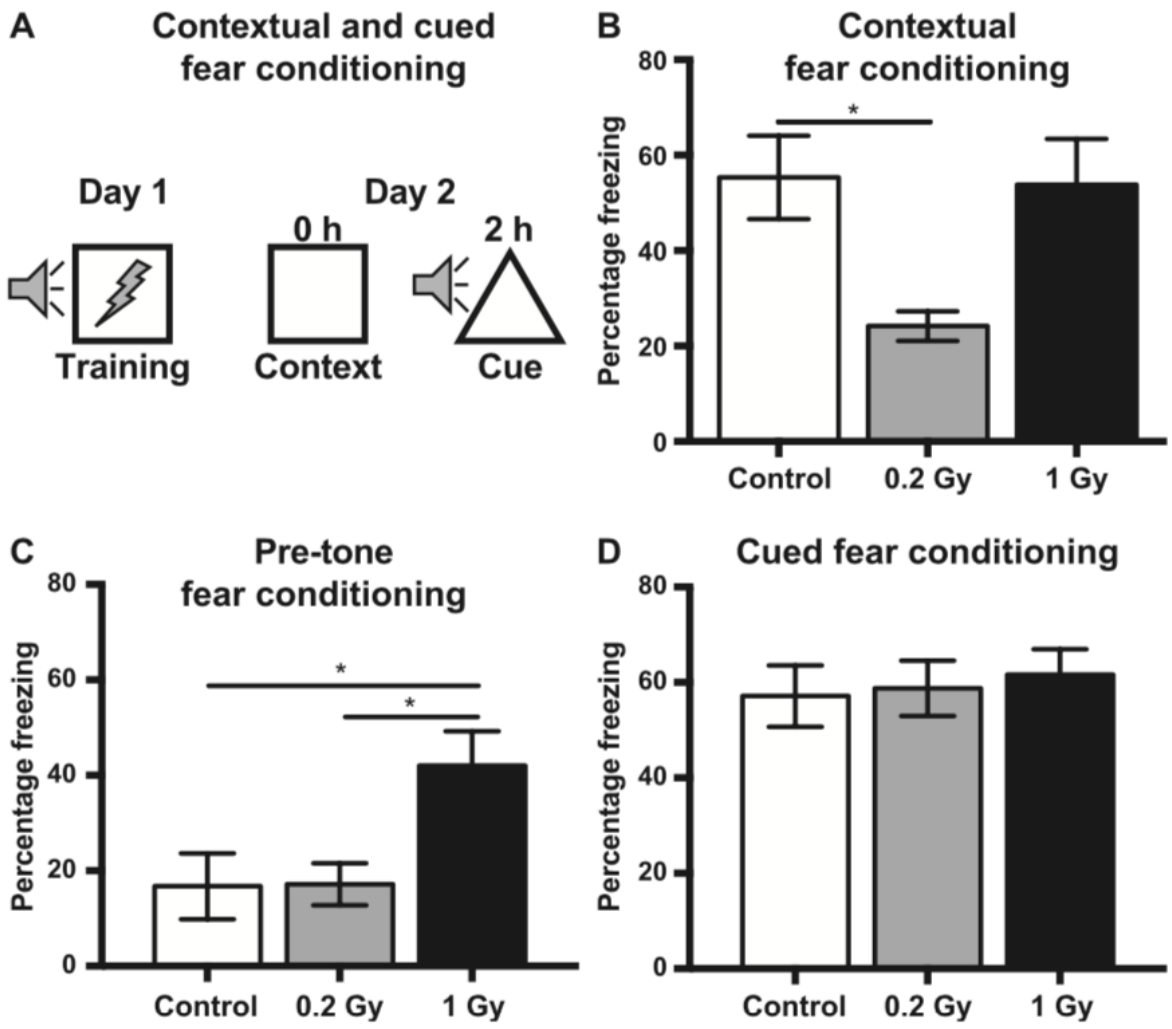

Figure 2-8. Three months post-irradiation, mice show a dose-dependent decrease in contextual fear conditioning (CFC) and dose-dependent appearance of anxiety-like trait. Panel A: Schematic of CFC pairing [pair a novel context with an auditory cue (speaker icon) that precedes a foot shock (lightning bolt)], CFC testing (context only, day 2) and cued fear conditioning (FC) (additional novel context with an auditory tone, day 2). Panels **B– D**: Percentage of time that mice froze in response to context (panel B), pretone in novel context (**panel C**) and cued FC (**panel D**). For controls, n = 8; for 0.2 Gy, n = 7; and for 1 Gy, n = 8. Mean ± SEM. *P < 0.05.

TABLE 1
Statistical Results, Short-Term Cohort (Figs. 2–4)

Antibody	Fig.				Bonferroni post hoc		
Ki67	2A	One-way ANOVA main effect **$F(2, 29) = 24.38$, $P < 0.0001$**			Controls vs. 0.2 Gy ns	Controls vs. 1 Gy **$P < 0.0001$**	0.2 Gy vs. 1 Gy **$P < 0.001$**
	2B	Two-way ANOVA main effects					
		Treatment **$F(2, 26) = 23.12$, $P < 0.0001$**	Sex **$F(1, 26) = 6.04$, $P < 0.05$**	Interaction $F(2, 26) = 1.90$, $P > 0.05$	Controls vs. 0.2 Gy	Controls vs. 1 Gy	0.2 Gy vs. 1 Gy
				Males	**$P < 0.05$**	**$P < 0.0001$**	**$P < 0.001$**
				Females	ns	**$P < 0.05$**	ns
	2C	Two-way ANOVA main effects					
		Treatment **$F(2, 233) = 78.06$, $P < 0.0001$**	Bregma **$F(12, 233) = 40.14$, $P < 0.0001$**	Interaction **$F(24, 233) = 3.42$, $P < 0.0001$**			
				Males	See Fig. 2C		
	2D	**$F(2, 126) = 19.67$, $P < 0.0001$**	**$F(13, 126) = 19.37$, $P < 0.0001$**	$F(26, 126) = 1.30$, $P > 0.05$			
				Females	See Fig. 2D		
BrdU	3A	One-way ANOVA main effect **$F(2, 29) = 33.86$, $P < 0.0001$**			Controls vs. 0.2 Gy ns	Controls vs. 1 Gy **$P < 0.0001$**	0.2 Gy vs. 1 Gy **$P < 0.0001$**
	3B	Two-way ANOVA main effects					
		Treatment **$F(2, 26) = 30.06$, $P < 0.0001$**	Sex $F(1, 26) = 3.90$, $P > 0.05$	Interaction $F(2, 26) = 1.21$, $P > 0.05$	Controls vs. 0.2 Gy	Controls vs. 1 Gy	0.2 Gy vs. 1 Gy
				Males	ns	**$P < 0.0001$**	**$P < 0.0001$**
				Females	ns	**$P < 0.01$**	**$P < 0.01$**
	3C	Two-way ANOVA main effects					
		Treatment **$F(2, 252) = 76.43$, $P < 0.0001$**	Bregma **$F(13, 252) = 24.80$, $P < 0.0001$**	Interaction **$F(26, 252) = 3.27$, $P < 0.0001$**			
				Males	See Fig. 3C		
	3D	**$F(2, 112) = 20.56$, $P < 0.0001$**	**$F(13, 112) = 11.56$, $P < 0.0001$**	**$F(26, 112) = 1.67$, $P < 0.05$**			
				Females	See Fig. 3D		
DCX	4A	One-way ANOVA main effect **$F(2, 29) = 33.34$, $P < 0.0001$**			Controls vs. 0.2 Gy **$P < 0.05$**	Controls vs. 1 Gy **$P < 0.0001$**	0.2 Gy vs. 1 Gy **$P < 0.0001$**
	4B	Two-way ANOVA main effects					
		Treatment **$F(2, 26) = 26.24$, $P < 0.0001$**	Sex $F(1, 26) = 0.20$, $P > 0.05$	Interaction $F(2, 26) = 0.09$, $P > 0.05$	Controls vs. 0.2 Gy	Controls vs. 1 Gy	0.2 Gy vs. 1 Gy
				Males	ns	**$P < 0.0001$**	**$P < 0.001$**
				Females	ns	**$P < 0.001$**	ns
	4C	Two-way ANOVA main effects					
		Treatment **$F(2, 237) = 62.91$, $P < 0.0001$**	Bregma **$F(13, 237) = 57.13$, $P < 0.0001$**	Interaction **$F(26, 237) = 2.99$, $P < 0.0001$**			
				Males	See Fig. 4C		
	4D	**$F(2, 112) = 25.92$, $P < 0.0001$**	**$F(13, 112) = 28.84$, $P < 0.0001$**	$F(26, 112) = 1.925$, $P > 0.05$			
				Females	see Fig. 4D		

Note. Significance indicated in bold face; ns = not significant.

Table 2-1. Statistical results, Short-Term Cohort (Figs. 2-2 through 2-4)

TABLE 2
Statistical Results, Long-Term Cohort (Figs. 5–7)

Antibody	Fig.				Bonferroni post hoc		
Ki67	5A	One-way ANOVA main effect F(2, 32) = 0.4007, $P > 0.05$			Controls vs. 0.2 Gy ns	Controls vs. 1 Gy ns	0.2 Gy vs. 1 Gy ns
	5B	Two-way ANOVA main effects					
		Treatment **F(2, 29) = 7.64, $P < 0.05$**	Sex **F(1, 29) = 75.17, $P < 0.0001$**	Interaction **F(2, 29) = 5.89, $P > 0.01$**	Controls vs. 0.2 Gy	Controls vs. 1 Gy	0.2 Gy vs. 1 Gy
				Males	ns	ns	**$P < 0.001$**
				Females	ns	ns	ns
	5C	Two-way ANOVA main effects					
		Treatment F(2, 210) = 8.84, $P > 0.05$	Bregma **F(13, 210) = 16.32, $P < 0.0001$**	Interaction F(26, 210) = 1.34, $P > 0.05$			
				Males	See Fig. 2C		
	5D	**F(2, 126) = 19.67, $P < 0.0001$**	**F(13, 126) = 19.37, $P < 0.0001$**	F(26, 126) = 1.30, $P > 0.05$			
				Females	See Fig. 2D		
BrdU	6A	One-way ANOVA main effect **F(2, 32) = 5.162, $P < 0.05$**			Controls vs. 0.2 Gy ns	Controls vs. 1 Gy **$P < 0.05$**	0.2 Gy vs. 1 Gy **$P < 0.05$**
	6B	Two-way ANOVA main effects					
		Treatment **F(2, 29) = 1.915, $P < 0.001$**	Sex **F(1, 29) = 16.72, $P < 0.001$**	Interaction F(2, 29) = 1.915, $P > 0.05$	Controls vs. 0.2 Gy	Controls vs. 1 Gy	0.2 Gy vs. 1 Gy
				Males	ns	**$P < 0.001$**	**$P < 0.01$**
				Females	ns	ns	ns
	6C	Two-way ANOVA main effects					
		Treatment **F(2, 210) = 34.29, $P < 0.0001$**	Bregma **F(13, 210) = 11.8, $P < 0.0001$**	Interaction **F(26, 210) = 2.151, $P < 0.01$**			
				Males	See Fig. 3C		
	6D	**F(2, 195) = 4.67, $P < 0.05$**	**F(13, 195) = 4.09, $P < 0.0001$**	F(26, 195) = 1.14, $P > 0.05$			
				Females	See Fig. 3D		
Percentage $BrdU^+$ and $NeuN^+/BrdU^+$	6F	Two-way ANOVA main effects					
		Treatment F(2, 18) = 0.3144, $P > 0.05$	Sex F(1, 18) = 0.9259, $P > 0.05$	Interaction F(2, 18) = 0.2526, $P > 0.05$	Controls vs. 0.2 Gy	Controls vs. 1 Gy	0.2 Gy vs. 1 Gy
				Males	na	na	na
				Females	na	na	na
Surviving $BrdU^+$ neurons (total $BrdU^+$ and $NeuN^+$ cells) (Fig. not shown.)		Two-way ANOVA main effects					
		Treatment **F(2, 18) = 12.75, $P < 0.001$**	Sex **F(1, 18) = 21.09, $P < 0.001$**	Interaction F(2, 18) = 2.437, $P > 0.05$	Controls vs. 0.2 Gy	Controls vs. 1 Gy	0.2 Gy vs. 1 Gy
				Males	ns	**$P < 0.001$**	**$P < 0.05$**
				Females	ns	ns	ns
DCX	7A	One-way ANOVA main effect **F(2, 32) = 4.359, $P < 0.05$**			Controls vs. 0.2 Gy ns	Controls vs. 1 Gy ns	0.2 Gy vs. 1 Gy **$P < 0.05$**
	7B	Two-way ANOVA main effects					
		Treatment **F(2, 29) = 3.58, $P < 0.05$**	Sex F(1, 29) = 0.06, $P > 0.05$	Interaction F(2, 29) = 0.42, $P > 0.05$	Controls vs. 0.2 Gy	Controls vs. 1 Gy	0.2 Gy vs. 1 Gy
				Males	ns	ns	ns
				Females	ns	ns	ns
	7C	Two-way ANOVA main effects					
		Treatment **F(2, 210) = 15.12, $P < 0.0001$**	Bregma **F(14, 210) = 52.80, $P < 0.0001$**	Interaction F(28, 210) = 1.14, $P > 0.05$			
				Males	See Fig. 4C		
	7D	F(2, 225) = 2.67, $P > 0.05$	**F(14, 225) = 40.53, $P < 0.0001$**	F(28, 225) = 1.08, $P > 0.05$			
				Females	See Fig. 4D		

Note. Significance indicated in bold face; ns = not significant; na = not applicable.

Table 2-2 Statistical results, Long-Term Cohort (Figs. 2-5 through 2-7)

TABLE 3
Statistical Results, Contextual Fear Conditioning (Fig. 8)

			Bonferroni post hoc		
Phase	Fig.	One-way ANOVA main effect	Controls vs. 0.2 Gy	Controls vs. 1 Gy	0.2 Gy vs. 1 Gy
Context	8B	**$F(2, 20) = 4.574$, $P < 0.05$**	**$P < 0.05$**	ns	ns, $P = 0.053$
Pretone	8C	**$F(2, 18) = 5.295$, $P < 0.05$**	ns	**$P < 0.05$**	**$P < 0.05$**
Cue	8D	$F(2, 18) = 0.1505$, $P > 0.05$	na	na	na

Note. Significance indicated in bold face; ns = not significant; na = not applicable.

Table 2-3 Statistical results, Contextual Fear Conditioning (Fig. 2-8)

CHAPTER 3: SPACE RADIATION UNEXPECTEDLY ENHANCES PATTERN SEPARATION YET DIMINISHES DENTATE GYRUS NEUROGENESIS IN C57BL/6J MICE

Whoolery CW, Lucero MJ, Reynolds RP, Ito N, Redfield RL, Richardson DR, Shih H, Rivera PD, Chen BPC, Yun S, Birnbaum SG, Stowe AM, Eisch AJ. *In preparation for submission, April 2018.*

Abstract (146/150)

Deep space exploration is accompanied by unavoidable exposure to galactic cosmic radiation. In young adult mice, exposure to ground-based particles of space radiation is detrimental to brain and behavior. Here we show mature mice (astronaut-age-equivalent) exposed to these particles perform better on two distinct pattern separation tasks relative to control mice. In context-dependent fear conditioning, mice exposed to whole-body, high-atomic number and -energy particles (either ^{56}Fe or ^{28}Si) discriminate similar contexts sooner than non-irradiated controls (Days 3-4 vs. Days 9-10). In touchscreen-based location discrimination, ^{56}Fe irradiated mice discriminate similar visual cues sooner and more accurately than non-irradiated controls (5 Days, 72% correct vs. 8 Days, 60% correct). While increased neurogenesis in young adult mice is sufficient to improve pattern separation, our mature irradiated mice had decreased neurogenesis. Taken together, this is the first evidence that space radiation particles can improve the mission-critical process of pattern separation.

Introduction

With interest in deep space travel on the rise, the highest priorities for space agencies is to gauge the hazards that deep space missions pose to human health (Vazquez 1998; Thirsk et al. 2009; Williams et al. 2009; Chang 2018). One major concern is exposure to galactic cosmic radiation (GCR), which is composed of high-(H)atomic number (Z) and -energy (E) (HZE) particles, such as heavy iron (^{56}Fe) or silicon (^{28}Si). HZE particles cannot be effectively blocked by shielding and thus pose a risk to mission success (Cucinotta et al. 2013; Nelson 2016). Due to the unavoidable nature of this radiation exposure, it is understandably concerning that studies exposing laboratory animals to ground-based space radiation generally conclude that HZE particles are detrimental to brain and behavior (Cucinotta et al. 2014; Jandial et al. 2018).

However, there are at least two reasons why it is worth revisiting the conclusion that space radiation is damaging to the central nervous system (CNS). First, most studies utilize young adult rodents (<3-month-old at HZE particle exposure), which - depending on the source consulted - is considered equivalent to a 14 to 20 year-old human (Jackson Laboratory 2018; NASA no date). Thus, tests using mature animals (6-month-old rodent), which are closer to the average age of an astronaut (~34 year old), are warranted. Second, most studies are based on general hippocampal-based learning and memory tasks, such as Contextual Fear Conditioning (CFC), Y Maze testing, Novel Object Recognition, Novel Location Recognition, Morris Water Maze, and Barnes Maze (Acharya et al. 2017; Kiffer et al. 2018; Rabin, Shukitt-Hale & Carrihill-Knoll 2014b;

Britten et al. 2017; Whoolery et al. 2017; Raber et al. 2015b; Carr et al. 2018; Parihar et al. 2018). Although these studies form our fundamental understanding of the impact space radiation has on behavior, converging evidence in both human and rodents suggests age-related shifts in network dynamics can affect high level cognitive tasks (Leal & Yassa 2018). For example, the hippocampal dentate gyrus supports contextual pattern separation, a translationally relevant, high-resolution, hippocampal-dependent learning ability required to distinguish two similar contexts (Clelland et al. 2009; McHugh et al. 2007). Specifically, previous literature has suggested hippocampal-based pattern separation may become less efficient as a result of normal aging in human and rodents (Holden & Gilbert 2012; Stark et al. 2010). Thus, as a result of radiation exposure occurring at later ages, pattern separation was assessed via tasks such as Context Discrimination Fear Conditioning (CDFC) in an aversive shock-based paradigm, or by Location Discrimination (LD) in an appetitive touchscreen-based paradigm (Sahay et al. 2011; T. J. McHugh et al. 2007; McTighe et al. 2009). Given the widely-published finding that space radiation reduces the generation of new neurons in the hippocampal dentate gyrus (Whoolery et al. 2017; DeCarolis et al. 2014; Rivera et al. 2013; Sweet et al. 2016; Rola, Otsuka, et al. 2004; Casadesus et al. 2005; Encinas et al. 2008), and given that adult neurogenesis in the rodent is both necessary and sufficient for pattern separation(Sahay et al. 2011; Nakashiba et al. 2012; Tronel et al. 2012), it is surprising that pattern separation ability has not yet been examined for its sensitivity to space radiation. This knowledge gap consequently leaves a disconnect between space radiation-induced central nervous system cellular deficits and the resulting behavioral deficits. Historically, there is a clear dose- and particle-dependent effect of space

radiation on brain and behavior (Rabin, Shukitt-Hale & Carrihill-Knoll 2014b). However, recent studies indicate improved performance in the shock-based, CFC test at specific doses of HZE radiation (Raber et al. 2015; Raber et al. 2014). These conflicting findings underscore the need for further studies to assess whether HZE particle exposure, given at relevant doses, are detrimental to CNS function and cognitive behavior, particularly in astronaut-age-equivalent rodents.

Here separate groups of mature mice, 6 months-old at the time of irradiation, were examined for their performance on a variety of cognitive behavioral tasks, including standard operant learning, a visual discrimination task, a cognitive flexibility task, a rule-based learning task, and two distinct pattern separation tasks. Our results surprisingly show radiation exposure at 6 months of age enhanced pattern separation in both the aversive CDFC (^{56}Fe or ^{28}Si) and appetitive touchscreen paradigms (^{56}Fe only). Interestingly, there was no effect (positive or negative) on any other cognitive task and these improvements were not correlated to the number of new neurons in mature mice. Thus it is possible that once outside the Earth's magnetosphere, astronauts exposed to HZE particles may show improvements in certain mission-critical tasks, such as pattern separation ability, which might increase the likelihood for mission success.

Methods

Animals

Animal procedures and husbandry were in accordance with the National Institutes of Health Guide for the Care and Use of Laboratory Animals, and performed in IACUC-approved facilities at UT Southwestern Medical Center (UTSW, Dallas TX) and

Brookhaven National Laboratories (BNL, Upton NY). 2-4-month old male C57BL/6J mice (Jackson Laboratories, stock #000664) were housed at UTSW and then shipped to BNL for irradiation at 6-months of age. During shipping and housing at BNL, mice were provided Shepherd Shacks (Bio-Serv). Mice were group-housed at UTSW or BNL (3-4/cage, light on 06:00, lights off 18:00, UTSW: room temperature 68-79°F, room humidity 30-70%, BNL: room temperature 70-74°F and room humidity 30-70%). At both facilities, food and water were provided *ad libitum*.

Particle Irradiation (IRR)

Mice received whole body HZE (^{56}Fe, **Figs. 1-3, Supp. Figs. 1-4, 6**; or ^{28}Si, **Supp. Fig. 5**) particle radiation at BNL's NASA Space Radiation Laboratory (NSRL). The ^{56}Fe and ^{28}Si ion beams were produced by the AGS Booster Accelerator at BNL and transferred to the experimental beam line in the NSRL. Delivered doses were ±0.5% of the requested value. Each day between 18:30 and 15:30, all mice - regardless of whether control (Sham) or experimental - were placed for 15 min in modified clear polystyrene cubes (AMAC Plastics, Cat #100C, W5.8 cm x L5.8 cm x H10.6 cm; modified with ten 5mm air holes). For ^{56}Fe experiments, mice received Sham IRR (placed in cubes Monday, Wednesday, Friday, but received no IRR) or either Fractionated (Frac) 20 cGy ^{56}Fe (600 MeV/n, LET 174 KeV/µ, Dose rate 20 cGy/min; placed in cubes and received 6.7 cGy on Monday, Wednesday, and Friday), or Non-Fractionated (Non-Frac) 20 cGy ^{56}Fe (placed in cubes Monday, Wednesday, and Friday but received 20 cGy only on Friday). For ^{28}Si IRR, mice received Sham IRR (placed in cubes Sunday, but received no IRR) or a single exposure of either 20 cGy or 100 cGy ^{28}Si (275 MeV/n, LET 72

KeV/μ, Dose rate 100 cGy/min). Post-IRR, mice were returned to UTSW and housed in quarantine for 4-6 weeks prior to initiation of behavior testing. Body weights (**Supp. Fig. 4**) were taken multiple times: prior to irradiation, at irradiation, and at least monthly (up to weekly) post-irradiation until collection of brain tissue.

Overview of behavioral testing

All mice began behavior testing 1-2 months post-IRR. Parallel groups of mice were tested for aversive behavioral tests (contextual fear conditioning, CFC; contextual discrimination fear conditioning, CDFC) vs. appetitive behavioral tests (operant touchscreen platform: Pairwise Discrimination, PD; Location Discrimination, LD; and Visiomotor Conditional Learning, VMCL). Subsets of mice were also tested for general activity (locomotor, LM, **Supp. Fig. 4**; open field, OF, **Supp. Fig. 3**) and pain sensitivity (pain threshold, PT, **Supp. Fig. 4**), methods for which are provided in **Supp. Methods.**

Aversive Behavior Testing. CDFC overview is provided below. See **Supp. Fig 1** and **Supp. Methods** for additional CDFC information, and for detailed information about CFC (**Supp. Fig. 2, 3**).

Contextual Discrimination Fear Conditioning (CDFC). A modified CDFC behavioral paradigm was utilized in which mice were exposed daily to two contexts (Context A and B) that shared similarities but had distinct visual and olfactory features (**Supp. Fig. 1**)(McHugh et al. 2007; Nakashiba et al. 2012), and were paired with distinct handling (**Supp. Methods**).

Over the course of 16 days, mice were exposed daily to both Context A and Context B. The order of exposure to Context A and B alternated between days (BAABABBABAABABBA) such that on days 2, 3, 5, 8, 10, 11, 13, 16 mice were exposed to Context A first and Context B second (**Supp. Fig. 1**). For CDFC data analysis, the percent freezing in Context A and Context B were measured each day, and data from each treatment group were collapsed and averaged across every two days, referred to as Blocks. Therefore, data were analyzed as 8 blocks (16 testing days) such that the grouping of days into blocks was as follows: [BA AB] [AB BA] [BA AB] [AB BA] etc. However, since Day 1 of exposure includes data from mice prior to their first tone/shock pairing and therefore their response does not reflect a learned association, Block 1 (Days 1-2) was removed from analysis. Percent of time freezing was measured using both discrete and linear analysis, with similar results; only linear results are presented in this study. The threshold for freezing was 20 arbitrary units detected using the proprietary Med Associates Software. Additional analysis parameters include bout length (0.5 sec), observation intervals (f):150, observation duration (f):6, and frames/sec (30).

Appetitive Behavior Testing. Separate groups of sham and IRR mice were trained on an operant touchscreen platform, an overview of which is provided below. Additional touchscreen methods are provided in **Supp. Methods.** Videos of mice performing all touchscreen assays are provided in **Supp. Video Files 1-3**.

Touchscreen platform and software. The touchscreen platform used was Model 80614 made by Lafayette Instruments (Lafayette, IN). Each operant chamber is encased in a sound-attenuating chamber. Each chamber is trapezoid-shaped, with the widest wall serving as the “touchscreen (238x170mm WxH)” and the opposite and narrowest wall (46mm W) containing a motion-sensitive center dispenser (tray) to deliver liquid reward (Strawberry Ensure, Abbott Laboratories, Chicago, IL). The touchscreen records Infrared (IR) light and has a delay of 10 milliseconds from the time of touch to the recording of the computer. The chamber has two lights (tray light, and overhead house light), and is equipped with a speaker (ceiling in each chamber) to play a tone. Aside from initial priming reward used during training (**Supp. Methods**), a “reward” is defined as 7uL Ensure delivered to the illuminated tray at the same time as a tone is played. Aside from training sessions, the term “initiate a trial” is defined as the mouse placing its head in the tray when the tray light is illuminated and the tone is played. The two remaining walls of the chamber are infrared-permeable to track rodents during testing. The floor is a perforated metal grid, and the solid roof is hinged for easy placement/removal of animal. A computer outside of the chamber allows recording and running of programs and each animal is tested in their light cycle Monday through Friday until testing was complete. Software used for the Touchscreen System is from ABET 2 (Lafayette Instruments), and individual ABET programs for specific touchscreen training and testing sessions are listed below or in **Supp. Methods**.

Food exposure/restriction. Three days prior to touchscreen training, each cage of sham or IRR behaviorally-naive, group-housed mice received daily access home cage to in a

volume sufficient to cover the bottom of a 2” plastic petri dish. Touchscreen training/testing occurred Monday through Friday during the light cycle. During touchscreen training and testing, mice were maintained on a food-restricted diet (**Supp. Methods**).

Touchscreen training (Abet 2 software, Cat 89505). Touchscreen training (**Fig. 2, Supp. Fig. 6**) consisted of 5 steps: Habituation, Initial Touch, Must Touch, Must Initiate, and Punish Incorrect (**Supp. Methods**). Latency (days) to complete each training step is reported.

Pairwise Discrimination (PD)/Reversal Testing (ABET2 software, Cat #89540). After training on the touchscreen platform (above, **Supp. Methods**), mice went through PD/Reversal training (**Fig. 2**). For PD, two images from the image bank that the mice have never seen before are simultaneously presented on the screen (e.g. plane vs. a spider). Only one of the images is rewarded (S+), and the image that is rewarded is counterbalanced within each group of mice. After the mouse initiates the trial, the rewarded image is presented on either the left or right side of the screen. The presentation side is pseudorandomly selected such that the S+ is not presented on the same side more than 3 times in a row. An incorrect choice leads to a correction trial, and the mouse must repeat the trial until it correctly selects the rewarded image displayed in the same location. The correction trial is not counted towards the final percent of trials correct. For Reversal testing, the S+ and S- are switched, and the previously-rewarded S+ image is now no longer rewarded. The mouse performs PD or

Reversal testing until it is able to complete 25 trials in 30 min at 80% accuracy for 2 days in a row, and latency (days) to completion is reported.

Location Discrimination (LD; ABET2 software, Cat #89546-6). For LD, mice receive one additional training step, termed LD1-choice, prior to the actual 2-choice LD test (LD2).

For LD 1-choice training, mice initiate the trial, which leads to the display of two identical white squares (25x25 pixels), that are presented with two black squares between them, a separation which is termed “intermediate” in difficulty. One of the location of the squares is rewarded (L+) and the other is not, and the L+ location (left or right) is counterbalanced within groups. On subsequent days, the rewarded square location is switched (becomes L-), then L+, then L-, etc. Once the animal reaches 25 trials in 30 min for 2 consecutive days (i.e. learns to press the right-most and then left-most square on consecutive days), the mouse advances to the LD 2-choice random test.

For the LD 2-choice random (or just LD), mice initate the trial, which leads to the display of two identical white squares, either with four black squares between them (“easy” separation) or directly next to each other (“hard” separation; **Fig. 2**). Like the LD 1-choice, only one of the square locations (right-most or left-most) is rewarded (L+, same side for both easy and hard separations, and counterbalanced within groups). The rewarded square location is switched the following day, and the location continues to alternate daily throughout training. Each day, the separation (easy vs. hard) is pseudorandomly displayed (same separation shown no more than 3 consecutive times). LD testing is complete when the mouse completes 50 trials in 30 min. For LD testing,

latency (days) to complete the test is reported, along with percent of easy vs. hard trials correct achieved on the last day of testing.

Tissue Collection

After completion of behavioral tests, mice underwent intracardial perfusion and fixation as previously described (Whoolery et al. 2017; Lagace, Whitman, Noonan, Ables, DeCarolis, Arguello, Donovan, Fischer, Farnbauch, Beech, DiLeone, et al. 2007). ^{56}Fe IRR mice were perfused 4-6 months post-IRR (10 to 12-months of age) and ^{28}Si IRR mice were perfused 6 months post-IRR (14-months of age). Briefly, mice were anesthetized with chloral hydrate (Sigma-Aldrich cat. #C8383, 400 mg/kg, stock solution 400 mg/ml made in 0.9 % NaCl solution, i.p.) and exsanguinated intracardially with 0.1M PBS (7 ml/min, 6 min) and followed by perfusion intracardially with 4% paraformaldehyde in 0.1M PBS (7 ml/min, 15 min). As stress can influence neurogenesis and thus doublecortin-immunoreactive (DCX+) cell number, steps were taken to minimize potential stress differences among mice in the same cage: each cage was gently removed from the housing room and brought to the adjacent procedure room immediately prior to anesthesia; mouse cage transfer was performed by a researcher with clean personal protective equipment; and all mice in a cage were anesthetized within 3 min and began exsanguination within 5 min of being brought into the procedure room. With these and other steps, we have found neurogenesis levels in mice can be reliably and accurately evaluated (Whoolery et al. 2017; Rivera et al. 2013; DeCarolis et al. 2014). Brains were harvested and placed in 4% paraformaldehyde at room temperature for 2 days, transferred to cryoprotectant (30% sucrose in 0.1 M PBS and

0.1% NaN_3) and stored at 4°C until sectioning. Brains were coronally sectioned on a freezing microtome (Leica), with 30 µm sections collected in serial sets through the entire anterior-posterior length of the hippocampus (distance range from Bregma: -0.82 to -4.24 µm)(Paxinos & Franklin 2004). These eight serial sets of sections (section sampling fraction, ⅛) were stored in 0.1% NaN_3 in 1x PBS (Fisher Scientific; Pittsburgh, PA) at 4°C until processed.

Immunohistochemistry

Immunohistochemistry was performed as previously described (Whoolery et al. 2017; DeCarolis et al. 2014; Rivera et al. 2013). One complete set of coronal sections from a 1:8 series was mounted onto glass slides (Superfrost/Plus, Fisher) in rostral to caudal order and allowed to dry. To visualize DCX+ cells using 3'3-diaminobenzidine (DAB), sections were treated for antigen retrieval (0.01M citric acid, pH 6.0, 95°C, 15 min) and quenching of endogenous peroxidases (0.3% hydrogen peroxide in 1xPBS, 30 min). Non-specific staining was blocked by incubation in 3% normal donkey serum (NDS) and 0.1% Triton X-100 in 1xPBS for 60 min. Sections were then incubated in goat-anti-DCX primary antibody (1:500, Santa Cruz) overnight at room temperature in 3% NDS, 0.1% Tween-20 in 1xPBS. The following day, sections were incubated for 60 min with biotinylated donkey anti-goat antibody (1:200, Jackson ImmunoResearch) in 1.5% normal donkey serum in 1xPBS followed by rinses. A 60-min incubation in avidin-biotin complex (ABC Elite, 1:50, Vector Laboratories) was then performed, followed by visualization of immunoreactive cells using DAB (Thermo Scientific Pierce) and Nuclear

Fast Red counterstaining (Vector Laboratories). Tissue was then dehydrated with a series of increasing ethanol concentrations and slides were cover slipped with DPX Mountant (Sigma-Aldrich).

Stereological Cell Quantification

DCX+ cell data are presented as number of cells Unbiased analysis of DCX+ cell number was performed via stereologic quantification on a BX51 System Microscope (Olympus America, Center Valley, PA, USA) as previously described (Whoolery et al. 2017; DeCarolis et al. 2014; Rivera et al. 2013). DCX+ cells in the subgranular zone (SGZ) and granular cell layer of the hippocampal dentate gyrus were visualized with a 40X, 0.63 NA oil-immersion objective and quantified with the formula:

Total population of cells = total cells counted x 1/ssf x 1/asf x 1/hsf

where ssf is the section sampling fraction (DCX: 1/8), asf is the area sampling fraction (1 for these rare populations of cells; thus, all cells were counted in 1/8 of the sections), hsf is the height sampling fraction (1 given the minimal effect edge artifacts have in counting soma <10um with ssf 1/8). As both hemispheres were counted for DCX, the resulting formula was:

Total population of DCX+ cells = total cells counted x 1/(1/8) x 1/1 x 1/1

Statistical Analyses

Statistical analyses were performed using Prism (GraphPad vs. 7.0). A detailed overview of all analyses performed is provided in **Table 3-1, 3-2, 3-3 and Sup. Table 3-1**. Data with one variable and two groups (e.g. Treatment, Sham vs. Frac 20 cGy) were

analyzed using an unpaired two-tailed Student's t-test **(Fig. 3-2C,E-G; Supp. Fig. 3-6C,E)**. Data with one variable with three groups (e.g. Treatment) were analyzed using a one-way ANOVA and Bonferroni post-hoc **(Fig. 3-3B; Supp. Fig. 3-3A)**. Data with two variables (e.g. Treatment and stress) with three groups were analyzed using a two-way ANOVA and Bonferroni post-hoc **(Supp. 3-4B-D).** Data with two variable and one repeated measure (e.g. Treatment x Context, Treatment x Training Stage) were analyzed using a two-way ANOVA and Bonferroni post-hoc **(Fig. 3-1E-G, 3-2B; Supp. Fig. 3-3B-C, 3-4A, 3-5E-G, 3-6B)**. Data with two repeated measures (e.g. Context x Block) were analyzed with two-way repeated measure ANOVA and Bonferroni post-hoc **(Fig. 3-1B-D; Supp. Fig. 3-5B-D)**. Statistical significance was defined as $P<0.05$ and is indicated by asterisks in graphs. Threshold significance value is presented rather than exact P values, although if $P\leq0.06$ a hashtag (#) is provided on relevant data.

Figure Preparation

For graphical data, figures for each data set were produced in Prism (GraphPad vs. 7.0) and transferred to Illustrator (Adobe 2017 version 21.1.0) so that uniformity in line thickness and figure size could be replicated across each figure. For photomicrographs, images were taken with an epifluorescence microscope (Olympus BX51) with 10x and 40x objectives and captured with the Olympus DP Manager Program before being prepared in Adobe Illustrator 2017 (version 21.1.0).

Transparency and Reproducibility

Behavioral experiments were performed by researchers blind to treatment (Sham or IRR), made feasible since these whole-body doses of space radiation did not have gross measurable impact on mouse weight gain or hair loss. Touchscreen testing criteria were set on rodent performance, i.e. did they hit criteria, (yes or no), thus avoiding any scoring discrepancies across researchers. For immunohistochemical experiments, tissue was coded to obscure treatment information, and code was not broken until data analyses were complete. After publication, raw data and images will be made provided upon reasonable request.

Results

Whole body ^{56}Fe IRR exposure improves pattern separation in a foot-shock based contextual discrimination task. To determine the effects of HZE radiation on pattern separation ability, whole body ^{56}Fe radiation was delivered via fractionated (Frac; 3 exposures of 6.7 cGy) or non-fractionated (Non-Frac; 1 exposure of 20 cGy) doses to C57BL/6J mice at 6-months of age. This dose closely aligns with the maximal dose and intermittent exposure predicted for a Mars mission (Gifford & Magazine 2014; Cucinotta & Durante 2006), but, similar to previously reported, does not cause hair loss or weight loss (data not shown) (Whoolery et al. 2017; DeCarolis et al. 2014; Rivera et al. 2013).

Beginning ~2 months post-IRR, mice began a battery of behavioral tests (**Fig. 3-1A**) to assess pattern separation (CDFC) and changes in locomotion (LM, **Fig. S3-4B, Table S3-1**), anxiety (open field test, OF, **Fig. S3-3C**), and pain sensitivity (pain threshold testing, PT, **Fig. S3-4C-E, Table S3-1**). For CDFC (**Fig. S3-1A-D,Table S3-1**), Sham mice learned over time to discriminate the two contexts by Days 9-10 (block 5), as they

froze more in the shock-paired context (context A) compared to the non-shock context (context B) (non-shock context, **Fig. 3-1B, Table 3-1**). However, mice exposed to either Frac or Non-Frac 20 cGy of ^{56}Fe irradiation learned to discriminate the contexts by Days 3-4 (block 2, **Fig. 3-1B, Table 3-1**). For the control tests using LM, OF, and PT, radiation exposure did not change beam breaks, duration in center, or response to a foot shock, respectively (**Fig. S3-3C, S3-4A-D, Table S3-1**). Thus, ^{56}Fe-irradiated mice learned to pattern separate earlier relative to Sham mice without any changes in locomotion, anxiety-like behavior, or sensitivity to pain.

To determine if all fear-based learning was improved, a second cohort of mice underwent the classical hippocampal-based CFC (**Fig. S3-2A-B, S3-3A,B, Table S3-1**). However, Sham and ^{56}Fe-IRR mice displayed normal performance in CFC (**Fig. S2A-B, S3-3A,B, Table S3-1**). Importantly, to see if the space radiation-induced improvement in contextual discrimination was dependent on the type of heavy particle used, similar behavior testing was performed with mice exposed to whole body ^{28}Si radiation, a particle with a smaller track structure as ^{56}Fe (**Fig. S3-5A-F, Table S3-1**)(Schaefer & Sullivan 1976). Sham mice were inconsistent with their ability to discriminate, spending more time freezing in A vs B only in block 5, Days 9-10, and block 8, Days 15-16 (**Fig. S3-5A-F, Table S3-1**). In contrast, mice irradiated with 1 Gy of ^{28}Si were able to discriminate between the two contexts as early as block 3, Days 5-6 (**Fig. S3-5A-F, Table S3-1**). Taken together, exposure to two different HZE particles results in earlier separation ability relative to Sham mice.

Whole body ^{56}Fe IRR exposure improves pattern separation in an appetitive-based touchscreen location discrimination task. To determine the effects of HZE radiation on pattern separation ability in a non-stressful behavioral paradigm, whole body ^{56}Fe radiation was delivered as a 20 cGy Fractionated dose (Frac; 3 exposures of 6.7 cGy). Mice then underwent an assortment of touchscreen tests for operant learning, visual discrimination, cognitive flexibility, rule-based learning, and pattern separation (**Fig. 2A, Fig. S6A**). These tests are depicted as touchscreen training, Pairwise Discrimination (PD), Reversal Learning (Rev), Visiomotor Conditional Learning (VMCL), and Location Discrimination (LD) (**Fig. 3-2A, Table 3-2, Fig. S3-6A-E, Table S3-1**). Surprisingly, we found that IRR Mice were able to finish Punish Incorrect (PI), the final stage of operant touch screen training, earlier relative to Sham mice (**Fig. 3-2B, Table 3-2**). Interestingly, IRR mice also were able to complete the LD pattern separation task earlier and more accurately (by Day 5 with a 72% accuracy for the hard display) compared to the Sham mice (Day 8, 60% accuracy for the hard display; **Fig 3-2 E,G, Table 3-2**). Both cohorts performed with similar accuracy on the easy display (60% and 57%, respectively; **Fig. 3-2F, Table 3-2**). For additional touchscreen based cognitive tasks, no changes were seen in the visual discrimination or cognitive flexibility tasks (PD and Reversal Learning, respectively; **Fig. 3-2C, Table 3-2**) or the rule-based learning task (VMCL; **Fig. S3-6A-E, Table S3-2**) when comparing Sham to the Fractionated cohort**.** Thus, this appetitive touchscreen experiment agrees with our finding that HZE-irradiated mice display improved pattern separation ability following HZE exposure.

^{56}Fe IRR decreases neurogenesis 4 months post-IRR As increasing neurogenesis

has been previously linked to improved pattern separation ability (Sahay et al. 2011), we measured doublecortin positive cells (**Fig. 3-3A**), a widely-accepted marker for neurogenesis (Francis et al. 1999; Couillard-Despres & Winner 2005; Brown et al. 2003), to determine if the HZE induced improvements on pattern separation ability was due to increased neurogenesis. However, mice IRR with either whole body, Fractionated or Non-Fractionated, ^{56}Fe radiation showed reduced DCX+ cell counts (**Fig. 3-3B, Table 3-3**).

Discussion

Astronauts on long-duration lunar missions or interplanetary missions will face unprecedented environmental, social, and technical challenges (Williams et al. 2009; Thirsk et al. 2009; Paris 2014). Exposure to galactic cosmic radiation is among the most concerning of these challenges, given the damaging nature of HZE particles (Jandial et al. 2018; Chancellor et al. 2014) and the current inability to effectively shield crew members (Chancellor et al. 2014; Cucinotta et al. 1998). Although missions to low Earth orbit (e.g. to the International Space Station) yield essential data on the impact of space flight on crew physiology, they do not yield information on the impact of HZE particles since the ISS and crew are protected by Earth's magnetosphere (Cucinotta et al. 2014). Thus, currently the best approach available to assess the unavoidable influence of HZE particles on mammalian brain and behavior is exposure of laboratory animals to ground-based radiation (Nelson 2003b). This approach has been intellectually profitable, as results from 75+ ground-based radiation studies suggest HZE radiation is detrimental to the central nervous system and therefore may pose a risk to mission completion (Jandial et al. 2018).

However, this conclusion overlooks two major caveats: almost all published data are from rodents that were young adult (<3-month-old) at time of irradiation, and from behavioral tests that rely on a broad network of brain regions, rather than those that rely on more specific brain subregions. While these early studies are undoubtedly important for the field, mounting evidence in both human and rodents suggest age-related shifts in network dynamics could be impairing high-level cognitive tasks, such as DG pattern separation ability (Leal & Yassa 2018). To address these two caveats, here we asked whether whole-body exposure to ground-based HZE particles in astronaut-age-equivalent rodents interferes with pattern separation, an ability that requires a functioning dentate gyrus (Gilbert et al. 2001; Goodrich-Hunsaker et al. 2008). We find mature mice exposed to HZE particles perform better in pattern separation tasks in both aversive (CDFC) and appetitive (LD touchscreen) platforms. These improvements were not correlated to the number of new dentate gyrus neurons. Contrary to the negative effect previously shown with young adult rodents, mature irradiated mice perform similarly to control non-irradiated mice in classical hippocampal-, striatal-, and amygdalar-based tasks. Taken together, these studies indicate that exposure to HZE particles may not be as damaging to the CNS as previously reported.

Neurogenesis is thought to be one of the major driving factors for pattern separation ability, with increases in neurogenesis being linked to improved pattern separation and vise versa (Sahay et al. 2011; Clelland et al. 2009; Nakashiba et al. 2012; Creer et al. 2010). As a result, one might view our data - pattern separation improved while

neurogenesis decreased - to be quite shocking since it contradicts this relatively well-accepted relationship between pattern separation and neurogenesis. However, this neurogenesis/pattern separation relationship was primarily based on manipulations performed on young adult rodents (2-3 months of age). Mounting evidence supports that manipulations performed on old mice (>17 months) can improve pattern separation ability such that it is equivalent to that of a young adult rodent (2-3 month) levels with minimal to no improvements in neurogenesis (Cès et al. 2018; Wu et al. 2015). Importantly, the improvements shown are not so broad as to affect every cognitive task tested but are unique to pattern separation ability yet unreliant on neurogenesis. While further studies are needed to investigate the effects decreased neurogenesis serves over the lifespan of the animal (Bizon et al. 2004), an in-depth systematic study targeting a variety of known functional pattern separation characteristics at the cellular and circuit level will also be be required to fully understand the underlying mechanism.

For example, some pattern separation characteristics that will need to be tested include region specific firing activity shifts from the Entorhinal Cortex (Ent) to the Hippocampus/CA3, changes in inhibitory signaling onto the hippocampus, or decreases in pattern completion or cognitive flexibility. Specifically, previous work has linked the lateral entorhinal cortex (Ent) to object-based pattern separation, and the medial Ent to spatial-based pattern separation (Reagh et al. 2018). Expanding on this in humans, recent high-resolution fMRI studies show age-related activity shifts in healthy aging adults (Reagh et al. 2018). In this study they suggest hypoactivity in the anterolateral Ent (alEnt) commensurate and dentate/CA3 hyperactivity can lead to deficits on an

object-based pattern separation task (Reagh et al. 2018). Interestingly, only subtle deficits between young and older adults were found in the spatial pattern separation task and in posteromedial Ent activity, demonstrating the various roles of the Ent across age in both object and spatial pattern separation (Reagh et al. 2018). Thus perhaps a similar approach can be taken with our spatial pattern separation data shown here, where future fMRI experiments in mice will target the medial Ent to monitor HZE induced activity shits. In addition, prior work has shown that manipulation to adult born granule cell firing can lead to alterations in pattern separation ability (Danielson et al. 2016; Nakashiba et al. 2012; McHugh et al. 2007). Thus a second characteristic change could be inhibitory hilar interneurons or mossy cells interacting with the perforant path (Myers & Scharfman 2009; McAvoy et al. 2015). This interaction could regulate pattern separation ability by lowering the firing probability of DG granule cells onto CA3 pyramidal cells, thus reducing the input necessary to activate the same subset of CA3 neurons (Myers & Scharfman 2009; McAvoy et al. 2015). Finally, although historically tied to learning and memory, recent work has suggested that neurogenesis plays a major role in forgetting (Akers et al. 2014; Epp et al. 2016). Specifically, some believe neurogenesis replaces old neurons/past memories that proactively interfere with new memory formation (Epp et al. 2016; Tello-Ramos et al. 2018). As a result, high levels of neurogenesis (say during childhood) can lead to increased levels of forgetting prior memories and thus increase cognitive flexibility (or the ability to adjust to change) (Epp et al. 2016; Tello-Ramos et al. 2018; Akers et al. 2014). In converse, as humans age, neurogenesis levels decrease (i.e less forgetting of prior memories) and as a result, prior memories begin to interfere with new memory formation (thus decreasing cognitive

flexibility) (Epp et al. 2016; Tello-Ramos et al. 2018). Here we show decreases in neurogenesis following HZE radiation exposure. If neurogenesis does have an impact on cognitive flexibility, we should expect irradiated mice to exhibit decreased cognitive flexibility via increased proactive interference from past memories (as forgetting would be decreased). Thus one strategy for testing this final pattern separation characteristic, would be to place a mouse on a more challenging reversal learning paradigm similar to the Pairwise Discrimination/Reversal learning cognitive flexibility task presented here. As the simplistic reversal learning ability presented here does not test a rodents memory retention, or appear to be affected following HZE radiation exposure, future studies can extend the task by including additional pairs of images prior to reversal testing. This should allow us to measure the extent to which the rodents retain the previous images as they are exposed to an increasing number of stimuli. The second strategy, would be to test the converse of pattern separation, which is the rodents pattern completion ability (i.e their ability to form an accurate generalization of partial sensory input) (Wilson et al. 2006; Yassa & Stark 2011; Vieweg et al. 2015). In ageing adult humans, there is a shift from pattern separation to pattern completion, where prior memories could be interfering with new memory formation (Wilson et al. 2006; Yassa & Stark 2011; Vieweg et al. 2015). As we have seen improvements in pattern separation (distinguishing between fine details) and a decrease in neurogenesis (increasing proactive interference), it is possible that IRR mice will exhibit a deficit in their pattern completion ability, or their ability to generalize information to form a solution. If correct, this in-depth systematic study targeting firing activity shifts from the Entorhinal Cortex (Ent) to the Hippocampus/CA3, changes in inhibitory signaling onto the hippocampus,

or decreases in pattern completion or cognitive flexibility will reveal the underlying mechanism behind the pattern separation improvements and allow us to move ahead accordingly.

In summary, prior to this study, space radiation was widely considered to be detrimental to brain function. However, the negative behavioral effects of high-energy particle exposure had been seen in young adult mice, with few studies assessing the behavioral effects on mature mice. Here we show improvements in various hippocampal-dependent pattern separation tasks when irradiating mice at 6 months of age. As increasing the age has lead to unexpected behavioral results previously not reported, more work is needed to clarify the broader implications of these data. Specifically, these finding highlight the important consideration that must be given to age when evaluating the impact space radiation has on the CNS during future deep space missions.

Chapter 3, Figures

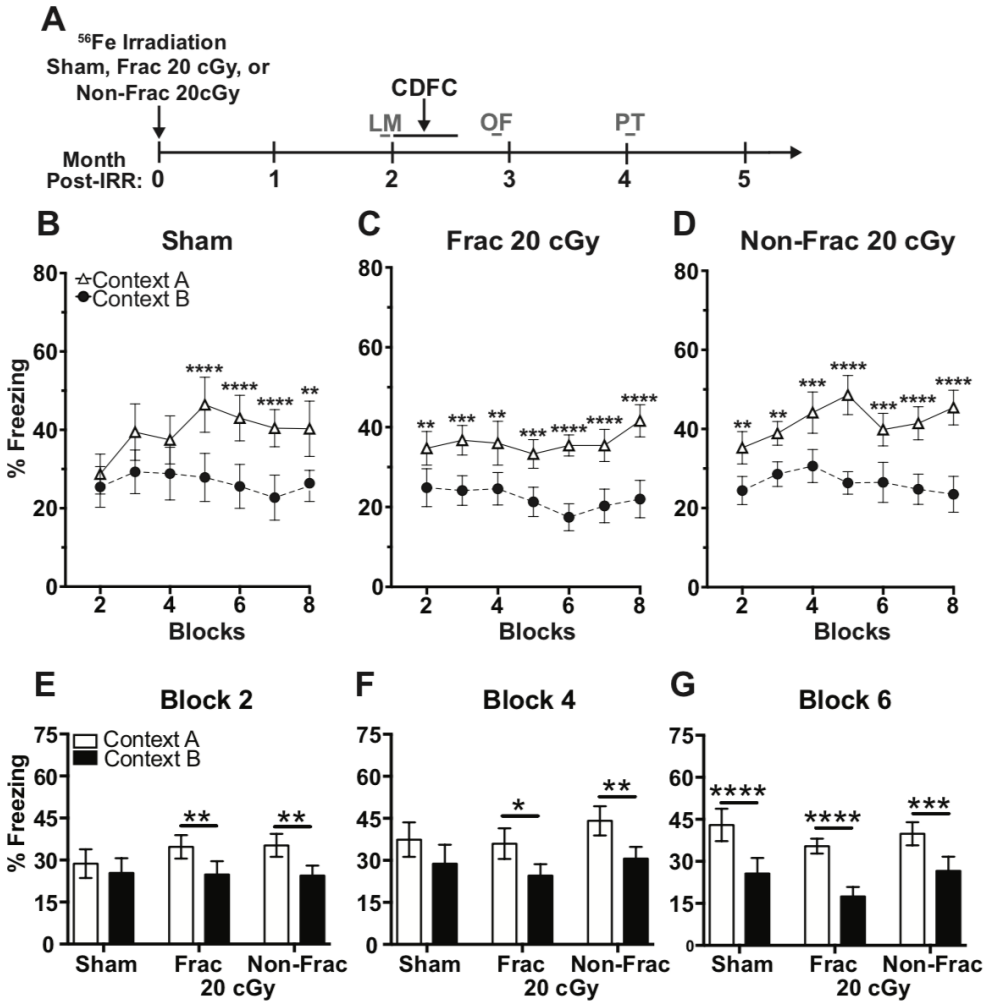

Figure 3-1. On an aversive contextual discrimination fear conditioning (CDFC) task, mice exposed to whole body ^{56}Fe irradiation (IRR) at 6-month of age discriminate two contexts earlier than mice exposed to Sham IRR. (A) Timeline of mouse exposure to whole-body Sham IRR or ^{56}Fe (600 MeV/n, LET 174 KeV/μ) - Sham 0 cGy, Fractionated (Frac 20 cGy) 3x6.7 cGy, and Non-Fractionated (Non-Frac 20 cGy) 1x20 cGy - and subsequent testing in CDFC (black arrow and line). Gray text and lines indicate behavioral data provided in Supplemental Figures: Locomotor LM, Open Field OF, Pain Threshold PT. **(B)** Sham mice (N=10) discriminate Context A (shock context)

from Context B (non-shock context) by Block 5. **(C)** Frac 20 cGy mice (N=10) and **(D)** Non-Frac 20 cGy mice (N=9) discriminate Context A from Context B by block 2. **(E-G)** When examined at Block 2 **(E)**, Block 4 **(F)**, and Block 6 **(G)**, Frac and Non-Frac 20 cGy discriminate by Block 2. Mean±SEM. **(B-D)** Two-way repeated measures ANOVA (RM factors Day and Animal), Bonferroni post-hoc tests. **(E-G)** One-way ANOVA, Bonferroni post-hoc tests. ∗P<0.05, ∗∗P< 0.01, ∗∗∗P< 0.001, ∗∗∗∗P< 0.0001.

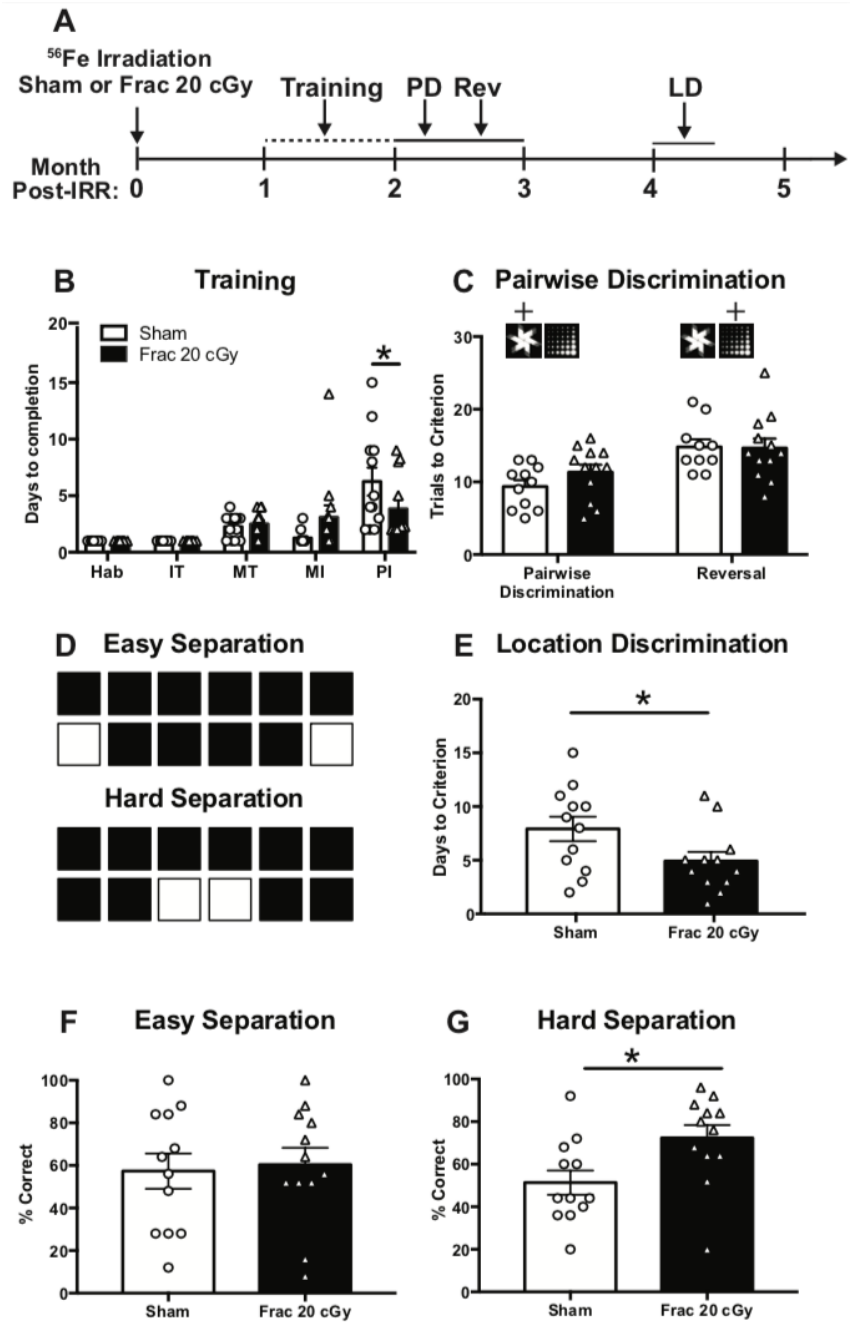

Figure 3-2. On an appetitive touchscreen task, mice exposed to whole body ^{56}Fe IRR at 6-month of age distinguish two similar visual cues earlier and with greater percent correct than mice exposed to Sham IRR. (A) Timeline of mouse exposure to whole body Sham IRR or ^{56}Fe (600 MeV/n, LET 174 KeV/μ) and subsequent testing on touchscreen platform for Pairwise Discrimination (PD) training, PD testing, PD reversal

(Rev), and location discrimination (LD). **(B)** Sham and ^{56}Fe IRR mice performed similarly in the 4 first steps of the 5 PD training stages, including Habituation (Hab), Initiate Touch (IT), Must Touch (MT), and Must Initiate (MI). However, ^{56}Fe IRR mice completed the punish incorrect (PI) stage of PD training faster than Sham **(B)**. **(C)** Sham and ^{56}Fe IRR mice performed similarly in the hippocampal-dependent but context-independent Pairwise Discrimination task, and in the cognitive flexibility hippocampal-dependent Reversal task. **(D)** Sample Easy and Hard separation images used for the hippocampal-dependent pattern separation task, Location Discrimination (LD). **(E)** Surprisingly, ^{56}Fe IRR mice completed the LD task faster than Sham. **(F, G)** Additionally, Sham and ^{56}Fe IRR mice performed similarly during the “Easy Separation” display, but the ^{56}Fe IRR mice had higher accuracy compared to Sham when presented the “Hard Separation” display. Mean±SEM. Unpaired, two-tailed, t test, ✱P<0.05.

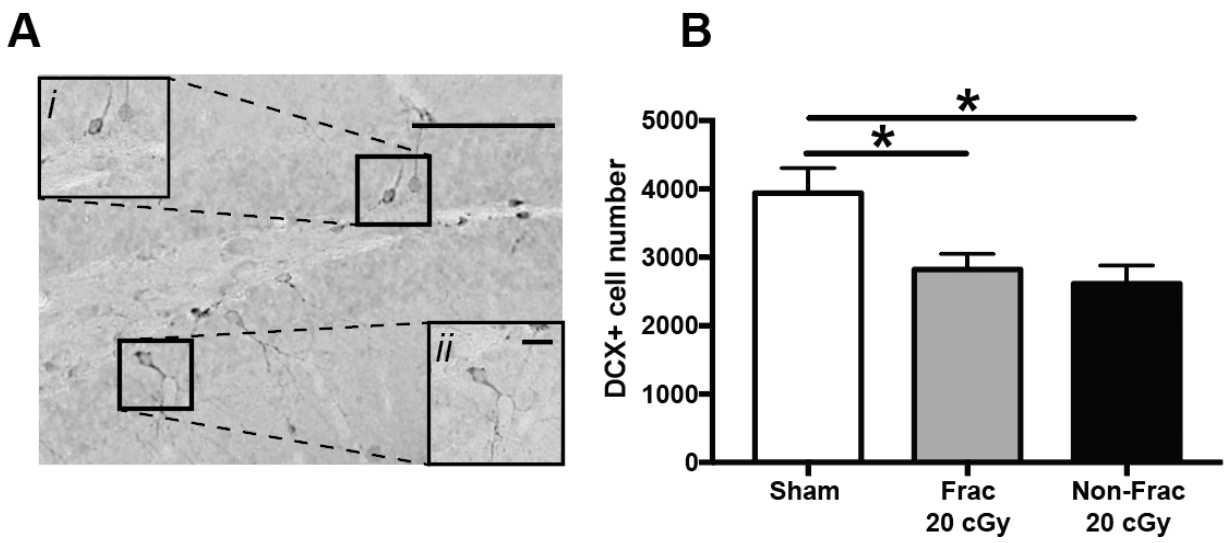

Figure 3-3. Stereological quantification reveals fewer immature dentate gyrus neurons (DCX+ cells) 4 months post-whole body ^{56}Fe particle radiation. (A) Representative photomicrograph of DCX+ cell in the mouse dentate gyrus subgranular zone. Inset: higher magnification of boxed area in main image. Scale bar=XX. **(B)** Relative to Sham mice, Frac 20 cGy and Non-Frac 20 cGy ^{56}Fe mice have fewer DCX+ dentate gyrus subgranular zone cells (N's=10, 10, 9). Mean±SEM. Two-way ANOVA, Bonferroni posthoc. ✱P<0.05.

Chapter 3, Statistics tables

Subject	Figure	n	Mean							
Sham Context Dependent Fear Conditioning (CDFC)	1B	10	Block	2	3	4	5	6	7	8
			Context A	28.71	39.43	37.43	46.43	43	40.43	40.29
			Context B	25.43	29.29	28.86	27.86	25.57	22.71	25.71
Fractionated (Frac) CDFC	1C	10	Block	2	3	4	5	6	7	8
			Context A	34.71	36.71	36	33.29	35.43	35.43	41.57
			Context B	24.86	24.14	24.57	21.28	17.43	20.29	22
Non-Fractionated (Non-Frac) CDFC	1D	9	Block	2	3	4	5	6	7	8
			Context A	35.24	38.89	44.13	48.57	39.84	41.43	45.4
			Context B	24.44	28.57	30.64	26.35	26.51	24.76	23.49
CDFC Block 2 across Treament	1E	Sham: 10 Frac 20 cGy: 10 Non-Frac 20 cGy: 9	Block	Sham	Frac 20 cGy	Non-Frac 20 cGy				
			Context A	28.71	34.71	35.24				
			Context B	25.43	24.86	24.44				
CDFC Block 4 across Treament	1F	Sham: 10 Frac 20 cGy: 10 Non-Frac 20 cGy: 9	Block	Sham	Frac 20 cGy	Non-Frac 20 cGy				
			Context A	37.43	36	44.13				
			Context B	28.86	24.57	30.64				
CDFC Block 6 across Treament	1G	Sham: 10 Frac 20 cGy: 10 Non-Frac 20 cGy: 9	Block	Sham	Frac 20 cGy	Non-Frac 20 cGy				
			Context A	43	35.43	39.84				
			Context B	25.57	17.43	26.51				
Operant Training	2B	Sham: 12 Frac 20 cGy: 12	Training Stage	HAB	IT	MT	MI	PI		
			Sham	1	1	2.25	1.25	6.25		
			Frac 20 cGy	1	1	2.5	3.083	3.833		
Pairwise Discrimination (PD)	2C	Sham: 12 Frac 20 cGy: 12		PD						
			Sham	9.364 ± 0.887						
			Frac 20 cGy	11.33 ± 1.04						
PD Reversal (Rev)	2C	Sham: 12 Frac 20 cGy: 12		Rev						
			Sham	14.8 ± 1.083						
			Frac 20 cGy	14.67 ± 1.305						
Location Discrimination (LD)	2E	Sham: 12 Frac 20 cGy: 12		LD (Mean ± SEM)						
			Sham	7.917 ± 1.145						
			Frac 20 cGy	4.917 ± 0.8569						
LD Easy Separation	2F	Sham: 12 Frac 20 cGy: 12		Easy						
			Sham	57.33 ± 8.288						
			Frac 20 cGy	60.33 ± 7.961						
LD Hard Separation	2G	Sham: 12 Frac 20 cGy: 12		Hard						
			Sham	51.33 ± 5.675						
			Frac 20 cGy	72.33 ± 6.059						
DCX cell counts 56Fe Mature	3B	Sham: 10 Frac 20 cGy: Non-Frac 20	Sham	3942						
			Frac 20 cGy	2825						
			Non-Frac	2614						

Subject	Figure	Statistics (variables)	Main Effect or	F Value	P value	Post hoc Test	Post hoc Results							
Sham Context Dependent Fear Conditioning (CDFC)	1B	ANOVA (Block X Context), two repeated measures (Block and Context)	Blocks	F (6, 54) = 3.106	P=0.0110	Bonferroni	Block	2	3	4	5	6	7	8
			Context	F (1, 9) = 38.45	P=0.0002		Context A vs.B	ns	ns	ns	****	****	****	**
			Interaction:	F (6, 54) = 2.478	P=0.0344			>0.9999	0.0518	0.1563	<0.0001	<0.0001	<0.0001	0.0014
Fractionated (Frac) CDFC	1C	ANOVA (Block X Context), two repeated measures (Block and Context)	Blocks	F (6, 54) = 0.8698	P=0.5232	Bonferroni	Block	2	3	4	5	6	7	8
			Context	F (1, 9) = 137.8	P<0.0001		Context A vs.B	**	***	**	***	****	****	****
			Interaction: Blocks x Context	F (6, 54) = 1.584	P=0.1698			0.008	0.0004	0.0014	0.0007	<0.0001	<0.0001	<0.0001
Non-Fractionated (Non-Frac) CDFC	1D	ANOVA (Block X Context), two repeated measures (Block	Blocks	F (6, 48) = 2.239	P=0.0551	Bonferroni	Block	2	3	4	5	6	7	8
			Context	F (1, 8) =	P=0.0005		Context A vs.B	**	**	***	****	***	****	****
				F (6, 48) =	P=0.0135			0.0027	0.0045	0.0001	<0.0001	0.0001	<0.0001	<0.00
CDFC Block 2 across Treament	1E	ANOVA (Treatment x Context), one repeated measure (Context)	Interaction	F (2, 26) = 1.917	P=0.1673	Bonferroni	Block	Sham	Frac 20 cGy	Non-Frac 20 cGy				
			Treatment	F (2, 26) =	P=0.8738		Context A vs.B	ns	**	**				
			Context	F (1, 26) =	P<0.0001			0.8114	0.0069	0.005				
			Subjects (matching)	F (26, 26) = 8.519	P<0.0001									
CDFC Block 4 across Treament	1F	ANOVA (Treatment x Context), one repeated measure (Context)	Interaction	F (2, 26) = 0.3829	P=0.6857	Bonferroni	Block	Sham	Frac 20 cGy	Non-Frac 20 cGy				
			Treatment	F (2, 26) =	P=0.6222		Context A vs.B	ns	*	**				
			Context	F (1, 26) =	P<0.0001			0.1113	0.0209	0.0088				
			Subjects (matching)	F (26, 26) = 6.533	P<0.0001									
CDFC Block 6 across Treament	1G	ANOVA (Treatment x Context), one repeated measure (Context)	Interaction	F (2, 26) = 0.8509	P=0.4386	Bonferroni	Block	Sham	Frac 20 cGy	Non-Frac 20 cGy				
			Treatment	F (2, 26) =	P=0.3953		Context A vs.B	****	****	***				
			Context	F (1, 26) =	P<0.0001			<0.0001	<0.0001	0.0002				
			Subjects (matching)	F (26, 26) = 10.49	P<0.0001									
Operant Training	2B	ANOVA (Treatment x Training Stage), one repeated measure (Training Stage)	Interaction	F (4, 88) = 3.169	P=0.0175	Bonferroni	Treatment	Hab	IT	MT	IT	PI		
			Training	F (4, 88) =	P<0.0001		Sham vs. Frac 20 cGy	ns	ns	ns	ns	*		
			Treatment	F (1, 22) = 0.03139	P=0.8610			>0.9999	>0.9999	>0.9999	0.1673	0.027		
			Subjects (matching)	F (22, 88) = 0.971	P=0.5076									
Pairwise Discrimination (PD)	2C	Student's T-test (Treatment)	Treatment	0.168		NA								
PD Reversal (Rev)	2C	Student's T-test (Treatment)	Treatment	0.940		NA								
Location Discrimination (LD)	2E	Student's T-test (Treatment)	Treatment	0.048		NA								
LD Easy Separation	2F	Student's T-test (Treatment)	Treatment	0.797		NA								
LD Hard Separation	2G	Student's T-test (Treatment)	Treatment	0.019		NA								
DCX cell counts 56Fe Mature	3B	ANOVA (Treatment)	Treatment	F (2, 26) = 5.863	P=0.0079	Bonferroni	Sham vs. Frac 20	*	0.0347					
							Sham vs. Non-Frac	*	0.0124					
							Frac 20 cGy vs. 100	ns	>0.9999					

Table 3-1 Statistical results; CDFC, Touchscreen training, PD, LD, and DCX+ cell counts Statistical analysis for each test are listed above with significance set at p≤0.05 (bold). Abbreviation not defined in table: Fractionation, Frac; Habituation, Hab; Initial Touch, IT; Must Initiate, MI; Must Touch, MT; Punish Incorrect, PI.

Chapter 3, Supplemental Figures

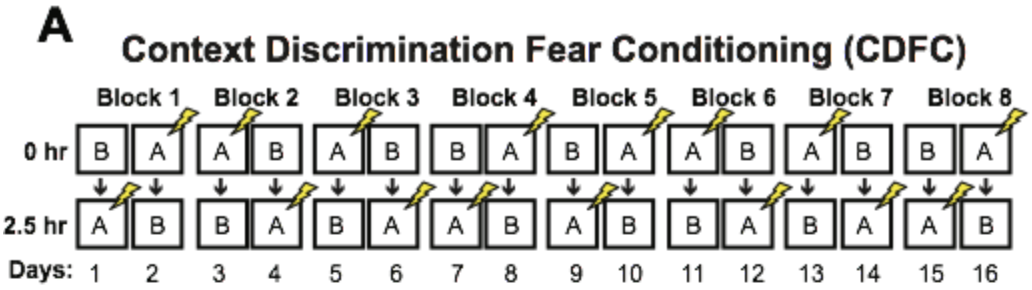

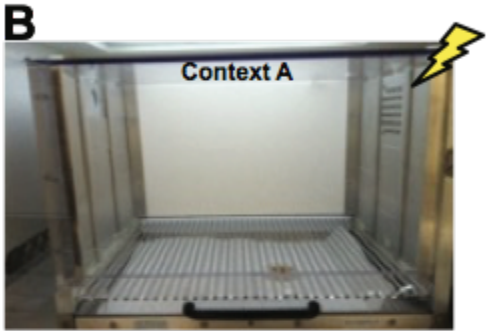

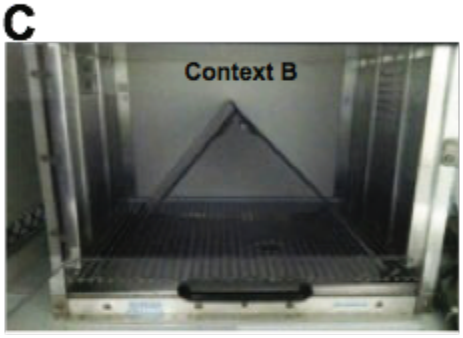

D

Context Discrimination Fear Conditioning (CDFC)

Parameter	Chamber A	Chamber B
Chamber Characteristic:		
Wall Shape	Standard	Triangular
Lighting	White light	Infrared
Odor	Vanilla	Mint
Floor	Grid bars	Grid bars
Holding Cage	Bedding	Paper towel
Shock Amplitude	0.25 mA	NA
Number of Shocks	1	0
Shock Length	2 sec	NA
Latency to Shock	3 min	NA
Length of Paradigm	4 min	4 min

Supplemental Figure 3-1. Contextual Discrimination Fear Conditioning (CDFC) paradigm. (A) Photographs of Context A (paired with mild foot shock) and **(B)** Context B (no shock). **(C)** Sixteen-day CDFC paradigm depicting daily, randomized placement

into Context A (shock-paired, indicated by yellow lightning bolt) and the contextually-similar Context B (no shock). **(D)** Parameters of Contexts A and B for CDFC.

A

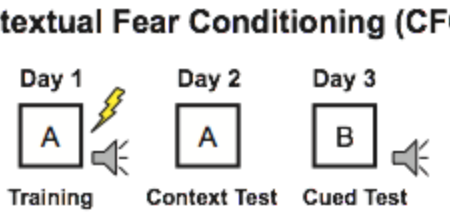

B

Contextual Fear Conditioning			
Parameter	**Training**	**Context Test**	**Cued Test**
Chamber Characteristic:			
Wall Shape	Standard	Standard	Triangular
Lighting	White light	White light	White light
Odor	None	None	Vanilla
Floor	Grid bars	Grid bars	Plastic floor
Shock Amplitude	0.50 mA	NA	NA
Number of Shocks	2	0	0
Shock Length	2 sec	NA	NA
Latency to First Shock	2.5 min	NA	NA
Interval Between Shocks	1.5 min	NA	NA
Auditory Sound	30 sec white noise	NA	3 min white noise
Total Test Time	5 min	5 min	6 min

Supplemental Figure 3-2. Contextual fear conditioning (CFC) paradigm. (A) Mice are placed in novel context which is paired with a cue (auditory tone, Day 1) and followed by testing in context and then additional novel context for cue testing. **(B)** Parameters of the training/testing in CFC.

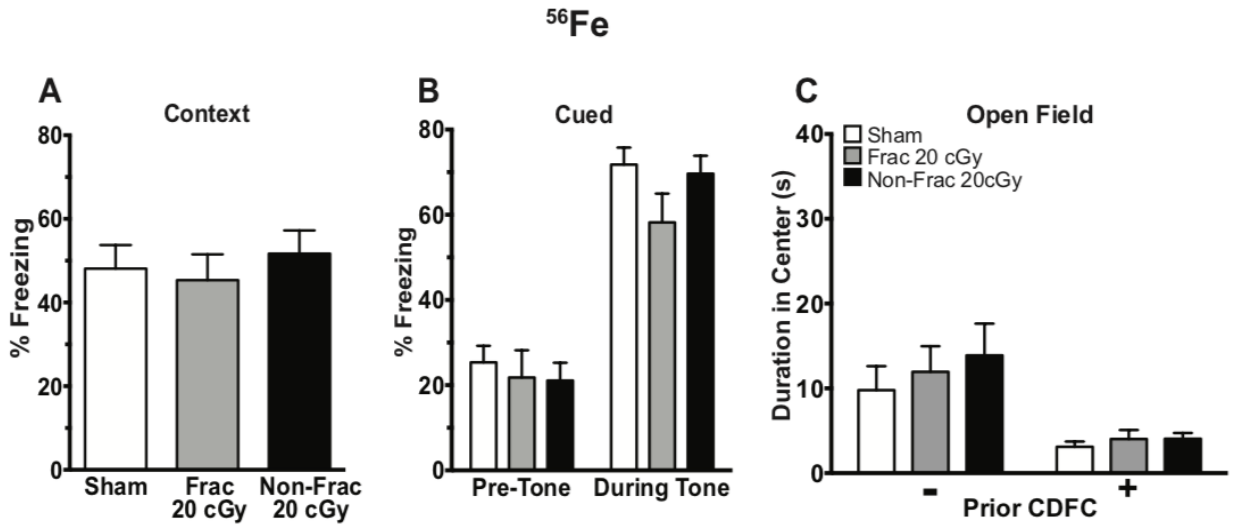

Supplemental Figure 3-3. CFC and anxiety are unaffected in mice exposed to whole body Fractionated (Frac) or Non-Fractionated (Non-Frac) ^{56}Fe radiation. Percent freezing in response to context **(A)** or cue **(B)** in the CFC test and time spent in the center of arena in the open field test **(C)** reveals a lack of effect with ^{56}Fe radiation. Rodents who did not receive CDFC testing (-) were compared to rodents with prior shock experience (+) to ensure prior CDFC exposure did not affect duration in center (s) across treatment **(C)**. Mean±SEM. Two-way ANOVA

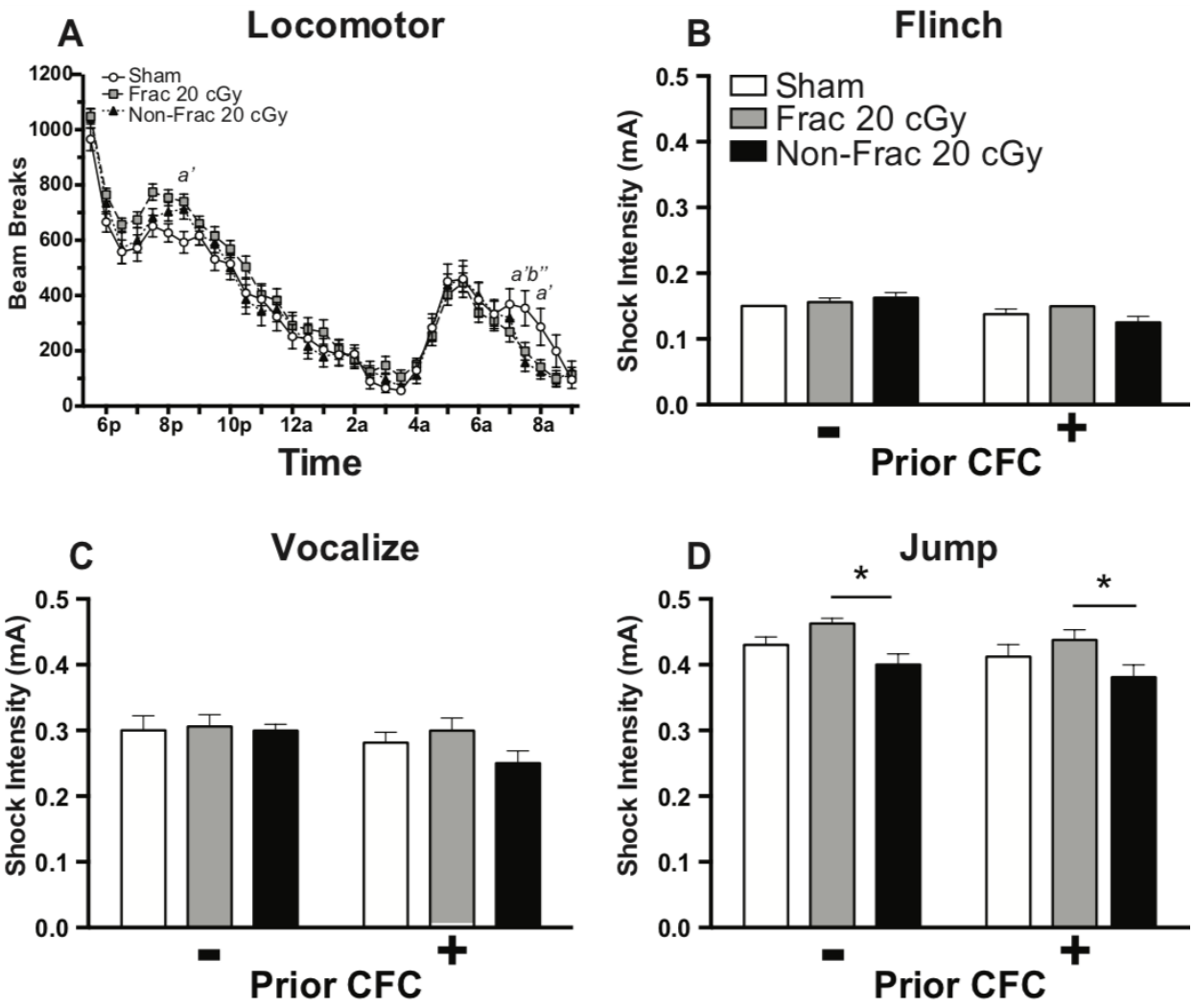

Supplemental Figure 3-4. Supplemental Figure 4. Locomotion and pain threshold are generally unaffected in mice exposed to whole body Frac or Non-Frac ^{56}Fe radiation in maturity. Locomotor activity measured in 30 minute bins **(A)**, and measurements for flinch **(B)**, vocalize **(C)**, and jump **(D)** in the pain threshold test reveal no gross changes after exposure to Sham or ^{56}Fe radiation. Rodents who did not receive CFC testing (-) were compared to rodents with prior shock experience (+) to ensure prior CFC exposure did not affect pain thresholds **(B-D)**. Mean±SEM. Two-way ANOVA, Bonferroni's post-hoc analysis. ✱ or ' P<0.05, '' P<0.01 main effect; a P<0.05, post-hoc Sham vs Frac; b P<0.05, post-hoc Sham vs Non-Frac.

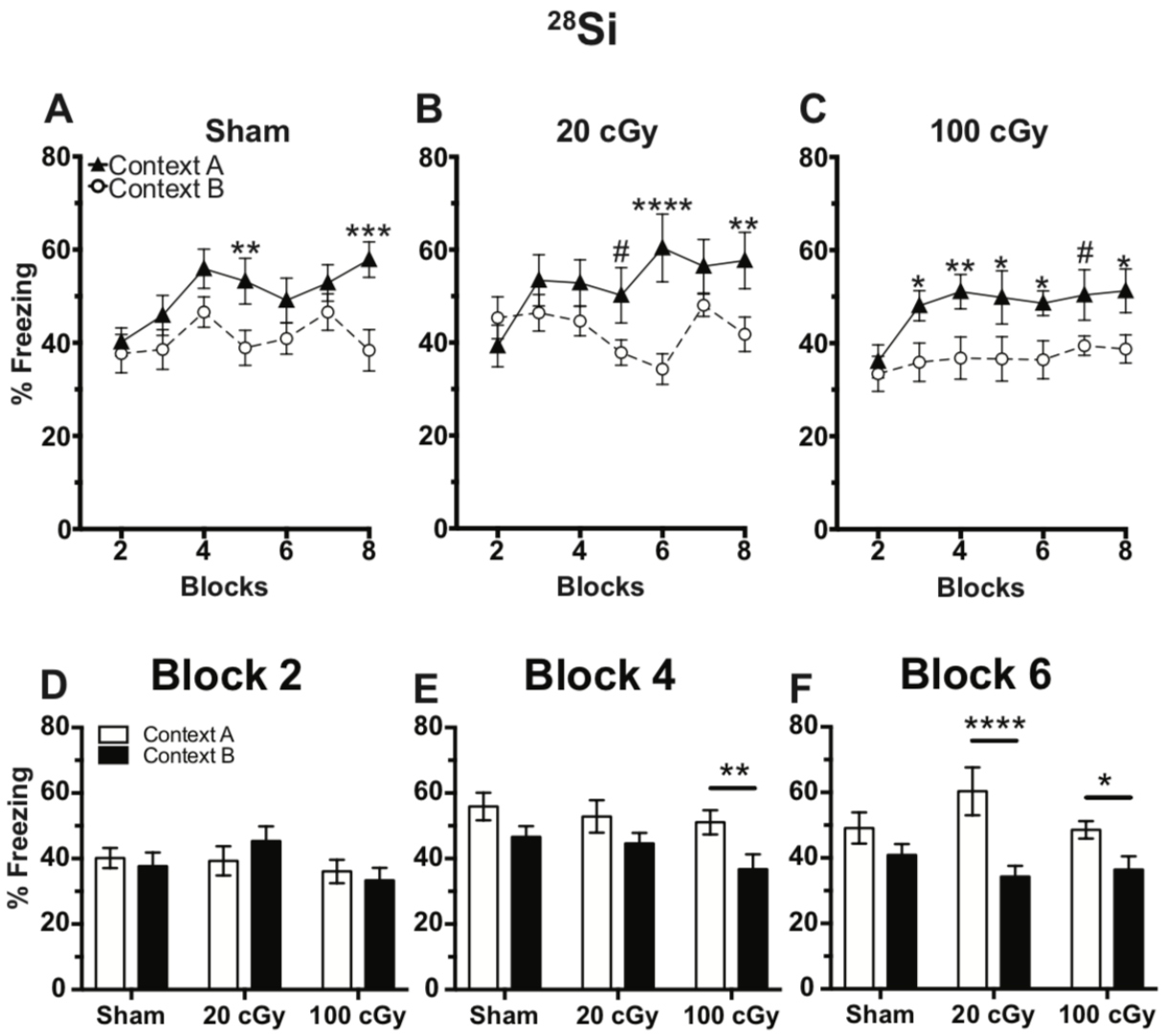

Supplemental Figure 3-5. On an aversive fear conditioning task, mice exposed to ^{28}Si irradiation (IRR) at 7-month of age discriminate two contexts faster and more consistently than mice exposed to Sham IRR. (A) Data are 2-day blocks from CDFC Days 3-16. Sham (**A**, N=8) and 20cGy (**B**, N=8) ^{28}Si IRR mice discriminate the shock-paired context (Context A; black triangle, solid line) from a highly-similar context (Context B; open circle, dotted line) by block 5, while 100cGy (**C**, N=8) ^{28}Si IRR mice discriminate earlier and more consistently. Mean±SEM. Two-way repeated measures

ANOVA, Bonferroni. #p<0.06 ∗P<0.05, ∗∗<0.01, ∗∗∗<0.001, ∗∗∗∗<0.0001, #P<0.06.

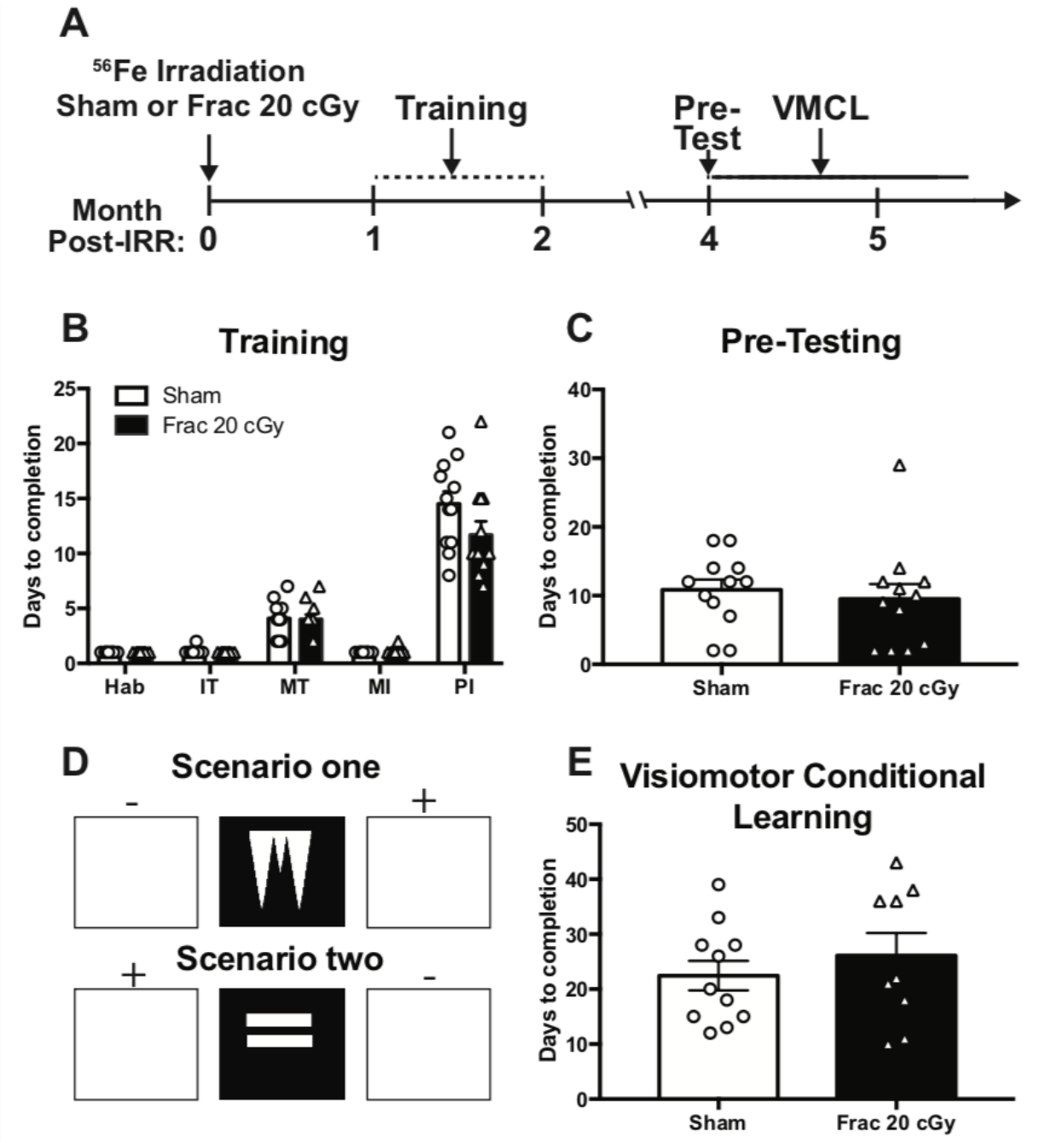

Supplemental Figure 3-6. On an appetitive touchscreen task, mice exposed to ^{56}Fe IRR at 6-month of age show no changes in rule based learning. Timeline of mouse exposure to whole body Sham IRR or ^{56}Fe (600 MeV/n, LET 174 KeV/μ) **(A)** and subsequent testing on touchscreen platform for Visiomotor Conditional Learning (VMCL) training **(B)**, VMCL pre-testing **(C)**, and VMCL **(E)**. Sham and ^{56}Fe IRR mice

performed similarly in the 4 first stages of the 5 VMCL training stages **(B)**. However, statistic reveal a trend for ^{56}Fe IRR mice to complete the punish incorrect (PI) stage of PD training faster than Sham. The VMCL reward paradigm is shown in **(D)** but there is no effect of treatment on rule based learning **(E)**.

Chapter 3, SUPPLEMENTARY STATS TABLE

Subject	Figure	n		Mean									Statistics (variables)	Main Effect or Interaction	F Value	P value	Post hoc Test	Post hoc Results							
Contextual Fear Conditioning (CFC) 56Fe Mature, Context	Supp. 3A	Sham: 8 Frac 56Fe: 8 Non-Frac 56Fe: 8	Sham Frac 56Fe Non-Frac 56Fe	48.09 45.34 51.89									ANOVA (Treatment)	Treatment	F(2,21) = 0.3035	P=0.7414	NA								
Contextual Fear Conditioning (CFC) 56Fe Mature, Cue	Supp. 3B	Sham: 8 Frac 56Fe: 8 Non-Frac 56Fe: 8	Session Pre-Tone During-Tone	Sham 25.36 71.79	Frac 56Fe 21.79 58.21	Non-Frac 56Fe 21.07 69.65							ANOVA (Treatment x Session), one repeated measure (Session)	Interaction **Session** Treatment Subjects	F(2,21) = 0.8047 **F (1,21) = 110.2** F(2,21) = 1.514 F(21,21)	P=0.4605 **P<0.0001** P=0.2430 P=0.5479	Bonferroni	Session Pre-Tone vs. During Tone	Sham <0.0001	Frac 56Fe 0.0002	Non-Frac 56Fe <0.0001					
Open field Time in center Prior CDFC (-)	Supp. 3C	Sham: 13 Frac 56Fe: 32 Non-Frac 56Fe: 16		9.76 11.95 13.89									ANOVA (Treatment x Stress), one repeated measure (Session)	Interaction Stress Treatment	F(2,84) = 0.08763 **F(1,84) = 7.524** F(2,84) = 0.226	P=0.9162 **P=0.0074** P=0.7982	NA								
Open field Time in center Prior CDFC (+)	Supp. 3C	Sham: 10 Frac 56Fe: 10 Non-Frac 56Fe: 9		3.102 4.021 4.058																					

Locomotor	Supp. 4A	Sham: 25 Frac 56Fe: 42 Non-Frac 56Fe: 28	Avg all each time not shown Avg all each time not shown	ANOVA (Time x Treatment), one repeated measure	Interaction Time Treatment	F (62, 2852) = 1.567 F (31, 2852) = 130.3 F (2, 92) = 0.7391	P=0.03 P=<0.0001 P=0.480	post hoc data not shown																		
Flinch Response on Pain Threshold test	Supp. 4B	Sham: (-)4, (+) 8 Frac 56Fe: (-) 8, (+) 8 Non-Frac 56Fe: (-) 8, (+) 8	Prior CFC	Sham		Frac 56Fe		Non-Frac 56Fe					ANOVA (Treatment x Stress),	Interaction Treatment **Stress**	F(2,39) = 2.852 F(2,39) = 1.193 **F(1,39) = 10.18**	P=0.0698 P=0.3142 **P=0.0028**	NA								
			-	0.15		0.1563		0.1625																	
			(+)	0.1375		0.15		0.125																	
Vocalize Response on Pain Threshold test	Supp. 4C	Sham: (-)4, (+) 8 Frac 56Fe: (-) 8, (+) 8 Non-Frac 56Fe: (-) 8, (+) 8	Prior CFC	Sham		Frac 56Fe		Non-Frac 56Fe					ANOVA (Treatment x Stress),	Interaction Treatment Stress	F(2,39) = 0.36031 F(2,39) = 1.425 F(1,39) = 3.061	P=0.4136 P=0.2527 P=0.0881	NA								
			-	0.3		0.3063		0.3																	
			(+)	0.2813		0.3		0.25																	
Jump Response on Pain Threshold test	Supp. 4D	Sham: (-)4, (+) 8 Frac 56Fe: (-) 8, (+) 8 Non-Frac 56Fe: (-) 8, (+) 8	Prior CFC	Sham		Frac 56Fe		Non-Frac 56Fe					ANOVA (Treatment x Stress),	Interaction **Treatment** Stress	F(2,39) = 0.33182 **F(2,39) = 7.44** F(1,39) = 2.399	P=0.9687 **P=0.0018** P=0.1295	Bonferroni	Treatment Stress (-) Stress (+)	Sham vs Frac 0.5943 0.7735	Sham vs Non-Frac 0.7023 0.4774	Frac vs Non-Frac 56Fe **0.0198** **0.0409**					
			-	0.43		0.4625		0.4																	
			(+)	0.4125		0.4375		0.3813																	

28Si Sham Context Dependent Fear Conditioning (CDFC)	Supp. 5B	8	Block	2	3	4	5	6	7	8	ANOVA (Block X Context), two repeated measures (Block and Context)	**Blocks** **Context** Interaction: Block x Context	**F(6, 42) = 4.152** **F(1,7) = 12.51** F(6, 42) = 1.937	**P=0.0023** **P=0.0095** P=0.0970	Bonferroni	Block Context A vs.B	2 ns >0.9999	3 ns 0.532	4 ns 0.182	5 ****** **0.0067**	6 ns 0.3328	7 ns 0.8953	8 ******* 0.0001
			Context A	40.18	45.89	55.89	53.22	49.11	52.86	57.86													
			Context B	37.68	38.57	46.61	38.93	40.89	46.61	38.39													
28Si 20 cGy CDFC	Supp. 5C	8	Block	2	3	4	5	6	7	8	ANOVA (Block X Context), two repeated measures (Block and Context)	Blocks **Context** **Interaction: Block x Context**	F(6, 42) = 2.27 **F (1,7) = 9.797** **F (6, 42) = 4.779**	P=0.0548 **P=0.0166** **P=0.0009**	Bonferroni	Block Context A vs.B	2 ns >0.9999	3 ns 0.8826	4 ns 0.5093	5 ns 0.0596	6 ******** **<0.0001**	7 ns 0.4686	8 ****** **0.0065**
			Context A	39.29	53.39	52.86	50.18	60.36	56.43	57.68													
			Context B	45.36	46.43	44.64	37.86	34.29	48.04	41.79													
28Si 100 cGy CDFC	Supp. 5D	8	Block	2	3	4	5	6	7	8	ANOVA (Block X Context), two repeated measures (Block and Context)	Blocks **Context** **Interaction: Block x Context**	**F(6, 42) = 2.777** **F (1,7) = 16.68** F (6, 42) = 0.979	**P=0.0229** **P=0.0047** P=0.4514	Bonferroni	Block Context A vs.B	2 ns >0.9999	3 * **0.0237**	4 ** **0.005**	5 * **0.011**	6 * **0.0237**	7 # 0.0557	8 * **0.0184**
			Context A	36.07	48.04	51.07	49.82	48.57	50.36	51.25													
			Context B	33.39	35.89	36.79	36.61	36.43	39.47	38.75													

28Si CDFC Block 2 across Treatment	Supp. 5E	Sham: 8 20 cGy: 8 100 cGy: 8	Block	Sham		20 cGy		100 cGy			ANOVA (Treatment x Context), two repeated measure	Interaction Treatment Context Subjects	F(2,21) = 0.4187 F(2,21) = 0.2147 F(1,21) = 0.9225 F(21,21) = 0.2668	P=0.4187 P=0.2147 P=0.9225 P=0.2668	NA								
			Context A	40.18	45.89	55.89	53.22	49.11	52.86	57.86													
			Context B	37.68	38.57	46.61	38.93	40.89	46.61	38.39													
28Si CDFC Block 4 across Treatment	Supp. 5F	Sham: 8 20 cGy: 8 100 cGy: 8	Block	Sham		20 cGy		100 cGy			ANOVA (Treatment x Context), two repeated measure	Interaction Treatment **Context** **Subjects**	F(2,21) = 0.5541 F(2,21) = 0.3334 **F(1,21) = 0.0002** F(21,21) = 0.1253	P=0.5541 P=0.3334 **P=0.0002** **P=0.0120**	Bonferroni	Treatment Context A vs.B	Sham ns 0.1096	20 cGy ns 0.1845	100 cGy ****** **0.0074**				
			Context A	46.61		44.64		36.79															
			Context B	55.89		52.86		51.07															
28Si CDFC Block 6 across Treatment	Supp. 5G	Sham: 8 20 cGy: 8 100 cGy: 8	Block	Sham		20 cGy		100 cGy			ANOVA (Treatment x Context), two repeated measure	Interaction Treatment **Context** **Subjects**	F(2,21) = 0.6859 F(1,21) = **F(1,21) = 0.0001** F(21,21) = **P=0.9932**	P=0.6859 **P=0.0001** **P=0.9932**	Bonferroni	Treatment Context A vs.B	Sham ns 0.2605	Frac 20 cGy ******** **<0.0001**	Non-Frac 20 cGy ***** **0.0444**				
			Context A	49.11		48.57		48.57															
			Context B	40.89		34.29		36.43															

VMCL Training	Supp. 6B	Sham: 12 Frac 20 cGy: 12	Training Stage Sham Frac 20 cGy	Hab 1	IT 1.08 1	MT 4.08 4	MI 1 1.08	PI 14.5 11.67	ANOVA (Treatment x Training Stage), one repeated measure (Training Stage)	*Interaction* **Training** Treatment Subjects	*F (4, 88) = 2.273* **F(4, 88) = 11.22** F (1, 22) = 0.7881	*P=0.0677* **P<0.0001** P=0.0866 P=0.7672	NA
Pre-testing	Supp. 6C	Sham: 12 Frac 20 cGy: 12	Rev (Mean ± SEM) 10.83 ± 1.512 9.5 ± 2.183						Student's T-test (Treatment)	Treatment	0.621		NA
Visiomotor conditional learning (VMCL)	Supp. 6E	Sham: 11 Frac 20 cGy: 9	Rev (Mean ± SEM) 22.45 ± 2.888 26.11 ± 4.114						Student's T-test (Treatment)	Treatment	0.452		NA

Table 3-2 Supplementary statistical results; all supplementary data. Statistical analysis for each test are listed above with significance set at p≤0.05 (bold). Abbreviation not defined in table: Fractionation, Frac; Habituation, Hab; Initial Touch, IT; Must Initiate, MI; Must Touch, MT; Punish Incorrect, PI.

Chapter 3, Supplemental Methods

Locomotor Activity (LM, ***Supp. Fig. 3-4****).* Within 2 months post-IRR (^{56}Fe experiments: 59 days post-IRR; ^{28}Si experiments: 49 days post-IRR), most mice underwent a single locomotor activity recording session from 5pm-9am under red light. After 1-hr acclimation to the testing suite, group-housed mice were individually placed into clean standard cages and were given *ad libitum* food and water. Beam breaks were recorded over 16 hrs using the Photobeam Activity System-Home Cage (San Diego Instruments; San Diego, CA). Data were collapsed into 30-min bins across the 16-hr session, and are presented as number of beam breaks. At the completion of recording, mice were placed back to their original group-housed cage and returned to their normal housing room.

Open Field (OF, ***Supp. Fig. 3-3****).* Mice were placed in a novel open field environment (W 44 cm x L 44 cm x H 30 cm) in a dimly lit room (60 lux) and allowed to explore for 10 min. Mice were monitored from above by a video camera and Ethovision video tracking software (Noldus, Leesburg, VA) to determine the duration of time spent in the center (W 14 cm x L 14 cm). After testing, the open field arenas were cleaned and allowed to dry between mice. Data are presented as duration of time spent in center of field, although distance traveled was also collected (data not shown).

Pain Threshold (PT, ***Supp. Fig. 3-4****).* Mice were individually placed into boxes equipped with a metal grid floor connected to a scrambled shock generator (Med Associates Inc., St. Albans, VT). After ~1 min, mice received a series of foot shocks (each 2-sec

duration) with increasing intensity. The initial shock intensity was 0.05 mA, and the amplitude was increased by 0.05 mA for each consecutive foot shock with a 15-sec intershock interval. The first shock intensity at which each animal displayed each behavior (flinch, vocalization, or jump) is reported. Once the animal displayed all three behaviors, it was removed from the chamber.

Contextual Discrimination Fear Conditioning (CDFC, ***Supp. Fig. 3-1****).* Context A consisted of a standard fear conditioning chamber (Med Associates) outfitted with a grid floor and white overhead house light, was scented with vanilla, and was paired with a shock. Context B consisted of a standard fear conditioning chamber with a grid floor, but with a near-infrared light and a black A-frame insert, was scented with mint, and was not paired with a shock. There were other subtle differences between the contexts. For example, prior to placement into Context A, mice were individually placed into a transfer cage (a standard cage with bedding), and then placed by the tail into Chamber A. After exposure to Context A, the mouse was removed and Context A was cleaned with Coverage Plus NPD solution (Steris, Mentor, OH). In contrast, prior to placement into Context B, mice were individually placed into a transfer cage lined with white paper towels, and each mouse was scooped by hand into both the transfer cage and testing chamber. After exposure to Context B, the mouse was removed and Context B was cleaned with 1% acetic acid. Each twice daily exposure over 16 days lasted 4 minutes and 2 seconds, during which freezing behavior was scored for the first 3 min. Mice in Context A, but not Context B, received a single, mild foot shock (0.25 mA, 2 sec duration) after 3 min in the context. Mice then remained in the chambers for one

additional minute until the session was complete. The interval between daily exposures to Context A or B was 2-2.5 hrs.

Contextual Fear Conditioning (CFC, ***Supp. Figs. 3-2, 3-3)****.* CFC consisted of two phases: training (Day 1), and testing (Day 2-3). Mice were habituated to the behavior room environment 1 hr each day prior to training and testing sessions. On Day 1, mice were trained to associate a novel context (standard fear conditioning chamber, grid flooring, no odor, house lights on; Med Associates Inc., St. Albans, VT) with a shock. Two minutes after placement in the novel context, an auditory cue was played (white noise, 30-sec duration, Med Associates Inc.), which co-terminated with the presentation of a 0.5 mA shock (2-sec duration). This cue-shock pairing was repeated twice during Day 1 (5-min training session), with 1.5 min between the cue-shock presentations. On Day 2, mice underwent context testing: 5 min in the same environment as Day 1 training, but no auditory cue or foot shock presented. On Day 2 (^{28}Si IRR mice, 2 hrs post-context testing) or on Day 3 (^{56}Fe IRR mice) mice underwent auditory cue testing: 6 min in another novel context (plastic flooring, triangular roof, vanilla odor, house lights on), with 3 min of cue followed by 3-min without the cue. For training and testing sessions, freezing behavior was assessed using VideoFreeze software (Med Associates Inc.), compiled for each phase of each session (e.g. Pre-Cue, During Cue, etc.), and presented as percent percent time freezing for each phase.

Food exposure/restriction. In brief, mouse chow (16% protein 2016 Teklad Global Diet, Envigo, Madison,WI) was removed from each cage the 5pm the day prior to training or

testing, and each cage was given *ad libitum* access to chow for 3 hrs (min) to 4 hrs (max) immediately following daily touchscreen training/testing, and from completion of training/testing on Friday until Sunday 5pm. Mice were weighed each Wednesday to ensure weights >80% initial body weight. While weights below this threshold merited removal of the mouse from the study, zero mice reached this threshold (data not shown).

Touchscreen training (Abet 2 software, Cat 89505). Touchscreen training (**Fig. 3-2, Supp. Fig. 3-6**) consisted of 5 steps: Habituation, Initial Touch, Must Touch, Must Initiate, and Punish Incorrect:

Habituation (Hab). Mice are placed in touchscreen chamber for 30-min (max) session with the tray light turned on (LED Light, 75.2 LUX). For the initial reward in each habituation session, a tone is played (70db at 500Hz, 1000 ms) at the same time as a priming reward (150uL Ensure) is dispensed to the chamber tray. After the mouse inserted head and then removed head from tray, the light turns off and a 10-sec delay begins. At the end of the delay, the light is turned on and tone is played again as a standard reward (7uL Ensure) is dispensed. If the mouse's head remains in the tray at the end of the 10-sec delay, an additional 1-sec delay is added. Mice complete Habituation training after they collect 25 rewards (25 x 7 ul) in 30 min. Mice that achieve habituation criteria faster than 30 min are removed from the chamber immediately after their 25th reward in order to minimize extinction learning.

Initial Touch (IT). Drawing from a bank of 40 preselected black and white images (240x240 pixels), a random image is displayed on the screen in a pseudo-random

location such that no image is displayed in that location more than 3 consecutive times. The mouse has 30 sec to touch the image (typically with their nose). If the mouse does not touch the image, the image is removed, a reward (7uL Ensure) is delivered into a lit tray and a tone is played. After the reward is collected, the tray light turns off and a 20-sec intertrial interval begins. If the mouse touches the image on the screen while it is displayed, the image is removed and the mouse receives 3 times the normal reward (21uL Ensure, tray lit, tone played). Mice advance from Initial Touch training after they complete 25 trials (irrespective of reward level received) in 30 min. Mice that achieve Initial Touch criteria faster than 30 min are removed from the chamber immediately after their 25th trial.

Must Touch (MT). Similar to Initial Touch training, a random image is displayed, but now the image remains on the screen until it is touched. If the mouse touches the screen, the mouse receives a reward (7uL Ensure, tray lit, tone played). There is no response (no reward dispensed, no light in tray, no tone) if the mouse touches the blank screen. Mice advance from Must Touch training after they complete 25 trials in 30 min. Mice that achieve Must Touch criteria faster than 30 min are removed from the chamber immediately after their 25th trial.

Must Initiate (MI). Must Initiate training is similar to Must Touch training, but a mouse is now required to initiate the training by placing its head into the already-lit tray. A random image from the image bank will then presented on the screen, and the mouse must touch the image to receive a reward (7uL Ensure, tray lit, tone played). Following the collection of the reward, the mouse must remove its head from the tray and then reinsert its head to initiate the next trial. Mice advance from Must Initiate training after

they complete 25 trials in 30 min. Mice that achieve Must Initiate criteria faster than 30 min are removed from the chamber immediately after their 25th trial.

Punish Incorrect (PI). Punish Incorrect training builds on Must Initiate training, but here if a mouse touches a portion of the screen that is blank (does not have an image), the overhead house light turns on and the image disappears from the screen. After a 5-sec timeout period, the house light turns off, and the mouse has to initiate a correction trial, where the same image appears in the same location on the screen. The correction trials are repeated until mouse successfully presses the image but are not counted towards the final % correct criteria. Mice advance from Punish Incorrect training and onto testing for PD/reversal after they complete 25 trials in 30 min at ≥76% (≥19 correct) for two consecutive days. Mice that achieve Punish Incorrect criteria faster than 30 min are removed from the chamber immediately after their 25th trial.

Visiomotor Conditional Learning (VMCL, ABET software, Cat #89542). For VMCL (**Supp. Fig. 3-6**), mice receive one additional training step, termed VMCL pre-testing, prior to the VMCL test.

VMCL pre-testing is designed to teach the mouse to touch two images on the screen in a specific order and rapid succession. The first touch must be to an image presented in the center of the screen, and the second touch must be to an image presented either on the left or right of the screen. Specifically, after trial initiation, the mouse must touch a center white square (200x200 pixels), which then disappears after touch. A second white square immediately appears on either the left or right side of the screen in a pseudorandom style, such that a square is located on each side 5 out of 10

times, but not more than 3 times in a row. If the mouse selects the location with the second white square, a reward is provided, and a 20-sec inter-trial-interval starts. However, if the mouse selects the location without a square, then the second stimulus is removed, and the house light illuminates for 5 sec to indicate a timeout period which must conclude prior to the 20-sec inter-trial-interval. Then the mouse is presented with a correction trial which must be completed prior to a new set of locations being displayed. VMCL pre-testing is complete when the mouse completes 2 consecutive days of 25 trials in 30 min with >75% correct.

After VMCL pre-testing, mice advance to VMCL testing. As shown in **Supp. Fig. 3-6**, mice are provided with a center black and white image (spike or bars). Once touched, the center image disappears and a white squares appear in both the right and left. For this task, the spike center image signals the rodent should touch the right square and the bar center image designates the rodents should touch the left square. The two center images are presented pseudorandomly for an equal number of times, and the mice have 2 sec to touch the white square on the right or left side of the central image. If they fail to touch the white square within 2 sec, a timeout period begins. The same timeout and inter-trial-intervals are used for VMCL testing as were used for VMCL pre-testing. As with VMCL pre-testing, correction trials are used to protect against side bias. VMCL testing is complete when the mouse completes 2 consecutive days of 25 trials in 30 min with ≥80% correct. Data are reported as days to completion.

CHAPTER 4: UNEXPECTED ENHANCEMENT IN PATTERN SEPARATION FOLLOWING ^{56}FE EXPOSURE IS TRANSIENT IN MALE MICE AND SEX SPECIFIC, YET DISRUPTS RULE-BASED LEARNING IN FEMALE C57BL/6J MICE

Whoolery CW, Torres VO, Reynolds RP, Zuurbier KR, Richardson DR, Desalle M, Yun S, Birnbaum SG, Stowe AM, Eisch AJ. *In preparation*

Abstract

Astronauts traveling to Mars will be exposed to space radiation made up of high-atomic number and -energy (HZE) particles, such as ^{56}Fe. This unavoidable radiation has been tied to decreases in hippocampal function (e.g. learning and memory) in rodents, and raises concerns that space radiation will compromise astronaut health or mission success. However, most data are from young adult male rodents (2 month-old at irradiation [IRR]) which are age-equivalent to teenage humans. In the previous chapter we show that HZE radiation exposure at 6 months of age can improve performance on the hippocampal-dependent pattern separation task in both an appetitive and aversive testing paradigm. To determine if this improvement in pattern separation is transient, mature male mice received whole-body radiation (^{56}Fe) at 6 months of age and pattern separation was evaluated 6 months post-IRR. To determine if this improvement in pattern separation is sex specific, mature female mice received whole-body radiation (^{56}Fe) at 6 months of age and followed a similar appetitive-base behavior testing paradigm as our previous male studies discussed in chapter 3. By providing 6 month recovery time before testing, we show male mice performed similarly in pattern

separation following HZE exposure, suggesting pattern separation improvements are only transient. In contrast, mature irradiated female mice performed similarly in the transient appetitive touchscreen pattern separation tasks but were impaired in a rule-based learning task; for example, female mice took longer to reach criterion than the Sham controls. Taken together, this work highlights the differences sex can play on the cognitive responses to HZE radiation exposure and warrants further investigation.

Introduction

With NASA's goal to reach Mars by 2030 fast approaching (United States. National Aeronautics and Space Administration 2015), more work must be done to understand the risk deep space flight will entail for the central nervous system (CNS), including exposure to high atomic number and energy (HZE) particles that comprise galactic cosmic radiation (GCR) (Jandial et al. 2018). Currently, a large body of literature indicates that much of the effect HZE particles will have on the CNS is detrimental to cognition (Jandial et al. 2018; Cucinotta et al. 2014). Although not necessarily incorrect, this conclusion may be misleading due to the small percentage of studies focusing on rodents at similar age-equivalents to the average astronaut (34 years of age) or studies using appropriate dosing regimens (**Table 1-1)**. For instance, in the previous chapter, our lab found improvements in rodents that were 6 months at the time of irradiation across both aversive and appetitive pattern separation paradigms. Although this was not the first study showing cognitive improvements following HZE exposure (Raber et al. 2015; Raber et al. 2014; Raber et al. 2013), the small body of literature supporting this conclusion leaves questions that will still need to be addressed.

For example, a trip to Mars will include approximately ~400 days of travel - or a little over 6 months each way- with an approximate 540 day stay on the martian surface in between (Cucinotta et al. 2013). Because of this prolonged stay on Mars, it is critical to determine long-term effects to the CNS for mission success. In addition, NASA has been increasing the proportion of woman astronauts with each recruiting class, with 42% (5/12) of the 2017 Astronaut candidates being woman (Whiting 2016). Surprisingly, only 15% (12/80) of CNS related HZE studies include female rodents (**Table 1-1)**.

To address these knowledge gaps and build on our previous data, separate groups of male and female mice were irradiated at 6 months of age. The male mice were then housed for 6 months prior to appetitive pattern separation testing to determine if the improvements in pattern separation persisted long-term. The female mice underwent a similar battery of touchscreen behavior testing, including the appetitive pattern separation task, to determine if the robust improvement to pattern separation seen in males could be seen in female mice.

Interestingly, the data presented indicate that the improvements in pattern separation are only transient in male mice, as the irradiated cohort required a similar number of trials to reach criterion and performed at a similar % correct. In addition, the females did not show any improvements pattern separation but did perform worse at a rule-based touchscreen test. When challenged long-term for their ability to recall the rules, the females performed similarly across treatment, (i.e taking a similar number and having similar accuracy) suggesting a learning (vs memory) impairment. Taken together, those

data highlight the time- and sex-specific effects HZE radiation can have on the CNS, and suggest that female mice might be more susceptible to radiation-induced cognitive decline.

Methods

Animals

Animal procedures and husbandry were in accordance with the National Institutes of Health Guide for the Care and Use of Laboratory Animals, and performed in IACUC-approved facilities at UT Southwestern Medical Center (UTSW, Dallas TX) and Brookhaven National Laboratories (BNL, Upton NY). 2-4-month old male C57BL/6J mice (Jackson Laboratories, stock #000664) were housed at UTSW (males) or the Perelman School of Medicine (females, University of Pennsylvania, Philadelphia PA) and then shipped to BNL for irradiation at 6-months of age. During shipping and housing at BNL, mice were provided Shepherd Shacks (Bio-Serv). Mice were group-housed at UTSW or BNL (3-4/cage, light on 06:00, lights off 18:00, UTSW: room temperature 68-79°F, room humidity 30-70%, BNL: room temperature 70-74°F and room humidity 30-70%). At all facilities, food and water were provided *ad libitum* until testing.

Particle Irradiation (IRR)

Mice received whole body HZE (^{56}Fe, **Figs. 4-1, 4-2, 4-3, 4-4, 4-5)** particle radiation at BNL's NASA Space Radiation Laboratory (NSRL) during the 2016 summer run (male data) and the 2017 spring run (female data). The ^{56}Fe beams were produced by the AGS Booster Accelerator at BNL and transferred to the experimental beam line in the NSRL. Delivered doses were ±0.5% of the requested value. Each day between 18:30

and 15:30, all mice - regardless of whether control (Sham) or experimental - were placed for 15 min in modified clear polystyrene cubes (AMAC Plastics, Cat #100C, W5.8 cm x L5.8 cm x H10.6 cm; modified with ten 5mm air holes). For ^{56}Fe experiments, mice received Sham IRR (placed in cubes Monday, Wednesday, Friday, but received no IRR) or either Fractionated (Frac) 20 cGy ^{56}Fe (600 MeV/n, LET 174 KeV/μ, Dose rate 20 cGy/min; placed in cubes and received 6.7 cGy on Monday, Wednesday, and Friday), or Non-Fractionated (Non-Frac) 20 cGy ^{56}Fe (placed in cubes Monday, Wednesday, and Friday but received 20 cGy only on Friday). Post-IRR, mice were returned to UTSW and housed in quarantine for 4-6 weeks prior to initiation of behavior testing. Body weights were taken multiple times: prior to irradiation, at IRR, and at least monthly (up to weekly) post-IRR until collection of brain tissue (data not shown).

Overview of behavioral testing

All mice began behavior testing 1-2 months post-IRR. Subsets of mice underwent appetitive behavioral tests (operant touchscreen platform: Pairwise Discrimination, PD; Location Discrimination, LD; and Visomotor Conditional Learning, VMCL, and VMCL recall testing; **Fig. 4-1, 4-2, 4-3, 4-4**) as well as general activity (open field, OF, **Fig. 4-5**) and motor function (rotarod, **Fig. 4-5)** as outlined in chapter 3.

Appetitive Behavior Testing. Separate groups of sham and IRR mice were trained on an operant touchscreen platform, an overview of which is provided below.

Touchscreen platform and software. The touchscreen platform used was Model 80614 made by Lafayette Instruments (Lafayette, IN). Each operant chamber is encased in a sound-attenuating chamber. Each chamber is trapezoid-shaped, with the widest wall serving as the “touchscreen (238x170mm WxH)” and the opposite and narrowest wall (46mm W) containing a motion-sensitive center dispenser (tray) to deliver liquid reward (Strawberry Ensure, Abbott Laboratories, Chicago, IL). The touchscreen records IR light and has a delay of 10 millisecond delay from the time of touch to the recording of the computer. The chamber has two lights (tray light, and overhead house light), and is equipped with a speaker (ceiling in each chamber) to play a tone. Aside from initial priming reward used during training, a “reward” is defined as 7uL Ensure delivered to the illuminated tray at the same time as a tone is played. Aside from training sessions, the term “initiate a trial” is defined as the mouse placing its head in the tray when the tray light is illuminated and the tone is played. The two remaining walls of the chamber are infrared-permeable to track rodents during testing. The floor is a perforated metal grid, and the solid roof is hinged for easy placement/removal of animal. A computer outside of the chamber allows recording and running the programs and each animal is tested in their light cycle Monday through Friday until testing was complete..

Food exposure/restriction. Three days prior to touchscreen training, each cage of sham or IRR behaviorally-naive, group-housed mice received daily access home cage to in a volume sufficient to cover the bottom of a 2” plastic petri dish. Touchscreen training/testing occurred Monday through Friday during the light cycle. During touchscreen training and testing, mice were maintained on a food-restricted diet.

Touchscreen training (Abet 2 software, Cat 89505). Touchscreen training (**Fig. 4-1, 4-4**) consisted of 5 steps: Habituation, Initial Touch, Must Touch, Must Initiate, and Punish Incorrect. Latency (days) to complete each training step is reported.

Pairwise Discrimination (PD)/Reversal Testing (ABET2 software, Cat #89540). After training on the touchscreen platform (above), mice went through PD/Reversal training (**Fig. 4-2**). For PD, two images from the image bank that the mice have never seen before are simultaneously presented on the screen (i.e. plane vs. a spider). Only one of the images is rewarded (S+), and the image that is rewarded is counterbalanced within each group of mice. After the mouse initiates the trial, the rewarded image is presented on either the left or right side of the screen. The presentation side is pseudorandomly selected such that the S+ is not presented on the same side more than 3 times in a row. An incorrect choice leads to a correction trial, and the mouse must repeat the trial until it correctly selects the rewarded image displayed in the same location. The correction trial is not counted towards the final percent of trials correct. For Reversal testing, the S+ and S- are switched, and the previously-rewarded S+ image is now no longer rewarded. The mouse performs PD or Reversal testing until it is able to complete 25 trials in 30 min at 80% accuracy for 2 days in a row, and latency (days) to completion is reported.

*Location Discrimination (LD; ABET2 software, Cat #89546-6)***(Fig.4-1, 4-2)**. For LD, mice receive one additional training step, termed LD1-choice, prior to the actual 2-choice LD test (LD2).

For LD 1-choice training, mice initiate the trial, which leads to the display of two identical white squares (25x25 pixels), that are presented with two black squares between them, a separation which is termed “intermediate” in difficulty. One of the location of the squares is rewarded (L+) and the other is not, and the L+ location (left or right) is counterbalanced within groups. On subsequent days, the rewarded square location is switched (becomes L-), then L+, then L-, etc. Once the animal reaches 25 trials in 30 min for 2 consecutive days (i.e. learns to press the right-most and then left-most square on consecutive days), the mouse advances to the LD 2-choice random test.

For the LD 2-choice random (or just LD), mice initiated the trial, which leads to the display of two identical white squares, either with four black squares between them (“easy” separation) or directly next to each other (“hard” separation). Like the LD 1-choice, only one of the square locations (right-most or left-most) is rewarded (L+, same side for both easy and hard separations, and counterbalanced within groups). The rewarded square location is switched the following day, and the location continues to alternate daily throughout training. Each day, the separation (easy vs. hard) is pseudorandomly displayed (same separation shown no more than 3 consecutive times). LD testing is complete when the mouse completes 50 trials in 30 min. For LD testing, latency (days) to complete the test **(Fig. 4-1, 4-2)** and percent of easy vs. hard trials correct achieved on the last day of testing **(Fig. 4-1, 4-2)**.

Visiomotor Conditional Learning (VMCL, ABET software, Cat #89542). For VMCL (**Fig.**

4-3), mice receive one additional training step, termed VMCL pre-testing, prior to the VMCL test.

VMCL pre-testing (PI2) is designed to teach the mouse to touch two images on the screen in a specific order and rapid succession. The first touch must be to an image presented in the center of the screen, and the second touch must be to an image presented either on the left or right of the screen. Specifically, after trial initiation, the mouse must touch a center white square (200x200 pixels), which then disappears after touch. A second white square immediately appears on either the left or right side of the screen in a pseudorandom style, such that a square is located on each side 5 out of 10 times, but not more than 3 times in a row. If the mouse selects the location with the second white square, a reward is provided, and a 20-sec inter-trial-interval starts. However, if the mouse selects the location without a square, then the second stimulus is removed, and the house light illuminates for 5 sec to indicate a timeout period which must conclude prior to the 20-sec inter-trial-interval. Then the mouse is presented with a correction trial which must be completed prior to a new set of locations being displayed. VMCL pre-testing is complete when the mouse completes 2 consecutive days of 25 trials in 30 min with >75% correct.

After VMCL pre-testing, mice advance to VMCL testing. Mice are provided with a center black and white image (spike or bars). Once touched, the center image disappears and a white squares appear in both the right and left. For this task, the spike center image signals the rodent should touch the right square and the bar center image designates the rodents should touch the left square. The two center images are presented pseudorandomly for an equal number of times, and the mice have 2 sec to

touch the white square on the right or left side of the central image. If they fail to touch the white square within 2 sec, a timeout period begins. The same timeout and inter-trial-intervals are used for VMCL testing as were used for VMCL pre-testing. As with VMCL pre-testing, correction trials are used to protect against side bias. VMCL testing is complete when the mouse completes 2 consecutive days of 25 trials in 30 min with ≥80% correct. Data are reported as days to completion.

VMCL recall testing began 1 month after the final rodent finished VMCL testing. As a result this occured between 1-3 months following VMCL testing with variability dependent on how long it took the mice to initially finish (faster learner meant more downtime). For this test, mice were place back on the VMCL test and days to hit 25 trials was recorded. Once they hit 25 trials, percent correct was calculated as a group **(Fig. 4-4)**.

General Activity and Motor Function

Open Field (OF, **Fig. 4-5***).* Mice were placed in a novel open field environment (W 44 cm x L 44 cm x H 30 cm) in a dimly lit room (60 lux) and allowed to explore for 5 min. Mice were monitored from above by a video camera and Ethovision video tracking software (Noldus, Leesburg, VA) to determine the duration of time spent in the center (W 14 cm x L 14 cm). After testing, the open field arenas were cleaned and allowed to dry between mice. Data are presented as distance traveled only (**Fig 4-5)** but duration of time spent in center of field or duration of time spent in periphery was also recorded.

*Rotarod (***Fig. 4-5***).* All rotarod data was collected on an IITC Life Science (Woodland Hills, CA) rotarod apparatus with 5 semi-enclosed lanes, automatic timers, and falling sensors to record rodents ability for 10 days. For this task, rodents are habituated in the testing room at least 30 minutes prior to rotarod testing. Testing begins once all rodents from their respective cage (4 mice/cage) have been placed on a stationary rod (1.25 inch diameter, 10 inch elevation) and had a chance to stabilize. The rod rotation parameters are set at 4 rpm start speed, 44 rpm top speed, 0.2 rpm/s acceleration rate (200 s from start to top speed) and the rotation direction was toward investigator to encourage mice to face away while walking. The total time spent on the rod is recorded from the initial start until the mouse trips the falling sensor. If a mouse would grip the rod and stop walking, the trip sensor was triggered manually by the experimenter when the rodent has performed one complete revolution (passive rotation). Once all the rodents had fallen, the times were recorded and the chambers were wiped down prior to the experimenter moving onto the next cage . Each cage would perform 4 trials/day (to average performance times) in a set order so that no cage was re-tested prior to all other cages going.

Statistical Analyses

Statistical analyses were performed using Prism (GraphPad vs. 7.0). A detailed overview of all analyses performed is provided in **Table 4-1**. Data with one variable and two groups (e.g. Treatment, Sham vs. Frac 20 cGy) were analyzed using an unpaired two-tailed Student's t-test **(Fig. 4-1 C-D,4-2 B-E, 4-3C,4-4,4-5A).** Data with two variable and one repeated measure (e.g. Treatment x Training Stage or day) were analyzed

using a two-way ANOVA and Bonferroni post-hoc **(Fig. 4-1B, 4-3B, 4-5B)**. Statistical significance was defined as $P<0.05$ and is indicated by asterisks in graphs. Threshold significance value is presented rather than exact P values.

Figure Preparation

For graphical data, figures for each data set were produced in Prism (GraphPad vs. 7.0) and transferred to Illustrator (Adobe 2017 version 21.1.0) so that uniformity in line thickness and figure size could be replicated across each figure.

Transparency and Reproducibility

Behavioral experiments were performed by researchers blind to treatment (Sham or IRR), made feasible since these whole-body doses of space radiation did not have gross measurable impact on mouse weight gain or hair loss. Touchscreen testing criteria was set on rodent performance, i.e. did they hit criteria,(yes or no), thus avoiding any scoring discrepancies across researchers. After publication, raw data and images will be made available to interested researchers.

Results

Whole body ^{56}Fe IRR at 6 months of age does not influence pattern separation in 12 month old male mice. To determine the long-term effects of HZE radiation on pattern separation ability, whole body ^{56}Fe radiation was delivered as a 20 cGy Fractionated dose (Frac; 3 exposures of 6.7 cGy) at 6 month of age. Mice were then tested at 12 months of age on the operant learning and pattern separation touchscreen platform (**Fig. 4-1)**. We found that IRR Mice trained on the touchscreen system at a

similar rate as Sham controls **(Fig. 4-1B, Table 4-1)**. Both cohorts also performed similarly on the LD pattern separation task, taking a similar number of trials to hit criterion (Sham ~19 days and Frac 20 cGy ~21 days) and responding with a similar accuracy to the easy (Sham ~65% and Frac 20 cGy ~69%) and hard (Sham ~57% and Frac 20 cGy ~52%) displays (**Fig. 4-1C, 4-1D; Table 4-1)**. Thus, any effect HZE-radiation exposure may have on pattern separation is undetectable by 6 months post-irradiation.

Whole body ^{56}Fe IRR exposure to 6 month female mice has effect on appetitive pattern separation ability but impairs rule-based learning 2 months post-IRR. To determine the effects of HZE radiation on pattern separation ability in female C57BL/6J mice, whole body ^{56}Fe radiation was delivered as a 20 cGy Fractionated dose (Frac; 3 exposures of 6.7 cGy). One month post-IRR mice began an assortment of touchscreen tests for operant learning, visual discrimination, cognitive flexibility, pattern separation, and rule-based learning with recall (**Fig. 4-2, 4-3, 4-4**). These tests are depicted as touchscreen training, Pairwise Discrimination (PD), Reversal Learning (Rev), Visiomotor Conditional Learning (VMCL), Recall, and Location Discrimination (LD) (**Fig. 4-2A, 4-3A)**. The Frac 20 cGy and Sham control group both performed similarly in the PD, Rev, and LD task (**Fig. 4-2B, 4-2C, 4-2D, 4-2E)**. Surprisingly, we found that IRR Mice spent less time on the final stage of operant touchscreen training (PI2) when being tested for VMCL (**Fig. 4-3B, Table 4-1**). This improvement is not seen in the PI stage for either the cohort undergoing the battery of tests with the LD (results on stats table only) or the cohort with the VMCL test (**Fig. 4-3B, Table 4-1**). However, these IRR rodents ended

up performing worse in the VMCL task, taking longer to reach the criterion of 80% correct in 25 trials (~45 day) compared to the Sham control group (26 days) (**Fig. 4-3C, Table 4-1**). To determine if this was a memory vs learning issue, Rodents were given between 1-3 months off before being placed back on the VMCL task to see how quickly they could recall the given parameters. Both cohorts ended up taking around 6 days to perform 25 trials in one testing and were still around 80% correct **(Fig. 4-4A, 4-4B, Table 4-1)**. In addition, these mice were tested on open field and rotarod to determine if this decrease was anxiety or motor function related. However, we did not see any differences in either of these tests between the Frac 20 cGy and Sham groups **(Fig. 4-5A, 4-5B, Table 4-1)**. Thus, rule-based learning ability in female mice appears to be impaired following ^{56}Fe radiation exposure.

Discussion

As HZE radiation exposure is generally viewed as detrimental to the CNS (Jandial et al. 2018; Cucinotta et al. 2014), it was surprising to discover that male mice irradiated at 6 months of age showed improvements in both appetitive and aversive pattern separation (**Chapter 3)**. Thus the overarching purpose of this chapter was to further advance our understanding of this phenomena two ways: 1) Are ^{56}Fe radiation-induced improvements in pattern separation (using appetitive touchscreen platform) long-lasting? 2) Do mature female mice exposed to whole body ^{56}Fe radiation have altered pattern separation ability when tested on an appetitive platform?

In doing so, this work demonstrates ^{56}Fe radiation-induced improvements in pattern separation are both tranient and sex specific. Specifically, the data show that male mice

starting pattern separation around 12 months of age (IRR at 6 months of age) have no differences in their performance compared to Sham controls. This suggests that HZE-induced cognitive effects are transient in male mice, and, although negative, we now have a narrowed down window for all future mechanistic studies (i.e within 6 months of radiation exposure).

In addition, female mice show a completely different response to HZE radiation. As we demonstrate, female mice irradiated at 6 months of age do not exhibit any differences in pattern separation ability. However, they demonstrate improved acquisition of the touchscreen training, yet require longer periods of time to acquire (as no difference were seen in the recall portion) the rule based learning task. Prior to this study, data evaluating the effects of HZE particles on 6 month female rodents at time of IRR was severely limited and only consisted of work using the aversive, shock-based, contextual fear condition paradigm (Raber et al. 2015a; Raber et al. 2016). Specifically these studies show ^{16}O exposure increases contextual fear conditioning at doses of 0.4 and 0.8 Gy (Raber et al. 2015); ^{28}Si, ^{48}Ti and proton exposure has no effect on contextual fear conditioning below 1.4 Gy (Raber et al. 2015a); and ^{40}Ca had no effect on contextual fear learning, memory or extinction but showed a decrease in their response to the shock compared to the males (Raber et al. 2016). From this literature and the work done here, a comparison could be drawn between the use of the hippocampal-based contextual fear conditioning paradigm (Fanselow & Dong 2010) in the literature and our hippocampal-based pattern separation test (Horner et al. 2013) both indicating HZE particles may not be detrimental to hippocampal based cognition. As this may

actually be the case, additional testing may still be necessary to confirm this theory as one of the studies (Raber et al. 2016) highlight the sex specific differences in shock responses females exhibit following IRR, yet the sex was not explicitly separated out in the other two articles from this group (Raber et al. 2015a). Also, IRR-induced behavioral responses would need to be validated across animal strain, as all three of these articles use B6D2F1 mice with various dosing regimens compared to the fractionated dose of 20 cGy on C57BL/6J mice that was shown here.

However, the negative pattern separation data presented here is only the partial story, as female C57BL/6J IRR mice completed the final stage of operant testing earlier than Sham controls but took on average 19 days longer to complete the striatum- and posterior cingulate cortex-dependent VMCL task (Horner et al. 2013). This sex-specific response was intriguing, as the striatum has been implemented in motor function and reward and the posterior cingulate cortex contributes to spatial orientation and memory (Vogt et al. 1992; Kravitz & Kreitzer 2012). As spatial learning was not affected in the location discrimination task, we tested the rodents on rotarod to measure motor function; and a VMCL recall stage to measure memory. Surprisingly both of these experiments revealed negative data and rodents did not show any indications of increased anxiety that would inhibit their responses. Importantly, as lesions to the medial prefrontal, perirhinal, or anterior cingulate cortex, hippocampus, and anterior or mediodorsal thalamus do not impair VMCL performance, more work will be needed to determine the underlying mechanism for this impairment and subsequently determine the risk to future female astronauts (Bussey et al. 1997; Chudasama et al. 2001; Bussey

et al. 2000; Horner et al. 2013).

Chapter 4, Figures

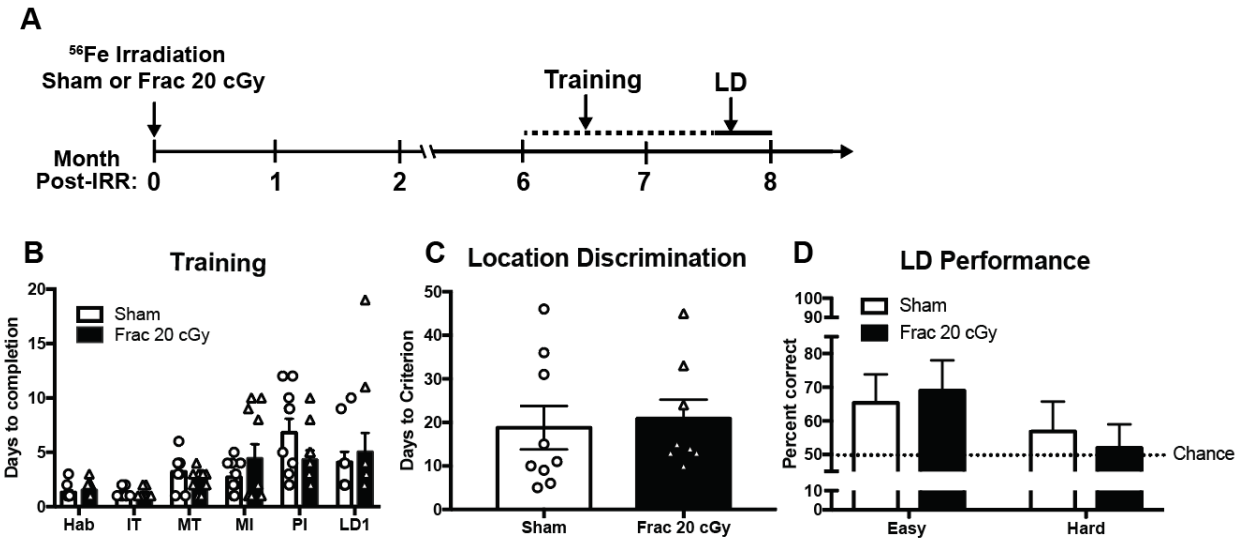

Figure 4-1. Analysis of Location Discrimination performance 6 months post-IRR reveal no differences in training or pattern separation performance in male mice. Timeline of mouse exposure to whole body Sham IRR or ^{56}Fe (600 MeV/n, LET 174 KeV/μ) **(A)** and subsequent training on touch screen platform for LD **(B)**, LD testing to learning latency **(C)** and accuracy **(D)**. Sham and ^{56}Fe IRR mice performed similarly in all stages of training **(B)** and on the Location discrimination task **(C-D)**. Mean±SEM. Two-Way Repeated Measures Anova and Unpaired, two-tailed, t test respectively.

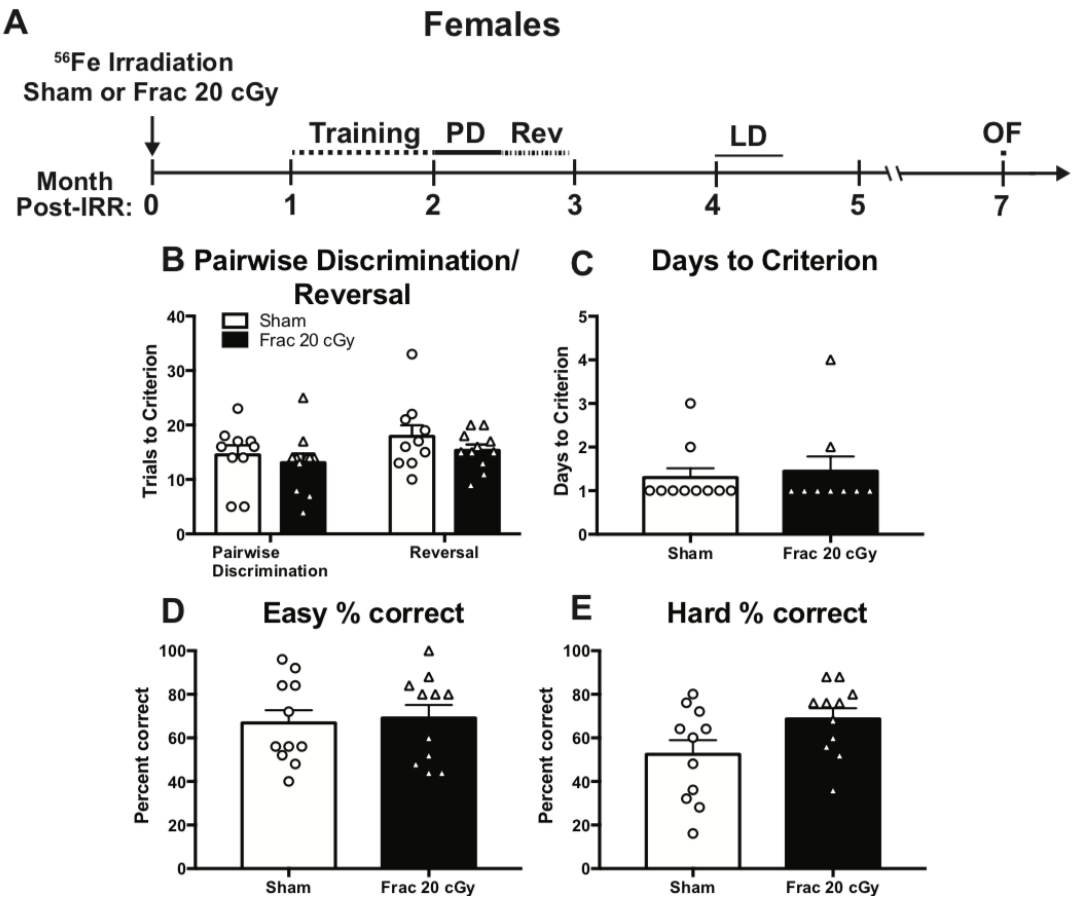

Figure 4-2. On an appetitive touch screen task, female mice exposed to ^{56}Fe IRR at 6-month of age show no differences, Pairwise Discrimination/Reversal learning, or Location Discrimination. Timeline of mouse exposure to whole body Sham IRR or ^{56}Fe (600 MeV/n, LET 174 KeV/μ) and subsequent testing on touch screen platform for Pairwise Discrimination (PD) training, PD testing, PD reversal (Rev), and location discrimination (LD) **(A)**. Sham and ^{56}Fe IRR mice performed similarly in the hippocampal-dependent but context-independent Pairwise Discrimination task, and in the cognitive flexibility hippocampal-dependent Reversal task **(B)**. ^{56}Fe IRR mice completed the LD task in a similar amount of time **(C)**. Additionally, Sham and ^{56}Fe IRR

mice performed similarly during the “Easy Separation” and “Hard Separation” display **(D-E)**. Mean±SEM. Unpaired, two-tailed, t test.

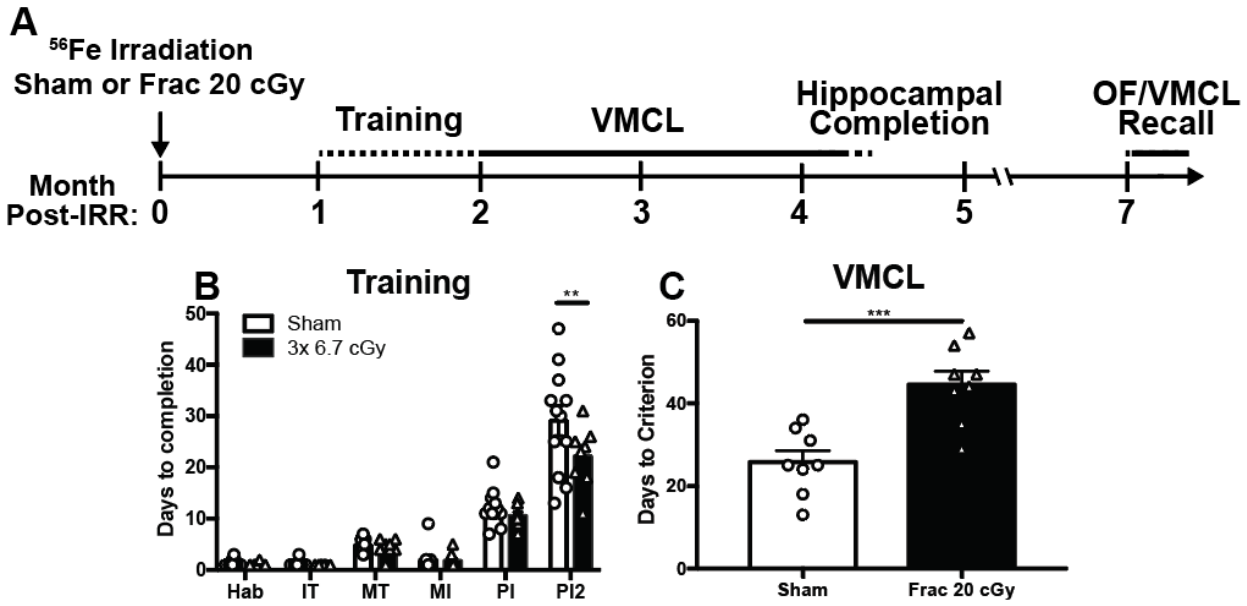

Figure 4-3. On an appetitive touch screen task, female mice exposed to ^{56}Fe IRR at 6-month of age show decreased ability in rule based learning. Timeline of mouse exposure to whole body Sham IRR or ^{56}Fe (600 MeV/n, LET 174 KeV/μ) **(A)** and subsequent testing on touch screen platform for Visiomotor Conditional Learning (VMCL) training (**B)** and VMCL **(C)**. Sham and ^{56}Fe IRR mice performed similarly in the 5 first stages of the 6 VMCL training stages **(B)**. However, ^{56}Fe IRR mice to complete the punish incorrect 2 (PI2) stage of VMCL training faster than Sham**.** However, IRR mice do worse at the rule based learning compared to Sham **(C).** Mean±SEM. Two-way repeated measures ANOVA, Bonferroni. Unpaired, two-tailed, t test. ✱✱<0.01, ✱✱✱<0.001.

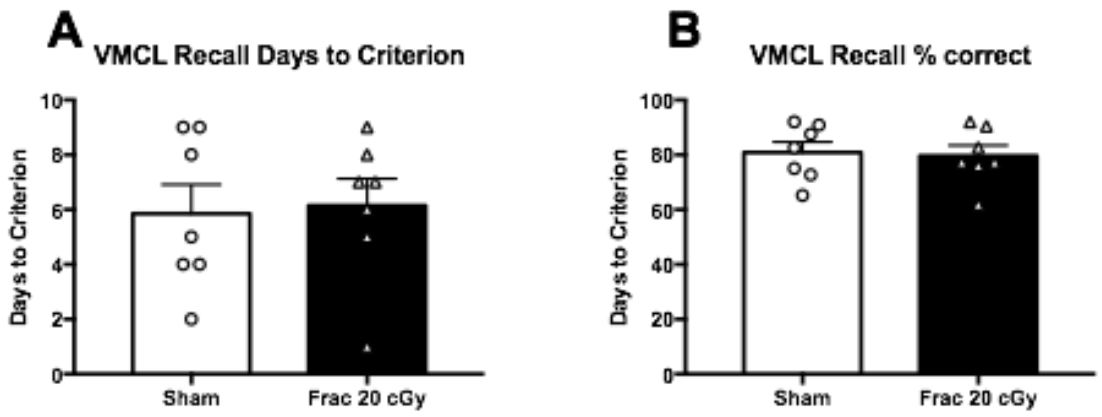

Figure 4-4. 1-month post-VMCL testing ^{56}Fe IRR female mice recall the VMCL test at a similar rate and to a similar accuracy. Mice were given a month or more off from VMCL testing prior to measuring their ability to recall the task. Although IRR mice took longer to initially learn the VMCL, Mice IRR take the same number of days as Sham to reach criterion in the recall test **(A)**. Importantly, both Sham and IRR mice are averaging 80% accuracy at criterion, similar to their initial learning criterion **(B)**. Mean±SEM. Unpaired, two-tailed, t test.

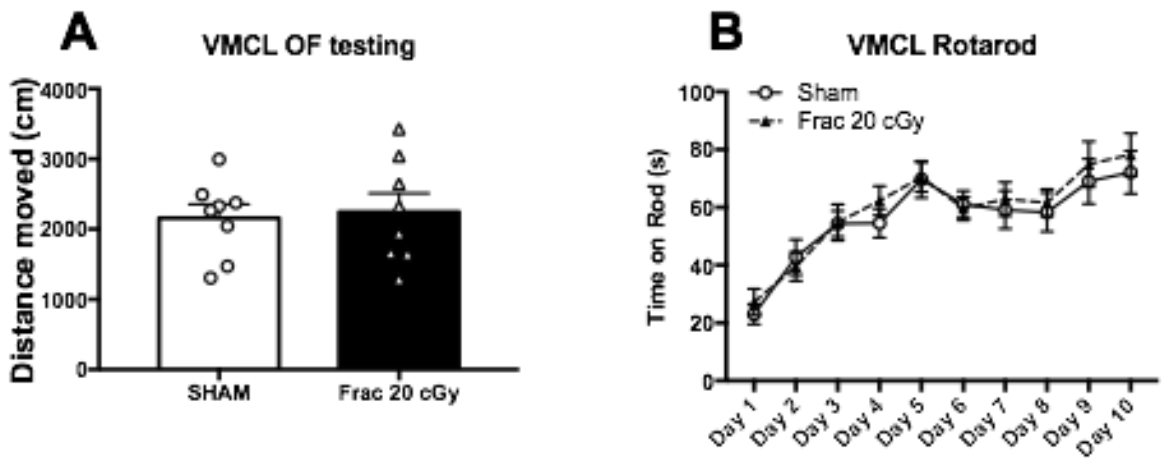

Figure 4-5. ^{56}Fe does not appear to increase anxiety or decrease motor function 6 months post-IRR. Following the VMCL recall task, Mice were run on OF to measure anxiety levels **(A)**. IRR traveled similar distances in the OF task and showed similar motor function compared to Sham in the Rotarod task **(B).** Mean±SEM. Unpaired, two-tailed, t test.

Chapter 4, Statistics Table

Subject	Figure	n	Mean							Statistics (variables)	Main Effect or Interaction	F Value	P value	Post hoc Test	Post hoc Results						
			Training Stage	Hab	IT	MT	MI	PI	LDI						Block	Hab	IT	MT	IT	PI	
Operant Training	4-1B	Sham: 10	Sham	1.3	1.2	3.2	2.7	6.8	4.1	ANOVA (Treatment x Training Stage), one repeated measure (Training Stage)	Interaction	F (5, 90) = 1.328	P=0.2596	NA	Context A vs B	-	-	-	-	-	-
		Frac 20 cGy 10	Frac 20 cGy	1.5	1.2	2.5	4.4	4.3	5		Training Stage / Treatment / Subjects (matching)	F (5, 90) = 7.535 / F (1, 18) = 0.0254 / F (18, 90) = 0.6689	P=0.0001 / P=0.8752 / P=0.8345			-	-	-	-	-	-
Location Discriminat ion (LD)	4-1C	Sham: 9	Sham	Rev Mean ± SEM)						Student's T-test (Treatment)											
		Frac 20 cGy 8	Frac 20 cGy	18.78 ± 4.483			20.88 ± 4.357				Treatment	0.759		NA							
LD Easy Separation	4-1D	Sham: 9	Sham							Student's T-test (Treatment)											
		Frac 20 cGy 8	Frac 20 cGy				65.33 ± 8.459				Treatment	0.770		NA							
							69 ± 8.968														
LD Hard Separation	4-1D	Sham: 9	Sham							Student's T-test (Treatment)											
		Frac 20 cGy 8	Frac 20 cGy				56.89 ± 8.839				Treatment	0.676		NA							
							52 ± 6.969														
Operant Training	Not shown	Sham: 11	Sham	HAB	IT	MT	MI	PI		ANOVA (Treatment x Training Stage), one repeated measure (Training Stage)	Interaction	F (4, 80) = 0.7056	P=0.5904	NA							
		Frac 20 cGy 11	Frac 20 cGy	1.091	1	3	5.909	5.273			Training Stage / Treatment / Subjects (matching)	F (4, 80) = 13.23 / F (1, 20) = 2.319 / F (20, 80) = 0.9369	P<0.0001 / P=0.1435 / P=0.9421								
				1.091	1	2.455	4	5.273													
Pyramix Discriminat ion (PD)	4-2B	Sham: 10	Sham	PD						Student's T-test (Treatment)											
		Frac 20 cGy 11	Frac 20 cGy	14.5																	
				13.09							Treatment	0.569		NA							
PD Reversal (Rev)	4-2B	Sham: 10	Sham	Rev						Student's T-test (Treatment)											
		Frac 20 cGy 11	Frac 20 cGy	17.9																	
				15.36							Treatment	0.271		NA							
Location Discriminat ion (LD)	4-2C	Sham: 11	Sham	LD Mean ± SEM)						Student's T-test (Treatment)											
		Frac 20 cGy 11	Frac 20 cGy	2.091 ± 0.639																	
				3 ± 1.087							Treatment	0.479		NA							
LD Easy Separation	4-2D	Sham: 11	Sham	Easy						Student's T-test (Treatment)											
		Frac 20 cGy 11	Frac 20 cGy	66.91 ± 5.836																	
				69.09 ± 6.008							Treatment	0.797		NA							
LD Hard Separation	4-2E	Sham: 11	Sham	Hard						Student's T-test (Treatment)											
		Frac 20 cGy 11	Frac 20 cGy	52.36 ± 6.505																	
				68.73 ± 4.879							Treatment	0.058		NA							

VMCL Training	4-3B	Sham: 12	Sham	1.33	1.167	4.75	1.917	12.17		29.08	ANOVA (Treatment x Training Stage), one repeated measure	Interaction	F (5, 90) = 120.6	P<0.0001	Sham vs. Frac 20 cGy	Hab	IT	MT	IT	PI	P12
		Frac 20 cGy 8	Frac 20 cGy	1	1	4	1.083	11.67		22.13		Training stage / Treatment / Subjects (matching)	F (1, 18) = 3.165 / F (18, 90) = 1.372	P<0.0741 / P<0.1653		ns	ns	ns	ns	ns	**
																>0.9999	>0.9999	>0.9999	>0.9999	0.9303	0.0012
Vistamotor control learning (VMCL)	4-3C	Sham: 8	Sham	VMCL						Student's T-test (Treatment)	Treatment	0.001		NA							
		Frac 20 cGy 8	Frac 20 cGy	25.75 ± 2.763																	
				44.5 ± 3.251																	
VMCL Recall (Hab)	4-4A	Sham: 8	Sham	Days to Criterion						Student's T-test (Treatment)	Treatment	0.847		NA							
		Frac 20	Frac 20 cGy	9.857 ± 1.056																	
				8.143 ± 0.9693																	
Recall % correct	4-4B	Sham: 8	Sham	Mean % correct						Student's T-test (Treatment)	Treatment	0.828		NA							
		Frac 20	Frac 20 cGy	80.85 ± 3.834																	
				78.65 ± 3.836																	
Open Field	4-5A	Sham: 8	Sham	Distance						Student's T-test (Treatment)	Treatment	0.795		NA							
		Frac 20	Frac 20 cGy	2159 ± 194.1																	
				2288 ± 264.7																	
Roland	4-5B	Sham: 8	Sham	ANOVA (Day x Treatment), one repeated measure (Day)	Interaction	F (9, 126) = 0.403	P=0.9314	NA													
		Frac 20 cGy: 8	Frac 20 cGy		Day	F (9, 126) = 29.2	P<0.0001														
			Avg at each time not shown		Treatment	F (1, 14) = 0.187	P=0.0001														

Table 4-1. Statistical analysis table investigating whether HZE improved pattern separation is transient or sex-specific. Statistical analysis for each test are listed above with significance set at p≤0.05 (bold). Abbreviation not defined in table: Fractionation, Frac; Habituation, Hab; Initial Touch, IT; Must Initiate, MI; Must Touch, MT; Punish Incorrect, PI; Punish Incorrect 2, PI2.

CHAPTER 5: CONCLUSIONS AND FUTURE DIRECTIONS

Summary

The potential threat high-atomic number and energy (HZE) particles, such as ^{28}Si and ^{56}Fe, pose to the CNS is currently a concern for both heavy ion radiation therapy patients and future astronauts embarking on deep space missions. In regard to future deep space missions, chronic low dose exposure to HZE particles will be unavoidable. Thus understanding their impact on the CNS is of utmost relevance for mission success. This dissertation was centered around both structural and behavioral implications these particles have on the hippocampal dentate gyrus (DG), a brain region critical for learning, memory, mood regulation, spatial memory, and pattern separation. Structurally, we expand on previous work that suggested HZE particles (almost exclusively ^{56}Fe) are detrimental to hippocampal-based neurogenesis, by being the first to investigate the neurogenic effect ^{28}Si poses for either male or female mice. In **Chapter 2,** we show that ^{28}Si dose-dependently disrupts proliferation and neurogenesis shortly after radiation exposure (24 hrs). Interestingly, proliferation and neurogenesis recover by three months, yet cell survival is still impaired in a dose- and sex-specific fashion.

Behaviorally, this dissertation expanded the field in a variety of ways. First, in **Chapter 2 we show** higher levels of anxiety in the long-term, and sex-specific decreases in cell survival following ^{28}Si exposure. Also, we are the first to show in **Chapter 3** that irradiating rodents at astronaut relevant ages (6 months) can lead to improvements in aversive (with ^{28}Si and ^{56}Fe) and appetitive (^{56}Fe only) pattern separation in a

neurogenesis independent manner. Specifically, male mice were able to distinguish two similar contexts earlier in a shock-based paradigm, and were able to reach criterion faster with a higher accuracy in a touchscreen-based paradigm. In addition, we were the first to train rodents to use the touchscreen apparatus following ^{56}Fe radiation exposure. This allowed us to be the first to show in **Chapter 3 and 4** that both males and females exhibit operant touchscreen training improvements. In **Chapter 4,** we are the first to show that female mice are impaired on the striatal- and posterior cingulate cortex-dependent rule based learning task. Taken as a whole, this dissertation suggests that sex, age, and timing of both IRR and data collection/behavior testing are all very important factors to consider when evaluating the risks HZE particles have on both heavy ion radiation therapy patients and future astronauts embarking on deep space missions. In the following sections, we will review the chapters' major points, discuss their implications in the field, and provide the future direction for each chapter.

CHAPTER 2 Review: Whole-body exposure to ^{28}Si-radiation dose-dependently disrupts dentate gyrus neurogenesis and proliferation in the short term and new neuron survival and contextual fear conditioning in the long term

Prior to this work, ^{56}Fe was almost exclusively the ion experimenters would use when evaluating the HZE-induced effects to DG neurogenesis. The sole manuscript using a heavy ion other than ^{56}Fe chose ^{12}C but irradiated with doses well over those an astronaut would experience in space (1 and 3 Gy) and only looked at one time point (9 months post-IRR) (Rola et al. 2005). Therefore, to determine if the previously seen detrimental effect on neurogenesis is particle- or time-dependent, we designed our study to best compare across the literature at the time (Rivera et al. 2013; DeCarolis et

al. 2014; Sweet et al. 2016; Raber et al. 2016; Encinas et al. 2008; Manda et al. 2008; Rola et al. 2008; Casadesus et al. 2005; Rola, Otsuka, et al. 2004). Specifically we look at two different timepoints, use more relevant doses, and use a variety of markers to determine cell fate. With this approach, our data suggest that ^{28}Si radiation has a more transient and less potent long-term influence on the process of DG neurogenesis than ^{56}Fe. In **Chapter 2** we show recovery of DCX+ cells 3 months following HZE exposure, yet earlier work from our group showed decreases using ^{56}Fe (Rivera et al. 2013). Furthermore, the sex-specific effects HZE had on neurogenesis are quite novel, as only our group previously used both sexes within the same neurogenesis experiment (Rivera et al. 2013; DeCarolis et al. 2014). While **Chapter 2** suggests there is a transient, ion-independent, effect of HZE particles on neurogenesis, it highlights the importance for further studies that vary timing of data collection across sex and particle. Thus further experiments are needed and discussed below.

Future directions Chapter 2

As **Chapter 2** points out (along with other previous non-neurogenic literature), dose, dose rate, ion, age, and ion energy can vary widely and affect the response to HZE particles (Rabin, Shukitt-Hale & Carrihill-Knoll 2014a; Rabin et al. 2011). In **Chapter 2** we show data with just ^{28}Si at 2 doses (0.2 and 1 Gy). However, in space astronauts will be exposed to an abundance of protons and ions with varying energies (Kim et al. 2015). Fortunately, recent technological advances allow researchers to move past these rudimentary mono-energetic beams and rapidly switch through a spectrum of ions that could be experienced in space (Kim et al. 2015). While this advancement can

complicate the comparison of studies across the field, particularly if set standards are not put in place to coordinate mixed beam content, the data produced will more closely represent the interactions that could be expected out in space. For instance, we show that male and female rodent neurogenesis and proliferation are transiently reduced following exposure to ^{28}Si. Future experiments (in both male and female mice) using primarily proton radiation with realistic levels of ^{28}Si (or other HZE particles) could shift this transient effect into a long lasting decrease or, as some recent literature has suggested with proton and ^{56}Fe, have no effect on neurogenesis (Raber et al. 2016).

Furthermore, environmentally-relevant means of depleting neurogenesis include binge ethanol consumption, high fat diets, sleep deprivation, stress, and the natural age-related decline (Becker 2017). Interestingly, none of these factors have been tested with HZE particle exposure, but are all highly relevant for either deep space missions (the basis for which we set our study parameters) or heavy ion radiation therapy patients. For instance, at this time, no study has tested the effects of sleep deprivation or chronic stress prior to radiation exposure, and excluding our data in **Chapter 3**, no work investigated neurogenesis with rodents at or above 6 months of age (male or female). Fortunately, as we show in **Chapter 3**, neurogenesis levels are still high enough to reveal biological changes when mice are irradiated at 6 months of age and evaluated later in life. In addition, astronauts will experience sleep deprivation and high levels of stress in space (Cucinotta et al. 2014). Thus many of these factors can and should be studied in the future radiation studies.

Finally, the existence of neurogenesis in adult humans is controversially up for debate. Classically, neurogenesis is linked to learning, memory, spatial navigation, mood regulation, and even forgetting (Becker 2017; Tello-Ramos et al. 2018; Gonçalves et al. 2016). Previous studies show the existence of neurogenesis in humans using the thymidine analog BrdU in cancer patients, and ^{14}C DNA labeling from nuclear-bomb test survivors (Spalding et al. 2013; Eriksson et al. 1998). Specially, this work suggests that neurogenesis does exist in humans at later stages in life (up to as many as 700 new neurons per day), but is significantly reduced as people age (Spalding et al. 2013; Eriksson et al. 1998). Interestingly, in the weeks leading up to this dissertation, contrasting studies were published debating the existence of neurogenesis in adult humans. Specifically, recent work suggests neurogenesis is non-existent in the dentate gyrus beyond 7 years of age in humans. This study shows that DCX+ and Ki67+ cell numbers are present in children but become essentially non-existent in the DG by 7 years of age using both epileptic and non-epileptic controls (Sorrells et al. 2018). However, less than a month later, contrasting data has indicated that neurogenesis does occur in healthy individuals up to 79 years of age by using some of the very same neuronal markers (Boldrini et al. 2018). While this debate continues to play out, more causative neurogenesis studies are needed to truly distinguish its role in cognition following HZE exposure. This can be done with transgenic mouse lines similar to those used to link neurogenesis and pattern separation (discussed in the introduction) (Sahay et al. 2011; Tronel et al. 2012).

CHAPTER 3 Review: Space radiation unexpectedly enhances pattern separation yet diminishes dentate gyrus neurogenesis in C57BL/6J mice

Prior to this work, no study investigated HZE radiation's effect on the hippocampal-dependent process of pattern separation. In addition, only 29% of studies **(Table 1-1)** evaluated the behavioral effects HZE radiation exposure at 6 months of age has on the CNS. In order to address both of these issues, rodents at 6 months of age were exposed to HZE radiation and the hippocampal-dependent process of pattern separation - with both the aversive, shock-based, context dependent fear conditioning task and appetitive, touchscreen-based, location discrimination task – was assessed. In **Chapter 3,** we show for the first time in male mice that exposure to either ^{56}Fe or ^{28}Si can induce earlier contextual discrimination between two similar environments. In addition, we show for the first time that male IRR mice are able to complete the punish incorrect stage (final stage of operant touchscreen testing) earlier than the Sham mice, and exhibit earlier and more accurate performance in the location discrimination task. Interestingly, this work was the first to show an inverse relationship between neurogenesis and pattern separation ability. This shocking discovery suggests that the improvement in pattern separation, following radiation exposure at maturity, was neurogenesis-independent and thus requires further experiments discussed below.

Future directions Chapter 3

The improvement in pattern separation across both the aversive and touchscreen platforms was quite unexpected. As this improvement is not tied to increases in neurogenesis, additional work is needed to determine the underlying mechanism.

However, as our group and others have shown, HZE particle exposure increases anxiety (Whoolery et al. 2017). Thus our initial experiments had to confirm these results were not anxiety or general health related. As most of the control experiments for the cohort that underwent CDFC testing were shown in **Chapter 3 supplemental**, this future direction section mostly focuses on similar control tests for the touchscreen tested cohort, with additional data provided that may or may not be included in submission. With this group, we looked at body weight across testing and a variety of anxiety indicators using blank screen touches and open field. In **this chapter** we show that bodyweight is not grossly different across treatment during the training, PD/Reversal testing, and LD testing (**Fig 5-1)**. Analyzing the blank touches allowed us to determine if the IRR mice were more driven to touch the screen or generally hyperactive in the chambers, and as a result, could have explained their ability to finish PI touchscreen training and LD earlier than Sham mice (**Fig 5-2)**. However, both cohorts touched the screen around 40 times during the LD inter trial interval (ITI) and would touch blank spaces around 100 times during the LD test, thus ruling out hyperactive screen pressing (**Fig 5-2)**. Finally, neither group exhibits heightened anxiety related behaviors based on similar distance traveled, frequency to enter center, and time spent in the center of the open field (**Fig 5-3)**. Interestingly, the improvement in pattern separation ability appears to be the only hippocampal-dependent task to show a response. For example, here we show no differences in percent freezing time using the hippocampal-based CFC test across treatment groups (Fanselow & Dong 2010). This suggests that the underlying mechanism is not a global response (e.g improved respiration, metabolism, etc.) but a process that is unique to the hippocampus. As a

result, a variety of theoretical perspectives about the hippocampus will be discussed in relation to future work.

For instance, although historically tied to learning and memory, recent work suggests that neurogenesis plays a major role in forgetting (Akers et al. 2014; Epp et al. 2016). Here they show high levels of neurogenesis during early ages can lead to increased levels of forgetting prior memories (Akers et al. 2014; Epp et al. 2016). In turn, this will lead to low levels of proactive interference from past memories and permit new memory formation, thus increasing cognitive flexibility (Epp et al. 2016; Tello-Ramos et al. 2018). However, as humans age, neurogenesis levels decrease (i.e. less forgetting of prior memories). As this occurs, prior memories begin to interfere with new memory formation and thus decrease cognitive flexibility (Epp et al. 2016; Tello-Ramos et al. 2018). Based on this theory, we hypothesized that the age induced decrease in neurogenesis would lead to impaired cognitive flexibility. However, as we show in **Chapter 3**, male IRR mice take a similar number of trials to reach criterion as the Sham mice for the reversal learning task. While this suggests cognitive flexibility is unimpaired, this reversal task does not allow testing for memory retention (Tello-Ramos et al. 2018). Thus a future experiment where male mice are trained on multiple sets of images prior to reversal learning is warranted. This will identify acquisition rates as the number of image sets are increased, identify memory retention issues from earlier image sets, and test for cognitive flexibility.

Another interesting perspective is the shift from pattern separation to pattern completion in adult humans, where pattern separation is the distinction of similar representations and pattern completion is accurate generalization of partial sensory input (Vieweg et al. 2015; Yassa & Stark 2011; Wilson et al. 2006). Based on the improvements shown in **Chapter 3** to pattern separation, we hypothesized that generalization, via pattern completion, would be impaired. For this type of experiment, our first attempt was to create a touchscreen-based pattern completion task **(Fig 5-4)**. For this task, rodents were trained to 80% accuracy out of 25 trials on the rule-based learning task. Once criteria is reached, the images that indicate which side is rewarding were slowly blocked out over a 5-day period **(Fig 5-4A)**. Our goal was to have the mouse mentally complete the image to resolve the rule. As IRR rodents exhibit improved pattern separation, our expected results would have been a decrease in pattern completion ability. Unfortunately, this particular experiment will need to be rerun for two reasons. First, this was done in female mice who showed baseline deficits in rule-based learning **(Fig 4-3)**. As this task is adapted from the rule-based learning task, we would need to exhibit zero baseline differences in the VMCL task prior to running the pattern completion portion. Second, the task did not offer the sufficient challenge needed to drop their percent correct down to chance alone, as the mice accuracy stayed above 65% correct. Thus, it is quite possible that male mice could show a deficit in the pattern completion task created. However, if creating a touchscreen pattern completion task is infeasible, a variant of the Morris water maze exists where rodents are trained to find a platform and then only given part of the cues required to navigate to the platform (Nakashiba et al. 2012).

In addition, previous work linked the lateral entorhinal cortex (Ent) to sensory cues required for object processing, and the medial Ent to configurational aspects of experience, such as space (Reagh et al. 2018). Expanding on this in humans, recent high-resolution fMRI studies show age-related hypoactivity in the anterolateral EC (alEnt) commensurate and dentate/CA3 hyperactivity in healthy adults (Reagh et al. 2018). These region-specific activity changes were tied to deficits on an object-based pattern separation task (Reagh et al. 2018). Interestingly, only subtle deficits between young and older adults were found in the spatial pattern separation task and in posteromedial Ent activity (Reagh et al. 2018). Importantly, this work demonstrates the various Ent regions across age in both object and spatial pattern separation, while highlighting the utility of fMRI for pattern separation studies. Thus, our spatial pattern separation data shown here warrants future fMRI experiments targeting the medial Ent, as much of the work done in this dissertation was spatial pattern separation should be performed to monitor activity levels following HZE exposure.

Beyond the potential experiments mentioned above, additional cellular work in our lab, begun by Ryan Reynolds, will sort out the driving factors behind this pattern separation phenomenon. For instance, one theory is that inhibitory mossy cells and hilar interneurons can interact with the perforant path to regulate pattern separation ability by lowering the firing probability of DG granule cells onto CA3 pyramidal cells, thus reducing the input necessary to activate the same subset of CA3 neurons (Myers & Scharfman 2009; McAvoy et al. 2015). While this mechanism might be true, initial work

by our group revealed this improvement in pattern separation is at least independent of GAD67+ (a inhibitory interneuron marker (Dayer et al. 2005)) cell number, as mice that received up to 1 Gy of ^{56}Fe had similar cell counts as Sham mice (data not shown). However, further functional interneuron experiments are needed to confirm this improvement in pattern separation is unrelated to interneurons by enhancing or repressing interneuron signaling during pattern separation tasks.

Mechanistically our group has also used an unbiased and cell-specific RNA screening strategy, called BAC-TRAP (Bacterial Artificial Chromosome-Translating Ribosomal Affinity Purification) (Doyle et al. 2008), to collect the whole translating RNA profile from DG glutamatergic neurons in mice exposed to 20 cGy of ^{56}Fe. With this, in collaboration with Dr. Sanghee Yun, our group identified over 150 genes upregulated or downregulated 2 fold or greater (data not shown). Surprisingly, a large majority of these genes are related to mitochondrial function or the control of oxidative phosphorylation following radiation exposure. While these studies are still ongoing, very early data using a mitochondria functional assay called seahorse suggests these changes may be due to a shift towards glycolysis and away from ATP production via the electron transport chain (data not shown). My role in this project has been minimal, and additional work will be needed to confirm any correlative effects found using the Seahorse assay. Specifically, I was only able to generate a single cohort of IRR mice for these mitochondrial studies. However, further mitochondrial manipulation studies will be done to increase sample size and determine whether non-IRR experiments can drive changes in pattern separation ability.

Lastly, the immune system in rodents has been shown to play a major role in cognitive performance and spatial navigation, but can be depleted with high enough doses of radiation (300 rad followed 2 days later by 950 rad) (Chen et al. 2008; Brynskikh et al. 2008). As result, the Stowe and Eisch groups isolated brain, cervical lymph node, thymus, spleen, blood, and bone marrow to determine if the behavioral improvements are driven by either the innate or adaptive immune system (Chen et al. 2008; Brynskikh et al. 2008). Our multi-objective approach was to first measure the ability of the immune system to mount a response and proliferate in the presence of foreign antigens. For this, spleen and cervical lymph node cells were stimulated with common antigens and their proliferative and cytokine-secretion responses were collected via flow cytometry. Our second objective was to investigate how radiation may alter the development and maturation of various immune cell types. Specifically, general leukocytes (identifying B cells, T cells, natural killer cells, macrophages, and granulocytes) as well as various B cell subsets from the spleen and blood were surveyed via flow cytometry and are currently under analysis. Once finished, our goal will be to causatively manipulate the immune system to verify its capacity to mount a pattern separation response.

CHAPTER 4 Review: Unexpected enhancement in pattern separation following ^{56}Fe exposure is transient in male mice and sex-specific, yet disrupts rule-based learning in female mice

Expanding on what was shown in **Chapter 3**, **Chapter 4** suggests that pattern separation improvement is transient in male mice. Specifically, we show that following a 6 month recovery period (with IRR at 6 months of age), IRR male mice require a similar

amount of time to complete the pattern separation task and exhibit similar accuracy in both easy and hard displays compared to sham mice. In addition, **Chapter 4** was the first experiment to train female rodents on the touchscreen platform and test pattern separation following HZE exposure. Contrary to the male data in **Chapter 3**, in **Chapter 4** we show for the first time that pattern separation ability (both time to reach criteria and accuracy) in female mice is not transiently affected following ^{56}Fe exposure. However, we are the first to show that female mice are transiently susceptible to HZE induced rule-based learning deficits. Thus further experiments discussed below will be necessary to explain why IRR female mice took longer to learn the VMCL touchscreen task.

Future directions Chapter 4

With **Chapter 4** we show that rule-based learning performance in female mice is susceptible to HZE particle exposure. However, these data leave one remaining question. Is the deficit seen learning-related or memory-related? To answer this question, our recollection data **(Fig. 4-4)** suggest female mice are capable of recalling the images for the VMCL task for at least 3 months past completion of the task. However, as the IRR cohort took longer to learn the task, some female mice had as little as a month between testing, compared to the faster non-IRR learners. Thus, our future plan will be to train female mice on the VMCL task prior to irradiation to confirm all mice have a similar gap in between testing. Once irradiated, we will retest the mice on the VMCL task to measure re-trainability. If there is no difference in recollection between

treatment groups, this work will suggest that the deficit is in fact in the learning/storage aspect of the test and not in the memory recollection portion.

From **Chapter 4**, we see sensitivity to both time of testing and sex-specific differences in pattern separation. As a result, these factors highlight the need to rerun the male rodents on the VMCL at an earlier time point. Specifically, the male mice were delayed in their start on the VMCL task because we attempted to train the mice on a Paired Associates Learning (PAL) task first. However this PAL task was rather labor intensive and after 40 days of Monday through Friday testing, both cohorts of mice (IRR and Sham) failed to reach the required 80% accuracy, and failed to diverge in performance levels (data not shown but provided in NSRL16B prism file). As a result, this PAL test was terminated prior to its completion and the male mice moved onto the VMCL test. With this delay prior to testing, we concluded that rule-based learning performance was unaffected in male mice 4 months post-IRR. However, as pattern separation was time-sensitive in males, it is possible that any effects HZE exposure might have had on rule-based learning may have recovered by 4 months post-IRR. Thus a replication experiment is currently being planned for the spring run of 2018 in male rodents, where they will be 6 month at the time of IRR and ill be immediately tested 1 month post-IRR on the VMCL test. This experiment will, to the best of its ability, mimic the female VMCL test that was run in 2017 **(Fig 4-3)**.

Finally, as mentioned throughout this dissertation, HZE particles have classically been viewed as detrimental to the CNS and unfortunately unavoidable (Cucinotta et al. 2014).

As a result, potential radiation countermeasures that can be given to protect astronauts from HZE-induced CNS damage is an appealing tactic. One such radioprotectant of interest is the synthetic triterpenoid 2-cyano-3,12-dioxooleana-1,9 (11)-dien-28-oic acid (CDDO) and its chemically-modified derivitive, CDDO-ethyl amide (CDDO-EA). Previously, rodents fed CDDO-EA three days prior to lethal dose (7.5 Gy) of whole body X-ray radiation exhibited an increase in survival rates by close to 2 fold (Kim et al. 2012). In addition to this drug potentially reducing the risk of cancer, our question now becomes whether it will be able to protect against this HZE induced decrease in rule-based learning performance in female mice. To answer this, we first ran 6 week exposure experiments in 3 month old male C57BL/6J mice to determine if CDDO had any baseline effect on animal body weight, food intake, or activity levels **(Fig 5-5)**. The need for this study becomes essential due to the food deprivation rodents undergo during touchscreen testing. As a result, body weight was closely monitored, thus any food related decreases in body weight could result in rodents omitted from the study. However, from these pilot experiments we concluded that 6 weeks of CDDO administration does not alter baseline body weight or food intake levels (**Fig 5-6)**. In addition, we looked at baseline activity level using running wheels and found no effects on the rodent's ability to exercise when given the opportunity (**Fig 5-7)**. Lastly, we also looked at the adaptive and innate immune response these rodents mounted after long-term exposure (**Fig 5-8, 5-9)**. While there was no effect on the adaptive immune response (**Fig 5-8)**, the lymphoid derived innate immune cells were decreased in sedentary mice (**Fig 5-9)**. Unfortunately, the overall consequences of this discovery has yet to be determined, as more work will be needed to differentiate these cells further to

determine their exact identity. In sum, the negative data was essential to collect prior to us moving forward with CDDO and touchscreen testing. From here, our lab, in collaboration with Dr. Jerry Shay's lab, has planned spring 2018 experiments to test CDDO food administration prior to whole body radiation to determine if this drug intervention can negate the detrimental effects seen in female mice rule-based learning.

Conclusion

The work done in this dissertation addresses multiple key knowledge gaps in the space radiation field, particularly those investigating the role HZE particles have on the CNS. First, we were interested in determining how ^{28}Si radiation exposure affects proliferation and neurogenesis in the young adult rodent hippocampus 24 hours post-irradiation and how it affects proliferation, neurogenesis, and survival in the young adult rodent hippocampus 3 months post-irradiation. Not only did we expand on what has been shown in regards to neurogenesis by irradiating both males and females with ^{28}Si, but we also address these goals by showing that hippocampal proliferation and neurogenesis is transiently affected by HZE particles yet only cell survival remains affected 3 months post-irradiation. Importantly, this ^{28}Si work also provides the groundwork for future mixed beam studies. Second, we were interested in determining if mature male mice exposed to whole body ^{56}Fe radiation have altered pattern separation ability when tested on an aversive platform and an appetitive platform. Here we show that HZE particles may not be as detrimental as previously believed, as male mice have shown transient improvements in pattern separation ability on both aversive and appetitive platforms. Finally, we were interested in determining if mature female mice exposed to whole body ^{56}Fe radiation have altered pattern separation ability when

tested on an appetitive platform and if ^{56}Fe radiation-induced improvements in pattern separation (using appetitive touchscreen platform) were long-lasting in male rodents. Here we provide critical female rodent data in a field that is severely lacking by showing sex-specific effects following HZE exposure. Specifically we found females mice might be more susceptible to rule-based learning deficits following exposure yet are unaffected for pattern separation ability. In addition, we discovered that radiation-induced improvements in pattern separation were not long-lasting using the appetitive touchscreen platform. While more work is needed to understand much of the HZE-induced cognitive changes that this dissertation has uncovered, this work will be crucial in evaluating its impact on future mission success.

Chapter 5, Figures

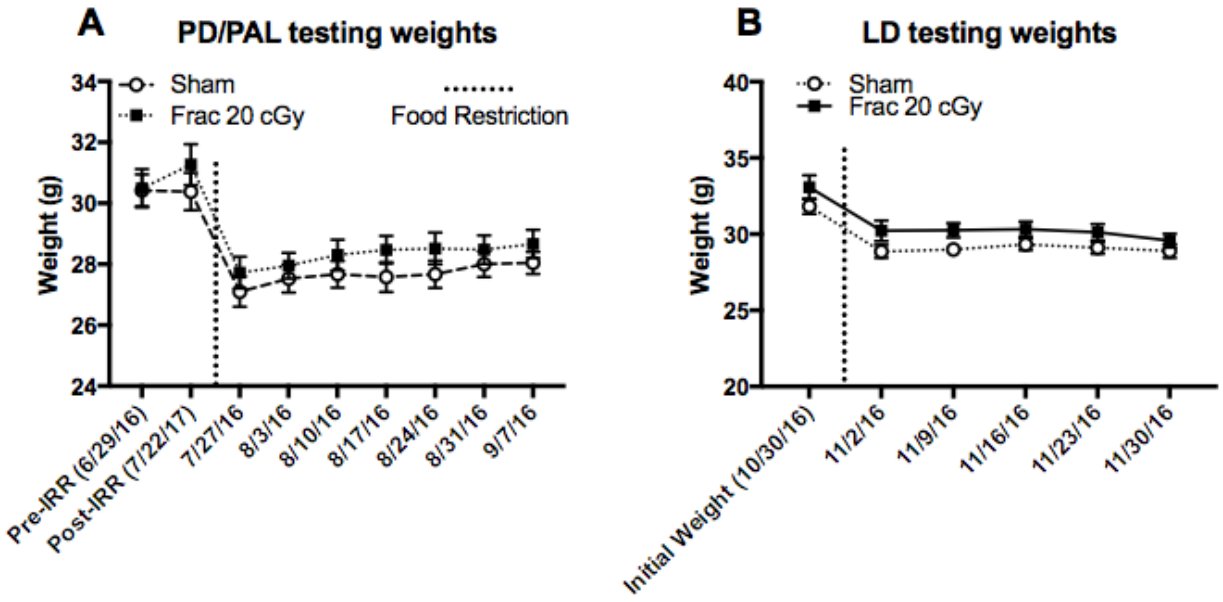

Figure 5-1. Analysis of post-irradiation weights reveal no differences in weight between IRR and Sham male mice during PD/Rev and LD testing. Body weight during PD and Rev touchscreen task **(A).** Body weight during LD touchscreen task **(B).** Mean±SEM. Two-way repeated measure ANOVA. *(See Fig 3-2 for rodent specifics)*

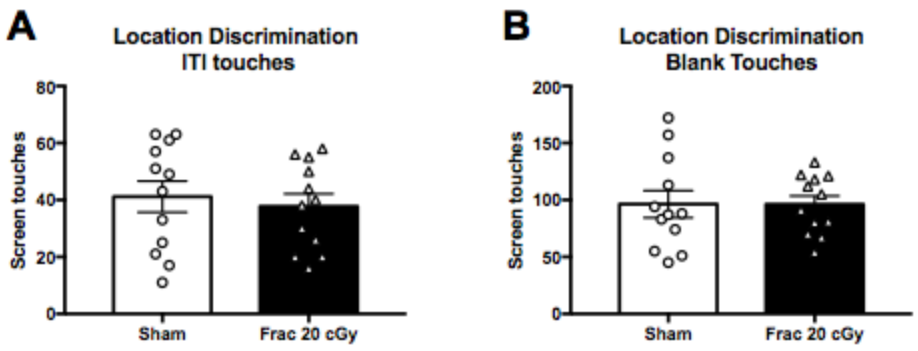

Figure 5-2. Analysis of Intertrial interval (ITI) touches and blank screen touches reveal no difference between Sham and IRR cohorts. Screen touches between each Location Discrimination trial show no difference **(A).** Screen touch counts for touches in blank window spaces do not show any differences between IRR and control **(B)**. Mean±SEM. Unpaired, two-tailed, t test. *(See Fig 3-2 for rodent specifics)*

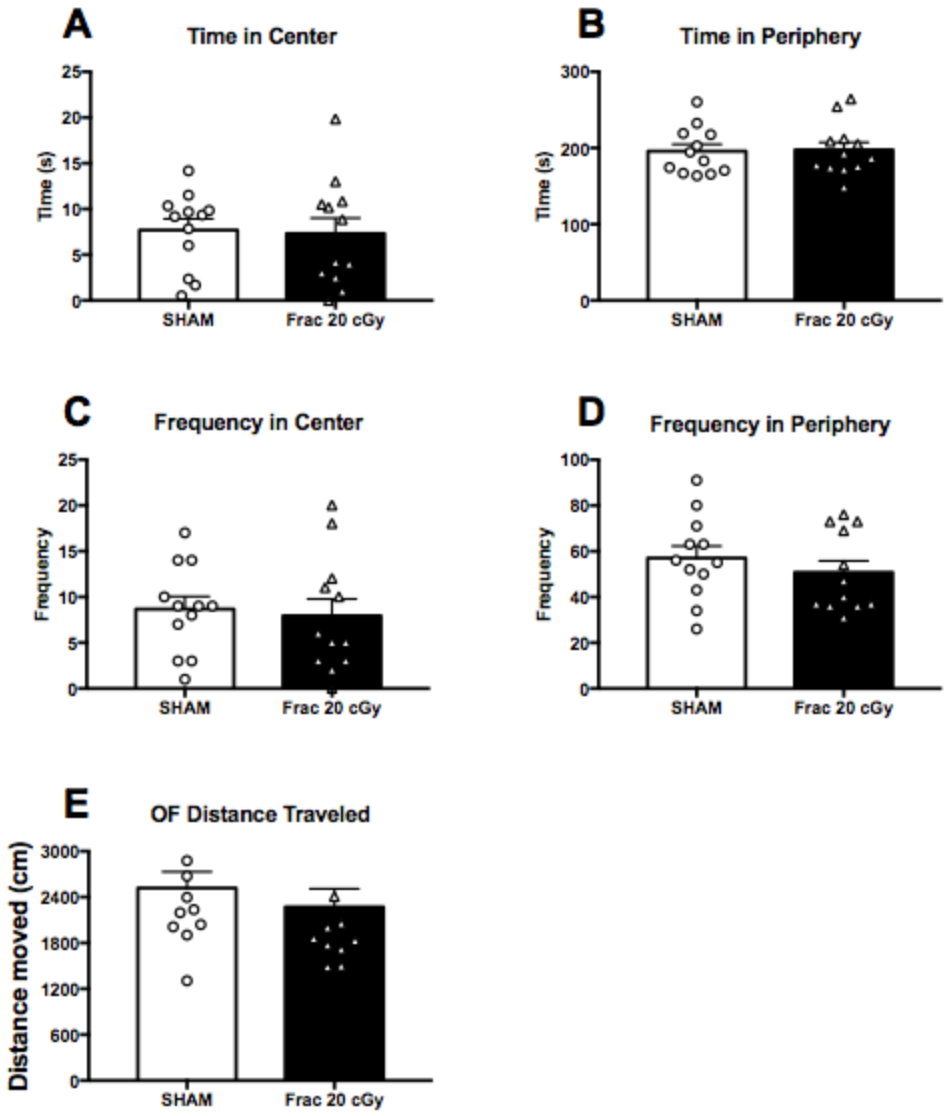

Figure 5-3. Analysis of time and frequency in center or periphery and distance traveled in the open field test show no differences in anxiety between IRR and Sham cohorts. Male Mice IRR with fractionated 20 cGy ^{56}Fe spend similar time in the center and periphery as the Sham cohort **(A-B)**. Mice also enter the center and periphery a similar amount of times, indicating that they are not just sitting still in either location **(C-D).** Finally, IRR and Sham are traveling similar distances **(E)**. Mean±SEM. Unpaired, two-tailed, t test. *(See Fig 3-2 for rodent specifics)*

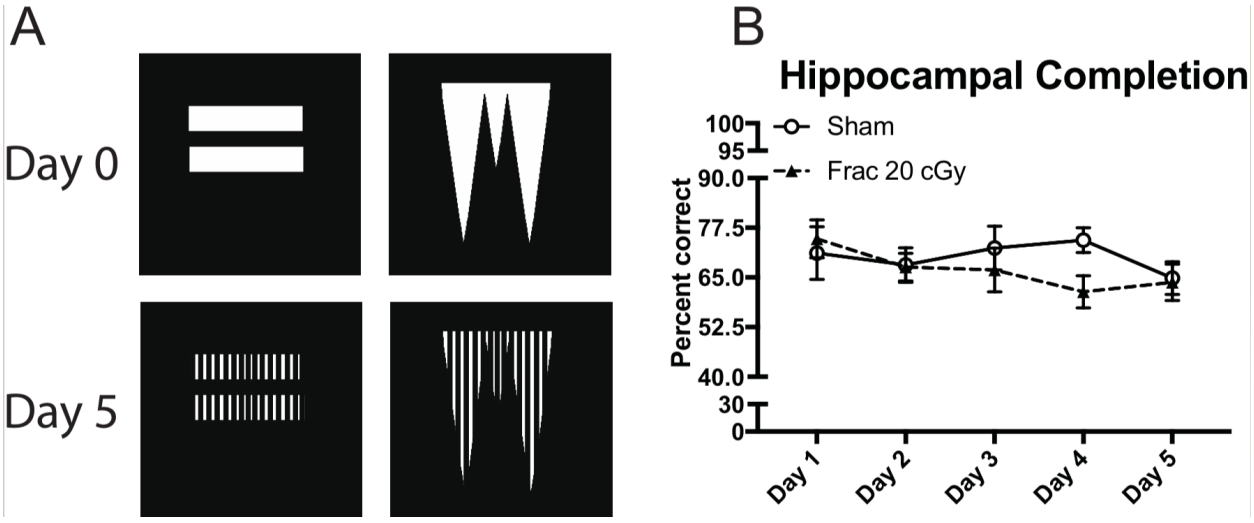

Figure 5-4. First attempt at developing a touchscreen-based hippocampal completion task suggests that the task needs to be more difficult for rodents.

Schematic showing the change in images from Day 0 (images during VMCL test) to Day 5 (last day of completion task)**(A).** Daily percent correct between groups show no difference **(B)**. Mean±SEM. Two-way repeated measure ANOVA. *(See Fig 4-3 for rodent specifics)*

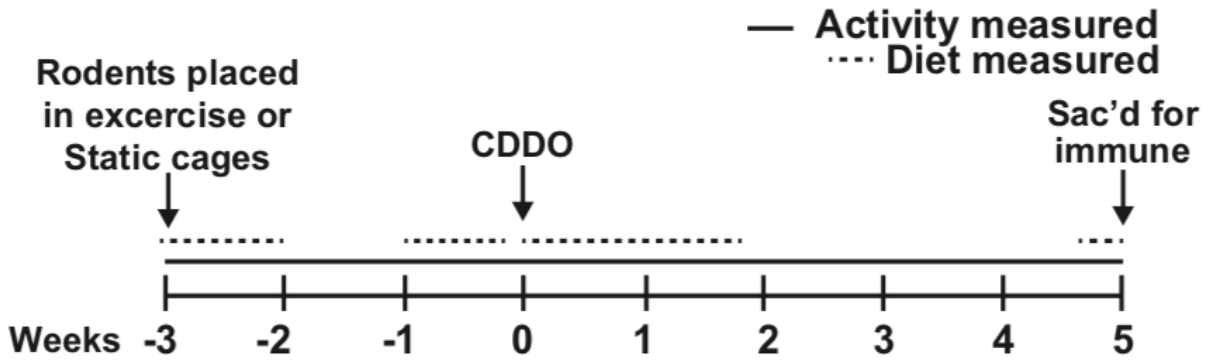

Figure 5-5. CDDO experimental timeline. Weeks relative to initial CDDO delivery. 2 month old C57BL/6J male mice body weights were measured once a week during the cage change. Manipulations (exercise vs static cages; Global Purina diet Control vs. CDDO). CDDO administration is indicated below timeline and was administered continuously following initial exposure.

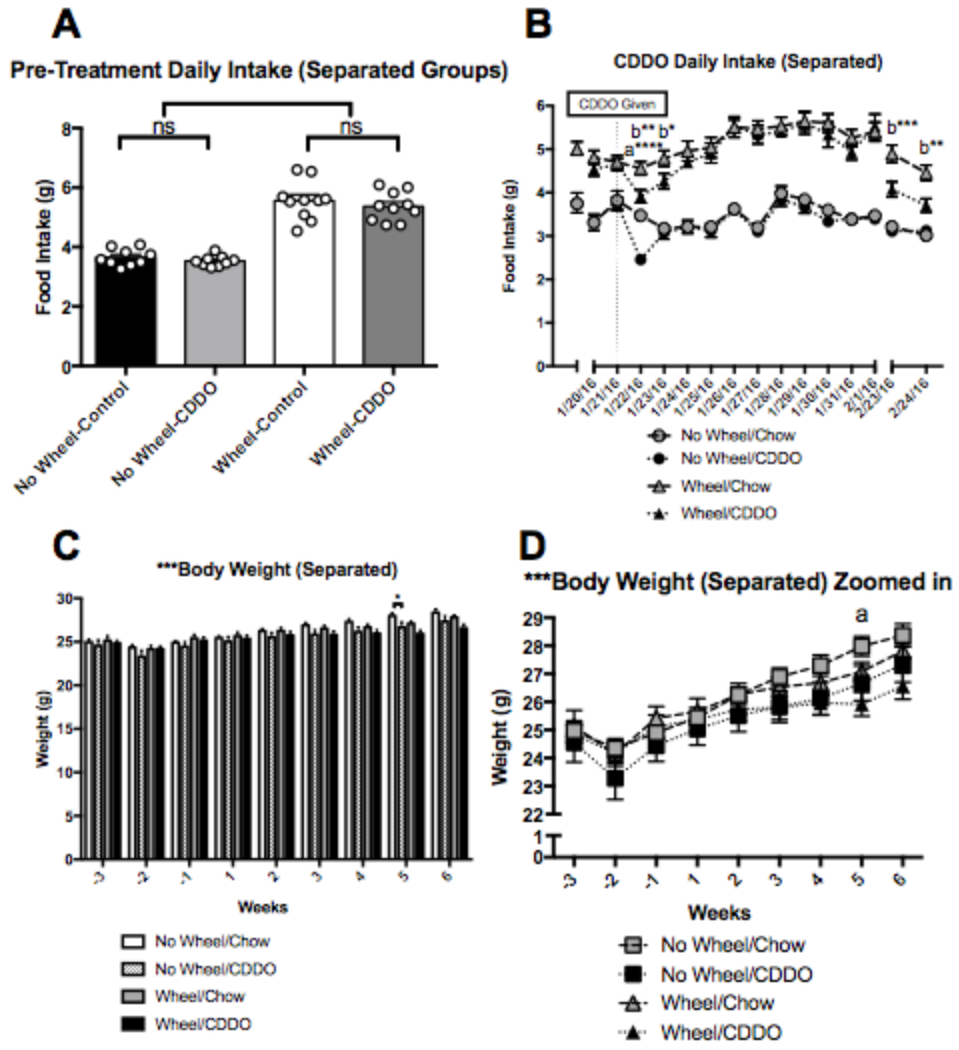

Figure 5-6. Long-term CDDO delivery does not change food intake or body weight in sedentary or exercise mice. (**A-C)** Food intake at Week -1, one week prior to Control or CDDO delivery, was similar across exercise matched groups (**A)**. Food intake was measured for 16 days (2 days prior and 12 days post-CDDO delivery and rechecked on the last two days of testing) **(B).** Data show differences in food intake from CDDO to control across both wheel and no wheel cohorts for the first day and then only for the wheel cohorts two days after and again on the last two days of testing **(B).** Body weight of the mice were measured weekly for 9 weeks and displayed as a bar

graph or line table, respectively **(C-D)**. There was not any significant body weight change within running-wheel exposure (exercise group) or no running-wheel exposure (sedentary group) over the CDDO administration, except week 5 between sedentary group **(C-D)**. This change was lost by week 6 **(C-D)**. Mean±SEM. One-way multiple comparisons ANOVA, uncorrected Fisher's LSD (**A**). Two-way multiple comparisons ANOVA, uncorrected Fisher's LSD (**B,C,D**). a=No Wheel/Chow vs No Wheel/CDDO, b=Wheel/Chow vs Wheel/CDDO; ✱P<0.05, ✱✱P<0.01, ✱✱✱P<0.001, ✱✱✱✱P<0.0001.

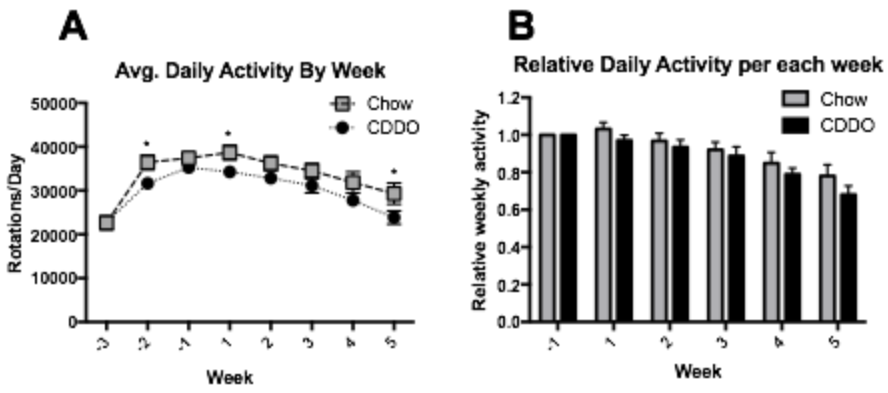

Figure 5-7. Long-term CDDO delivery does not change running wheel activity in exercise mice. *Note: The CDDO cohort was running significantly less than the control matched diet cohort prior to CDDO administration, Week -2, and was lost by week -1*. The average daily activity was calculated for each week and graphed to compare across weeks **(A).** Mice on CDDO ran significantly less week 1 and week 5 following CDDO administration **(A).** Because of the initial difference in running, running activity was normalized to the cohort activity levels 1 week prior to CDDO administration **(B).** When comparing relative activity, animals did not show any significant difference between groups **(B)**. Mean±SEM. Two-way repeated measures ANOVA, uncorrected Fisher's LSD. ✱P<0.05.

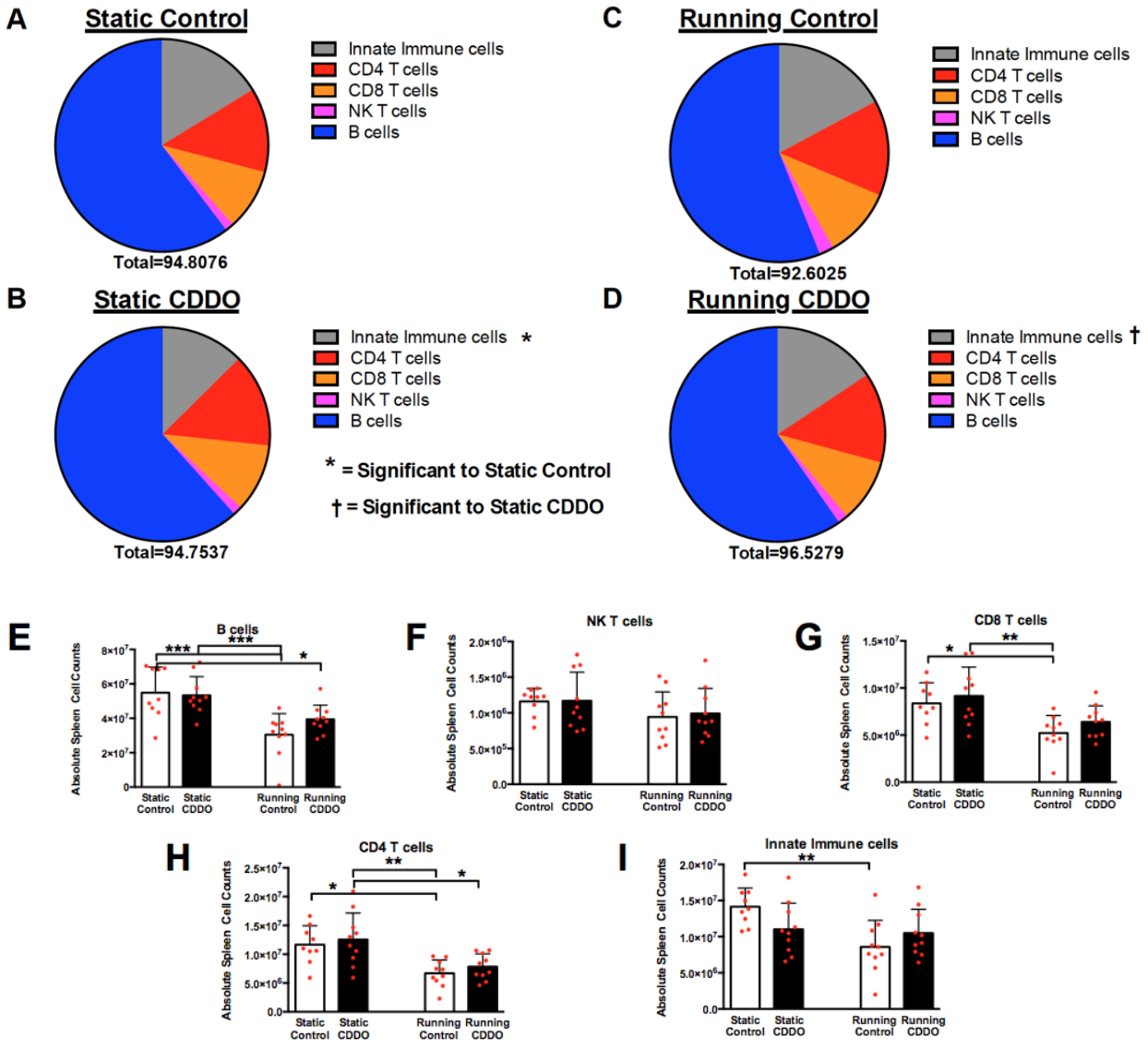

Figure 5-8. Long-term CDDO delivery alters the adaptive immune response. Immune system cell characterization from the spleen by flow cytometry shows cell population percentages **(A-D)** and absolute cell counts **(E-I)**. CDDO significantly reduces overall percentage and number of innate immune cells in sedentary mice **(A, B, I)**. Exercise reduced only the number of splenic adaptive immune cells; B, NK T, CD8 T, and CD4 T cells **(C, D, E-H)**. Two-way ANOVA using Bonferroni's multiple comparisons test. * P<0.05, ** P<0.01, *** P<0.001.

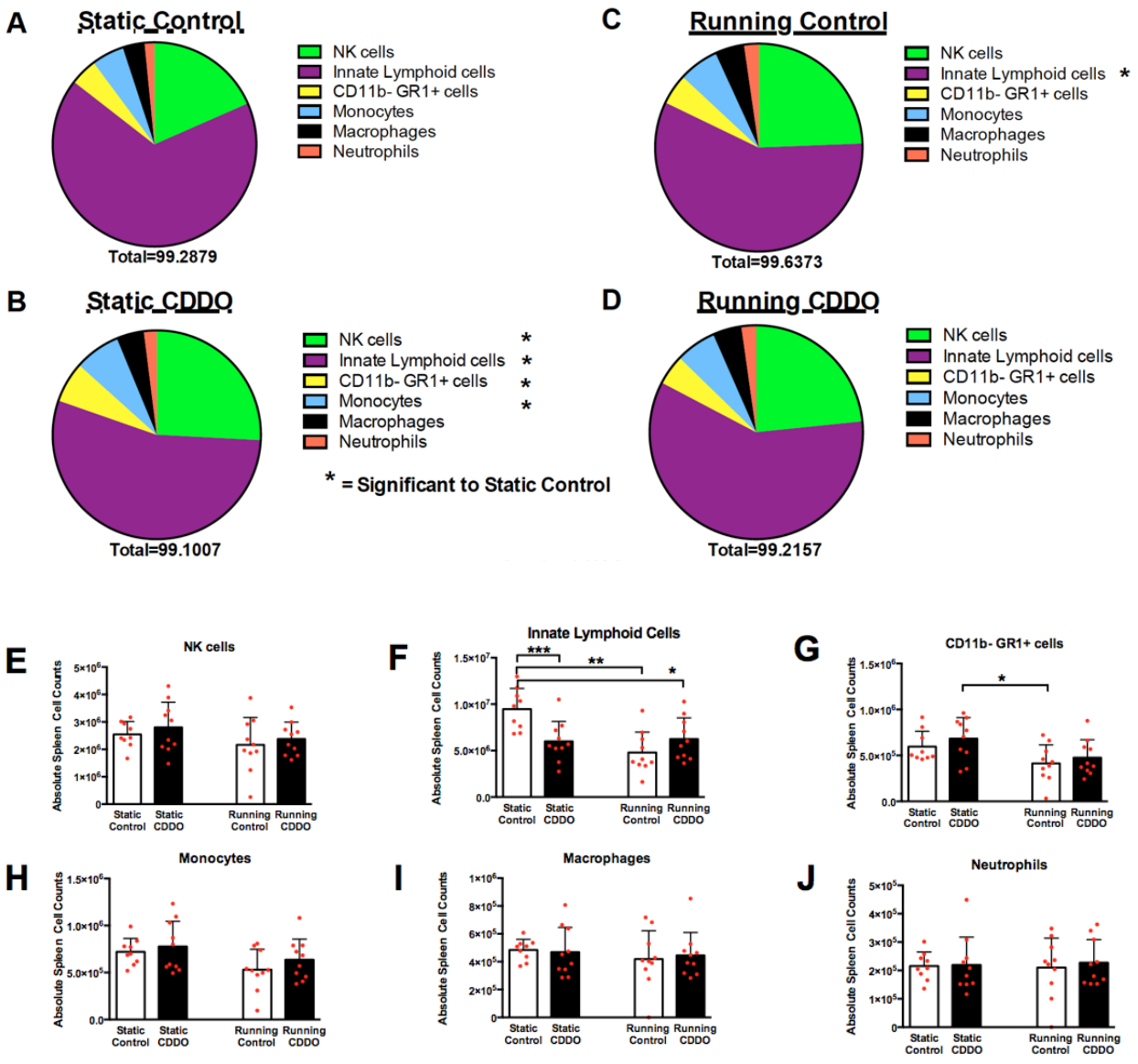

Figure 5-9. Long-term CDDO delivery decreases the innate lymphoid cells in Sed mice. Flow cytometry revealed CDDO significantly increased percentages of NK, CD11b- GR1+, and Monocytic innate immune cells in spleens of Sedentary mice **(A, B)**. In contrast, the percentage **(C)** and absolute cell number **(F)** of Innate Lymphoid cells was significantly reduced in spleen tissue of mice that were either subjected to exercise or treated with CDDO. There was no change in any innate immune cell percentage of running CDDO mice **(D)**, and neither CDDO nor exercise independently altered

absolute cell numbers of NK cells, CD11b- GR1+ cells, monocytes, macrophages, or neutrophils **(E, G-J)**. Two-way ANOVA using Bonferroni's multiple comparisons test. * P<0.05, ** P<0.01, *** P<0.001.

REFERENCES

Abchiche, A. & Others, 2016. Contributions of the Cherenkov Telescope Array (CTA) to the 6th International Symposium on High-Energy Gamma-Ray Astronomy (Gamma 2016). *arXiv [astro-ph.HE]*. Available at: http://arxiv.org/abs/1610.05151.

Acharya, M.M. et al., 2017. Epigenetic determinants of space radiation-induced cognitive dysfunction. *Scientific reports*, 7, p.42885.

Aimone, J.B. et al., 2014. Regulation and function of adult neurogenesis: from genes to cognition. *Physiological reviews*, 94(4), pp.991–1026.

Akers, K.G. et al., 2014. Hippocampal neurogenesis regulates forgetting during adulthood and infancy. *Science*, 344(6184), pp.598–602.

Altman, J. & Das, G.D., 1965. Autoradiographic and histological evidence of postnatal hippocampal neurogenesis in rats. *The Journal of comparative neurology*, 124(3), pp.319–335.

Amaral, D.G., Scharfman, H.E. & Lavenex, P., 2007. The dentate gyrus: fundamental neuroanatomical organization (dentate gyrus for dummies). In H. E. Scharfman, ed. *Progress in Brain Research*. Elsevier, pp. 3–790.

Antunes, M. & Biala, G., 2012. The novel object recognition memory: neurobiology, test procedure, and its modifications. *Cognitive processing*, 13(2), pp.93–110.

Becker, S., 2017. Neurogenesis and pattern separation: time for a divorce. *Wiley interdisciplinary reviews. Cognitive science*, 8(3). Available at:

http://dx.doi.org/10.1002/wcs.1427.

Bellone, J.A. et al., 2015. A Single Low Dose of Proton Radiation Induces Long-Term Behavioral and Electrophysiological Changes in Mice. *Radiation research*, 184(2), pp.193–202.

Ben Abdallah, N.M.-B. et al., 2010. Early age-related changes in adult hippocampal neurogenesis in C57 mice. *Neurobiology of aging*, 31(1), pp.151–161.

Bird, C.M. & Burgess, N., 2008. The hippocampus and memory: insights from spatial processing. *Nature reviews. Neuroscience*, 9(3), pp.182–194.

Bizon, J.L., Lee, H.J. & Gallagher, M., 2004. Neurogenesis in a rat model of age-related cognitive decline. *Aging cell*, 3(4), pp.227–234.

BNL | NASA Space Radiation Laboratory (NSRL). Available at: https://www.bnl.gov/nsrl/ [Accessed March 6, 2018b].

von Bohlen Und Halbach, O., 2007. Immunohistological markers for staging neurogenesis in adult hippocampus. *Cell and tissue research*, 329(3), pp.409–420.

Boice, J.D., Jr, 2017. Space: The Final Frontier—Research Relevant to Mars. *Health physics*, 112(4), p.392.

Boldrini, M. et al., 2018. Human Hippocampal Neurogenesis Persists throughout Aging. *Cell Stem Cell,* 22(4), pp. 589-599.

Bonaguidi, M.A. et al., 2012. A unifying hypothesis on mammalian neural stem cell properties in the adult hippocampus. *Current opinion in neurobiology*, 22(5),

pp.754–761.

Bond, A.M., Ming, G.-L. & Song, H., 2015. Adult Mammalian Neural Stem Cells and Neurogenesis: Five Decades Later. *Cell stem cell*, 17(4), pp.385–395.

Britten, R.A. et al., 2017. Changes in the Hippocampal Proteome Associated with Spatial Memory Impairment after Exposure to Low (20 cGy) Doses of 1 GeV/n 56Fe Radiation. *Radiation research*, 187(3), pp.287–297.

Britten, R.A. et al., 2014. Exposure to mission relevant doses of 1 GeV/Nucleon (56)Fe particles leads to impairment of attentional set-shifting performance in socially mature rats. *Radiation research*, 182(3), pp.292–298.

Britten, R.A. et al., 2011. Low (20 cGy) Doses of 1 GeV/u 56Fe-Particle Radiation Lead to a Persistent Reduction in the Spatial Learning Ability of Rats. *Radiation research*, 177(2), pp.146–151.

Brown, J.P. et al., 2003. Transient expression of doublecortin during adult neurogenesis. *The Journal of comparative neurology*, 467(1), pp.1–10.

Brynskikh, A. et al., 2008. Adaptive immunity affects learning behavior in mice. *Brain, behavior, and immunity*, 22(6), pp.861–869.

Bucker, H. & Facius, R., 1981. The role of HZE particles in space flight: results from spaceflight and ground-based experiments. *Acta astronautica*, 8(9-10), pp.1099–1107.

Bussey, T.J. et al., 2000. Distinct patterns of behavioural impairments resulting from

fornix transection or neurotoxic lesions of the perirhinal and postrhinal cortices in the rat. *Behavioural brain research*, 111(1-2), pp.187–202.

Bussey, T.J. et al., 1997. Triple dissociation of anterior cingulate, posterior cingulate, and medial frontal cortices on visual discrimination tasks using a touchscreen testing procedure for the rat. *Behavioral neuroscience*, 111(5), pp.920–936.

Cameron, H.A. et al., 1993. Differentiation of newly born neurons and glia in the dentate gyrus of the adult rat. *Neuroscience*, 56(2), pp.337–344.

Canales, J.J., 2016. *Adult Neurogenesis in the Hippocampus: Health, Psychopathology, and Brain Disease*, Academic Press.

Carr, H. et al., 2018. Early effects of 16O radiation on Neuronal Morphology and Cognition in a Murine Model. *Life Sciences in Space Research*. Available at: http://www.sciencedirect.com/science/article/pii/S2214552417301323.

Carrihill-Knoll, K.L. et al., 2007. Amphetamine-induced taste aversion learning in young and old F-344 rats following exposure to 56Fe particles. *Age* , 29(2-3), pp.69–76.

Casadesus, G. et al., 2005. Hippocampal neurogenesis and PSA-NCAM expression following exposure to 56Fe particles mimics that seen during aging in rats. *Experimental gerontology*, 40(3), pp.249–254.

Cès, A. et al., 2018. Age-related vulnerability of pattern separation in C57BL/6J mice. *Neurobiology of aging*, 62, pp.120–129.

Chancellor, J.C., Scott, G.B.I. & Sutton, J.P., 2014. Space Radiation: The Number One

Risk to Astronaut Health beyond Low Earth Orbit. *Life* , 4(3), pp.491–510.

Chang, K., 2018. Falcon Heavy, in a Roar of Thunder, Carries SpaceX's Ambition Into Orbit. *The New York Times*. Available at: https://www.nytimes.com/2018/02/06/science/falcon-heavy-spacex-launch.html [Accessed February 6, 2018].

Chen, J. et al., 2008. Neuroinflammation and disruption in working memory in aged mice after acute stimulation of the peripheral innate immune system. *Brain, behavior, and immunity*, 22(3), pp.301–311.

Christie, B.R. & Cameron, H.A., 2006. Neurogenesis in the adult hippocampus. *Hippocampus*, 16(3), pp.199–207.

Chudasama, Y., Bussey, T.J. & Muir, J.L., 2001. Effects of selective thalamic and prelimbic cortex lesions on two types of visual discrimination and reversal learning. *The European journal of neuroscience*, 14(6), pp.1009–1020.

Clark, R.E., Zola, S.M. & Squire, L.R., 2000. Impaired recognition memory in rats after damage to the hippocampus. *The Journal of neuroscience: the official journal of the Society for Neuroscience*, 20(23), pp.8853–8860.

Clelland, C.D. et al., 2009. A functional role for adult hippocampal neurogenesis in spatial pattern separation. *Science*, 325(5937), pp.210–213.

Couillard-Despres, S. & Winner, B., 2005. Doublecortin expression levels in adult brain reflect neurogenesis. *European Journal of*. Available at: http://onlinelibrary.wiley.com/doi/10.1111/j.1460-9568.2004.03813.x/full.

Creer, D.J. et al., 2010. Running enhances spatial pattern separation in mice. *Proceedings of the National Academy of Sciences of the United States of America*, 107(5), pp.2367–2372.

Cucinotta, F.A. et al., 2013. How safe is safe enough? Radiation risk for a human mission to Mars. *PloS one*, 8(10), p.e74988.

Cucinotta, F.A. et al., 2015. Safe days in space with acceptable uncertainty from space radiation exposure. *Life sciences and space research*, 5, pp.31–38.

Cucinotta, F.A. et al., 2014. Space radiation risks to the central nervous system. *Life Sciences in Space Research*, 2, pp.54–69.

Cucinotta, F.A. & Durante, M., 2006. Cancer risk from exposure to galactic cosmic rays: implications for space exploration by human beings. *The lancet oncology*, 7(5), pp.431–435.

Cucinotta, F.A., Nikjoo, H. & Goodhead, D.T., 2000. Model for radial dependence of frequency distributions for energy imparted in nanometer volumes from HZE particles. *Radiation research*, 153(4), pp.459–468.

Cucinotta, F.A., Nikjoo, H. & Goodhead, D.T., 1998. The effects of delta rays on the number of particle-track traversals per cell in laboratory and space exposures. *Radiation research*, 150(1), pp.115–119.

Curtis, M.A., Kam, M. & Faull, R.L.M., 2011. Neurogenesis in humans. *The European journal of neuroscience*, 33(6), pp.1170–1174.

Danielson, N.B. et al., 2016. Distinct Contribution of Adult-Born Hippocampal Granule Cells to Context Encoding. *Neuron*, 90(1), pp.101–112.

Dayer, A.G. et al., 2005. New GABAergic interneurons in the adult neocortex and striatum are generated from different precursors. *The Journal of cell biology*, 168(3), pp.415–427.

DeCarolis, N.A. et al., 2014. (56)Fe Particle Exposure Results in a Long-Lasting Increase in a Cellular Index of Genomic Instability and Transiently Suppresses Adult Hippocampal Neurogenesis in Vivo. *Life sciences and space research*, 2, pp.70–79.

DeCarolis, N.A. et al., 2013. In vivo contribution of nestin- and GLAST-lineage cells to adult hippocampal neurogenesis. *Hippocampus*, 23(8), pp.708–719.

Doyle et al., 2008. Application of a Translational Profiling Approach for the Comparative Analysis of CNS Cell Types. *Cell,* 135(4), pp. 749-762

Dranovsky, A. et al., 2011. Experience dictates stem cell fate in the adult hippocampus. *Neuron*, 70(5), pp.908–923.

Drew, M.R., Denny, C.A. & Hen, R., 2010. Arrest of adult hippocampal neurogenesis in mice impairs single- but not multiple-trial contextual fear conditioning. *Behavioral neuroscience*, 124(4), pp.446–454.

Durante, M., 2014. Space radiation protection: Destination Mars. *Life sciences and space research*, 1, pp.2–9.

Duvernoy, H.M., 2005. *The Human Hippocampus: Functional Anatomy, Vascularization and Serial Sections with MRI*, Springer Science & Business Media.

Ehninger, D. & Kempermann, G., 2006. Paradoxical effects of learning the Morris water maze on adult hippocampal neurogenesis in mice may be explained by a combination of stress and physical activity. *Genes, brain, and behavior*, 5(1), pp.29–39.

Eisch, A.J., 2002. Adult neurogenesis: implications for psychiatry. *Progress in brain research*, 138, pp.315–342.

Eisch, A.J. et al., 2000. Opiates inhibit neurogenesis in the adult rat hippocampus. *Proceedings of the National Academy of Sciences of the United States of America*, 97(13), pp.7579–7584.

Eisch, A.J. & Mandyam, C.D., 2007. Adult neurogenesis: can analysis of cell cycle proteins move us “Beyond BrdU”? *Current pharmaceutical biotechnology*, 8(3), pp.147–165.

Encinas, J.M. et al., 2008. Quiescent adult neural stem cells are exceptionally sensitive to cosmic radiation. *Experimental neurology*, 210(1), pp.274–279.

Epp, J.R. et al., 2016. Neurogenesis-mediated forgetting minimizes proactive interference. *Nature communications*, 7, p.10838.

Eriksson, P.S. et al., 1998. Neurogenesis in the adult human hippocampus. *Nature medicine*, 4(11), pp.1313–1317.

Fanselow, M.S. & Dong, H.W., 2010. Are the dorsal and ventral hippocampus functionally distinct structures? *Neuron*, 65(1), pp.7–19.

Filippov, V. et al., 2003. Subpopulation of nestin-expressing progenitor cells in the adult murine hippocampus shows electrophysiological and morphological characteristics of astrocytes. *Molecular and cellular neurosciences*, 23(3), pp.373–382.

Francis, F. et al., 1999. Doublecortin is a developmentally regulated, microtubule-associated protein expressed in migrating and differentiating neurons. *Neuron*, 23(2), pp.247–256.

Fukuda, S. et al., 2003. Two distinct subpopulations of nestin-positive cells in adult mouse dentate gyrus. *The Journal of neuroscience: the official journal of the Society for Neuroscience*, 23(28), pp.9357–9366.

Gebara, E. et al., 2015. Taurine increases hippocampal neurogenesis in aging mice. *Stem cell research*, 14(3), pp.369–379.

Gemignani, J., Gheysens, T. & Summerer, L., 2015. Beyond astronaut's capabilities: The current state of the art. *Conference proceedings: ... Annual International Conference of the IEEE Engineering in Medicine and Biology Society. IEEE Engineering in Medicine and Biology Society. Conference*, 2015, pp.3615–3618.

Ge, S. et al., 2008. Synaptic integration and plasticity of new neurons in the adult hippocampus. *The Journal of physiology*, 586(16), pp.3759–3765.

Gifford, S.E. & Magazine, A., 2014. Calculated Risks: How Radiation Rules Manned Mars Exploration. *Space.com*. Available at: https://www.space.com/24731-mars-

radiation-curiosity-rover.html [Accessed January 31, 2018].

Gilbert, P.E., Kesner, R.P. & Lee, I., 2001. Dissociating hippocampal subregions: double dissociation between dentate gyrus and CA1. *Hippocampus*, 11(6), pp.626–636.

Gleeson, J.G. et al., 1998. Doublecortin, a brain-specific gene mutated in human X-linked lissencephaly and double cortex syndrome, encodes a putative signaling protein. *Cell*, 92(1), pp.63–72.

Gonçalves, J.T., Schafer, S.T. & Gage, F.H., 2016. Adult Neurogenesis in the Hippocampus: From Stem Cells to Behavior. *Cell*, 167(4), pp.897–914.

Goodrich-Hunsaker, N.J., Hunsaker, M.R. & Kesner, R.P., 2008. The interactions and dissociations of the dorsal hippocampus subregions: how the dentate gyrus, CA3, and CA1 process spatial information. *Behavioral neuroscience*, 122(1), pp.16–26.

Gresack, J.E. et al., 2010. Isolation rearing-induced deficits in contextual fear learning do not require CRF(2) receptors. *Behavioural brain research*, 209(1), pp.80–84.

Grivas, I. et al., 2003. Vascular network of the rat hippocampus is not homogeneous along the septotemporal axis. *Brain research*, 971(2), pp.245–249.

Hagen, U., 1989. Radiation biology in space: a critical review. *Advances in space research: the official journal of the Committee on Space Research* , 9(10), pp.3–8.

Haley, G.E. et al., 2013. Early effects of whole-body (56)Fe irradiation on hippocampal function in C57BL/6J mice. *Radiation research*, 179(5), pp.590–596.

Hill, A.S., Sahay, A. & Hen, R., 2015. Increasing Adult Hippocampal Neurogenesis is Sufficient to Reduce Anxiety and Depression-Like Behaviors. *Neuropsychopharmacology: official publication of the American College of Neuropsychopharmacology*, 40(10), pp.2368–2378.

Hladik, D. & Tapio, S., 2016. Effects of ionizing radiation on the mammalian brain. *Mutation research*, 770(Pt B), pp.219–230.

Holden, H.M. & Gilbert, P.E., 2012. Less efficient pattern separation may contribute to age-related spatial memory deficits. *Frontiers in aging neuroscience*, 4, p.9.

Horner, A.E. et al., 2013. The touchscreen operant platform for testing learning and memory in rats and mice. *Nature protocols*, 8(10), pp.1961–1984.

Howard, V. & Reed, M., 2004. *Unbiased Stereology: Three-Dimensional Measurement in Microscopy*, Garland Science.

Izquierdo, I., Furini, C.R.G. & Myskiw, J.C., 2016. Fear Memory. *Physiological reviews*, 96(2), pp.695–750.

Jackson Laboratory, 2018. Life span as a biomarker. *The Jackson Laboratory*. Available at: https://www.jax.org/research-and-faculty/research-labs/the-harrison-lab/gerontology/life-span-as-a-biomarker [Accessed March 13, 2018].

Jandial, R. et al., 2018. Space-brain: The negative effects of space exposure on the central nervous system. *Surgical neurology international*, 9, p.9.

Jarrard, L.E., Luu, L.P. & Davidson, T.L., 2012. A study of hippocampal structure-

function relations along the septo-temporal axis. *Hippocampus*, 22(4), pp.680–692.

Jinno, S., 2011. Topographic differences in adult neurogenesis in the mouse hippocampus: A stereology-based study using endogenous markers. *Hippocampus*, 21(5), pp.467–480.

Jonas, P. & Lisman, J., 2014. Structure, function, and plasticity of hippocampal dentate gyrus microcircuits. *Frontiers in neural circuits*, 8, p.107.

Jung, M.W., Wiener, S.I. & McNaughton, B.L., 1994. Comparison of spatial firing characteristics of units in dorsal and ventral hippocampus of the rat. *The Journal of neuroscience: the official journal of the Society for Neuroscience*, 14(12), pp.7347–7356.

Kee, N. et al., 2002. The utility of Ki-67 and BrdU as proliferative markers of adult neurogenesis. *Journal of neuroscience methods*, 115(1), pp.97–105.

Kempermann, G. et al., 2003. Early determination and long-term persistence of adult-generated new neurons in the hippocampus of mice. *Development* , 130(2), pp.391–399.

Kempermann, G. et al., 2004. Milestones of neuronal development in the adult hippocampus. *Trends in neurosciences*, 27(8), pp.447–452.

Kempermann, G., 2002. Why new neurons? Possible functions for adult hippocampal neurogenesis. *The Journal of neuroscience: the official journal of the Society for Neuroscience*, 22(3), pp.635–638.

Kempermann, G., Song, H. & Gage, F.H., 2015. Neurogenesis in the Adult Hippocampus. *Cold Spring Harbor perspectives in biology*, 7(9), p.a018812.

Kesner, R.P., 2007. A behavioral analysis of dentate gyrus function. *Progress in brain research*, 163, pp.567–576.

Kheirbek, M.A. & Hen, R., 2011. Dorsal vs ventral hippocampal neurogenesis: implications for cognition and mood. *Neuropsychopharmacology: official publication of the American College of Neuropsychopharmacology*, 36(1), pp.373–374.

Kiffer, F. et al., 2018. Effects of 1H + 16O Charged Particle Irradiation on Short-Term Memory and Hippocampal Physiology in a Murine Model. *Radiation research*, 189(1), pp.53–63.

Kim et al., 2012. Targeting of Nrf2 induces DNA damage signaling and protects colonic epithelial cells from ionizing radiation. *Proceedings of the National Academy of Sciences of the United States of America*, 109(43).

Kim, J.J. & Fanselow, M.S., 1992. Modality-specific retrograde amnesia of fear. *Science*, 256(5057), pp.675–677.

Kim, J.-S. et al., 2009. Differences in immunoreactivities of Ki-67 and doublecortin in the adult hippocampus in three strains of mice. *Acta histochemica*, 111(2), pp.150–156.

Kim, M.-H.Y., Rusek, A. & Cucinotta, F.A., 2015. Issues for Simulation of Galactic Cosmic Ray Exposures for Radiobiological Research at Ground-Based Accelerators. *Frontiers in oncology*, 5, p.122.

Kjelstrup, K.G. et al., 2002. Reduced fear expression after lesions of the ventral hippocampus. *Proceedings of the National Academy of Sciences of the United States of America*, 99(16), pp.10825–10830.

Klein, C. et al., 2016. Physical exercise counteracts MPTP-induced changes in neural precursor cell proliferation in the hippocampus and restores spatial learning but not memory performance in the water maze. *Behavioural brain research*, 307, pp.227–238.

Knobloch, M. et al., 2013. Metabolic control of adult neural stem cell activity by Fasn-dependent lipogenesis. *Nature*, 493(7431), pp.226–230.

Knoth, R. et al., 2010. Murine features of neurogenesis in the human hippocampus across the lifespan from 0 to 100 years. *PloS one*, 5(1), p.e8809.

Kohler, S.J. et al., 2011. Maturation time of new granule cells in the dentate gyrus of adult macaque monkeys exceeds six months. *Proceedings of the National Academy of Sciences of the United States of America*, 108(25), pp.10326–10331.

Koike, Y. et al., 2005. Effects of HZE particle on the nigrostriatal dopaminergic system in a future Mars mission. *Acta astronautica*, 56(3), pp.367–378.

Kravitz, A.V. & Kreitzer, A.C., 2012. Striatal mechanisms underlying movement, reinforcement, and punishment. *Physiology* , 27(3), pp.167–177.

Kronenberg, G. et al., 2003. Subpopulations of proliferating cells of the adult hippocampus respond differently to physiologic neurogenic stimuli. *The Journal of comparative neurology*, 467(4), pp.455–463.

Kuhn, H.G. & Peterson, D.A., 2008. Detection and phenotypic characterization of adult neurogenesis. *Cold Spring Harbor Monograph Series*, 52, p.25.

Lagace, D.C. et al., 2010. Adult hippocampal neurogenesis is functionally important for stress-induced social avoidance. *Proceedings of the National Academy of Sciences of the United States of America*, 107(9), pp.4436–4441.

Lagace, D.C. et al., 2008. Cdk5 is essential for adult hippocampal neurogenesis. *Proceedings of the National Academy of Sciences of the United States of America*, 105(47), pp.18567–18571.

Lagace, D.C., Whitman, M.C., Noonan, M.A., Ables, J.L., DeCarolis, N.A., Arguello, A.A., Donovan, M.H., Fischer, S.J., Farnbauch, L.A., Beech, R.D. & Others, 2007. Dynamic contribution of nestin-expressing stem cells to adult neurogenesis. *The Journal of neuroscience: the official journal of the Society for Neuroscience*, 27(46), pp.12623–12629.

Lagace, D.C., Whitman, M.C., Noonan, M.A., Ables, J.L., DeCarolis, N.A., Arguello, A.A., Donovan, M.H., Fischer, S.J., Farnbauch, L.A., Beech, R.D., DiLeone, R.J., et al., 2007. Dynamic contribution of nestin-expressing stem cells to adult neurogenesis. *The Journal of neuroscience: the official journal of the Society for Neuroscience*, 27(46), pp.12623–12629.

Lagace, D.C. et al., 2006. Juvenile administration of methylphenidate attenuates adult hippocampal neurogenesis. *Biological psychiatry*, 60(10), pp.1121–1130.

Latchney, S.E. et al., 2014. Developmental and adult GAP-43 deficiency in mice

dynamically alters hippocampal neurogenesis and mossy fiber volume. *Developmental neuroscience*, 36(1), pp.44–63.

Leal, S.L. & Yassa, M.A., 2018. Integrating new findings and examining clinical applications of pattern separation. *Nature neuroscience*, 21(2), pp.163–173.

Lee, C.-Y., Robinson, K.J. & Doe, C.Q., 2006. Lgl, Pins and aPKC regulate neuroblast self-renewal versus differentiation. *Nature*, 439(7076), pp.594–598.

Leuner, B., Gould, E. & Shors, T.J., 2006. Is there a link between adult neurogenesis and learning? *Hippocampus*, 16(3), pp.216–224.

Liu, X. et al., 2012. Optogenetic stimulation of a hippocampal engram activates fear memory recall. *Nature*, 484(7394), pp.381–385.

Mahaney, B.L., Meek, K. & Lees-Miller, S.P., 2009. Repair of ionizing radiation-induced DNA double-strand breaks by non-homologous end-joining. *Biochemical Journal*, 417(3), pp.639–650.

Mahar, I. et al., 2016. Effects of neuregulin-1 administration on neurogenesis in the adult mouse hippocampus, and characterization of immature neurons along the septotemporal axis. *Scientific reports*, 6, p.30467.

Manda, Ueno, K.;. & K., M.;. A., 2008. Space radiation-induced inhibition of neurogenesis in the hippocampal dentate gyrus and memory impairment in mice: ameliorative potential of the melatonin metabolite, AFMK. *Journal of pineal research*, 45, pp.430–438.

Mandyam, C.D., Harburg, G.C. & Eisch, A.J., 2007. Determination of key aspects of precursor cell proliferation, cell cycle length and kinetics in the adult mouse subgranular zone. *Neuroscience*, 146(1), pp.108–122.

Maren, S., Phan, K.L. & Liberzon, I., 2013. The contextual brain: implications for fear conditioning, extinction and psychopathology. *Nature reviews. Neuroscience*, 14(6), pp.417–428.

Marty, V.N. et al., 2014. Radiation-induced alterations in synaptic neurotransmission of dentate granule cells depend on the dose and species of charged particles. *Radiation research*, 182(6), pp.653–665.

McAvoy, K., Besnard, A. & Sahay, A., 2015. Adult hippocampal neurogenesis and pattern separation in DG: a role for feedback inhibition in modulating sparseness to govern population-based coding. *Frontiers in systems neuroscience*, 9, p.120.

McHugh et al., 2007. Dentate Gyrus NMDA Receptors Mediate Rapid Pattern Separation in the Hippocampal Network. *Science*, 317(94), pp.94–99.

McHugh, T.J. et al., 2007. Dentate gyrus NMDA receptors mediate rapid pattern separation in the hippocampal network. *Science*, 317(5834), pp.94–99.

McTighe, S.M. et al., 2009. A new touchscreen test of pattern separation: effect of hippocampal lesions. *Neuroreport*, 20(9), pp.881–885.

Ming, G.L. & Song, H., 2011. Adult neurogenesis in the mammalian brain: significant answers and significant questions. *Neuron*, 70(4), pp.687–702.

Moser, M.B. et al., 1995. Spatial learning with a minislab in the dorsal hippocampus. *Proceedings of the National Academy of Sciences of the United States of America*, 92(21), pp.9697–9701.

Moser, M.B. & Moser, E.I., 1998. Functional differentiation in the hippocampus. *Hippocampus*, 8(6), pp.608–619.

Mouton, P., 2009. Applications of Modern Stereology to Quantitative Light Microscopy. *Microscopy and Microanalysis; Cambridge*, 15(S2), pp.1526–1527.

Mumby, D.G. et al., 2002. Hippocampal damage and exploratory preferences in rats: memory for objects, places, and contexts. *Learning & memory* , 9(2), pp.49–57.

Myers, C.E. & Scharfman, H.E., 2009. A role for hilar cells in pattern separation in the dentate gyrus: a computational approach. *Hippocampus*, 19(4), pp.321–337.

Nakashiba, T. et al., 2012. Young dentate granule cells mediate pattern separation, whereas old granule cells facilitate pattern completion. *Cell*, 149(1), pp.188–201.

NASA, Astronaut Frequently Asked Questions. Available at: https://astronauts.nasa.gov/content/faq.htm.

Nelson, G.A., 2003a. Fundamental Space Radiobiology. *Gravitational and space biology bulletin: publication of the American Society for Gravitational and Space Biology*, 16, pp.29–36.

Nelson, G.A., 2003b. Fundamental space radiobiology. *Gravitational and space biology bulletin: publication of the American Society for Gravitational and Space Biology*,

16(2), pp.29–36.

Nelson, G.A., 2016. Space Radiation and Human Exposures, A Primer. *Radiation research*, 185(4), pp.349–358.

Nelson, G.A., Simonsen, L. & Huff, J.L., 2016. Evidence Report: Risk of Acute and Late Central Nervous System Effects from Radiation Exposure. Available at: https://ntrs.nasa.gov/search.jsp?R=20160004368 [Accessed March 6, 2018].

Noonan, M.A. et al., 2010. Reduction of adult hippocampal neurogenesis confers vulnerability in an animal model of cocaine addiction. *The Journal of neuroscience: the official journal of the Society for Neuroscience*, 30(1), pp.304–315.

Norbury, J.W. et al., 2016. Galactic cosmic ray simulation at the NASA Space Radiation Laboratory. *Life sciences and space research*, 8, pp.38–51.

O'Banion, M.K., Space Radiation and the Central Nervous System: Potential Risks. Available at: https://three.jsc.nasa.gov/articles/OBanionCNS.pdf.

O'Keefe, J. & Dostrovsky, J., 1971. The hippocampus as a spatial map. Preliminary evidence from unit activity in the freely-moving rat. *Brain research*, 34(1), pp.171–175.

O'Leary, O.F. & Cryan, J.F., 2014. A ventral view on antidepressant action: roles for adult hippocampal neurogenesis along the dorsoventral axis. *Trends in pharmacological sciences*, 35(12), pp.675–687.

Oomen, C.A. et al., 2014. Adult hippocampal neurogenesis and its role in cognition.

Wiley interdisciplinary reviews. Cognitive science, 5(5), pp.573–587.

Parihar et al., 2015. What happens to your brain on the way to Mars. *Science Advances*, 1(4).

Parihar, V.K. et al., 2016. Cosmic radiation exposure and persistent cognitive dysfunction. *Scientific reports*, 6, p.34774.

Parihar, V.K. et al., 2018. Persistent nature of alterations in cognition and neuronal circuit excitability after exposure to simulated cosmic radiation in mice. *Experimental neurology*. Available at: http://dx.doi.org/10.1016/j.expneurol.2018.03.009.

Parihar, V.K. et al., 2015. Targeted overexpression of mitochondrial catalase prevents radiation-induced cognitive dysfunction. *Antioxidants & redox signaling*, 22(1), pp.78–91.

Paris, A., 2014. Physiological and Psychological Aspects of Sending Humans to Mars. *The Center for Planetary Science*. Available at: http://planetary-science.org/wp-content/uploads/2014/11/The-Physiological-and-Psychological-Aspects-of-Sending-Humans-to-Mars-Edited-and-Updated1.pdf.

Paxinos, G. & Franklin, K.B.J., 2004. *The Mouse Brain in Stereotaxic Coordinates*, Gulf Professional Publishing.

Pecaut et al., 2004. The Effects of Low-Dose, High-LET Radiation Exposure on Three Models of Behavior in C57BL/6 Mice. *Radiation research*, 162, pp.148–156.

Petrik, D. et al., 2012. Functional and mechanistic exploration of an adult neurogenesis-promoting small molecule. *FASEB journal: official publication of the Federation of American Societies for Experimental Biology*, 26(8), pp.3148–3162.

Phillips, R.G. & LeDoux, J.E., 1992. Differential contribution of amygdala and hippocampus to cued and contextual fear conditioning. *Behavioral neuroscience*, 106(2), pp.274–285.

Plümpe, T. et al., 2006. Variability of doublecortin-associated dendrite maturation in adult hippocampal neurogenesis is independent of the regulation of precursor cell proliferation. *BMC neuroscience*, 7, p.77.

des Portes, V. et al., 1998. A novel CNS gene required for neuronal migration and involved in X-linked subcortical laminar heterotopia and lissencephaly syndrome. *Cell*, 92(1), pp.51–61.

Pothuizen, H.H.J. et al., 2004. Dissociation of function between the dorsal and the ventral hippocampus in spatial learning abilities of the rat: a within-subject, within-task comparison of reference and working spatial memory. *The European journal of neuroscience*, 19(3), pp.705–712.

van Praag, H., Kempermann, G. & Gage, F.H., 1999. Running increases cell proliferation and neurogenesis in the adult mouse dentate gyrus. *Nature neuroscience*, 2(3), pp.266–270.

Raber, J., Marzulla, T., Kronenberg, A. & Turker, M.S., 2015. (16)Oxygen irradiation enhances cued fear memory in B6D2F1 mice. *Life sciences and space research*, 7,

pp.61–65.

Raber, J., Marzulla, T., Stewart, B., Kronenberg, A., et al., 2015b. (28)Silicon Irradiation Impairs Contextual Fear Memory in B6D2F1 Mice. *Radiation research*, 183(6), pp.708–712.

Raber, J. et al., 2014. 28Silicon Radiation-Induced Enhancement of Synaptic Plasticity in the Hippocampus of Naïve and Cognitively Tested Mice. *Radiation research*, 181(4), pp.362–368.

Raber, J. et al., 2016. Effects of Proton and Combined Proton and (56)Fe Radiation on the Hippocampus. *Radiation research*, 185(1), pp.20–30.

Raber, J. et al., 2013. Effects of whole body 56Fe radiation on contextual freezing and Arc-positive cells in the dentate gyrus. *Behavioural brain research*, 246, pp.162–167.

Raber, J. et al., 2004. Radiation-induced cognitive impairments are associated with changes in indicators of hippocampal neurogenesis. *Radiation research*, 162(1), pp.39–47.

Raber, J. et al., 2016. Sex- and dose-dependent effects of calcium ion irradiation on behavioral performance of B6D2F1 mice during contextual fear conditioning training. *Life sciences and space research*, 9, pp.56–61.

Rabin, B.M., Shukitt-Hale, B., Carrihill-Knoll, K.L., et al., 2014. Comparison of the Effects of Partial- or Whole-Body Exposures to 16O Particles on Cognitive Performance in Rats. *Radiation research*, 181(3), pp.251–257.

Rabin, B.M. et al., 2013. Effects of 17β-Estradiol on Cognitive Performance of Ovariectomized Female Rats Exposed to Space Radiation. *Journal of behavioral and brain science*, 3(01), p.67.

Rabin, B.M. et al., 2009. Effects of heavy particle irradiation and diet on object recognition memory in rats. *Advances in space research: the official journal of the Committee on Space Research* , 43(8), pp.1193–1199.

Rabin, B.M. et al., 2012. Interaction between age of irradiation and age of testing in the disruption of operant performance using a ground-based model for exposure to cosmic rays. *Age* , 34(1), pp.121–131.

Rabin, B.M. et al., 2015. Lack of reliability in the disruption of cognitive performance following exposure to protons. *Radiation and environmental biophysics*, 54(3), pp.285–295.

Rabin, B.M. et al., 2007. Relative effectiveness of different particles and energies in disrupting behavioral performance. *Radiation and environmental biophysics*, 46(2), pp.173–177.

Rabin, B.M., Carrihill-Knoll, K.L. & Shukitt-Hale, B., 2011. Operant responding following exposure to HZE particles and its relationship to particle energy and linear energy transfer. *Advances in space research: the official journal of the Committee on Space Research* , 48(2), pp.370–377.

Rabin, B.M., Hunt, W.A. & Joseph, J.A., 1989. An assessment of the behavioral toxicity of high-energy iron particles compared to other qualities of radiation. *Radiation*

research, 119(1), pp.113–122.

Rabin, B.M. & Shukitt-Hale, B., 2014. A voyage to Mars: space radiation, aging, and nutrition. *Nutrition and Aging*, 2(4), pp.233–241.

Rabin, B.M., Shukitt-Hale, B. & Carrihill-Knoll, K.L., 2014a. Effects of age on the disruption of cognitive performance by exposure to space radiation. *Journal of behavioral and brain science*, 4(07), p.297.

Rabin, B.M., Shukitt-Hale, B. & Carrihill-Knoll, K.L., 2014b. Effects of Age on the Disruption of Cognitive Performance by Exposure to Space Radiation. *Journal of behavioral and brain science*, 04(07), pp.297–307.

Rao, M.S., Hattiangady, B. & Shetty, A.K., 2006. The window and mechanisms of major age-related decline in the production of new neurons within the dentate gyrus of the hippocampus. *Aging cell*, 5(6), pp.545–558.

Rao, M.S. & Shetty, A.K., 2004. Efficacy of doublecortin as a marker to analyse the absolute number anddendritic growth of newly generated neurons in the adult dentate gyrus. *The European journal of neuroscience*, 19(2), pp.234–246.

Reagh, Z.M. et al., 2018. Functional Imbalance of Anterolateral Entorhinal Cortex and Hippocampal Dentate/CA3 Underlies Age-Related Object Pattern Separation Deficits. *Neuron*, 97(5), pp.1187–1198.e4.

Rivera, P.D. et al., 2013. Acute and fractionated exposure to high-LET (56)Fe HZE-particle radiation both result in similar long-term deficits in adult hippocampal neurogenesis. *Radiation research*, 180(6), pp.658–667.

Rola, R. et al., 2005. High-LET radiation induces inflammation and persistent changes in markers of hippocampal neurogenesis. *Radiation research*, 164(4 Pt 2), pp.556–560.

Rola, R. et al., 2008. Hippocampal neurogenesis and neuroinflammation after cranial irradiation with (56)Fe particles. *Radiation research*, 169(6), pp.626–632.

Rola, R., Otsuka, S., et al., 2004. Indicators of hippocampal neurogenesis are altered by 56Fe-particle irradiation in a dose-dependent manner. *Radiation research*, 162(4), pp.442–446.

Rola, R., Raber, J., et al., 2004. Radiation-induced impairment of hippocampal neurogenesis is associated with cognitive deficits in young mice. *Experimental neurology*, 188(2), pp.316–330.

Sahay, A. et al., 2011. Increasing adult hippocampal neurogenesis is sufficient to improve pattern separation. *Nature*, 472(7344), pp.466–470.

Sahay, A., Drew, M.R. & Hen, R., 2007. Dentate gyrus neurogenesis and depression. In H. E. Scharfman, ed. *Progress in Brain Research*. Elsevier, pp. 697–822.

Sawamoto, K. et al., 2001. Generation of dopaminergic neurons in the adult brain from mesencephalic precursor cells labeled with a nestin-GFP transgene. *The Journal of neuroscience: the official journal of the Society for Neuroscience*, 21(11), pp.3895–3903.

Schaefer, H.J. & Sullivan, J.J., 1976. Atlas of nuclear emulsion micrographs from personnel dosimeters of manned space missions. Available at:

https://ntrs.nasa.gov/search.jsp?R=19770009784 [Accessed February 8, 2018].

Scharfman, H.E., 2011. *The Dentate Gyrus: A Comprehensive Guide to Structure, Function, and Clinical Implications*, Elsevier.

Scharfman, H.E. & Hen, R., 2007. Is More Neurogenesis Always Better? *Science*, 315(5810), pp.336–338.

Schlaff, C.D. et al., 2014. Bringing the heavy: carbon ion therapy in the radiobiological and clinical context. *Radiation oncology* , 9(1), p.88.

Scholzen, T. & Gerdes, J., 2000. The Ki-67 protein: from the known and the unknown. *Journal of cellular physiology*, 182(3), pp.311–322.

Scoville, W.B. & Milner, B., 1957. Loss of recent memory after bilateral hippocampal lesions. *Journal of neurology, neurosurgery, and psychiatry*, 20(1), pp.11–21.

Sierra, A. et al., 2010. Microglia shape adult hippocampal neurogenesis through apoptosis-coupled phagocytosis. *Cell stem cell*, 7(4), pp.483–495.

Snyder, J.S., Ferrante, S.C. & Cameron, H.A., 2012. Late maturation of adult-born neurons in the temporal dentate gyrus. *PloS one*, 7(11), p.e48757.

Sorrells, S.F. et al., 2018. Human hippocampal neurogenesis drops sharply in children to undetectable levels in adults. *Nature*. Available at: http://dx.doi.org/10.1038/nature25975.

Spalding, K.L. et al., 2013. Dynamics of hippocampal neurogenesis in adult humans. *Cell*, 153(6), pp.1219–1227.

Stark, S.M., Yassa, M.A. & Stark, C.E.L., 2010. Individual differences in spatial pattern separation performance associated with healthy aging in humans. *Learning & memory* , 17(6), pp.284–288.

Steiner, B. et al., 2004. Differential regulation of gliogenesis in the context of adult hippocampal neurogenesis in mice. *Glia*, 46(1), pp.41–52.

Suzuki, S. et al., 2010. The neural stem/progenitor cell marker nestin is expressed in proliferative endothelial cells, but not in mature vasculature. *The journal of histochemistry and cytochemistry: official journal of the Histochemistry Society*, 58(8), pp.721–730.

Sweet, T.B. et al., 2014. Central nervous system effects of whole-body proton irradiation. *Radiation research*, 182(1), pp.18–34.

Sweet, T.B. et al., 2016. Neurogenic Effects of Low-Dose Whole-Body HZE (Fe) Ion and Gamma Irradiation. *Radiation research*, 186(6), pp.614–623.

Tannenholz, L., Jimenez, J.C. & Kheirbek, M.A., 2014. Local and regional heterogeneity underlying hippocampal modulation of cognition and mood. *Frontiers in behavioral neuroscience*, 8, p.147.

Tanti, A. & Belzung, C., 2013. Neurogenesis along the septo-temporal axis of the hippocampus: are depression and the action of antidepressants region-specific? *Neuroscience*, 252, pp.234–252.

Taupin, P., 2007. BrdU immunohistochemistry for studying adult neurogenesis: paradigms, pitfalls, limitations, and validation. *Brain research reviews*, 53(1),

pp.198–214.

Tello-Ramos, M.C. et al., 2018. Spatial memory and cognitive flexibility trade-offs: to be or not to be flexible, that is the question. *Animal behaviour*. Available at: http://www.sciencedirect.com/science/article/pii/S0003347218300691.

Thirsk, R. et al., 2009. The space-flight environment: the International Space Station and beyond. *Canadian Medical Association journal*, 180(12), pp.1216–1220.

Tozuka, Y. et al., 2005. GABAergic excitation promotes neuronal differentiation in adult hippocampal progenitor cells. *Neuron*, 47(6), pp.803–815.

Treves, A. et al., 2008. What is the mammalian dentate gyrus good for? *Neuroscience*, 154(4), pp.1155–1172.

Tronel, S. et al., 2012. Adult-born neurons are necessary for extended contextual discrimination. *Hippocampus*, 22(2), pp.292–298.

United States. National Aeronautics and Space Administration, 2015. *NASA's Journey to Mars: Pioneering Next Steps in Space Exploration*, Government Printing Office.

Vazquez, M.E., 1998. Neurobiological problems in long-term deep space flights. *Advances in space research: the official journal of the Committee on Space Research* , 22(2), pp.171–183.

Vieweg, P. et al., 2015. Changes in pattern completion--a key mechanism to explain age-related recognition memory deficits? *Cortex; a journal devoted to the study of the nervous system and behavior*, 64, pp.343–351.

Vivar, C. & van Praag, H., 2013. Functional circuits of new neurons in the dentate gyrus. *Frontiers in neural circuits*, 7, p.15.

Vogt, B.A., Finch, D.M. & Olson, C.R., 1992. Functional heterogeneity in cingulate cortex: the anterior executive and posterior evaluative regions. *Cerebral cortex* , 2(6), pp.435–443.

Vorhees, C.V. & Williams, M.T., 2014. Assessing spatial learning and memory in rodents. *ILAR journal / National Research Council, Institute of Laboratory Animal Resources*, 55(2), pp.310–332.

Vuolo, M. et al., 2016. Monte Carlo simulations for the space radiation superconducting shield project (SR2S). *Life sciences and space research*, 8, pp.22–29.

Walker, A.K. et al., 2015. The P7C3 class of neuroprotective compounds exerts antidepressant efficacy in mice by increasing hippocampal neurogenesis. *Molecular psychiatry*, 20(4), pp.500–508.

Walter, J. et al., 2011. Age-related effects on hippocampal precursor cell subpopulations and neurogenesis. *Neurobiology of aging*, 32(10), pp.1906–1914.

Wang, L.-P., Kempermann, G. & Kettenmann, H., 2005. A subpopulation of precursor cells in the mouse dentate gyrus receives synaptic GABAergic input. *Molecular and cellular neurosciences*, 29(2), pp.181–189.

Ward, J.F., 1988. DNA damage produced by ionizing radiation in mammalian cells: identities, mechanisms of formation, and reparability. *Progress in nucleic acid research and molecular biology*, 35, pp.95–125.

West, M.J., 2012. *Basic Stereology for Biologists and Neuroscientists*, Cold Spring Harbor, New York.

Whiting, M., 2016. NASA Astronaut Candidates. Available at: https://www.nasa.gov/astronauts/biographies/candidates [Accessed March 26, 2018].

Whoolery, C.W. et al., 2017. Whole-Body Exposure to (28)Si-Radiation Dose-Dependently Disrupts Dentate Gyrus Neurogenesis and Proliferation in the Short Term and New Neuron Survival and Contextual Fear Conditioning in the Long Term. *Radiation research*. Available at: http://dx.doi.org/10.1667/RR14797.1.

Williams, D. et al., 2009. Acclimation during space flight: effects on human physiology. *CMAJ: Canadian Medical Association journal = journal de l'Association medicale canadienne*, 180(13), pp.1317–1323.

Wilson, I.A. et al., 2006. Neurocognitive aging: prior memories hinder new hippocampal encoding. *Trends in neurosciences*, 29(12), pp.662–670.

Wolf, S.A. et al., 2010. Cannabinoid receptor CB1 mediates baseline and activity-induced survival of new neurons in adult hippocampal neurogenesis. *Cell communication and signaling: CCS*, 8, p.12.

Wolf, S.A., Melnik, A. & Kempermann, G., 2011. Physical exercise increases adult neurogenesis and telomerase activity, and improves behavioral deficits in a mouse model of schizophrenia. *Brain, behavior, and immunity*, 25(5), pp.971–980.

Wu, M.V. & Hen, R., 2014. Functional dissociation of adult-born neurons along the

dorsoventral axis of the dentate gyrus. *Hippocampus*, 24(7), pp.751–761.

Wu, M.V., Luna, V.M. & Hen, R., 2015. Running rescues a fear-based contextual discrimination deficit in aged mice. *Frontiers in systems neuroscience*, 9, p.114.

Yamaguchi, M. et al., 2000. Visualization of neurogenesis in the central nervous system using nestin promoter-GFP transgenic mice. *Neuroreport*, 11(9), pp.1991–1996.

Yan, J. et al., 2016. 56Fe irradiation-induced cognitive deficits through oxidative stress in mice. *Toxicology research*, 5(6), pp.1672–1679.

Yassa, M.A. & Stark, C.E.L., 2011. Pattern separation in the hippocampus. *Trends in neurosciences*, 34(10), pp.515–525.

Yun, S. et al., 2016. Re-evaluating the link between neuropsychiatric disorders and dysregulated adult neurogenesis. *Nature medicine*, 22(11), pp.1239–1247.

Yun, S. et al., 2016. Stress-Induced Anxiety- and Depressive-Like Phenotype Associated with Transient Reduction in Neurogenesis in Adult Nestin-CreERT2/Diphtheria Toxin Fragment A Transgenic Mice. *PloS one*, 11(1), p.e0147256.

Zhao, C., Deng, W. & Gage, F.H., 2008. Mechanisms and functional implications of adult neurogenesis. *Cell*, 132(4), pp.645–660.

VITAE

Cody William Whoolery began his academic career at the University of Pittsburgh. Here he was offered an HHMI sponsored undergraduate summer internship through the University of Pittsburgh to research the role tRNA codon usage has in *Mycobacterium smegmatis*. In 2013, Mr. Whoolery graduated with a Bachelors of Science dual Business/Biology degree and was offered a research technician position at West Virginia University. His work investigating the role RNA splice variants have on diabetes at West Virginia drove his passion for science and space. In 2014, Mr. Whoolery was accepted into the graduate program at the UTSW Medical Center where he furthered his studies under the direction of Dr. Amelia Eisch. Mr. Whoolery, soon to be Doctor, has accepted a full time position at Reata Pharmaceuticals in Irving, Texas. Here he has been offered a role in the company's biopharmaceutical leadership development program where they will train him in four separate departments over a two-year span. Upon the completion of the program, he will transition into a leadership role in the company.

Permanent Address: 4859 Cedar Springs Rd #251 Dallas, TX 75219